Synthesis and Reactions of
Iron and Ruthenium Dinitrogen Complexes

A thesis submitted in partial fulfilment of the

requirements for admission to the degree of

Doctor of Philosophy

by

Ruth Guest

School of Chemistry

The University of Sydney

March 2008

Preface

This thesis is a report of original research undertaken by the author and is submitted for admission to the degree of Doctor of Philosophy at the University of Sydney. The work was completed in the School of Chemistry at the University of Sydney during the period March 2004 to December 2005 and in the School of Chemistry at the University of New South Wales during the period January 2006 to March 2008. The work and results presented in this thesis are those of the author, unless otherwise acknowledged.

Sections of this work have been presented at Scientific Conferences:

Investigation of a Dinitrogen Bridged Homobimetallic Complex

L. D. Field, R. Guest

6th Reactive Organometallics Symposium, Sydney University, Sydney, 28th May **2004**. Oral Presentation.

Investigation of a Dinitrogen Bridged Homobimetallic Complex

L. D. Field, R. Guest

7th Reactive Organometallics Symposium, ANU, Canberra, 11th February **2005**. Oral Presentation.

Investigation of a Dinitrogen Bridged Homobimetallic Complex

L. D. Field, R. Guest, H. L. Li

12th The Royal Australian Chemical Institute Convention (RACI Connect 2005), Sydney Convention and Exhibition Centre, Darling Harbour, Sydney, 3rd-7th July, **2005**. Poster Presentation, Poster T137.

Investigation of a Dinitrogen Bridged Homobimetallic Complex

L. D. Field, R. Guest

8th Reactive Organometallics Symposium, UNSW, Sydney, 11th August **2005**. Oral Presentation.

Investigation of a Dinitrogen Bridged Homobimetallic Complex

L. D. Field, R. Guest, H. L. Li

2005 International Chemical Congress of Pacific Basin (Pacifichem 2005), Honolulu, Hawaii, 15th-20th December, **2005**. Poster Presentation, Poster 244.

Synthesis of Iron and Ruthenium Dinitrogen Complexes

L. D. Field, R. Guest

11th Reactive Organometallics Symposium, UNSW, Sydney, 24th November **2006**. Oral Presentation.

Crystals on the Way To Reduction of Dinitrogen at a Metal Centre

L. D. Field, R. Guest

13th Reactive Organometallics Symposium, ANU, Canberra, 24th July **2007**. Oral Presentation.

Abstract

This thesis is primarily concerned with the synthesis and reactions of iron and ruthenium dinitrogen complexes of tripodal phosphine ligands. Of particular interest is the cationic dinitrogen bridged iron complex $[(FeH(PP_3))_2(\mu-N_2)]^{2+}$ **23**, containing the tetradentate ligand $P(CH_2CH_2PMe_2)_3$, PP$_3$ **1**, and its potential for facilitating the reduction of the bound dinitrogen upon treatment with acid.

The synthesis of a selection of novel and known tripodal phosphine and amino phosphine ligands is described. New ligands $N(CH_2CH_2CH_2PMe_2)_3$ N^{3}P$_3$ **7** and $P(CH_2CH_2CH_2P^iPr_2)_3$ P^{3}P$^i_3$ **11** were synthesised by nucleophilic displacement of bromide from the bromoalkylphosphine and bromoalkylamine precursors with the relevant phosphide. A new method for synthesis of known ligand $P(CH_2CH_2CH_2PMe_2)_3$ P^{3}P$_3$ **19** by the nucleophilic substitution of its chloroalkylphosphine oxide with dimethylphosphide and subsequent reduction is also reported.

The reaction of $[(FeH(PP_3))_2(\mu-N_2)]^{2+}$ **23** with base produced the singly deprotonated mixed valence species $[(FeH(PP_3))(\mu-N_2)(Fe(PP_3))]^{+}$ **37** and subsequently the iron(0) dinuclear species $(Fe(PP_3))_2(\mu-N_2)$ **38** and mononuclear complex $Fe(N_2)(PP_3)$ **44**. The ^{15}N labelling of complexes has allowed the ^{15}N NMR spectra of **23**, **37** and **44** to be reported along with the observation of a long-range $^5J_{P-P}$ coupling across the bridging dinitrogen of **37**. Complexes **23** and **37** were also structurally characterised by X-ray crystallography. The treatment of a variety of iron PP$_3$ **1** dinitrogen complexes, including the mononuclear species

$[(Fe(N_2)H(PP_3)]^+$ **22**, with acid, or base then acid, did not result in the formation of ammonia from reduction of the complexed dinitrogen.

The reactions of $FeCl_2(PP_3)$ **24** and $FeClH(PP_3)$ **25** with ammonia and hydrazine afforded the complexes $[FeCl(N_2H_4)(PP_3)]$ **48**, $[FeH(N_2H_4)(PP_3)]$ **47**, $[FeCl(NH_3)(PP_3)]$ **49** and $[FeH(NH_3)(PP_3)]$ **46**. Complexes **47** and **46** are considered potential intermediates in any reduction of the dinitrogen ligand of **23** to ammonia. Complexes **49** and **46** were also formed from the decomposition of the hydrazine complexes **48** and **47**. The ^{15}N NMR shifts, derived from both the ^{15}N labelling of complexes and from ^1H-^{15}N 2D NMR experiments at natural abundance are reported. In addition, complex **47** was characterised by X-ray crystallography.

The novel ligand $P(CH_2CH_2P^iPr_2)_3$ PP^i_3 **12** was used in the successful synthesis of $[FeCl(PP^i_3)]^+$ **51** and $[RuCl(PP^i_3)]^+$ **56**. Reduction of **51** and **56** with potassium graphite under dinitrogen afforded the complexes $Fe(N_2)(PP^i_3)$ **52** and $Ru(N_2)(PP^i_3)$ **57** respectively. This is the first report of a Ru(0) dinitrogen complex. Treatment of **52** and **57** with lutidinium tetrafluoroborate resulted in protonation and oxidation of the metal centre to afford the hydrido complexes $[Fe(N_2)H(PP^i_3)]^+$ **53** and $[Ru(N_2)H(PP^i_3)]^+$ **58** respectively. ^{15}N labelled analogues of **52**, **53**, **57** and **58** were achieved by exchange reactions with $^{15}N_2$ gas, allowing for analysis by ^{15}N NMR spectroscopy. Species **52**, **57** and **58** have also been structurally characterised by X-ray crystallography. Treatment of **52** with excess acid in THF afforded both **53** and the dihydrogen complex $[Fe(H_2)H(PP^i_3)]^+$ **54**.

The mechanism of formation of **54** probably involves the C-H activation of the solvent THF.

The complex cation $[RuCl(P^3P^i_3)]^+$ **65** was synthesised using the novel ligand $P^3P^i_3$ **11**. A polymeric iron(II) complex, $[Fe_2Cl_4(N^3P_3)_2]_n$ **66**, of the tridentate ligand N^3P_3 **7** was also synthesised. Characterisation of both **65** and **66** by X-ray crystallography is reported. $(FeCl)_2(\mu\text{-}Cl)_2(\mu\text{-}P^i_2)_2$ **68**, an unusual bridged dimer of the known ligand $CH_2(P^iPr_2)_2$ P^i_2 **67**, and iron(II) and iron(0) tetramers of the PP_3 **1** ligand, namely $[Fe_4Cl_4(PP_3)_5]^{4+}$ **71** and $Fe_4(PP_3)_5$ **72** were also characterised by X-ray crystallography.

Acknowledgements

The last four years have been a little crazy for me and quite a lot harder than I had imagined they would be. To say I couldn't have done it without some help would be a big understatement. So here we go...

Mark is the best husband you could wish for and I recognise his complete indulgence and support of me in this rather low income pursuit. He and my beautiful daughter Nicola are the lights of my life. I love and thank them both especially. Thanks also go to Thelma and Tommy for taking an active role in Nicola's care and making life that much easier.

Professor Les Field was a great supervisor when you could get your hands on him and a really good guy when you needed him to be. You can't ask for more than that so thankyou Les. Thanks also to Dr Rob Baker for being a superlative "silent" supervisor at Sydney University.

Dr Ian Luck was a great friend when I really needed one, and a good boss to a very casual employee. I extend special thanks to him.

The LDF group has been a 'slow burn' experience. However, I got there with just about all of 'em eventually. I'd like to thank the following for their friendship and a little bit more to boot: Dr Hsiu Lin Li for her diligence and good humour in proof reading this thesis for me; Dr Adelle Shasha for her kindness and generosity; Dr Olivia Allen for being a good mate as well as a fellow coffee loving, mad woman from the Motherland; Dr Alison Magill for her tremendously useful IT troubleshooting prowess and Tim Shearer for being very tall with the voice of a lark. I'd also like to thank Dr Khoung Vhuong who was key in kick starting some of my synthetic successes.

It may seem obvious but it is worth acknowledging that everything is easier when you have a great family to fall back on and in Sarah, William, Irene, Claire and Mum I have the absolute best.

In finishing, I'd like to thank my Mum for making me promise faithfully not to give my PhD away after losing my Dad. Here it is ... done and dusted.

Dedicated to my Dad, John David Guest, who died 17th November 2005.

Ruth Guest

March 2008

List of Abbreviations

1D	one dimensional
2D	two dimensional
AIBN	azo-2.2'-bis(isobutyronitrile)
approx.	approximately
atm	atmosphere(s)
$BAr^F_4{}^-$	$(B(3,5-C_6H_3(CF_3)_2)_4)^-$
br	broad (NMR)
b.p.	boiling point
Bu	butyl
ca.	circa
COSY	correlation spectroscopy
δ	chemical shift (ppm)
d	deutero
d	doublet (NMR)
DCM	dichloromethane
ddd	doublet of doublet of doublets (NMR)
ddq	doublet of doublet of quartets (NMR)
ddt	doublet of doublet of triplets (NMR)
δ	chemical shift
EI	electron impact ionisation
ESI	electrospray ionisation
Et	ethyl
EtOH	ethanol
FID	free induction decay
h	heptet (NMR)
HOMO	highest occupied molecular orbital
HRMS	high resolution mass spectrometry
HSQC	heteronuclear correlation through single quantum coherence
Hz	hertz (s^{-1})
^{i}Pr	isopropyl

IR	infrared
J	scalar coupling constant (NMR)
LRMS	low resolution mass spectroscopy
LUMO	lowest unoccupied molecular orbital
m	multiplet (NMR)
m	meta
M	metal
m/z	mass to charge ratio
Me	methyl
min.	minute(s)
MS	mass spectrometry
NMR	nuclear magnetic resonance
n	normal
o	ortho
p	pentet (NMR)
p	para
Ph	phenyl
ppm	parts per million
q	quartet (NMR)
ref.	reference
s	singlet (NMR)
t	triplet (NMR)
^{t}Bu	tertiary butyl
THF	tetrahydrofuran
w/v	weight by volume

Nomenclature and Naming Conventions

Tripodal Ligands:

N^3P_3 = $N(CH_2CH_2CH_2PMe_2)_3$

PP^i_3 = $P(CH_2CH_2P^iPr_2)_3$

The first letter of the label refers to the central atom of the ligand which is trisubstituted. The superscript number after the first atom denotes the number of methylene units between the central atom and terminal donor atoms. The default, i.e. no superscript number, is two methylene units. The second atom label refers to the terminal donor atoms. The superscript letter after this label refers to the substituent groups of the terminal atoms. The default, i.e. no superscript letter, refers to methyl substituents. The letter i denotes isopropyl substituents. The subscript after the terminal atom label denotes the number of arms. In all cases this is 3.
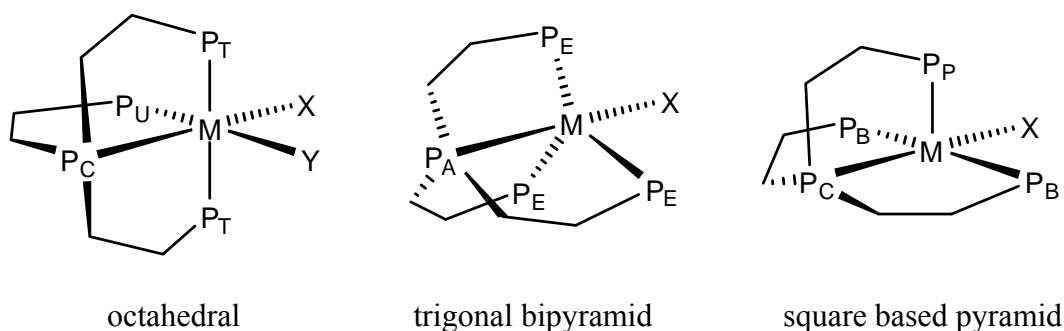
Bidentate Ligand:

P^i_2 = $CH_2(P^iPr_2)_2$

Complexes:

The IUPAC recommendations[*] have been followed in compiling the formal names for each complex presented in Chapter 6 of this thesis. In addition, several structure labelling conventions have been adopted throughout this work and these are described here.

---

[*] Connelly N.G. Ed., Nomenclature of Inorganic Chemistry (IUPAC recommendations 2005), Royal Society of Chemistry, **2005**

| octahedral | trigonal bipyramid | square based pyramid |

The majority of complexes dealt with in this work are octahedral, trigonal bipyramidal or square planar with tripodal tetradentate ligands, as illustrated above.

The 'central' phosphine of the ligand in each octahedral complex is denoted by the labelling P_C. A plane of symmetry renders the two terminal 'trans' phosphines, P_T, equivalent. The third 'unique' terminal phosphine is labelled P_U.

In the trigonal bipyramid structure all three terminal phosphines of the ligand are 'equivalent' by symmetry and assigned P_E. The 'apical' phosphine has been termed P_A to distinguish the ligand's central phosphine from that of alternative structures.

The square based pyramid structure has the 'central' phosphine of the ligand denoted as P_C. The two terminal phosphines which are on the 'base' of the structure, and are equivalent by symmetry, are denoted P_B. The third terminal phosphine is at the 'pinnacle' of the pyramid and is assigned as P_P.

Table of Contents

List of Figures

xviii

List of Tables

Chapter 1

Introduction

1 Introduction

1.1 Nitrogen and Nitrogen Fixation

Nitrogen gas makes up 78 percent by volume of the atmosphere that we breathe.[1] Reduction or 'fixation' of dinitrogen is essential for life. In reduced form it is an essential part of nucleic acids, proteins and most other biomolecules.[2] Industrially nitrogen is a component of many synthetic materials such as polymers, acrylics, dyes, explosives, resins and man-made fertilisers. In 2001 it was estimated that 40 percent of nitrogen used to grow crops came from man made fertilisers, and one third of human protein consumption was dependent upon man-made fertiliser.[3] This statistic gives some idea of the importance of 'fixed' nitrogen in agriculture today.

Dinitrogen is an extremely inert non polar molecule with a negative electron affinity.[4] It has an enthalpy of dissociation of 945 kJ mol^{-1} which is large[1] and an ionization enthalpy of 15.58 eV comparable with that of the noble gas argon (15.75 eV).[4] It is principally the strength of the N-N triple bond which is responsible for the molecule's inertness leading to the fact that most reactions involving nitrogen are endothermic.[1] In addition, dinitrogen has a large HOMO-LUMO gap making it resistant to simple electron transfer redox processes and its low polarisability discourages formation of the highly polar transition states often involved in electrophilic and nucleophilic displacement reactions.[5] These facts make the development of an efficient catalytic cycle for the reduction of dinitrogen to a useful organic species at ambient conditions a difficult and, as yet, unconquered task in the field of organometallic chemistry.

1.2 Haber-Bosch Process

In 1913 Fritz Haber, a German chemist, developed a chemical process to convert nitrogen into ammonia. This process was realised by the construction of a chemical plant designed by Carl Bosch, a German chemical engineer. Such was this achievement, in the as yet unchartered waters of large scale high pressure technology, that it won both men a Nobel Prize.[5] Today the Haber-Bosch process is used almost exclusively in the worldwide industrial production of ammonia. In this process, ammonia is produced from nitrogen and hydrogen gases at high temperature (400-500°C) and pressure (10^2-10^3 atm) using heterogeneous iron- or ruthenium-based catalysts (Equation 1.1).[6]

$$N\equiv N_{(g)} \; + \; 3H_{2(g)} \quad \xrightarrow[\substack{10^2 \text{-} 10^3 \text{ atm} \\ 400 \text{ - } 500^{o}C}]{\text{Fe or Ru catalyst}} \quad 2NH_{3(g)} \quad \substack{\Delta H^{o} = \text{-}46.2 \text{ kJ mol}^{-1} \\ \Delta S^{o} = \text{-}99 \text{ J mol}^{-1} \text{ K}^{-1}} \quad (1.1)$$
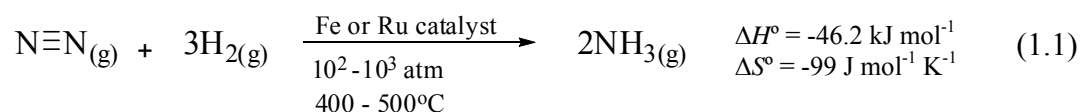
The high temperature is required to overcome the kinetic inertness of dinitrogen whilst the pressure is needed to overcome the thermodynamic effect of an unfavourable equilibrium constant at the elevated temperature.[5] The Haber-Bosch process is an energy intensive process accounting for approximately one percent of the world's energy consumption.[7] Such energy usage provides ample incentive in terms of both cost and environmental impact to develop a system capable of reducing dinitrogen under significantly milder conditions.

1.3 Nitrogenases

In nature, dinitrogen is 'fixed' to the biologically available form, ammonia, by diazotrophic microorganisms which contain enzymes known as nitrogenases.[8]

These microorganisms live in the root nodules of legumes with which they have a symbiotic relationship. There are at least three distinct kinds of nitrogenase based on molybdenum and iron, vanadium and iron and iron with no other metal present.[9] The most common contain two metal-centred proteins one with molybdenum and iron, the other with iron only. A representation of the crystal structure of the protein of *Azotobacter vinelandii* nitrogenase, which falls into the molbdenum and iron category, is shown in Figure 1.1.[10]
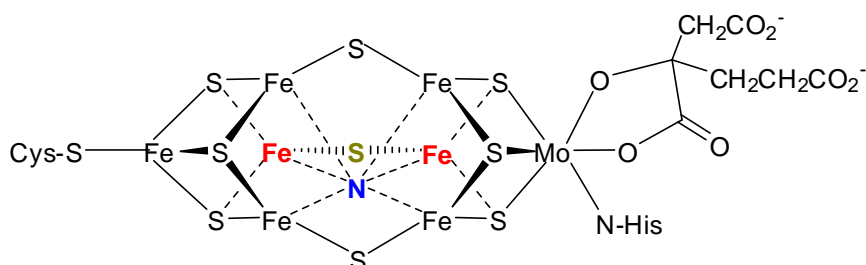
Figure 1.1 Core structure of the molybdenum-iron cluster in the *Azotobacter vinelandii* nitrogenase protein.

Crystallographic studies have determined that the central ligand, shown here in blue, is either C, N,or O.[10] However, theoretical studies have given strong support to the fact that it is a nitrogen atom.[11, 12] Debate over the binding and reduction mechanism of dinitrogen by the nitrogenase enzyme is ongoing. Mechanisms proposed include the central ligand initially as a dinitrogen bridging two iron centres which is converted to an ammonia molecule (released) and the nitrogen atom seen in the crystal structure. This second nitrogen is then reduced and itself released as ammonia leaving the central site free for complexation of another dinitrogen molecule.[12]

More recently, density-functional theory calculations have been used to support a mechanism whereby dinitrogen binds in an end-on or bridging fashion between iron centres (shown in red) prior to its reduction. In this mechanism the central nitrogen ligand plays no direct role in the protonation.[13] Whatever the mechanism, it is clear that the transition metal centres play an important role in the reduction of dinitrogen to ammonia by nitrogenase.

1.4 Chemistry of Dinitrogen Complexes

Since the discovery of the first dinitrogen complex $[Ru(NH_3)_5(N_2)]^{2+}$ in 1965,[14] chemists have sought to catalyse the reduction of dinitrogen through metal complexes capable of binding and thereby activating this relatively inert molecule.

1.4.1 Dinitrogen-Metal Binding

The binding between dinitrogen and a metal centre involves both σ bonding and π back-bonding components as illustrated in Figure 1.2.
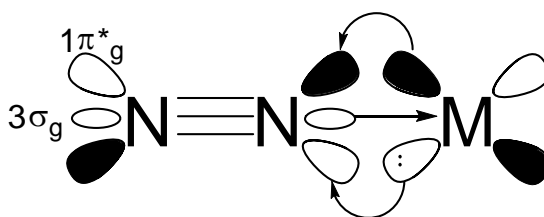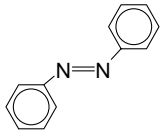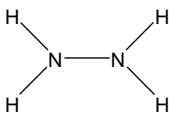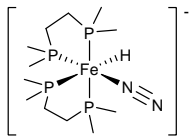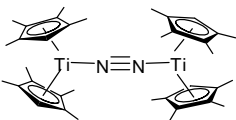
Figure 1.2 Bonding between dinitrogen and a metal centre involves both σ and π components.

The dinitrogen acts a Lewis base by donating electron density from its HOMO into an empty metal *d*-orbital. Conversely, it acts as a Lewis acid accepting electron density from a filled metal *d*-orbital of appropriate symmetry into a

degenerate $1\pi^*_g$ orbital. As a result of the symmetry of the dinitrogen molecular orbitals and the degeneracy of the $1\pi^*_g$ orbitals, dinitrogen can coordinate to metal centres via several different modes, the most common of which is end-on binding.[15] Donation of electron density into the π^*-orbitals by the metal centre weakens or 'activates' the triple bond and this weakening is characterised by an increase in bond length. Activation results in an increase in electron density on the terminal N which renders it more nucleophilic in nature. Hence, it is relatively common for dinuclear nitrogen-bridged complexes to occur. Table 1.1 illustrates the range of dinitrogen complexes, binding modes and levels of dinitrogen activation in the literature.

Table 1.1   Selection of N_2 Complexes and related species with binding mode and N-N bond lengths.

Binding Mode	Compound	N-N bond length (Å)	ref.
-	N≡N gas	1.0975	16
-		1.255	17
-		1.460	16
End-on Mononuclear		1.13(3)	18
End-on Dinuclear		1.170(4)	19
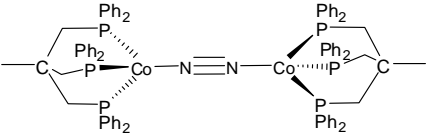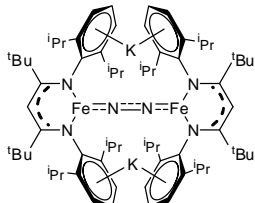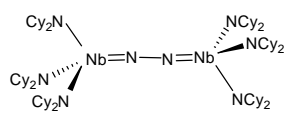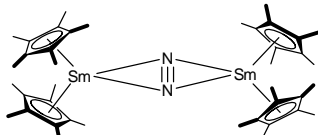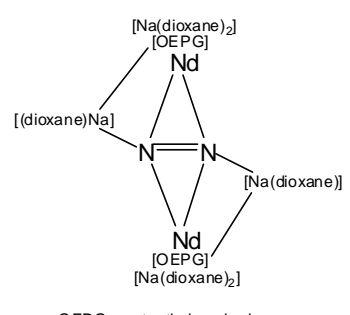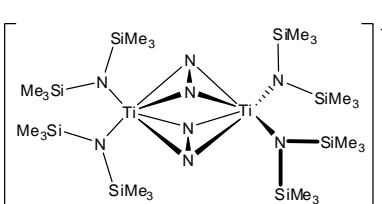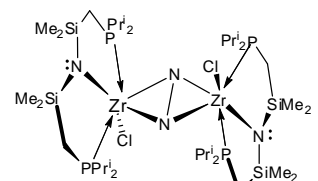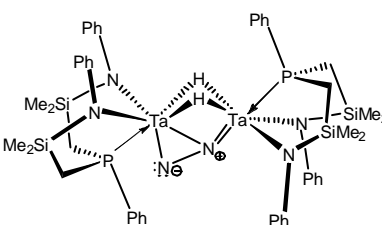
End-on Dinuclear		1.18(2)	[20]

Table 1.1 (cont'd)   Selection of N_2 Complexes and related species with binding mode and N-N bond lengths.

End-on Dinuclear		1.239(4)	[21]
End-on Dinuclear		1.34(1)	[22]
Side-on Dinuclear		1.088(12)	[23]
Side-on Dinuclear		1.234(8)	[24]
Side-on Dinuclear		1.379	[25]
Side-on Dinuclear		1.548(7)	[26]
Side-on End-on Dinuclear		1.319(6)	[27]

1.4.2   Dinitrogen Complex Synthesis

The synthesis of dinitrogen complexes from dinitrogen gas can be achieved by three general routes:[28]

1)   The displacement of a weakly bound ligand by an N_2 ligand.

The ruthenium complex $(SNNS)(P^iPr_3)Ru(N_2)$ (SNNS = 1,2-ethanediamine-N,N'-dimethyl-N,N'-bis(2-benzenethiolate)) shown in Scheme 1.1 is generated by the spontaneous reaction of its acetonitrile analogue with dinitrogen under 1 atmosphere of nitrogen at 50-60°C.[29]
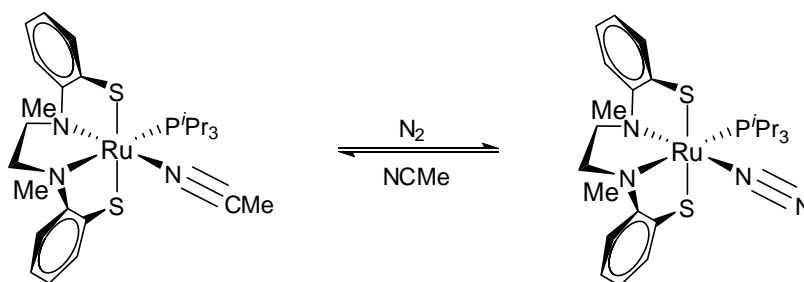
Scheme 1.1

This is an interesting complex in that iron sulfur complexes are often reluctant to ligate dinitrogen. Ruthenium, being more amenable to the task, is often used in attempts to mimic the workings of nitrogenase.[28]

The manganese complex $[Mn(CO)(dppe)_2(N_2)]^+$ (where dppe = $Ph_2PCH_2CH_2PPh_2$) is an example of a coordinated σ-bond being displaced by a dinitrogen (Scheme 1.2).
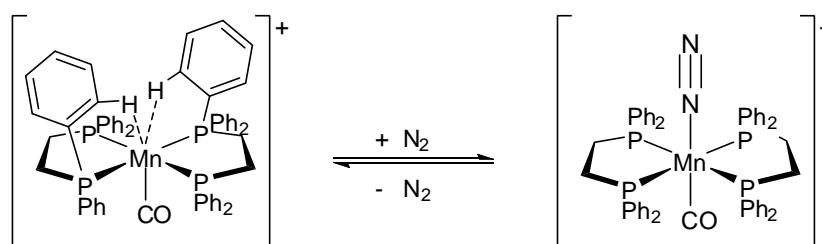
Scheme 1.2

Here the electron deficient carbonyl is stabilised by two agostic interactions with the dppe ligands. In solution, under an atmosphere of dinitrogen, the compound is in equilibrium with the six co-ordinate nitrogen complex.[30, 31]

2) Spontaneous co-ordination of dinitrogen at a vacant site within the co-ordination sphere.

A mixed valent uranium (III)/(IV) dimer ([N$_3$N^t]U)$_2$(μ-Cl) (where N$_3$N^t = N(CH$_2$CH$_2$NSi^{t}BuMe$_2$)$_3$) can be synthesised by reduction of the monomeric chloride [N$_3$N^t]UCl with potassium. Sublimation of this dimer affords [N$_3$N^t]U which, when placed under an atmosphere of dinitrogen, is converted completely to the nitrogen bridged dimer as illustrated in Scheme 1.3.

R = Si^{t}BuMe$_2$
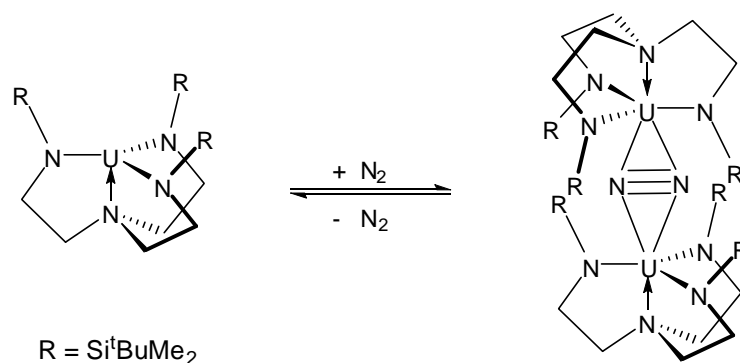
Scheme 1.3

The activation of the bridged dinitrogen is slight with an N-N bond length of 1.109(7) Å, essentially that of free dinitrogen. Application of a vacuum easily

removes the dinitrogen in this reversible reaction. Highlighting the importance of the ligand structure, it is interesting to note that replacing SiMe$_3$ for the Si^{t}BuMe$_2$ results in a complex which is unreactive towards dinitrogen, whereas, the SiPh$_2$Me analogue leads to a series of unidentifiable products.[32, 33]

3) Reduction of metal complexes leading to low-valent metal fragments that bind and activate dinitrogen.

There are several examples of zirconium side-on bound dinitrogen dimers in the literature.[34] The zirconium(IV) dimer ([PNP](THF)Zr)$_2$(μ-η^2:η^2-N$_2$) (where NPN = PhP(CH$_2$SiMe$_2$NPh)$_2$) shown in Scheme 1.4 has been generated by treatment of the dichloride precursor with two equivalents of potassium graphite at low temperature (-78 °C) under an atmosphere of dinitrogen.[35]
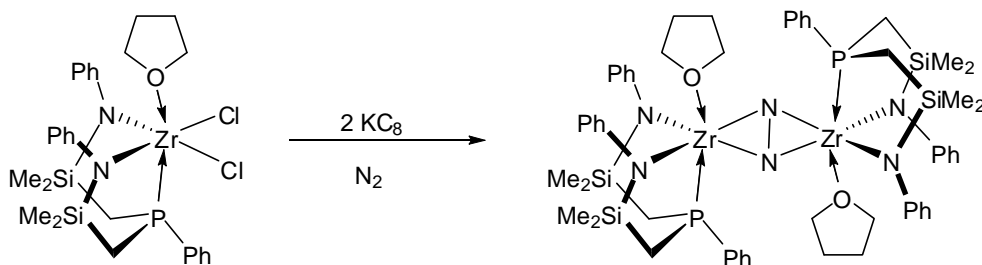
Scheme 1.4

In this complex there is strong N-N bond activation typical of these types of compounds[15] with a bond length (1.503(3) Å) that implies reduction of the dinitrogen to (N$_2$)$^{4-}$.

1.4.3   Reduction of Dinitrogen at a Metal Centre

The reduction of dinitrogen to ammonia requires the addition of six protons and six electrons according to the following equation.

$$N \equiv N \; + \; 6H^+ \; + \; 6e^- \longrightarrow \; 2NH_3 \hspace{2cm} (1.2)$$

In 1975, Chatt *et al.*[36] achieved the first protonation of a dinitrogen complex to give ammonia. This occurred by reacting *cis*-W(N$_2$)$_2$(PMe$_2$Ph)$_4$ with sulfuric acid in methanol. Numerous studies have been undertaken to clarify the process of this reduction, one possibility of which is shown in Figure 1.3 with the metal centre transferring a total of six electrons to the ligand.[37]
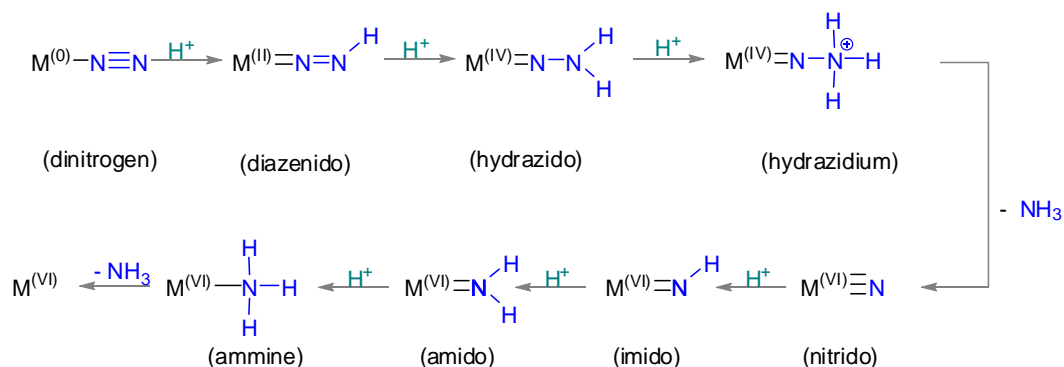
Figure 1.3   Model for reduction of a monometallic dinitrogen complex with electrons being provided by the metal centre.

During the process, available oxygen ligands such as methanol and bisulfate are thought to donate electron density to the metal centre and thereby promote the reduction of dinitrogen and stabilise the high oxidation state of the metal. The dinitrogen triple bond is sequentially degraded by transfer of its π electron density into a multiple M-N bond and to N-H σ bonds. Once the hydrazidium complex has been formed, the extent of the N-N bond weakening is such that it can

undergo cleavage resulting in an easily hydrolysable metal nitrido complex. This reaction sequence is supported by the fact that all of the stages, excepting the hydrazidium, have been recognised in stable complexes.[38] Hydrazidium complexes of tungsten with the bidentate ligand $Et_2PCH_2CH_2PEt_2$ and monodentate phosphine ligand PMe_3 have been reported in the literature.[39, 40]

The first report of ammonia derived from dinitrogen at a single iron centre was provided in 1991 by Leigh *et al.*[41] In this work, the iron(II) complex $[FeH(N_2)(dmpe)_2][BPh_4]$ (where dmpe $= Me_2PCH_2CH_2PMe_2$) was deprotonated with base to give the iron (0) complex $Fe(N_2)(dmpe)_2$ *in situ* which, upon treatment with acid, gave yields of ammonia up to twelve percent. This reaction is illustrated in Scheme 1.5.
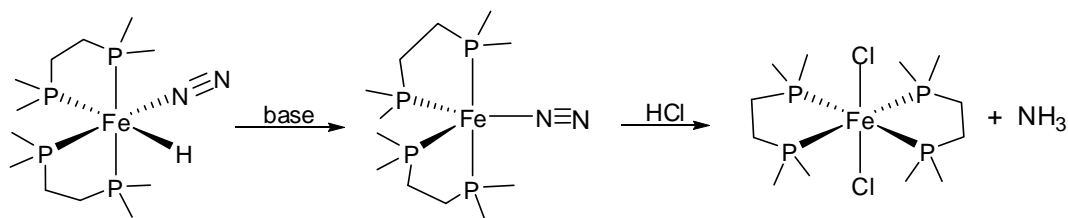
Scheme 1.5

Subsequent work showed that low yields of ammonia (up to twenty percent) could also be derived through this scheme with other phosphine ligands such as bidentate depe ($Et_2PCH_2CH_2PEt_2$) and tetradentate $P(CH_2CH_2PPh_2)_3$.[42] No mechanism for this reduction to ammonia has been proposed although it is believed the reduction power is derived from the formal two electron oxidation of the metal centre. Interestingly, Komiya *et al.*[43] were unable to replicate the production of ammonia when treating the depe iron(0) dinitrogen complex with acid. In this work the iron(0) dinitrogen complex was derived directly from the

iron(II) dichloride by treatment with sodium-naphthalene under an atmosphere of nitrogen.

In an analogous reaction George *et al.*[44] treated an iron(0) dinitrogen complex $Fe(N_2)(NP_3)$ (NP_3 = $N(CH_2CH_2PPh_2)_3$) with hydrobromic acid to produce hydrazine in 22% yield, and a very small amount of ammonia. In this work, the iron(0) dinitrogen complex $Fe(N_2)(NP_3)$ was synthesised by treatment of the hydride precursor $[FeH(N_2)(NP_3)][BPh_4]$ with *n*-butyllithium. The $[FeH(N_2)(NP_3)][BPh_4]$ was prepared by the addition of sodium borohydride to an ethanol solution of $[FeCl(NP_3)][BPh_4]$ under dinitrogen.[45]

In 1990 Schrock *et al.*[46] successfully protonated a complexed dinitrogen by addition of acid to the bimetallic system $[MoCp*Me_3](\mu-N_2)[WCp'Me_3]$ ($Cp*$ = C_5Me_5, Cp' = C_5Me_4Et) in the presence of excess zinc amalgam. This is one of several examples in the literature where reactions of dinitrogen bridged complexes have given rise to the reduction products hydrazine and ammonia.[47]

1.4.4 Catalytic Cycle for the Production of Ammonia from Nitrogen

In the presence of an external source of electrons as well as protons the process by Chatt *et al.* illustrated in Figure 1.3 can be modified to develop a catalytic cycle. In this cycle, the dinitrogen ligand is reduced and released as ammonia and the central metal cycles through a series of oxidation states ultimately returning to its initial state to complex another dinitrogen. Such a cycle is known as the Chatt cycle and is illustrated in Figure 1.4.[28, 48]
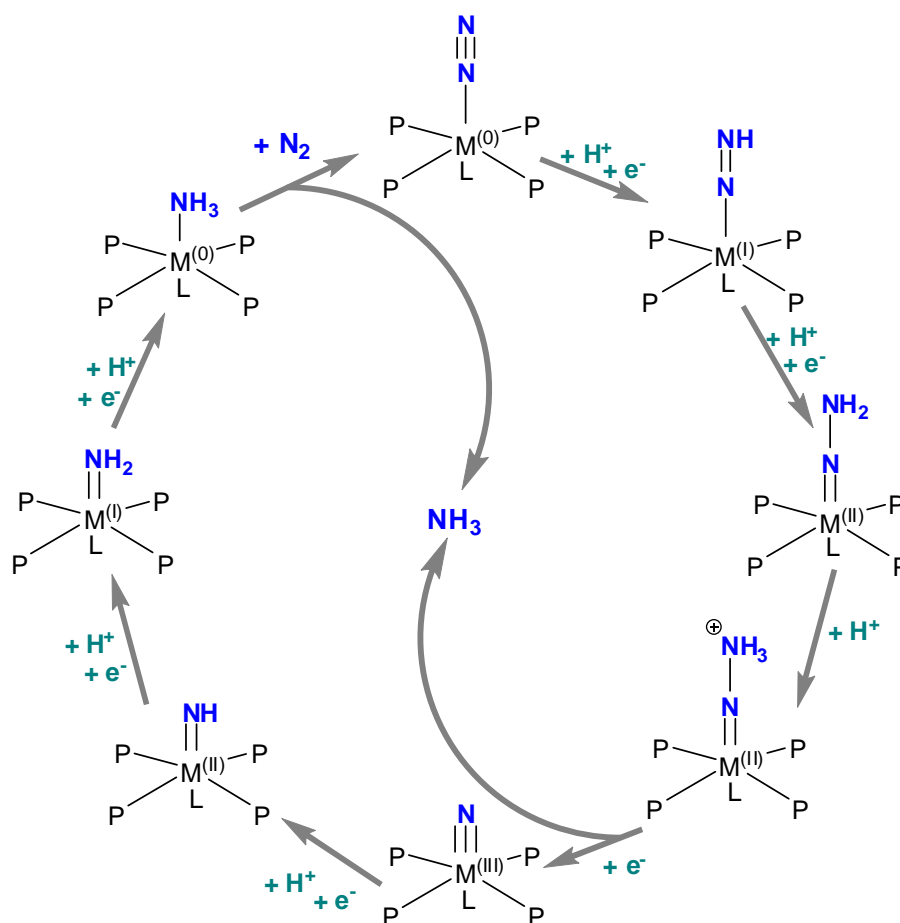
Figure 1.4 The Chatt cycle for the catalytic reduction of dinitrogen at a metal centre.

The first catalytic cycle for the production of ammonia from nitrogen was realised by Schrock *et al.* in 2003.[49] This was achieved with the molybdenum(III) dinitrogen complex [(HIPT)N$_3$N](N$_2$)Mo (where [(HIPT)(N$_3$N)] = [N(CH$_2$CH$_2$N(3,5-(2,4,6-^{i}Pr$_3$C$_6$H$_2$)$_2$C$_6$H$_3$))$_3$]$^{3-}$) shown in Figure 1.5.

HIPT = 3,5-(2,4,6-^{i}Pr$_3$C$_6$H$_2$)$_2$C$_6$H$_3$
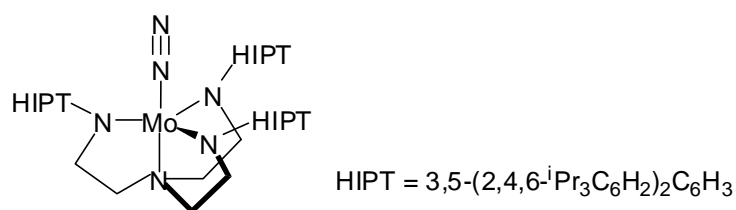
Figure 1.5 Drawing of [(HIPT)N$_3$N](N$_2$)Mo

When this complex was treated with 36 equivalents of CrCp*$_2$ and 48 equivalents of (2,6-lutidinium)[BAr$^F_4$] (Ar^F = 3,5-(CF$_3$)$_2$C$_6$H$_3$), under an atmosphere of dinitrogen, the complexed dinitrogen was reduced to ammonia and the catalyst regenerated. A total of 7 to 8 equivalents of ammonia were formed out of a possible 12 suggesting an efficiency of around 65%. Direct reaction of the reductant with the proton source to generate hydrogen was believed to be the primary cause for the loss in efficiency.[50]

During the proposed catalytic cycle, which involves sequential additions of an electron and then a proton, the molybdenum metal centre is proposed to cycle through 4 oxidation states from the Mo(III) dinitrogen complex to the Mo(VI) nitride and back to the dinitrogen complex. In support of this 'Chatt-like' cycle 8 of the intermediates have been characterised, namely, the Mo(III)-N$_2$, [Mo(IV)-N$_2$]$^-$, Mo(IV)-N=N-H, [Mo(VI)=N-NH$_2$]$^+$, Mo(VI)≡N, [Mo(VI)=NH]$^+$, [Mo(IV)(NH$_3$)]$^+$ and Mo(III)(NH$_3$) species.[49, 51-53]

The ligand in this work is worthy of note. It is a tripodal tetradentate amido amine which complexes to form trigonal bipyramidal molybdenum complexes. The bulky aromatic groups provide two main functions: they prevent dimerisation through a bridging dinitrogen ligand; and they form an approximately trigonal pocket in which dinitrogen, or its reduced products, are located and afforded a high degree of protection.

1.4.5 Hydrogenation of Dinitrogen Complexes

A potential source of both electrons and protons for the reduction of nitrogen to ammonia is hydrogen gas, as utilised in the Haber-Bosch process. In general, hydrogenation of ligated nitrogen complexes leads to displacement of the N_2 ligand by H_2. However, Fryzuk et al.[54] have shown that hydrogenation of the complex $([P_2N_2]Zr)_2(\mu-\eta^2:\eta^2-N_2)$ $([P_2N_2] = PhP(CH_2SiMe_2NSiMe_2CH_2)_2PPh)$ leads to addition of a bridging hydride and reduction of a dinitrogen by formation of an N-H bond (Scheme 1.6).

Methyl groups on Si omitted
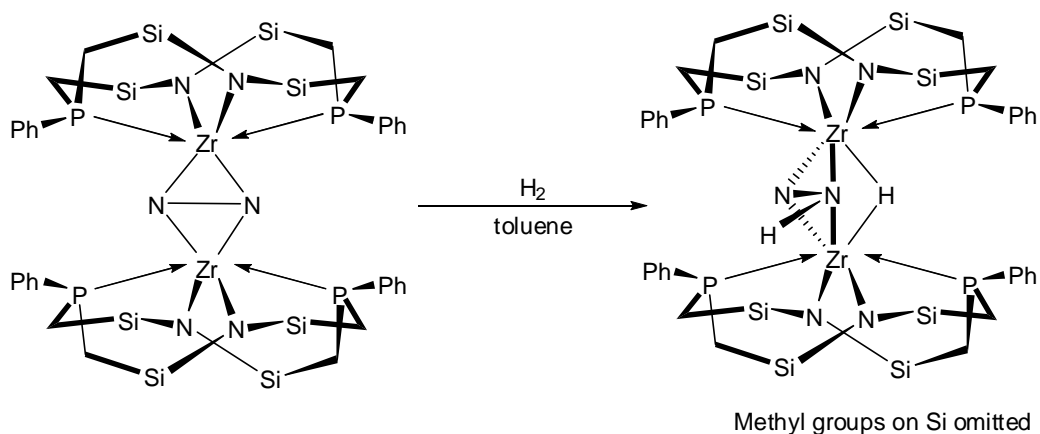
Scheme 1.6

In 2004 Chirik et al. achieved reduction and subsequent cleavage of a side on bound bridging dinitrogen in the complex $[(\eta^5-C_5Me_4H)_2Zr]_2(\mu^2, \eta^2, \eta^2-N_2)$ by reaction with dihydrogen. In this work it was also shown that, under certain conditions, the dinitrogen could be reduced to ammonia in low yield (10-15%, Scheme 1.7).[55-57]
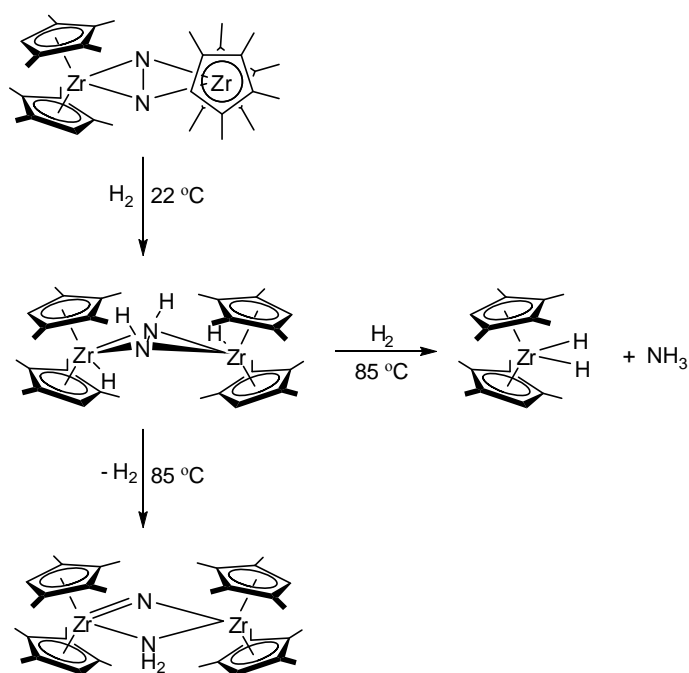
Scheme 1.7

This is the first example of reduction of dinitrogen to ammonia at ambient conditions using dihydrogen. If a pentamethyl version of the complex is utilised the dinitrogen acts as an end-on bridging ligand and no ammonia is formed in the reaction with hydrogen. This highlights how dramatically subtle changes in the ligand can affect the activation and reactivity of the complexed dinitrogen.

Earlier work by Hidai *et al*. has utilised dihydrogen in the form of a ruthenium dihydrogen complex, $[RuCl(\eta^2\text{-}H_2)(dppp)_2]PF_6$ (dppp = $Ph_2PCH_2CH_2CH_2PPh_2$), to reduce dinitrogen at a tungsten centre, *cis*-$W(N_2)_2(PMe_2Ph)_4$, to ammonia.[58] In turn, the ruthenium dihydrogen complex is converted to its hydride. In this instance, the ruthenium complex acts as an acid to provide a proton, with electrons being donated from the tungsten metal centre. Although this is not a true hydrogenation, as only one proton is derived from each dihydrogen, it is an

interesting reaction, nonetheless, as it formally represents the addition of hydrogen gas to dinitrogen to form ammonia.

1.4.6 Cleavage of Dinitrogen Bonds and Formation of Nitride Complexes

The formation of highly stable nitrides from the reaction of dinitrogen with the alkaline earth metals and many transition metals are well known.[15, 59] Although most of these reactions require heat, the reaction with lithium to produce lithium nitride occurs at room temperature. Despite these facts, the cleavage of dinitrogen to its nitride at a well characterised transition metal centre under mild conditions, without an accompanying functionalisation of part of the dinitrogen ligand, was not achieved until quite recently.

In 1995 cleavage of the nitrogen-nitrogen triple bond, by a bridged dinuclear complex, to afford a metal nitride was demonstrated by Laplaza and Cummins.[60] The co-ordinatively unsaturated molybdenum complex $Mo(N(R)Ar)_3$ (R = $C(CD_3)_2CH_3$ Ar = 3,5-$Me_2C_6H_3$) under certain conditions (namely cooled under N_2) formed the dinitrogen bridged $[(N(R)Ar)_3Mo]_2(\mu\text{-}\eta^1\text{:}\eta^1\text{-}N_2)$ complex. At 35°C, the Mo(III) species decomposed in a first-order process to generate the Mo(VI) nitride complex $Mo(\equiv N)[N(R)Ar]_3$[61] (Scheme 1.8).
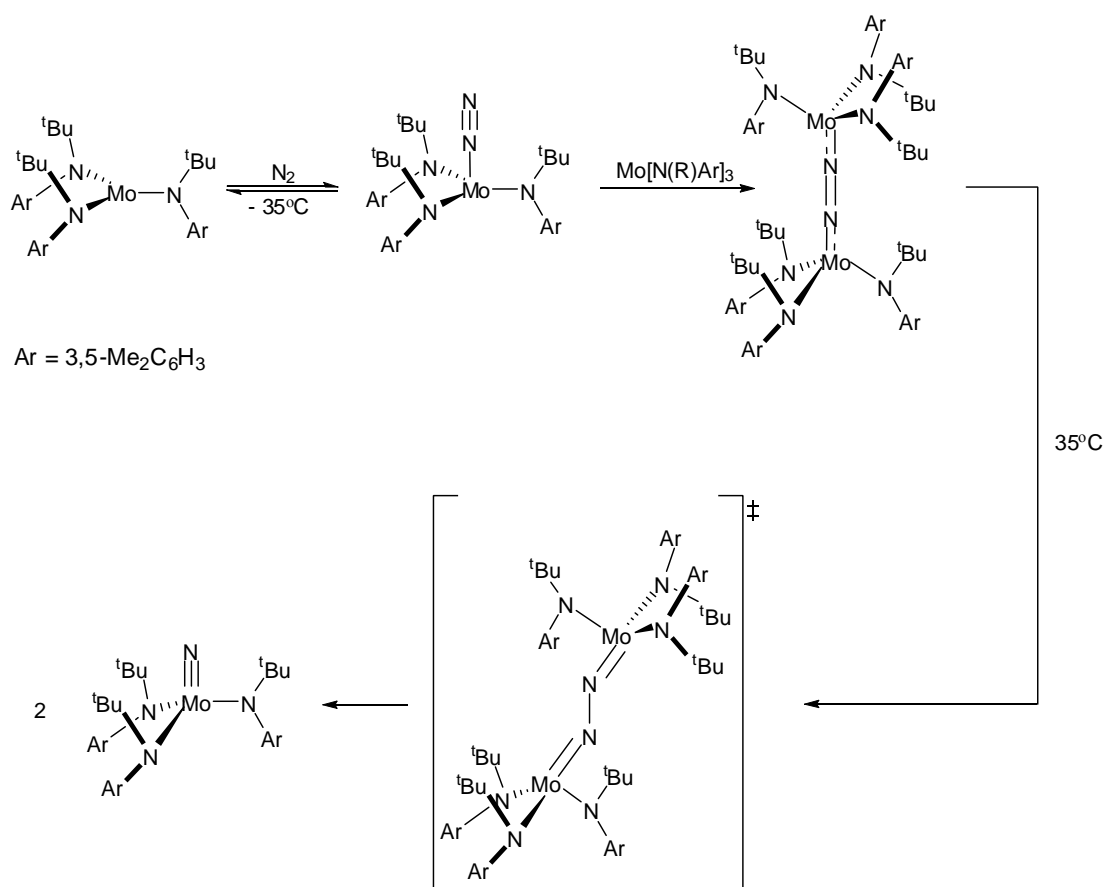
Scheme 1.8

In 2004, the first terminal iron(IV) nitride complex was reported by Betley and Peters.[62] This discovery was of significance given that such a nitride would be required in a Chatt-like scheme for reduction of dinitrogen at a single iron site. In a process, ostensibly the reverse of that illustrated for the molybdenum nitride in Scheme 1.8, the pseudotetrahedrally arranged $[PnBP^{iPr}_3]Fe^{IV}\equiv N$ ($[PnBP^{iPr}_3]$ = $[PhB(CH_2P^iPr_2)_3]^-$) species undergoes bimolecular condensation via nitride coupling under argon or upon concentration by application of a vacuum.[62, 63] The synthesis of the nitride and the transformation to a bridged species are depicted in Scheme 1.9.
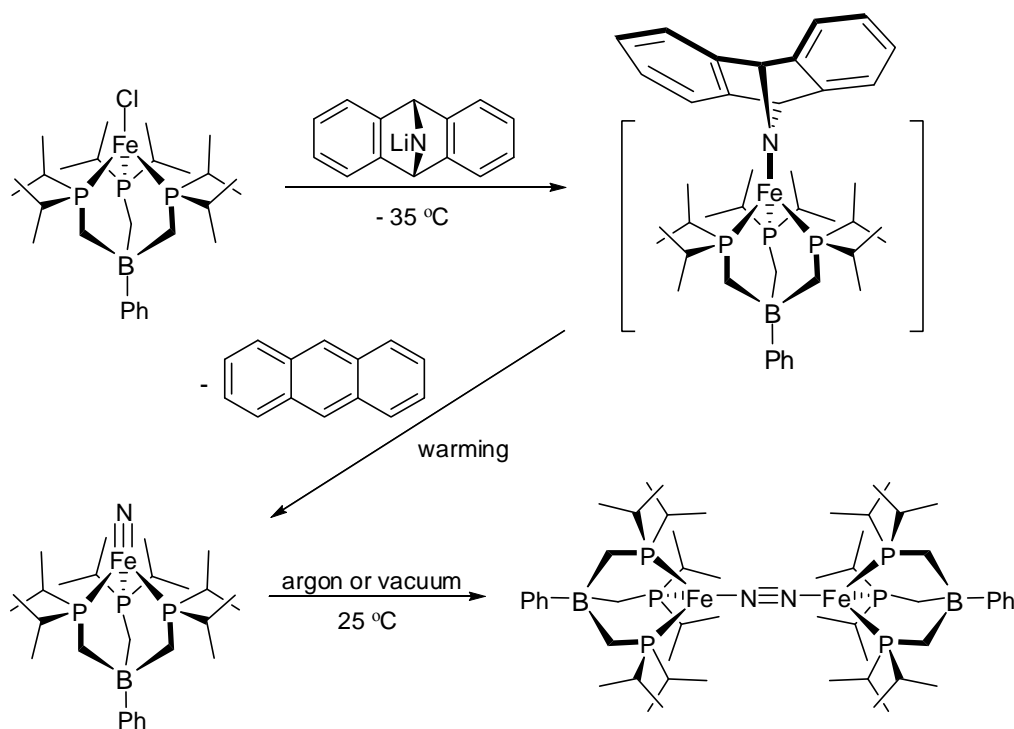
Scheme 1.9

During the nitride coupling reaction, the formally iron(IV) species is reduced to iron(I) whilst simultaneously the nitrogen is oxidised from a nitride (3-) to dinitrogen (0).

1.4.7 Functionalisation of Dinitrogen and Synthesis of Nitrogen Containing Organic Compounds

A line of research which has run in parallel with that described in this introduction is the functionalisation of molecular nitrogen to produce nitrogen containing compounds.[47, 64] For example, catalytic cycles for the formation of pyrrole and N-aminopyrrole, as illustrated in Scheme 1.10, have been achieved from the complexes *trans*-M(N$_2$)$_2$(dppe)$_2$ (M = W or Mo, dppe = Ph$_2$PCH$_2$CH$_2$PPh$_2$).
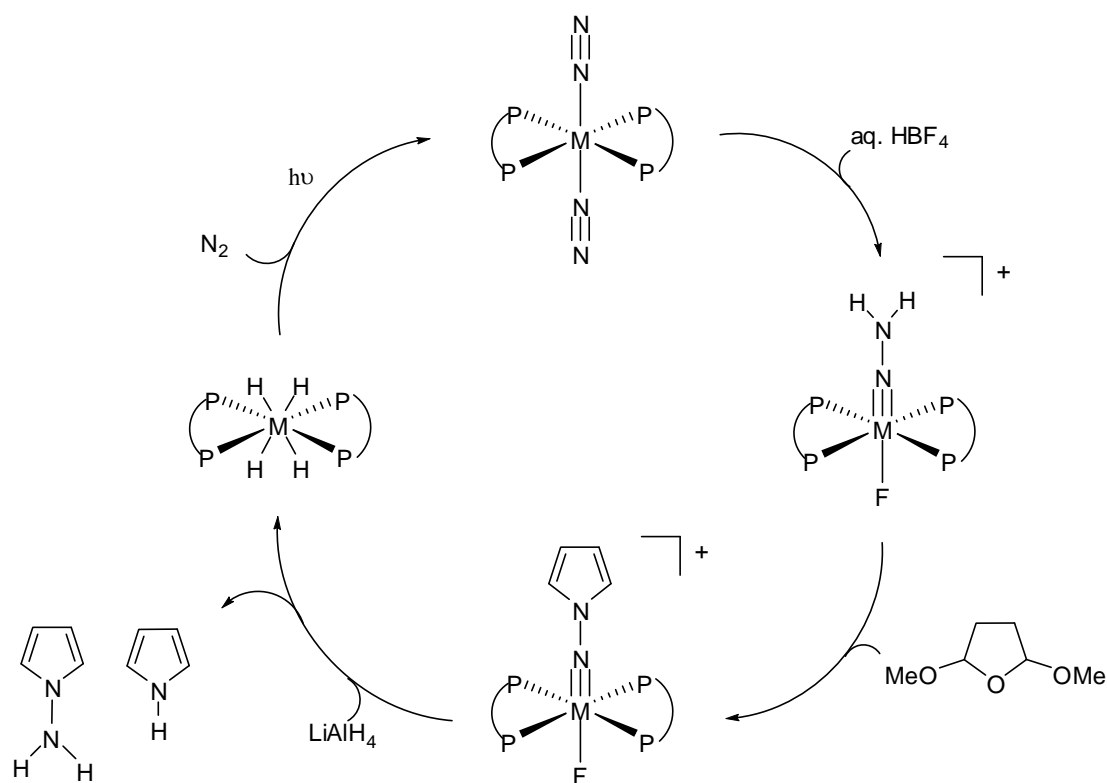
Scheme 1.10

More recently, Cummins *et al.*[65] have developed a cycle for synthesising organic nitriles from the molybdenum nitride complex described in Section 1.4.6. This cycle is illustrated in Scheme 1.11.

N-atom transfer from the molybdenum centre occurs via a Lewis-acid induced reaction with benzoyl chloride to produce a benzoylimido salt. This is then converted into the trimethylsiloxy-substituted ketimide and cyanobenzene is released by reaction with tin or zinc chloride. The molybdenum is returned in the form of a chloromolybdenum(IV) complex which is reductively recycled and treated with sodium hydride under an atmosphere of nitrogen to regain the nitride species.
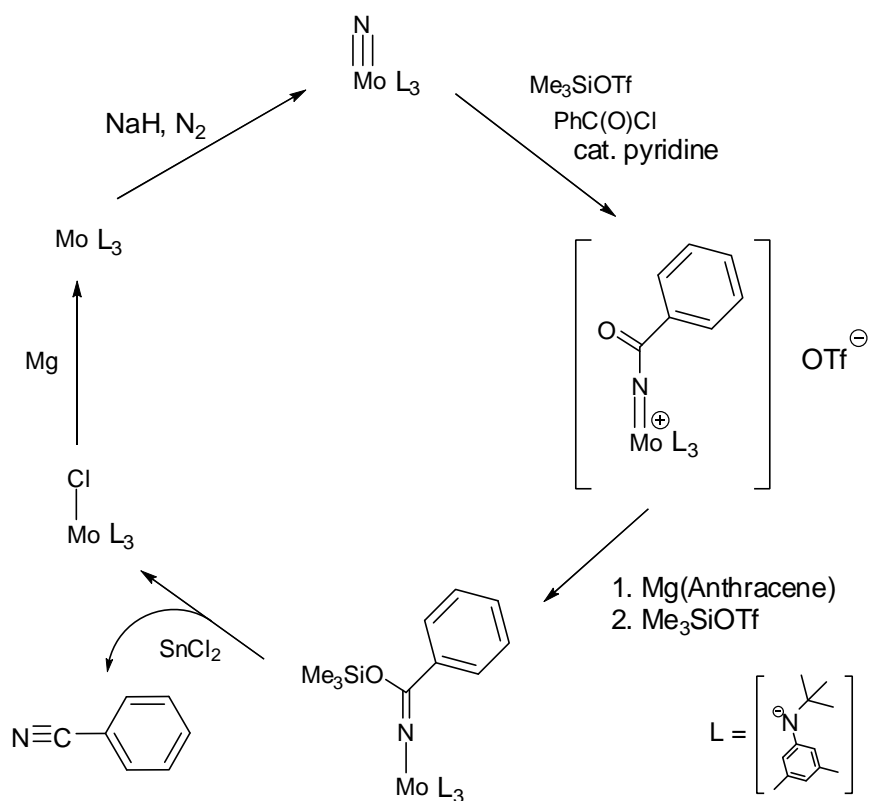
Scheme 1.11

In other work, Fryzuk *et al*. have shown significant functionalisation of the ditantalum complex ([NPN]Ta)$_2\mu$-η^1:η^2-N$_2$)(μ-H)$_2$ (NPN = (PhNSiMe$_2$CH$_2$)$_2$PPh) which has a unique side-on end-on bound dinitrogen. The complex undergoes reaction with electrophiles such as benzyl bromide to generate the N-C bond of the benzyl-hydrazido unit in ([NPN]TaBr)(μ-H)$_2$(μ-η^1:η^2-NNCH$_2$Ph)(Ta[NPN]).[66] It can also undergo hydroboration and hydroalumination where N-N bond cleavage is observed after functionalisation of the nitrogen. When reacted with 9-borabicyclo[3.3.1]nonane the Ta-N bond is hydroborated to generate ([NPN]TaH)(μ-H)$_2$(μ-η^1:η^2-NNBC$_8$H$_{11}$)Ta[NPN]). Functionalisation of the nitrogen is accompanied by the generation of a tantalum hydride.[67] Most recently, various hydrosilylation reactions have been performed on this complex.[68] This includes the formation of a dinuclear disilylimide by reaction of the dinitrogen

complex with just over two equivalents of butylsilane as illustrated in Scheme 1.12.
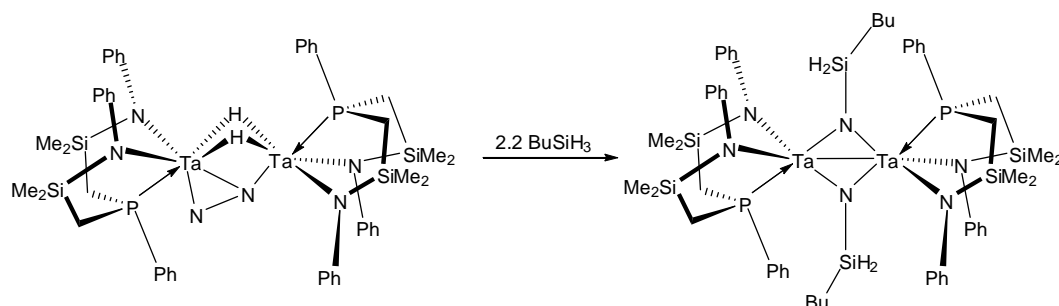
Scheme 1.12

Contributing to the high reactivity of this dinitrogen complex is the existence of a lone pair on the exposed terminal nitrogen affording it Lewis basicity.[69] In addition there is pronounced π character to the Ta-N bonding.[67]

More recent, closely related, work by Kawaguchi *et al.*[70] has shown that a diniobium tetrahydride complex [K(dme)]$_2$[{(*anti*-O$_3$)Nb}$_2$(μ-H)$_4$] (O$_3$ = CH(2-(O⁻)-3,5-(^{t}Bu)$_2$C$_6$H$_2$)$_3$, dme = dimethoxyethane) reacts with dinitrogen to give a bridging nitride complex [K(dme)]$_2$[{(*anti*-O$_3$)Nb}$_2$(μ-N)$_2$]. The nitride complex undergoes stepwise methylation to produce the bismethylimide complex.

1.5   Aims of this work

The primary aims of the work described in this thesis are to investigate the chemistry of a known dinitrogen bridged complex, namely [(FeH(PP$_3$))$_2$(μ-N$_2$)]$^{2+}$[71] **23** (PP$_3$ **1** = P(CH$_2$CH$_2$PMe$_2$)$_3$). This was done with particular regard to the potential for activation and reduction of the complexed dinitrogen and to the synthesis of intermediates that might be envisaged in any successful reduction. In addition, routes to new iron and ruthenium complexes,

with emphasis on the synthesis and characterisation of dinitrogen complexes and their chemistry with an organic acid, were sought. This required the design of synthetic routes to both new and known phosphine ligands.

The specific aims of this work were to:

i) Synthesise and further characterise a dinitrogen bridged iron(II) complex $[(FeH(PP_3))_2(\mu\text{-}N_2)]^{2+}$ [71] **23**, and investigate its potential for reduction of the bound dinitrogen at ambient conditions by treatment with acid and base.

ii) Synthesise and characterise hydrazine and ammine complexes considered as potential intermediates in any reduction of the dinitrogen ligand of **23.**

iii) Design and carry out the syntheses of new phosphine and amino phosphine ligands with the potential to form stable iron and/or ruthenium complexes.

iv) Synthesise and characterise new iron and ruthenium complexes with emphasis on dinitrogen complex preparation.

v) Investigate the chemistry of new iron and ruthenium dinitrogen complexes with an organic acid.

1.6   Structure of this Thesis

Chapter 1

Introduction to nitrogen fixation, dinitrogen metal complexation and the chemistry of dinitrogen bound to a metal centre.

Chapter 2

Synthesis of tris(2-dimethylphosphinoethyl)phosphine (PP$_3$) **1**. Design and synthesis of new tripodal ligands tris(3-dimethylphosphinopropyl)amine (N^{3}P$_3$) **7**

and tris(3-diisopropylphosphinopropyl)phosphine ($P^3P^i_3$) **11**, and a new synthetic route to tris(3-dimethylphosphinopropyl)phosphine (P^3P_3) **19**.

Chapter 3

Synthesis and characterisation of iron-dinitrogen complexes of PP_3. Investigation into the reactions of these complexes with base and acid, including characterisation of a mixed valance dinitrogen bridged dinuclear complex $[(FeH(PP_3))(\mu-N_2)(Fe(PP_3))]^+$ **37**. Synthesis and characterisation of iron(II) hydrazine and ammine complexes of PP_3 by ligand substitution reactions of the iron(II) dichloride and chlorohydride complexes.

Chapter 4

Synthesis and characterisation of iron and ruthenium dinitrogen complexes of tris(2-diisopropylphosphinoethyl)phosphine (PP^i_3) **12** and investigation into their reactions with an organic acid. Synthesis and characterisation of a range of iron and ruthenium complexes of tri and tetradentate phosphine and amino phosphine ligands.

Chapter 5

Summary, conclusions and future work.

Chapter 6

Experimental.

Appendix 1

X-ray crystallographic data (CD format).

1.7   References

1.   Cotton, F. A.; Wilkinson, G.; Gaus, P. L., *Basic Inorganic Chemistry*. 2nd ed.; John Wiley & Sons: New York, **1987**.

2.   Kim, J.; Rees, D. C., *Biochemistry* **1994,** *33*, (2), 389-97.

3.   Lomborg, J., *The Skeptical Environmentalist*. Cambridge University Press: Cambridge, **2001**.

4.   Sellmann, D.; Sutter, J., *Acc. Chem. Res.* **1997,** *30*, (11), 460-469.

5.   Shriver, D. F.; Atkins, P. W.; Langford, C. H., *Inorganic Chemistry*. 2nd ed.; Oxford University Press: Oxford, **1995**.

6.   Moore, J. W.; Stanitski, C. L.; Wood, J. L.; Kotz, J. C., *The Chemical World: Concepts and Applications*. 2nd ed.; Harcourt Brace & Company: Orlando, **1998**.

7.   Smith, B. E., *Science* **2002,** *297*, (5587), 1654-1655.

8.   Burgess, B. K.; Lowe, D. J., *Chem. Rev.* **1996,** *96*, (7), 2983-3011.

9.   Durrant, M. C., *Biochemistry* **2002,** *41*, (47), 13934-13945.

10.   Einsle, O.; Tezcan, F. A.; Andrade, S. L. A.; Schmid, B.; Yoshida, M.; Howard, J. B.; Rees, D. C., *Science* **2002,** *297*, (5587), 1696-1700.

11.   Hinnemann, B.; Norskov Jens, K., *J. Am. Chem. Soc.* **2003,** *125*, (6), 1466-7.

12.   Huniar, U.; Ahlrichs, R.; Coucouvanis, D., *J. Am. Chem. Soc.* **2004,** *126*, (8), 2588-2601.

13.   Kastner, J.; Hemmen, S.; Blochl, P. E., *J. Chem. Phys.* **2005,** *123*, (7), 074306/1-074306/8.

14.   Allen, A. D.; Senoff, C. W., *Chem. Commun.* **1965**, (24), 621-2.

15.   Fryzuk, M. D.; Johnson, S. A., *Coord. Chem. Rev.* **2000,** *200-202*, 379-409.

16.   Sutton, L. E., *Tables of Interatomic Distances and Configuration in Molecules and Ions*. The Chemical Society: London, **1958**.

17.   Allen, F. H.; Kennard, O.; Watson, D. G.; Brammer, L.; Orpen, A. G.; Taylor, R., *J. Chem. Soc., Perkin Trans. 2* **1987**, (12), S1-S19.

18.   Hills, A.; Hughes, D. L.; Jimenez-Tenorio, M.; Leigh, G. J., *J. Organomet. Chem.* **1990,** *391*, (3), C41-C44.

19.   de Wolf, J. M.; Blaauw, R.; Meetsma, A.; Teuben, J. H.; Gyepes, R.; Varga, V.; Mach, K.; Veldman, N.; Spek, A. L., *Organometallics* **1996,** *15*, (23), 4977-4983.

20.   Cecconi, F.; Ghilardi, C. A.; Midollini, S.; Moneti, S.; Orlandini, A.; Bacci, M., *J. Chem. Soc., Chem. Commun.* **1985**, (11), 731-3.

21.   Smith, J. M.; Lachicotte, R. J.; Pittard, K. A.; Cundari, T. R.; Lukat-Rodgers, G.; Rodgers, K. R.; Holland, P. L., *J. Am. Chem. Soc.* **2001,** *123*, (37), 9222-9223.

22.   Berno, P.; Gambarotta, S., *Organometallics* **1995,** *14*, (5), 2159-61.

23.   Evans, W. J.; Ulibarri, T. A.; Ziller, J. W., *J. Am. Chem. Soc.* **1988,** *110*, (20), 6877-9.

24.   Campazzi, E.; Solari, E.; Floriani, C.; Scopelliti, R., *Chem Commun* **1998**, (23), 2603-2604.

25.   Duchateau, R.; Gambarotta, S.; Beydoun, N.; Bensimon, C., *J. Am. Chem. Soc.* **1991,** *113*, (23), 8986-8.

26.   Cohen, J. D.; Fryzuk, M. D.; Loehr, T. M.; Mylvaganam, M.; Rettig, S. J., *Inorg. Chem.* **1998,** *37*, (1), 112-119.

27.   Fryzuk, M. D.; Johnson, S. A.; Rettig, S. J., *J. Am. Chem. Soc.* **1998,** *120*, (42), 11024-11025.

28.   MacKay, B. A.; Fryzuk, M. D., *Chem. Rev.* **2004,** *104*, (2), 385-401.

29.   Sellmann, D.; Hautsch, B.; Rosler, A.; Heinemann, F. W., *Angew. Chem., Int. Ed.* **2001,** *40*, (8), 1505-1507.

30.   King, W. A.; Luo, X.-L.; Scott, B. L.; Kubas, G. J.; Zilm, K. W., *J. Am. Chem. Soc.* **1996,** *118*, (28), 6782-6783.

31.   King, W. A.; Scott, B. L.; Eckert, J.; Kubas, G. J., *Inorg. Chem.* **1999,** *38*, (6), 1069-1084.

32.   Roussel, P.; Scott, P.; D. Tinker, N., *J. Alloys Compd.* **1998,** *271-273*, 150-153.

33.   Roussel, P.; Scott, P., *J. Am. Chem. Soc.* **1998,** *120*, (5), 1070-1071.

34.   MacLachlan, E. A.; Fryzuk, M. D., *Organometallics* **2006,** *25*, (7), 1530-1543.

35.   Morello, L.; Yu, P.; Carmichael, C. D.; Patrick, B. O.; Fryzuk, M. D., *J. Am. Chem. Soc.* **2005,** *127*, (37), 12796-12797.

36.   Chatt, J.; Pearman, A. J.; Richards, R. L., *Nature* **1975,** *253*, (5486), 39-40.

37.   Chatt, J.; Pearman, A. J.; Richards, R. L., *J. Chem. Soc., Dalton Trans.* **1977**, (19), 1852-60.

38.   Chatt, J.; Pearman, A. J.; Richards, R. L., *J. Organomet. Chem.* **1975,** *101*, (3), C45-C47.

39.   Barclay, J. E.; Hills, A.; Hughes, D. L.; Leigh, G. J.; MacDonald, C. J.; Abu Baker, M.; Mohd.-Ali, H., *J. Chem. Soc., Dalton Trans.* **1990**, (8), 2503-7.

40. Galindo, A.; Hills, A.; Hughes, D. L.; Richards, R. L.; Hughes, M.; Mason, J., *J. Chem. Soc., Dalton Trans.* **1990**, (1), 283-8.

41. Leigh, G. J.; Jimenez-Tenorio, M., *J. Am. Chem. Soc.* **1991,** *113*, (15), 5862-3.

42. Hall, D. A.; Leigh, G. J., *J. Chem. Soc., Dalton Trans.* **1996**, (17), 3539-3541.

43. Hirano, M.; Akita, M.; Morikita, T.; Kubo, H.; Fukuoka, A.; Komiya, S., *J. Chem. Soc., Dalton Trans.* **1997**, (19), 3453-3458.

44. George, T. A.; Rose, D. J.; Chang, Y.; Chen, Q.; Zubieta, J., *Inorg. Chem.* **1995,** *34*, (5), 1295-8.

45. Stoppioni, P.; Mani, F.; Sacconi, L., *Inorg. Chim. Acta* **1974,** *11*, (3), 227-30.

46. Schrock, R. R.; Kolodziej, R. M.; Liu, A. H.; Davis, W. M.; Vale, M. G., *J. Am. Chem. Soc.* **1990,** *112*, (11), 4338-45.

47. Hidai, M., *Coord. Chem. Rev.* **1999,** *185-186*, 99-108.

48. Donovan-Mtunzi, S.; Richards, R. L.; Mason, J., *J. Chem. Soc., Dalton Trans.* **1984**, (7), 1329-32.

49. Yandulov, D. V.; Schrock, R. R., *Science* **2003,** *301*, (5629), 76-78.

50. Schrock, R. R., *Acc. Chem. Res.* **2005,** *38*, (12), 955-962.

51. Yandulov, D. V.; Schrock, R. R., *J. Am. Chem. Soc.* **2002,** *124*, (22), 6252-6253.

52. Yandulov, D. V.; Schrock, R. R., *Inorg. Chem.* **2005,** *44*, (4), 1103-1117.

53. Yandulov, D. V.; Schrock, R. R.; Rheingold, A. L.; Ceccarelli, C.; Davis, W. M., *Inorg. Chem.* **2003,** *42*, (3), 796-813.

54. Fryzuk, M. D.; Love, J. B.; Rettig, S. J.; Young, V. G., *Science* **1997,** *275*, (5305), 1445-1447.

55. Fryzuk, M. D., *Nature* **2004,** *427*, (6974), 498-499.

56. Pool, J. A.; Bernskoetter, W. H.; Chirik, P. J., *J. Am. Chem. Soc.* **2004,** *126*, (44), 14326-14327.

57. Pool, J. A.; Lobkovsky, E.; Chirik, P. J., *Nature* **2004,** *427*, (6974), 527-530.

58. Nishibayashi, Y.; Takemoto, S.; Iwai, S.; Hidai, M., *Inorg. Chem.* **2000,** *39*, (26), 5946-5957.

59. Jones, L., Atkins, A., *Chemistry Molecules, Matter, and Change*. Fourth ed.; W.H. Freeman and Company: New York, **2000**.

60. Laplaza, C. E.; Cummins, C. C., *Science* **1995,** *268*, (5212), 861-3.

61. Laplaza, C. E.; Johnson, M. J. A.; Peters, J.; Odom, A. L.; Kim, E.; Cummins, C. C.; George, G. N.; Pickering, I. J., *J. Am. Chem. Soc.* **1996,** *118*, (36), 8623-8638.

62. Betley, T. A.; Peters, J. C., *J. Am. Chem. Soc.* **2004,** *126*, (20), 6252-6254.

63. Hendrich, M. P.; Gunderson, W.; Behan, R. K.; Green, M. T.; Mehn, M. P.; Betley, T. A.; Lu, C. C.; Peters, J. C., *Proc. Natl. Acad. Sci. U. S. A.* **2006,** *103*, (46), 17107-17112.

64. Hidai, M.; Mizobe, Y., *Can. J. Chem.* **2005,** *83*, (4), 358-374.

65. Curley, J. J.; Sceats, E. L.; Cummins, C. C., *J. Am. Chem. Soc.* **2006,** *128*, (43), 14036-14037.

66. Fryzuk, M. D.; Johnson, S. A.; Patrick, B. O.; Albinati, A.; Mason, S. A.; Koetzle, T. F., *J. Am. Chem. Soc.* **2001,** *123*, (17), 3960-3973.

67.   MacKay, B. A.; Johnson, S. A.; Patrick, B. O.; Fryzuk, M. D., *Can. J. Chem.* **2005,** *83*, (4), 315-323.

68.   MacKay, B. A.; Munha, R. F.; Fryzuk, M. D., *J. Am. Chem. Soc.* **2006,** *128*, (29), 9472-9483.

69.   Studt, F.; MacKay, B. A.; Johnson, S. A.; Patrick, B. O.; Fryzuk, M. D.; Tuczek, F., *Chem. Eur. J.* **2005,** *11*, (2), 604-618.

70.   Akagi, F.; Matsuo, T.; Kawaguchi, H., *Angew. Chem., Int. Ed.* **2007,** *46*, (46), 8778-8781.

71.   Field, L. D.; Messerle, B. A.; Smernik, R. J., *Inorg. Chem.* **1997,** *36*, (26), 5984-5990.

Chapter 2

Ligand Synthesis

2   Phosphine Ligand Synthesis

2.1   Introduction

Phosphines are, in general, quite a difficult class of compounds to work with. They tend to be air sensitive, reacting with atmospheric oxygen to form stable phosphine oxides. The more volatile phosphines are pyrophoric igniting spontaneously in air. These volatiles are also the most malodorous and toxic of the phosphines.[1] Handling of these compounds must be undertaken with great care in an inert atmosphere of argon or nitrogen. Syntheses should aim to use the fewest steps possible involving the free phosphine groups.

A brief search of the literature will soon reveal that tertiary phosphine ligands are used widely in transition metal chemistry. Phosphines are chemically similar to their amine counterparts but tend to be less basic and more nucleophilic.[2] The binding between a phosphorus donor atom and a metal centre primarily involves σ bonding. The phosphorus donor atom has a free lone pair of electrons and thus behaves as a Lewis base donating electron density into the empty d-orbital of the metal. Alkyl phosphines are also capable of a degree of π-back bonding, whether into hybrid phosphorus $3d$- and phosphorus-alkyl σ^*-orbitals or the phosphorus-alkyl σ^*-antibonding orbitals alone is open for debate. In some tertiary aliphatic phosphines, the effect of any backbonding is questioned with stability of complexes attributed primarily to the strong metal-phosphorus σ-bond.[2,3]

Phosphorus ligands, as well as forming stable complexes with transition metals, have the added advantage of being NMR active. The ^{31}P nucleus is 100% abundant with spin ½ and a gyromagnetic ratio 40.5% that of ^{1}H.[4] In metal

complexes, the proximity of the phosphorus nucleus to the metal centre results in good sensitivity to changes in the complex, both in terms of chemical shift and ^{31}P-^{31}P scalar coupling. These facts make NMR spectroscopy an important handle in providing structural information about the metal complexes.

The use of polydentate tripodal ligands in metal complexes can serve two main purposes. They are generally more stable than their monodentate counterparts due to the chelate effect.[5] Also, they have the advantage of controlling the stereochemistry. For example, when a tripodal tetradentate PP$_3$ ligand P((CH$_2$)$_n$PR$_2$)$_3$ is complexed to a metal in an octahedral complex, the two other substituents will always be constrained to be *cis* to each other. In bidentate PP ligand systems, with two ligands binding a metal centre in an octahedral arrangement, there is the possibility of the two remaining substituents being either *cis* or *trans* with regards to one another. This is illustrated in Figure 2.1.

cis-M(PP$_3$)XY   trans-M(PP)$_2$XY   cis-M(PP)$_2$XY
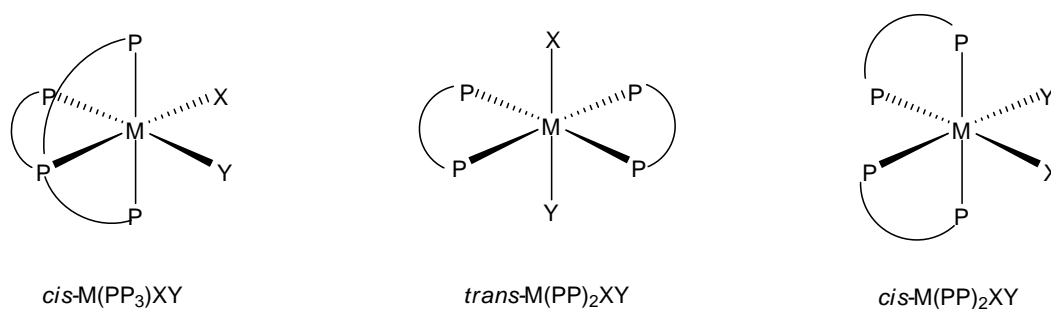
Figure 2.1. Arrangement of PP$_3$ and PP ligands at a six coordinate octahedral metal centre.

The nature of the substituents in a phosphine ligand influences the ability of the donor atom to bind the metal. The smaller the substituent on the phosphorus, typically the stronger the metal-ligand bonds.[6] The reactivity of the complex is also modified by the relative steric bulk of the substituents through distortion of

other ligands and shielding of the metal centre from attack from other potential donors.

There are several strategies for the synthesis of phosphine ligands in the literature.[7] The main methods involve the reaction of alkyl chlorides or alkyl/aryl phosphites with phosphide nucleophiles or the reaction of chlorophosphines or alkoxyphosphines with Grignard reagents. Other methods include reduction of a stable phosphorus-oxygen or phosphorus-sulfur compound, base-catalysed addition of a P-H bond across an alkene double bond and free radical addition of a P-H bond across an alkene double bond. In this chapter, several of these methods are employed in the synthesis of both known and new tripodal phosphine ligands.

2.2 Synthesis of Tris(2-dimethylphosphinoethyl)phosphine, P(CH$_2$CH$_2$P(CH$_3$)$_2$)$_3$, PP$_3$ 1

Originally synthesised by King and Cloyd[8] in a classical multistep route, the tripodal ligand PP$_3$ **1** has been obtained by the radical addition of dimethylphosphine **2** across trivinylphosphine **3**[9] as illustrated in Scheme 2.1.
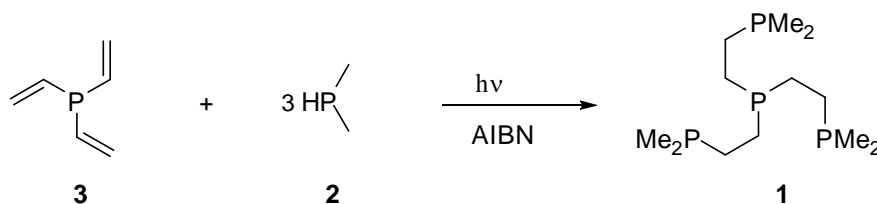
Scheme 2.1

Recently the ligand **1** has also been prepared by the base catalysed addition of dimethylphosphine **2** to trivinylphosphine **3**[10] in a method modified from that of Morris *et al*[11] used in the synthesis of analogous tripodal tetradentate phosphine

ligands. The primary advantage of the latter method is in avoiding unwanted byproducts in the radical reaction (Scheme 2.2) caused by competing radical coupling and fragmentation of the 1,2-diphosphine intermediates. Base-catalysed addition was the route to PP$_3$ **1** used in this work.

Dimethylphosphine 2 from tetramethyldiphosphine disulfide 4

Tetramethyldiphosphine disulfide **4** is a convenient precursor to dimethylphosphine as it is air stable and can be synthesised on a relatively large scale. Its desulfurisation and cleavage can be performed in a one pot synthesis in high yield. Tetramethyldiphosphine disulfide **4** was prepared via the addition of a methyl Grignard reagent to trichlorophosphine sulfide **5** following a method first reported by Parshall[12] (Scheme 2.2).
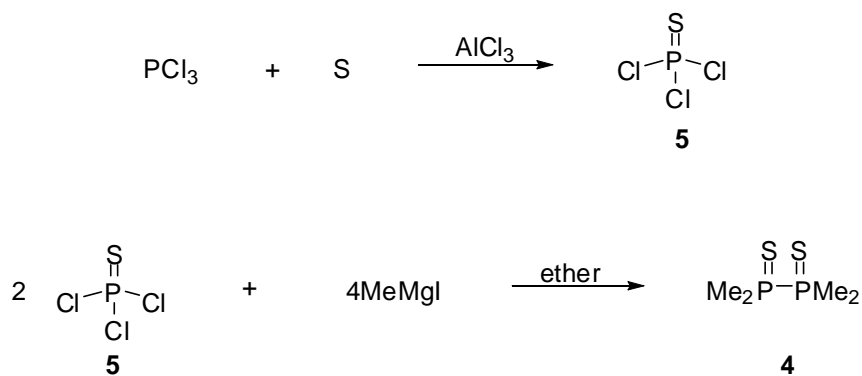
Scheme 2.2

Trichlorophosphine sulfide **5** was synthesised by sulfurising phosphorus trichloride with elemental sulfur and this was subsequently reacted with an ethereal solution of methylmagnesium iodide to give **4** as a white solid which was recrystallised from hot ethanol.

The air stable tetramethyldiphosphine disulfide **4** was desulfurised and cleaved by reaction with water and tri-*n*-butylphosphine.[13]   Dimethylphosphine **2** was distilled from the reaction mixture as a colourless volatile liquid in 88% yield (Scheme 2.3).
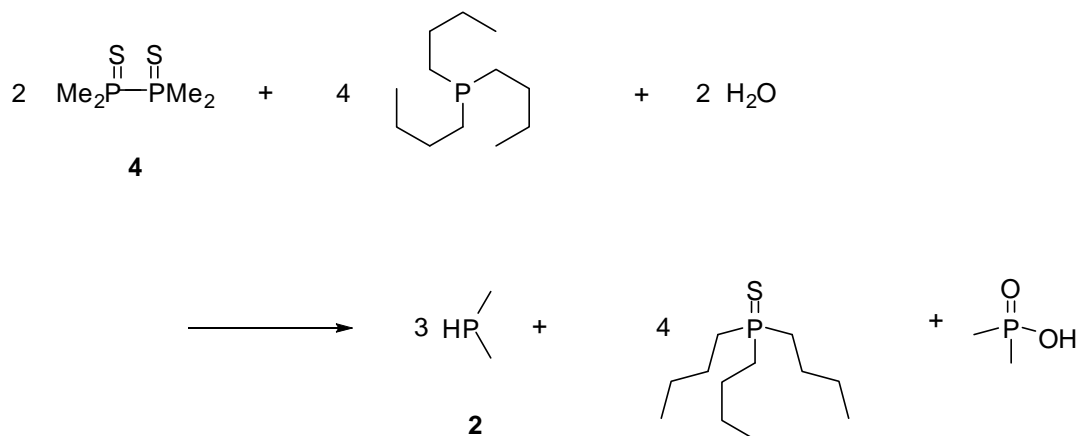
Scheme 2.3

Preparation of Tris(2-dimethylphosphinoethyl)phosphine, PP$_3$ 1

Trivinylphosphine **3** was synthesised by the addition of trimethyl phosphite to a THF solution of vinylmagnesium bromide at 0°C (Scheme 2.4).[9]
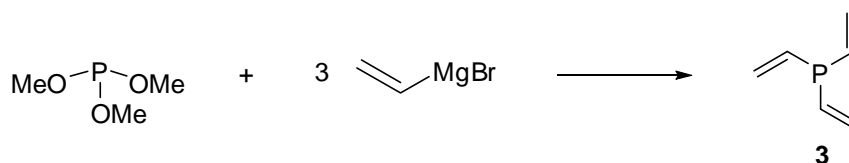
Scheme 2.4

Trivinylphosphine was isolated by distillation. The reaction mixture was distilled and after an initial forerun of neat THF, **3** was distilled, as a mixture with THF, directly from the crude reaction mixture and this solution was used in further reactions without attempting to isolate the trivinylphosphine **3**. If allowed to

stand, especially when undiluted, **3** can polymerise rapidly. Therefore, solutions

of **3** in THF were used as quickly as possible after preparation.

The target ligand **1** was prepared by addition of dimethylphosphine **2** to

trivinylphosphine **3** (Scheme 2.5).
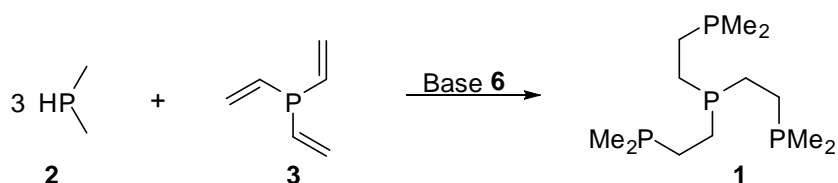
Scheme 2.5

The base used to catalyse the addition of **2** across the double bonds of **3** was

lithium diisopropylamide **6**.   Not only is this amide sufficiently basic to

deprotonate **2** but it is also sufficiently bulky to inhibit its activity as a nucleophile

in competing reactions with **3**.   The amide **6** was prepared by reaction of

diisopropylamine with *n*-butyllithium (Scheme 2.6). **6** is not stable in solution. In

THF, over the course of several hours, a precipitate forms, presumably

incorporating lithium salts. Even when isolated as a white solid under nitrogen,

discolouration was evident over the course of 2 days. **6** was always prepared

immediately prior to use.
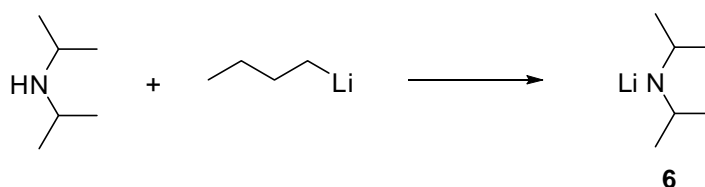
Scheme 2.6

The reaction of dimethylphosphine **2** with trivinylphosphine **3** was performed at

room temperature in THF, with addition of the base **6** intermittently over a period

of 15 minutes to control the vigour of the reaction. After 2 hours the reaction was complete by $^{31}P\{^{1}H\}$ NMR, the singlet for **3** at -19.8 ppm disappeared and the characteristic resonances of **1** appeared as a quartet at -19.6 ppm and a doublet at -47.7 ppm, representing the central and three terminal phosphines respectively. After workup, the ligand PP$_3$ **1** was obtained as a white solid in 50% yield (based on trimethyl phosphite).

In this synthesis addition of the phosphide nucleophile, formed by deprotonation of dimethylphosphine **2** by **6**, always occurs at the β-carbon of **3**. Although the mechanism for this is unclear it is likely that steric and/or electronic effects, due to the proximity of the tertiary phosphine to the double bond, are important.

2.3   Synthesis of Tris(3-dimethylphosphinopropyl)amine, N(CH$_2$CH$_2$CH$_2$P(CH$_3$)$_2$)$_3$, N^{3}P$_3$ 7

The ligand N^{3}P$_3$ **7** has not been synthesised previously. The analogue with 2-carbon bridges between the P and N donors, tris(2-dimethylphosphinoethyl)amine, has been prepared by reaction of tris(2-chloroethyl)ammonium chloride with four equivalents of lithium dimethylphosphide **8**.[14] Analogous tripodal tridentate phosphinoamines have also been prepared by reaction of three equivalents of the appropriate lithium phosphide with tris(2-chloroethyl)amine.[15] This strategy, of nucleophilic substitution of a halide, has been employed here in the synthesis of target ligand **7** (Scheme 2.7).
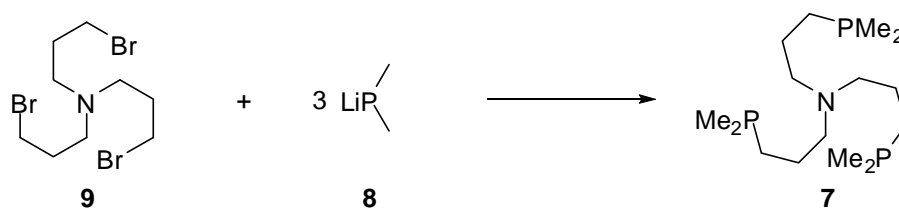
Scheme 2.7

As well as being a ligand of interest in its own right, the route to ligand **7** is air insensitive until the step shown in Scheme 2.7. This allowed it to be used as a testing ground for the potential synthesis of propylene-bridged, phosphine-centred tetradentate phosphine ligands.

Tris(3-bromopropyl)amine, $N(CH_2CH_2CH_2Br)_3$ 9

The synthesis of tris(3-bromopropyl)amine was based on the method of Piguet *et al.*[16] (Scheme 2.8).
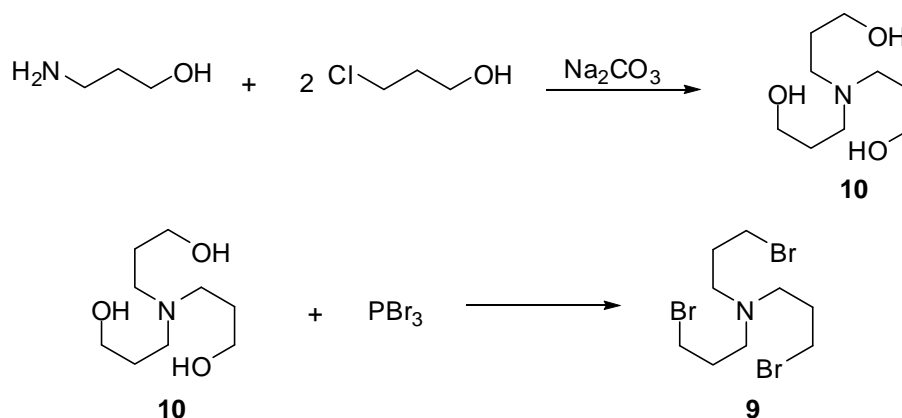
Scheme 2.8

The tris(3-hydroxypropyl)amine **10** was prepared by refluxing 3-chloro-1-propanol (2 equivalents) and 3-amino-1-propanol with sodium carbonate in ethanol for 24 hours.

In order to achieve the bromoalkylamine **9**, phosphorus tribromide was added dropwise to a chloroform solution of **10** and the reaction mixture refluxed overnight. Piguet *et al.*[16] used fifteen equivalents of phosphorus tribromide in their work. This excess was found to be unnecessary with six equivalents shown to be sufficient in this work. Once the reaction mixture was cooled and the excess phosphorus tribromide was quenched with ethanol the solvents were removed *in vacuo* to afford a colourless liquid. ^{1}H NMR of this liquid showed the presence of a significant byproduct, shown by ^{31}P NMR to be a phosphorus containing species presenting as a doublet of pentets. The large J_{P-H} doublet coupling of 692 Hz and the smaller pentet J_{POCH} coupling of 9.1 Hz allowed identification of this product as diethyl phosphite, $(EtO)_2P(O)H$.[17] Diethyl phosphite is likely the product of the quenching reaction of any excess PBr_3 with ethanol. Attempts to separate the two compounds by crystallisation of **9** from ethyl acetate (as has been reported by Piguet[16]) or by chromatography were unsuccessful. However, when left overnight the desired product, **9,** crystallised from the mixture. This product was filtered and washed with a mixture of ice cold water and methanol to give the target amine as large colourless crystals, with high purity by ^{1}H NMR, in 38% yield.

Lithium Dimethylphosphide, LiP(CH$_3$)$_2$ 8

Lithium dimethylphosphide **8** was prepared by the treatment of dimethylphosphine **2** with a hexane solution of *n*-butyllithium at low temperature following a modified method by Fryzuk *et al.*[18] (Scheme 2.9).
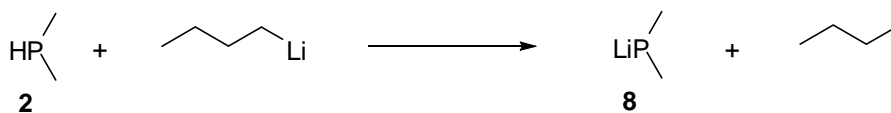
Scheme 2.9

A solution of *n*-butyllithium in hexane was added to **2** at -78°C with stirring affording a white suspension. It was very important not to add excess butyllithium as this would not be removed in the workup of **8** and would interfere in the final step of the ligand synthesis. The reaction mixture was allowed to warm to room temperature and the solvent removed *in vacuo* to afford a white solid. This solid was dissolved in THF resulting in a bright yellow solution of **8**. The yellow solution was used directly in the next step**.**

Preparation of Tris(3-dimethylphosphinopropyl)amine, N^{3}P$_3$ 7

The final step to the target ligand **7** (Scheme 2.7) was performed by dropwise addition of the THF solution of phosphide **8** (slight excess) to a THF solution of the bromoalkylamine **9** at 0°C. After an aqueous workup, N^{3}P$_3$ **7** was obtained as a clear oil in 80% yield. The ^{31}P$\{^1$H$\}$ NMR of this ligand presents as a singlet at -51.8 ppm with a chemical shift similar to that of the terminal phosphines of PP$_3$ **1** (-47.7 ppm) as would be expected given the similarity of their chemical environments.

2.4   Synthesis of Tris(3-diisopropylphosphinopropyl)phosphine,
   P(CH$_2$CH$_2$CH$_2$P(CH(CH$_3$)$_2$)$_2$)$_3$, P^{3}P$^i_3$ 11

The ligand P^{3}P$^i_3$ **11** has not been synthesised previously. The ethyl-bridged analogue tris(2-diisopropylphosphinoethyl)phosphine **12** has been prepared by the base catalysed addition of diisopropylphosphine **13** to trivinylphosphine **3**.[19] This approach is unlikely to work for the synthesis of **11** as the central phosphine is too distant to impart a directing influence on the position of the nucleophilic attack across the double bond of triallylphosphine **14** (see Section 2.5 for further

discussion). Given the successful synthesis of N^3P_3 **7**, by nucleophilic displacement of the bromides of **9** with the phosphide **8,** an analogous route was chosen for the synthesis of $P^3P^i_3$ **11** (Scheme 2.10).
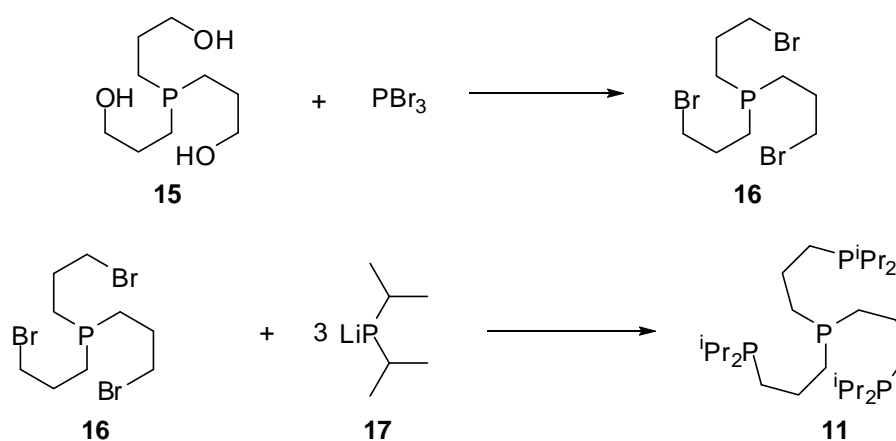
Scheme 2.10

Tris(3-bromopropyl)phosphine 16

Tris(3-hydroxypropyl)phosphine **15** was purchased (Strem) as an 80% pure, highly viscous, clear liquid which is not soluble is common solvents. It was used as received and reacted with phosphorus tribromide to afford tris(3-bromopropyl)phosphine **16** in 64% yield and 82% purity (by $^{31}P\{^1H\}$ NMR) after an aqueous workup. The bromoalkylphosphine **16** polymerises, probably by nucleophilic attack of the lone electron pair of the central phosphine on a brominated γ-carbon, to form an insoluble solid mass within a few hours. Hence, it was used immediately in the next step without any attempt at purification.

It is worth noting that, unlike in the synthesis of the bromoalkylamine **9** (Section 2.3), only one third of an equivalent of phosphorus tribromide was used i.e. the reagent was not in excess. It is likely, given the similarities in the chemistry, that this more efficient stoichiometry would have been sufficient in the case of the

synthesis of **9** (Section 2.3) and this could avoid complications arising from byproduct formation on workup.

Diisopropylphosphine, $((CH_3)_2CH)_2PH$ 13

Diisopropylphosphine **13** was prepared by the reaction of chlorodiisopropylphosphine **17** with lithium aluminium hydride following a modified method by Krogh-Jerspersen et al.[20] (Scheme 2.11).
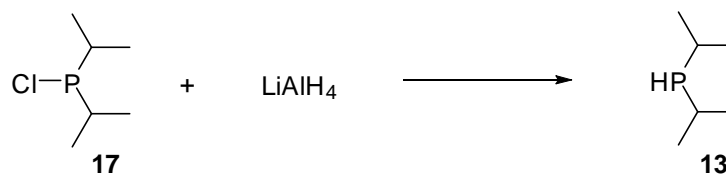
Scheme 2.11

A solution of two equivalents of **17** in diethyl ether was added dropwise to a suspension of lithium aluminium hydride at 0°C over the course of an hour with stirring. The reaction mixture, which appeared as a grey suspension, was then stirred overnight before being filtered and then distilled. Distillation afforded an azeotropic mixture of **13** and diethyl ether which was used directly in the next step, the amount of **13** (60% yield) being determined by integration of the ^{1}H NMR spectrum. Although filtering of a solution containing fine lithium and aluminium salts is never an ideal workup procedure, it was found to be the method of choice in this preparation. Attempts to perform an aqueous workup led to relatively poor yields presumably due to entrapment of the phosphine within the emulsion formed upon addition of water to the reaction mixture.[20]

The methyl groups of diisopropylphosphine are diastereotopic and present at separate chemical shifts in the ^{1}H NMR spectrum. The nitrogen analogue,

diisopropylamine, has four methyl groups which are identical by ^{1}H NMR due to fast inversion at the nitrogen centre.[21, 22] This is not the case for the phosphorus centre of **13,** where inversion is slow on the NMR timescale.

Lithium Diisopropylphosphide, LiP(CH(CH$_3$)$_2$))$_2$ 18

Lithium diisopropylphosphide **18** was prepared in a manner analogous to that for lithium dimethylphosphide **8** (Section 2.3) following a modified method by Fryzuk *et al.*[18] A hexane solution of *n*-butyllithium was added to one equivalent of diisopropylphosphine in diethyl ether at 0°C with stirring. The reaction mixture was allowed to warm to room temperature and THF was added to the white suspension until a red solution of **18** formed which was used directly in the next step.

Tris(3-diisopropylphosphinopropyl)phosphine,

P(CH$_2$CH$_2$CH$_2$P(CH(CH$_3$)$_2$)$_2$)$_3$, P^{3}P$^i_3$ 11

The target ligand **11** was prepared by addition of the red solution of lithium diisopropylphosphide **18** to slightly less than a one third equivalent of tris(3-bromopropyl)phosphine **16** at 0°C (Scheme 2.10). After an aqueous workup, the resulting brown liquid was purified by distillation. Byproducts were distilled from the liquid under an active vacuum leaving the target ligand P^{3}P$^i_3$ **11** as a brown oil residue in good purity by ^{1}H NMR.

The ^{31}P{^{1}H} NMR spectrum of **11** shows two singlets, representing the terminal phosphines at δ 1.9 and the central phosphine at -34.7 ppm. The chemical shift of the terminal phosphines shows a marked shift downfield relative to the terminal

phosphine shifts of PP$_3$ **1** (-47.7 ppm) and N^{3}P$_3$ **7** (-51.8 ppm) due to an effective deshielding[21] of the phosphine with isopropyl substituents compared to that with methyl substituents. This relative downfield chemical shift is typical for phosphines with alkyl substituents; for example, dimethylphosphine **2** has a ^{31}P{^{1}H} NMR chemical shift of -99 ppm, whilst diisopropylphosphine **13** has a chemical shift significantly lower field at -16 ppm.

2.5 Synthesis of Tris(3-dimethylphosphinopropyl)phosphine P(CH$_2$CH$_2$CH$_2$P(CH$_3$)$_2$)$_3$, P^{3}P$_3$ 19

The ligand tris(3-dimethylphosphinopropyl)phosphine, P^{3}P$_3$, **19** has been synthesised previously by the radical-initiated addition of dimethylphosphine **2** across the double bond of triallylphosphine **14** (Scheme 2.12).[23]
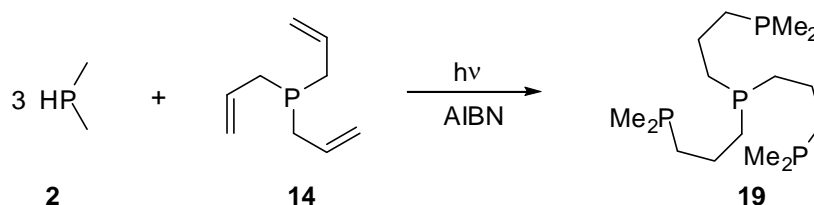
Scheme 2.12

This synthesis has two main drawbacks. The first is that often a significant amount of bis(dimethylphosphino)propane is formed as a byproduct caused by competing fragmentation of the 1,3-diphosphine intermediates. The second drawback is the very long (greater than two days) reaction time that increases the risks inherent with handling of the highly pyrophoric and volatile starting material **2**.[24]

Modifying the synthesis of the ethyl-bridged analogue PP$_3$ **1** (Section 2.2), to prepare P^{3}P$_3$ by base catalysed addition of **2** across triallylphosphine **14** has been found to be unsuccessful.[10] This is due to the non stereoselective addition of the phosphide intermediate at the β-carbons of **14** resulting in two pairs of enantiomeric isomers of tris(2-dimethylphosphinopropyl)phosphine, and none of the desired product **19** (Scheme 2.13).
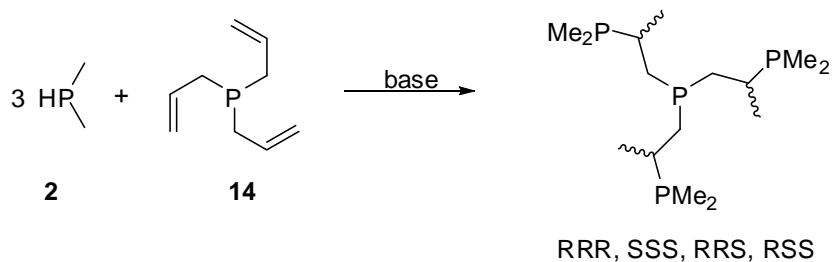
Scheme 2.13

The addition of the phosphine at the β-carbon position is believed to be due to base catalysed migration of the double bond prior to addition of **2** across the three double bonds.

Given the successful syntheses of N^{3}P$_3$ **7** and P^{3}P$^i_3$ **11** by substitution of the halogenated precursor with the required phosphide, a similar approach was taken in the synthesis of the target ligand **19**. As a modification from the synthesis of **7** and **11**, thionyl chloride (SOCl$_2$) was used as the halogenating agent. This was considered to have the potential advantage of easily removable byproducts, namely SO$_2$ and HCl. Kaden *et al.*[25] have successfully used this reagent in the chlorination of tris(2-hydroxyethyl)amine to tris(2-chloroethyl)amine. Somewhat surprisingly, treatment of the hydroxyalkylphosphine precursor **15** with thionyl

chloride under nitrogen resulted, not in tris(3-chloropropyl)phosphine but its

oxide **20** in 65% yield (Scheme 2.14).
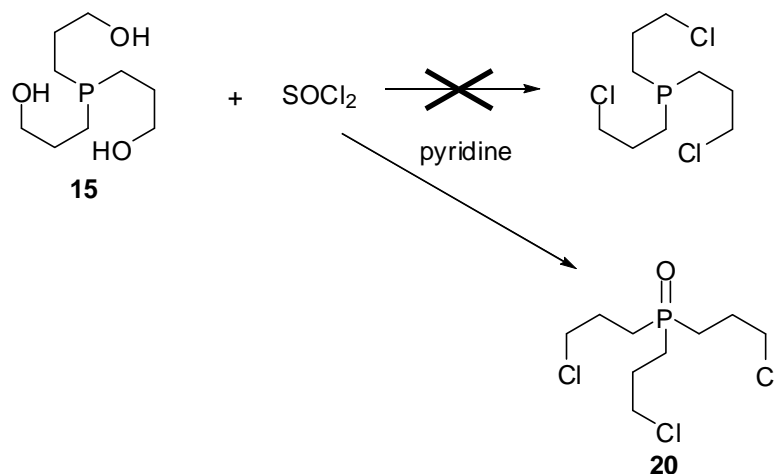
Scheme 2.14

An analogous reaction for the treatment of phosphines with thionyl chloride could

not be found in the literature. However, a patent for the treatment of **15** with HCl

gas resulting in the formation of **20** is available[26] (Scheme 2.15).
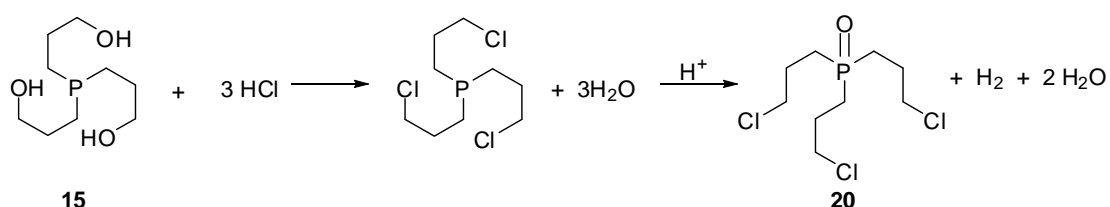
Scheme 2.15

In this work it is proposed that the role of the acid is catalytic in the oxidation of

the central phosphine by water. Given that HCl is one of the byproducts in a

standard chlorination of an alkylhydroxy species with thionyl chloride (Equation

2.1), then this type of mechanism can account for the oxidised product **20**. The

$^{31}P\{^{1}H\}$ NMR of **20** showed a single resonance at δ 47.3 ppm. This chemical

shift is characteristic of tertiary phosphine oxides which typically appear between 25 and 50 ppm.[27, 28]

$$R\text{-}OH + SOCl_2 \longrightarrow R\text{-}Cl + SO_2 + HCl \qquad\qquad (2.1)$$

This competing route to halogenation of **15** (Scheme 2.15) could probably be inhibited by the addition of an excess of base, rather than adding base in a catalytic amount only.

A better synthetic approach was to proceed with the synthesis using the oxide to advantage and incorporating a reduction step at the end. The phosphine oxide **20** has the advantage of removing the potentially nucleophilic polymerisation that might occur through attack of the central phosphine on the halogenated γ-carbon.

Tris(3-dimethylphosphinopropyl)phosphine oxide,
P(O)(CH$_2$CH$_2$CH$_2$P(CH$_3$)$_2$)$_3$, 21

Reaction of **20** with lithium dimethylphosphide **8** (Scheme 2.16) in THF at 0°C gave tris(3-dimethylphosphinopropyl)phosphine oxide **21** as a white solid in 67% yield.
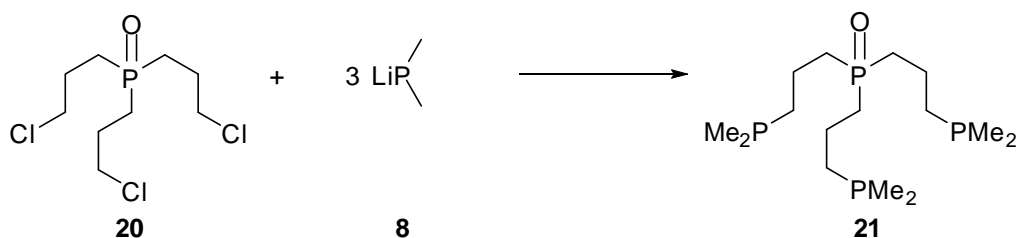
Scheme 2.16

The ^{31}P{^{1}H} NMR spectrum exhibited two singlets; a resonance for the oxidised central phosphine oxide at δ 46.2 ppm with a singlet for the terminal phosphines at -52.4 ppm. Here the terminal phosphine has a chemical shift very close to those

for the terminal phosphines of PP$_3$ **1** (-47.7 ppm) and N^{3}P$_3$ **7** (-51.8 ppm) as expected given the similarities in chemical environment. The chemical shift for the central phosphine is significantly downfield due to the oxidised state of the phosphine.

Tris(3-dimethylphosphinopropyl)phosphine, P(CH$_2$CH$_2$CH$_2$P(CH$_3$)$_2$)$_3$, P^{3}P$_3$ 19

The target ligand **19** was formed by reducing the oxide **21** with an excess of trichlorosilane (Scheme 2.17).[29]
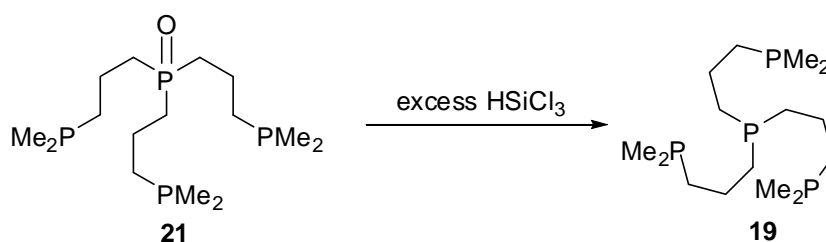
Scheme 2.17

Approximately 8 equivalents of trichlorosilane were added to a THF solution of **21** and the reaction mixture was refluxed under nitrogen overnight. Following an aqueous workup the target ligand **19** was obtained as a white solid in 70% yield. The ^{31}P{^{1}H} NMR showed the central phosphine resonance now at the higher field chemical shift of δ -31.5 ppm with that of the terminal phosphines very close to those of **21** at -51.2 ppm (these chemical shifts correlate well with the literature values[23]). The literature preparations of **19,** by radical addition (Scheme 2.13), report the product as a colourless oil.[23, 24]

2.6   Summary of Ligand Synthesis

The synthesis and characterisation of known ligand $P(CH_2CH_2PMe_2)_3$ PP_3 **1** was achieved by base-catalysed addition of dimethylphosphine **2** across the double bonds of trivinylphosphine **3**.   The phosphine adds regioselectively to the β-carbon due to the directing influence of the central phosphine.

The synthesis and characterisation of previously unknown ligands $N(CH_2CH_2CH_2PMe_2)_3$ N^3P_3 **7** and $P(CH_2CH_2CH_2P(iPr)_2)_3$ $P^3P^i_3$ **11** was achieved by the nucleophilic substitution of their bromoalkyl amine **9** and phosphine **16** precursors with dimethylphosphide **8** and diisopropylphosphide **18** respectively.

The synthesis and characterisation of known ligand $[P(CH_2CH_2CH_2)PMe_2)_3]$ P^3P_3 **19** was achieved by the nucleophilic substitution of its chloroalkylphosphine oxide with dimethylphosphide **8**, with subsequent reduction of the central phosphine oxide.

2.7 References

1. Luxon, S. G., *Hazards in the Chemical Laboratory*. 5th ed.; The Royal Society of Chemistry: Cambridge, **1992**.

2. Emsley, J.; Hall, D., *The Chemistry of Phosphorus*. Harper and Row Ltd: London, **1976**.

3. Song, S.; Alyea, E. C., *Comments Inorg. Chem.* **1996,** *18*, (3), 145-164.

4. Harris, R. K., *Nuclear Magnetic Resonance Spectroscopy*. Longman Group UK Limited: Avon, **1986**.

5. Cotton, F. A.; Wilkinson, G., *Advanced Inorganic Chemistry*. 5th ed.; Wiley- Interscience: New York, **1988**.

6. Tolman, C. A., *J. Am. Chem. Soc.* **1970,** *92*, (10), 2953-6.

7. Barton, D.; Ollis, D., *Comprehensive Organic Chemistry*. 1st ed.; Pergamon Press Ltd.: Oxford, **1979**; Vol. 2.

8. King, R. B.; Cloyd, J. C., *J. Am. Chem. Soc.* **1975,** *97*, (1), 53-60.

9. Bampos, N.; Field, L. D.; Messerle, B. A.; Smernik, R. J., *Inorg. Chem.* **1993,** *32*, (19), 4084-8.

10. Tronoff, A. B., PhD Thesis, University of Sydney, **2008**.

11. Jia, G.; Drouin, S. D.; Jessop, P. G.; Lough, A. J.; Morris, R. H., *Organometallics* **1993,** *12*, (3), 906-16.

12. Parshall, G. W., *Org. Synth.* **1965,** *45*, 102-4.

13. Trenkle, A.; Vahrenkamp, H., *Z. Naturforsch., B* **1979,** *34B*, (4), 642-3.

14. Dahlenburg, L.; Kerstan, S.; Werner, D., *J. Organomet. Chem.* **1991,** *411*, (3), 457-69.

15.   MacBeth, C. E.; Harkins, S. B.; Peters, J. C., *Can. J. Chem.* **2005,** *83*, (4), 332-340.

16.   Renaud, F.; Decurnex, C.; Piguet, C.; Hopfgartner, G., *J. Chem. Soc., Dalton Trans.* **2001**, (12), 1863-1871.

17.   Crutchfield, M. M.; Dungan, C. H.; Letcher, J. H.; Mark, V.; Wazer, J. R. V., *^{31}P Nuclear Magnetic Resonance*. John Wiley & Sons, Inc.: New York, **1967**.

18.   Fryzuk, M. D.; Carter, A.; Westerhaus, A., *Inorg. Chem.* **1985,** *24*, (5), 642-8.

19.   Vuong, K. V.; Field, L. D., Unpublished Work, University of New South Wales, **2006**.

20.   Zhu, K.; Achord, P. D.; Zhang, X.; Krogh-Jespersen, K.; Goldman, A. S., *J. Am. Chem. Soc.* **2004,** *126*, (40), 13044-13053.

21.   Gunther, H., *NMR Spectroscopy*. John Wiley & Sons, Ltd.: Chichester, **1980**.

22.   Pretsch, E.; Buhlmann, P.; Affolter, C., *Structure Determination of Organic Compounds*. Spinger-Verlag Berlin Hedelberg NewYork: Berlin, **2000**.

23.   Antberg, M.; Prengel, C.; Dahlenburg, L., *Inorg. Chem.* **1984,** *23*, (25), 4170-4.

24.   Bampos, N., PhD Thesis, University of Sydney, **1993**.

25.   Baumeister, J. M.; Alberto, R.; Ortner, K.; Spingler, B.; August Schubiger, P.; Kaden, T. A., *J. Chem. Soc., Dalton Trans.* **2002**, (22), 4143-4151.

26.   Lee, F. T. H., European Patent Office, EP0098251, **1984**.

27.   Derencsenyi, T. T., *Inorg. Chem.* **1981,** *20*, (3), 665-70.

28.   Rezvukhin, A. I.; Dolenko, G. N.; Krupoder, S. A., *Magn. Reson. Chem.* **1985,** *23*, (4), 221-4.

29.   Baldwin, L. C.; Fink, M. J., *J. Organomet. Chem.* **2002,** *646*, (1-2), 230-238.

Chapter 3

Iron-Nitrogen

Complexes of PP$_3$

3. Synthesis and Reactions of Iron-Nitrogen Complexes of PP_3

3.1 Introduction

Leigh and co-workers[1, 2] have described reduction of dinitrogen to ammonia at an

iron centre complexed by bidentate or tetradentate phosphine ligands. These

reductions were performed by treatment of iron(II) dinitrogen hydride complexes

with base to form iron(0) dinitrogen complexes which, upon treatment with acid,

gave low yields of ammonia (see Section 1.4.3). The mechanism for this

dinitrogen reduction is not known. However, if the metal centre is considered a

source of electrons and the hydride a source of protons and/or electrons then the

reduction potential of a bimetallic dinitrogen bridged iron(II) hydride complex

might be greater than that of its monometallic analogue. In this Chapter, the

synthesis and extended characterisation of a previously published dinitrogen

bridged iron(II) hydride complex[3] and its monometallic precursor is discussed.

Attempts to reduce the bound dinitrogen by treatment with base, and subsequently

with acid are reviewed. Finally, work towards the synthesis and characterisation

of hydrazine and ammine complexes, which could conceivably be involved in any

reduction mechanism, is described.

3.2 Preparation of Iron-Nitrogen Complexes of PP_3 1

The preparation of the iron(II) dinitrogen complexes $[Fe(N_2)H(PP_3)]Cl$ **22.Cl** and

$[(FeH(PP_3))_2(\mu\text{-}N_2)]Cl_2$ **23.Cl$_2$** was modified from that in the literature[3] and is

illustrated in Scheme 3.1.

Scheme 3.1
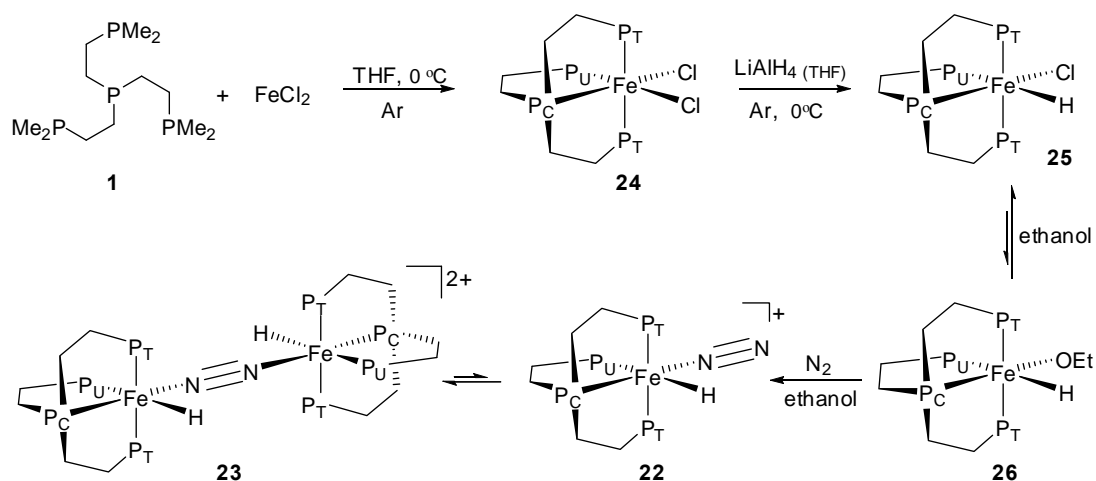
3.2.1 Preparation of FeCl$_2$(PP$_3$) 24

The synthesis of FeCl$_2$(PP$_3$) **24** requires the simultaneous addition of THF solutions of anhydrous iron(II) chloride and PP$_3$ **1**. This reaction tends to form a THF-insoluble red residue due to oligomerisation (with a PP$_3$ ligand bridging four FeCl(PP$_3$) moieties), previously described by Smernik,[4] and potentially little of the desired product. The best yields of the dichloride **24** (determined by the least amount of residue) were achieved by addition of the PP$_3$ **1** and iron(II) chloride solutions at equimolar rates and very low concentrations ($\leq$ 10^{-5} M) utilising syringe pumps. In this way, attachment of all four phosphorus atoms from a PP$_3$ **1** ligand appears to occur at a single iron centre before any other iron centre is able to interfere. Improved yields were observed by conducting the reaction at 0°C under an atmosphere of argon. In this work, crystals of the tetramer, proposed by Smernik[4] as the probable oligomeric impurity, have been obtained (see Section 4.8.1).

3.2.2   Preparation of FeClH(PP$_3$) 25

A THF solution of lithium aluminium hydride was added dropwise to the red solution of FeCl$_2$(PP)$_3$ **24** in THF at 0°C causing a colour change from red to bright yellow. The colour change was used to estimate the endpoint of the reaction. After workup, FeClH(PP$_3$) **25** was obtained as an orange solid in low yield (16%). In earlier work,[4] the THF solution of **24** was filtered prior to addition of lithium aluminium hydride. However, it was found in this work, that further reduction of **25** to its dihydride was easier to avoid by using the reaction mixture directly. This is possibly due to the preferential reduction of the residue, rather than **25**, providing a safety margin in the titration.

The chlorohydride **25** gives ^{31}P{^{1}H} and highfield ^{1}H NMR spectra which are characteristic of the octahedral complexes of iron(II) with PP$_3$ **1** and hydride ligands. Figure 3.1 illustrates the three phosphorus resonances P$_C$, P$_T$ and P$_U$ which appear at δ 184.8 (doublet of triplets), 61.5 (doublet of doublets) and 60.2 (doublet of triplets) in the ratio 1:2:1 respectively. The central phosphine P$_C$ has a significantly lower chemical shift compared to the terminal phosphines, P$_T$ and P$_U$, due to strain within the chelate ring.[5]

The high field ^{1}H NMR spectrum (Figure 3.2) shows the characteristic resonance for a hydride ligand coupled to all four phosphorus atoms (P$_C$, 2 x P$_T$ and P$_U$) as an unresolved doublet of doublet of triplets at δ -11.7 ppm. The resonances of metal-bound hydrides, such as this, appear in the high field region of the ^{1}H spectrum due to the mixing of low lying electronic excited states into the ground

state upon application of a magnetic field.[6] Previous work by Smernik[4] has

determined the hydride position as *trans* to the P$_U$ phosphine.
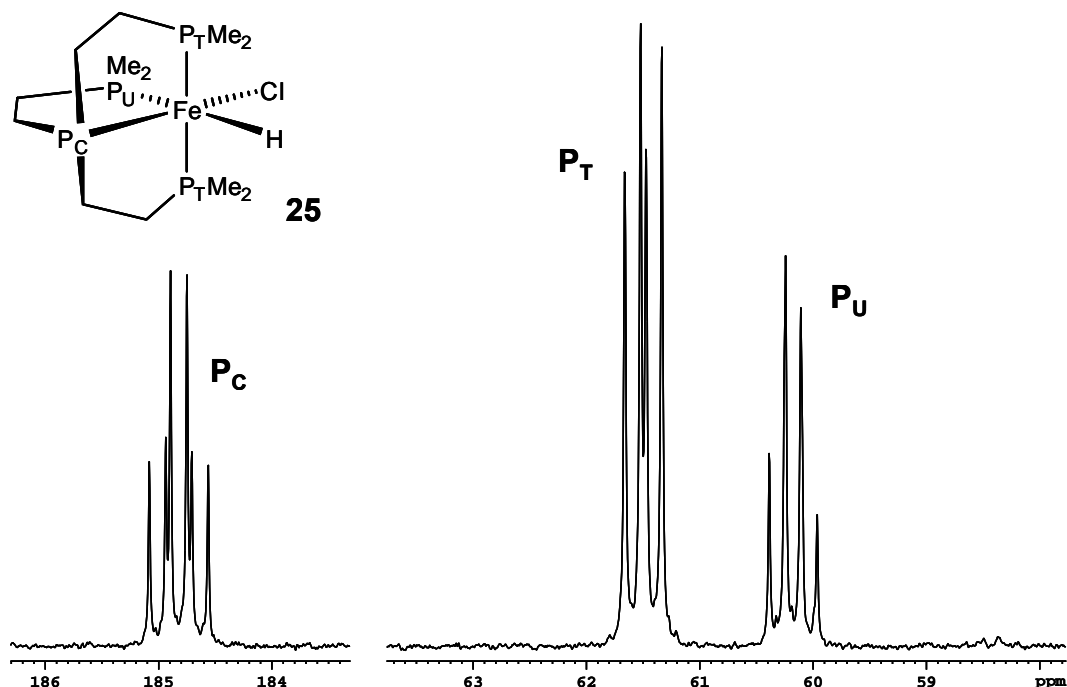
Figure 3.1 ^{31}P{^{1}H} NMR spectrum of FeClHPP$_3$ **25** in benzene-d_6
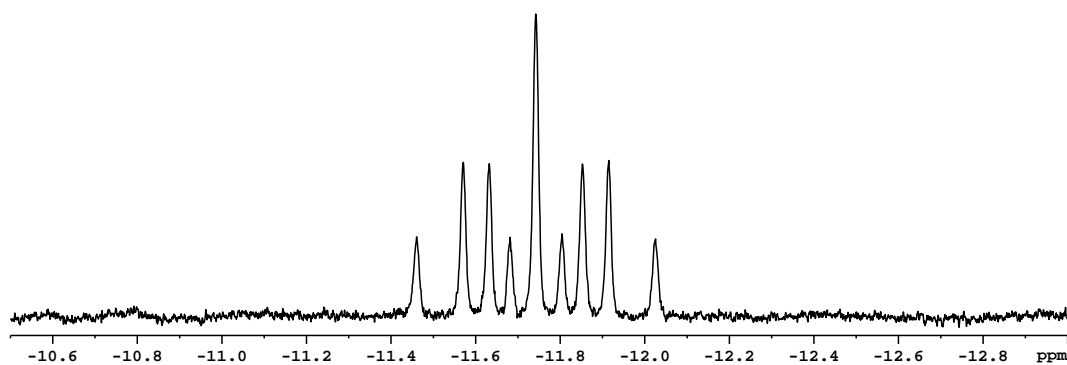
Figure 3.2 Hydride region of ^{1}H NMR spectrum of FeClHPP$_3$ **25** in benzene-d_6

3.2.3 Preparation of [FeH(N$_2$)(PP$_3$)]Cl 22.Cl and [(FeH(PP$_3$))$_2$(μ-N$_2$)]Cl$_2$ 23.Cl$_2$

Dissolution of complex **25** in ethanol results in an equilibrium being set up

between **25** and the ethoxy hydrido complex **26**.[3] This dissolution facilitates the

ligation of dinitrogen, whether this occurs by exchange with the more labile

ethoxide ligand or with the chloride ligand whose displacement is facilitated by the polar nature of the protic solvent is not known. An ethanol solution of **25** placed under an atmosphere of dinitrogen results in the immediate formation of the dinitrogen hydrido complex [FeH(N$_2$)(PP$_3$)]Cl **22.Cl** and the slower formation of the dinitrogen bridged complex [(FeH(PP$_3$))$_2$(μ-N$_2$)]Cl$_2$ **23.Cl$_2$**.[3] Over time the equilibrium favours the dinitrogen bridged species as illustrated in Scheme 3.2.
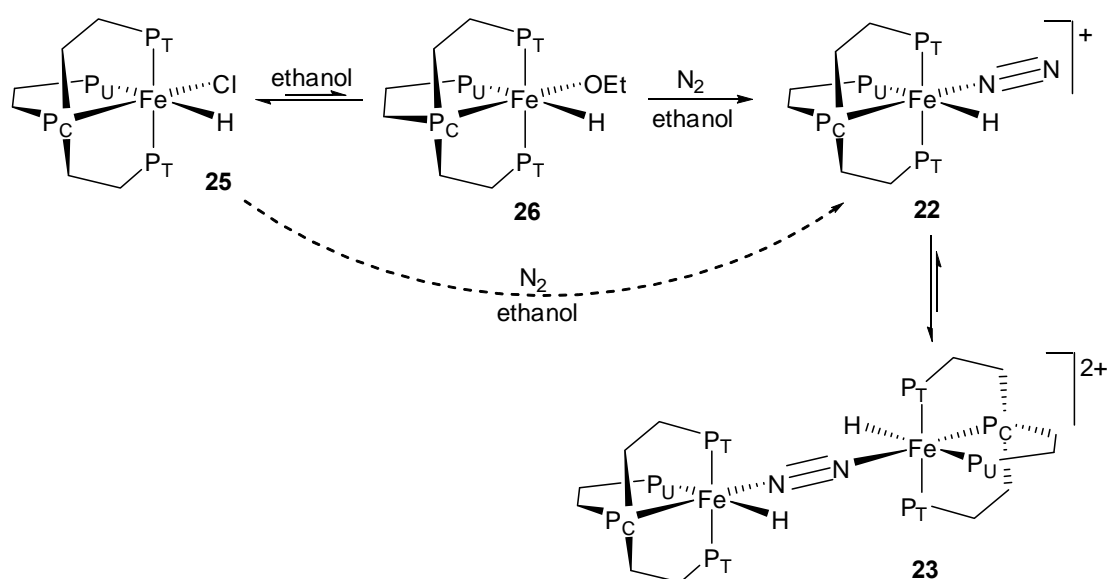
Scheme 3.2

Three species are apparent in the ^{31}P{^{1}H} NMR spectrum of an ethanol solution of **25** taken after *ca.* 48 hours under N$_2$ (Figure 3.3). The hydrido chloride **25** to ethoxy hydrido **26** ratio at equilibrium is 18:1[3] hence **26** is not observed. Resonances at δ 184.7 (P$_C$), 60.0 (P$_T$) and 58.1 (P$_U$) are assigned to FeHCl(PP$_3$) **25**, resonances at δ 62.9 (P$_T$) and 60.9 (P$_U$) are assigned to [Fe(N$_2$)H(PP$_3$)]$^+$ **22** whilst resonances at 62.1 (P$_T$) and 59.4 (P$_U$) are assigned to [(FeH(PP$_3$))$_2$(μ-N$_2$)]$^{2+}$ **23** with overlap at *ca.* 172 (P$_C$) of the central phosphine resonances of the latter two complexes. The chemical shifts of the assigned species in ethanol are slightly

different to those observed in other solvents,[3, 7] however the ^{31}P-^{31}P coupling constants vary little. The high field region of the ^{1}H{^{31}P} NMR spectrum (Figure 3.4) shows three resonances at δ -11.8, -12.7 and -12.9, assigned to **25**, **23** and **22** respectively (lit[3] **25** -11.63 (toluene-d_8), **23** -12.50, **22** -12.66 (acetone-d_6)).
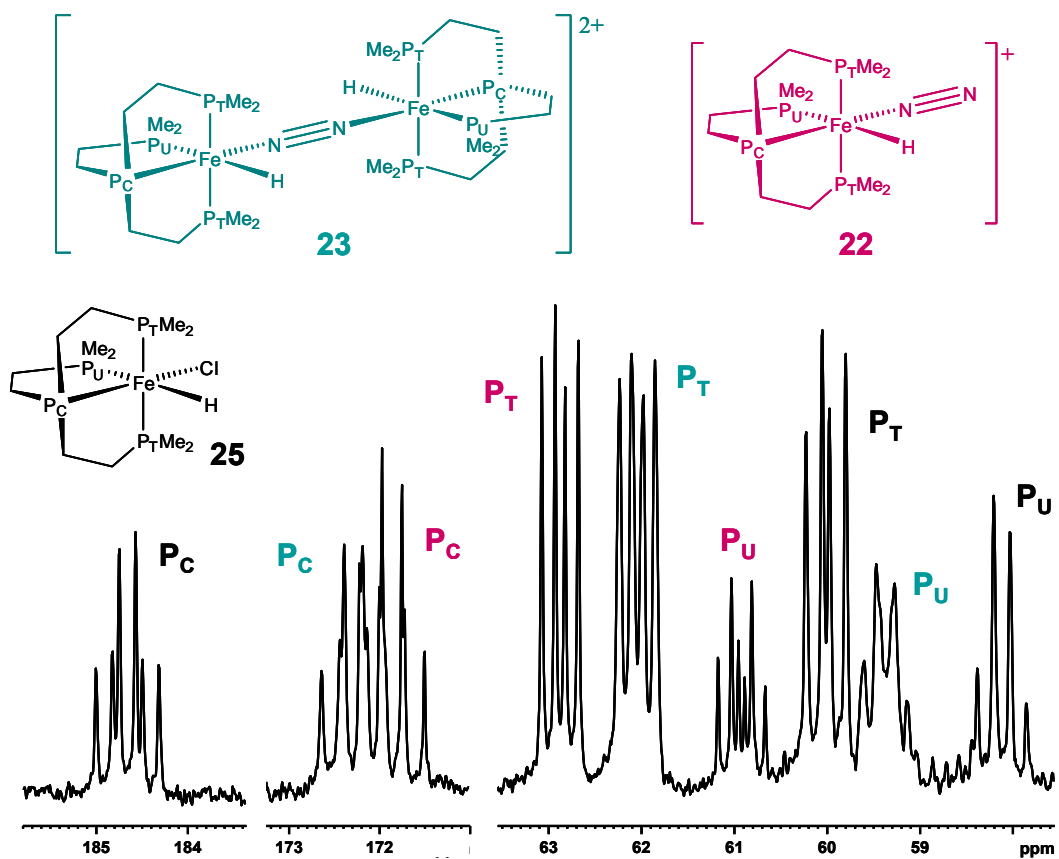
Figure 3.3 ^{31}P{^{1}H} NMR spectrum of FeClHPP$_3$ **25** in ethanol/benzene-d_6 after *ca*. 48 hours under an atmosphere of dinitrogen.
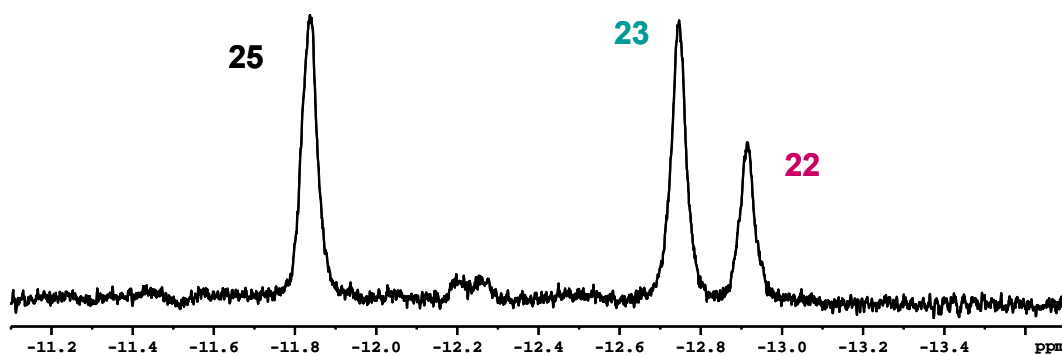
Figure 3.4   Hydride region of ^{1}H{^{31}P} NMR spectrum of FeClHPP$_3$ **25**, [Fe(N$_2$)H(PP$_3$)]$^+$ **22** and [(FeH(PP$_3$))$_2$(μ-N$_2$)]$^{2+}$ **23** in ethanol/benzene-d_6.

3.2.4 Preparation of ^{15}N labelled [Fe(^{15}N₂)H(PP₃)]Cl ^{15}N-22 and [(FeH(PP₃))₂(μ-^{15}N₂)]Cl₂ ^{15}N-23.

The ^{15}N labelled analogues of **23.Cl₂** and **22.Cl** were synthesised on an NMR scale by dissolution of FeClH(PP₃) in nitrogen free ethanol, to which ^{15}N labelled dinitrogen, at a pressure of less than 1 atmosphere, was added. Initially this led to a single peak at δ -58.7 ppm in the ^{15}N NMR spectrum corresponding to the symmetrical nitrogen bridged species **^{15}N₂-23**. The ^{31}P{^{1}H} NMR spectrum shows the appearance of the three resonances of **^{15}N₂-23** with an additional 11 Hz $^3J_{P-N}$ coupling clearly apparent in the splitting of the central phosphorus P_C. There is no ^{15}N₂ peak present in the ^{15}N NMR spectrum and no resonances which might correspond to dinitrogen species **^{15}N₂-22**. This result is in contrast to previous work[3] which has shown that at higher pressures of dinitrogen (greater than 1 atmosphere) the monometallic species **22** is initially the dominant species. The driving force under these conditions is likely to be the preference of the [FeH(PP₃)]$^+$ moiety to ligate a dinitrogen (bridged or otherwise) over an ethoxide or chloride in ethanol. Where there is a large excess of chlorohydride **25** all the dinitrogen is complexed in the form of the nitrogen bridged species **^{15}N₂-23**.

Further addition of ^{15}N₂ over the course of several days resulted in the increase in intensity of resonances for **^{15}N₂-23**, and the appearance of signals for **^{15}N₂-22** in both the ^{31}P{^{1}H} and ^{15}N NMR spectra as well as free ^{15}N₂ at δ -71.6 ppm in the ^{15}N NMR spectrum. It was not possible to introduce sufficient labelled dinitrogen to the sample to completely convert **25** to either dinitrogen species **^{15}N₂-23** or **^{15}N₂-22**. The generation of the dinitrogen species, monitored by ^{31}P{^{1}H} NMR, is illustrated in Figure 3.5. The corresponding high field ^{1}H{^{31}P} NMR spectra

showed the reduction of the hydride resonance of **25** at -10.8 ppm with the increase in that of **^{15}N$_2$-23** at -12.7 ppm and subsequently the appearance of a very small **^{15}N$_2$-22** signal at -12.9 ppm.
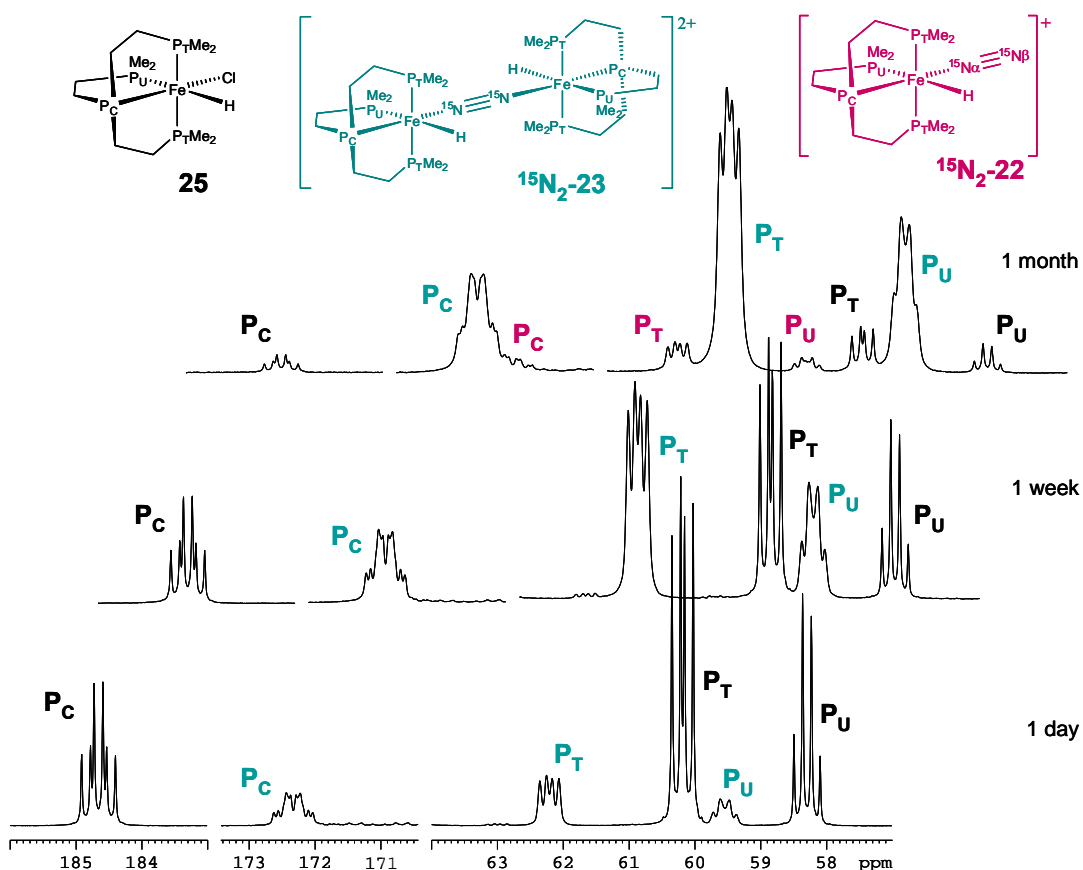
Figure 3.5 ^{31}P{^{1}H} NMR spectra showing the generation of **^{15}N$_2$-23** and **^{15}N$_2$-22** with the addition of ^{15}N$_2$ over time to an ethanol/benzene-d_6 solution of FeClHPP$_3$ **25**.

A computer enhancement of the ^{15}N{^{1}H} NMR resonances of the two dinitrogen containing species **^{15}N$_2$-22** and **^{15}N$_2$-23** is given in Figure 3.6. The monometallic species **^{15}N$_2$-22** has two resonances at δ -34.4 and -63.6 ppm assigned to N$_\beta$ and N$_\alpha$ respectively. This assignment is based on the larger ^{31}P-^{15}N coupling of N$_\alpha$ apparent in the computer enhanced spectrum and its relatively high field chemical shift with respect to N$_\beta$.[8] **^{15}N$_2$-22.[BPh$_4$]** has been prepared previously by

exchange of ^{15}N labelled dinitrogen with dinitrogen of unlabelled **22.[BPh$_4$]** in THF.[9] The ^{15}N{^{1}H} resonances of N$_\beta$ and N$_\alpha$ in THF were reported as -35.0 and -63.7 ppm which correspond well with the chemical shifts assigned to ^{15}N$_2$-**22** here. Due to its symmetry, the bridged species ^{15}N$_2$-**23** has only a single resonance at δ -58.9 ppm. This shift is within 5 ppm of the signal for ^{15}N$_2$-**22** N$_\alpha$ a result which might be expected given the similarity in chemical environment of these two nitrogen donors. The ^{15}N chemical shifts of ^{15}N$_2$-**22** are typical for mononuclear iron-phosphine dinitrogen complexes.[9] No other ^{15}N data for dinuclear iron(II) dinitrogen bridged species could be found in the literature for comparison with ^{15}N$_2$-**23**.
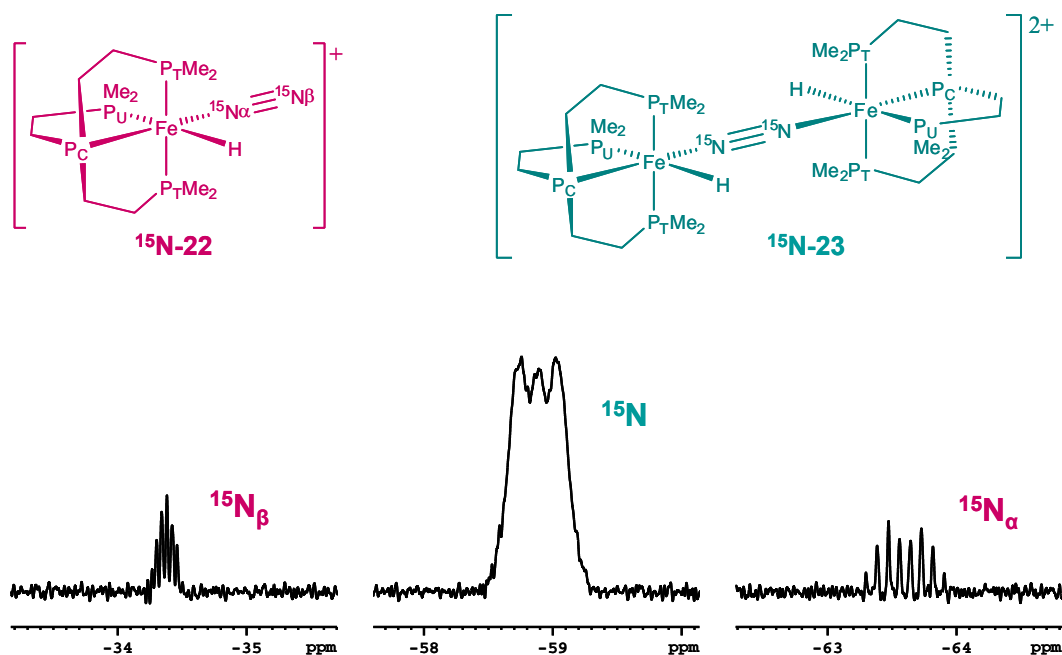
Figure 3.6 Computer enhanced ^{15}N{^{1}H} NMR resonances of ^{15}N$_2$-**22** and ^{15}N$_2$-**23** in ethanol/benzene-d_6.

3.2.5 Preparation and X-Ray Crystallography of [(FeH(PP$_3$))$_2$(μ-^{15}N$_2$)][BAr$^F_4$]$_2$ 23.[BAr$^F_4$]$_2$

Diffraction quality crystals of the ^{15}N labelled dication [(FeH(PP$_3$))$_2$(μ-N$_2$)]$^{2+}$ as its tetra(3,5-bis(trifluoromethyl)phenyl)borate [BAr$^F_4$]$^-$ salt were grown by addition of sodium tetra(3,5-bis(trifluoromethyl)phenyl)borate to an ethanol solution of the ^{15}N labelled dinitrogen complexes ^{15}N$_2$-22 and ^{15}N$_2$-23. The solution was left under an atmosphere of argon for several weeks during which time pale orange crystals formed.
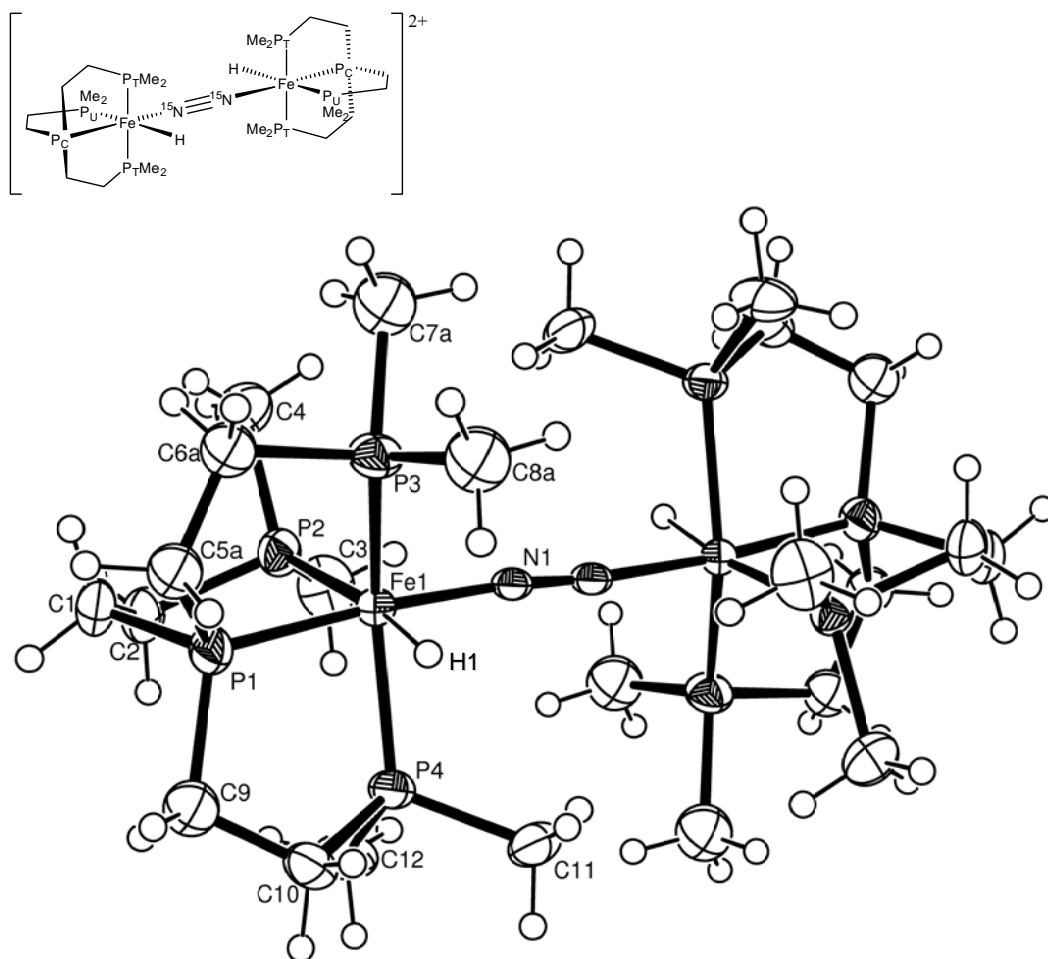
Figure 3.7 ORTEP plot (50% thermal ellipsoids, non-hydrogen atoms) of the complex cation of ^{15}N$_2$-23.[BAr$^F_4$]$_2$. Atoms of 30% occupancy have been excluded for clarity.

The crystal has a centre of symmetry about the N-N triple bond and contains slight disorder within the PP$_3$ ligand and the counteranion. Selected bond lengths and angles are presented in Table 3.1 and 3.2 respectively. Further crystallographic data is contained in Appendix 1 (CD format).

Table 3.1 Bond lengths (Å) for [(FeH(PP$_3$))$_2$(μ-^{15}N$_2$)][BAr$^F_4$]$_2$ **23.[BAr$^F_4$]$_2$**

Fe(1)-P(1)	2.163(1)	Fe(1)-H(1)	1.47(2)
Fe(1)-P(2)	2.2274(9)	Fe(1)-N(1)	1.858(2)
Fe(1)-P(3)	2.225(1)	N(1)-N(1)	1.130(3)
Fe(1)-P(4)	2.1979(9)		

Table 3.2 Bond angles (°) for [(FeH(PP$_3$))$_2$(μ-^{15}N$_2$)][BAr$^F_4$]$_2$ **23.[BAr$^F_4$]$_2$**

Fe(1)-N(1)-N(1)	174.5(2)	N(1)-Fe(1)-P(1)	175.27(6)
P(2)-Fe(1)-P(1)	85.96(3)	P(3)-Fe(1)-P(1)	85.06(4)
P(4)-Fe(1)-P(1)	84.47(4)	N(1)-Fe(1)-P(2)	94.76(6)
P(3)-Fe(1)-P(2)	105.19(4)	P(4)-Fe(1)-P(2)	104.24(3)
N(1)-Fe(1)-P(3)	99.24(7)	P(4)-Fe(1)-P(3)	147.89(3)
N(1)-Fe(1)-P(4)	90.82(7)	N(1)-Fe(1)-H(1)	93.1(10)
P(1)-Fe(1)-H(1)	86.0(10)	P(2)-Fe(1)-H(1)	171.6(10)
P(3)-Fe(1)-H(1)	76.2(10)	P(4)-Fe(1)-H(1)	72.8(10)

The four phosphorus atoms of the PP$_3$ ligand and the dinitrogen and hydride ligands of **23.[BAr$^F_4$]$_2$** are arranged around the iron(II) centres in distorted octahedra. This distortion is due, in part, to the bite angles of the PP$_3$ ligand which are 84.8° (average) and 85.0° for P$_C$-Fe-P$_T$ and P$_C$-Fe-P$_U$ respectively. In addition, the steric bulk of the methyl constituents on the phosphorus atoms combined with the small size of the hydride ligand results in a narrowing of the P-Fe-H angles with these angles being 74.5° (average), 86.0° and 171.6° for P$_T$-Fe-H$_1$, P$_C$-Fe-H$_1$ and P$_U$-Fe-H$_1$ respectively. The N-N bond length at

1.130(3) Å is representative of a small degree of activation of the dinitrogen triple

bond compared to free dinitrogen (1.10 Å).[10]

A search of the Cambridge Structural Database[11, 12] provides comparative

structures which can be grouped into three categories. A selection of bond lengths

and angles of these complexes, an unpublished complex **27** and **23.[BAr$^F_4$]$_2$** are

presented in Table 3.3.

Table 3.3 Selected bond lengths (Å) and angles (º) of complexes **23.[BAr$^F_4$]$_2$**
(this work), **27**[13], **28**[14], **29**[15], **30**[16], **31**[7], **32**[17], **33**[18], **34**[20], **35**[20] and **36**[21].

	23	27	28	29
Fe$_1$-N$_1$	1.858(2)	1.846(3)	1.809(9)	1.804(3)
Fe$_1$-H$_1$	1.47(2)	1.41(3)	1.4(1)	1.53(4)
N$_1$-N$_1$/N$_2$	1.130(3)	1.097(4)	1.10(1)	1.113(4)
Fe$_1$-P$_C$/N$_C$	2.163(1)	2.1644(9)	2.119(8)	2.142(3)
Fe$_1$-P$_U$	2.2274(9)	2.2538(9)	2.257(4)	2.286(1)
Fe$_1$-P$_T$ *	2.224(1)	2.2394(9)	2.216(4)	2.245(1)
Fe$_1$-P$_T$ *	2.1979(9)	2.2195(9)	2.210(3)	2.250(1)
N$_1$-Fe$_1$-H$_1$	93(1)	96(1)	95(4)	95(2)
Fe$_1$-N$_1$-N$_1$/N$_2$	174.5(2)	177.3(3)	178.2(9)	176.7(3)
P$_C$/N$_C$-Fe$_1$-N$_1$	175.27(6)	172.8(1)	176.8(4)	176.4(1)
P$_C$/N$_C$-Fe$_1$-H$_1$	86(1)	77(1)	84(4)	88(2)
P$_C$/N$_C$-Fe$_1$-P$_U$	85.96(3)	86.06(3)	86.0(3)	84.90(9)
P$_C$/N$_C$-Fe$_1$-P$_T$ *	85.06(4)	85.15(3)	84.9(3)	85.93(9)
P$_C$/N$_C$-Fe$_1$-P$_T$ *	84.47(4)	84.84(3)	87.2(2)	85.10(9)
P$_U$-Fe$_1$-N$_1$	94.76(6)	100.95(9)	95.0(4)	92.6(1)
P$_U$-Fe$_1$-H$_1$	172(1)	163(1)	170(3)	172(2)
P$_U$-Fe$_1$-P$_T$ *	105.19(4)	103.56(3)	107.4(1)	112.71(4)
P$_U$-Fe$_1$-P$_T$ *	104.24(3)	99.27(3)	108.2(1)	105.83(4)
P$_T$-Fe$_1$-N$_1$ *	99.24(7)	94.84(9)	92.0(3)	92.7(1)

Table 3.3 (cont'd) Selected bond lengths (Å) and angles (°) of complexes **23.[BAr$^F_4$]$_2$** (this work), **27**[13], **28**[14], **29**[15], **30**[16], **31**[7], **32**[17], **33**[18], **34**[20], **35**[20] and **36**[21].

	23	**27**	**28**	**29**
P$_T$-Fe$_1$-N$_1$ *	90.82(7)	92.20(9)	95.3(3)	98.1(1)
P$_T$-Fe$_1$-H$_1$ *	76(1)	77(1)	70(4)	70(2)
P$_T$-Fe$_1$-H$_1$ *	73(1)	78(1)	73(5)	71(2)
P$_T$-Fe$_1$-P$_T$	147.89(3)	154.32(4)	142.8(1)	139.36(4)

	23	**30**	**31**	**32**
Fe$_1$-P$_C$	2.163(1)	2.140(2)	2.202(2)	2.178(2)
Fe$_1$-P$_U$	2.2274(9)	2.218(2)	2.234(2)	2.234(2)
Fe$_1$-P$_T$ *	2.224(1)	2.266(2)	2.312(2)	2.230(2)
Fe$_1$-P$_T$ *	2.1979(9)	2.280(2)	2.312(2)	2.246(2)
P$_C$-Fe$_1$-P$_U$	85.96(3)	87.45(8)	83.85(9)	85.27(7)
P$_C$-Fe$_1$-P$_T$ *	85.06(4)	83.32(7)	83.66(9)	84.76(7)
P$_C$-Fe$_1$-P$_T$ *	84.47(4)	83.58(7)	83.24(90	83.6(1)
P$_U$-Fe$_1$-P$_T$ *	105.19(4)	99.38(7)	98.74(9)	96.51(6)
P$_U$-Fe$_1$-P$_T$ *	104.24(3)	93.84(7)	93.40(9)	100.14(7)
P$_T$-Fe$_1$-P$_T$	147.89(3)	160.91(7)	161.07(9)	158.8(1)

	23	**33**	**34**	**35**	**36**
Fe$_1$-N$_1$	1.858(2)	1.811(5)	1.813(2)	1.87(1)	1.876(9)
Fe$_2$-N$_2$		1.818(5)		1.89(2)	
N$_1$-N$_1$/N$_2$	1.130(3)	1.138(6)	1.171(4)	1.13(2)	1.13(1)

* Two *trans* terminal phosphines.

1. Iron complexes of a tripodal tetradentate phosphine ligand with two-carbon arms plus a dinitrogen and a hydride ligand:

These structures are [Fe(H)(N$_2$)(PP$^{Ph}_3$)][BPh$_4$] **27** (PP$^{Ph}_3$ = P(CH$_2$CH$_2$PPh$_2$)$_3$),[13] [FeH(N$_2$)(NP$^{Ph}_3$)][BPh$_4$] **28** (NP$^{Ph}_3$ = N(CH$_2$CH$_2$PPh$_2$)$_3$)[14] and [FeH(N$_2$)(NP$^{iPr}_3$)][PF$_6$] **29** (NP$^{iPr}_3$ = N(CH$_2$CH$_2$P^{i}Pr$_2$)$_3$).[15]
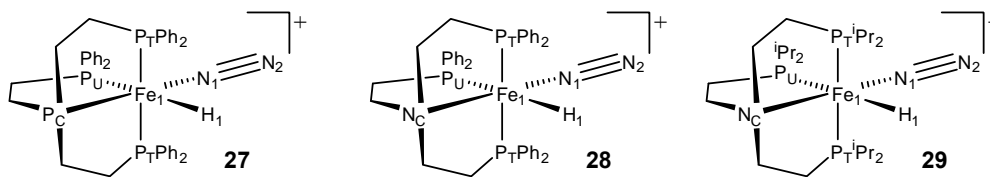
In all cases, the ligands are arranged around the iron(II) centre in a distorted octahedron and the dinitrogen ligand is *trans* to the central ligand atom. The N-N bond lengths of complexes **27**, **28** and **29** are slightly less than that of **23.[BAr$^F_4$]$_2$** and comparable with free dinitrogen which has a triple bond length of 1.10 Å.[10] Likewise the Fe-H bond lengths are very similar in all four structures. In common with the structure of **23.[BAr$^F_4$]$_2$**, the ligand bite angles are significantly less than 90º in **27**, **28** and **29**. However, the distribution of the terminal phosphines around the iron centre differs considerably with, for example, the P$_T$-Fe-P$_T$ of **27**, **28** and **29** being 154.3º, 142.8º and 139.4º respectively compared to 147.9º for **23.[BAr$^F_4$]$_2$**. Given the difference in this bond angle between structures **27** and **28,** which are identical in all but the central atom of the ligand, these differences are considered to be due both to the steric interactions of the terminal phosphine substituents and to the nature of the central atom of the ligand.

2. Iron complexes of PP$_3$ **1**:

These structures are [Fe(η^3-PhC≡C-C=CHPh)(PP$_3$)][BPh$_4$][16] **30**, [FeCl(PPh$_3$)(PP$_3$)][BPh$_4$][7] **31** and [FeCO(CH$_3$)(PP$_3$)]Cl[17] **32**.
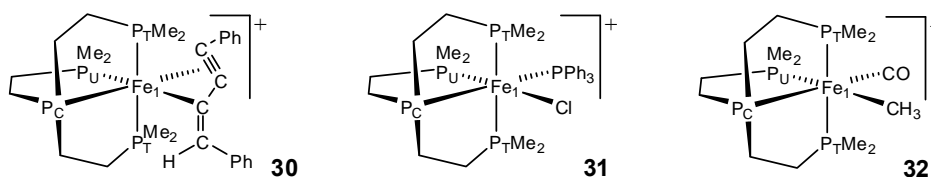
In these structures, the ligands are arranged around the iron(II) centre in a distorted octahedron. All Fe-P bond lengths are comparable with those of **23.[BAr$^F_4$]$_2$.** The P$_T$-Fe-P$_T$ angles of **30**, **31** and **32** are 160.9º, 161.1º and 158.8º respectively all of which are significantly greater than that of **23.[BAr$^F_4$]$_2$** which is 147.9º. This most likely reflects the small size of the hydride ligand of **23.[BAr$^F_4$]$_2$** which allows for greater P$_U$-Fe-P$_T$ angles favoured by the steric repulsion of the ligand's methyl substituents.

3. Dinitrogen bridged iron complexes:

These structures are [Fe(PhBP$^{iPr}_3$)]$_2$(μ-N$_2$)[18] **33** (PhBP$^{iPr}_3$ = PhB(CHP^{i}Pr$_2$)$_3$), [Na(THF)$_6$][(Fe(PhBP$^{iPr}_3$))$_2$(μ-N$_2$)] [19] **34**, [Fe(CO)$_2$(PEt$_3$)$_2$]$_2$(μ-N$_2$)[20] **35** and [Fe(CO)$_2$(P(OCH$_3$)$_3$)$_2$]$_2$(μ-N$_2$)[21] **36.**

n = 0 **33**, n = 1 **34**   X = Et **35**, X = (OCH$_3$) **36**
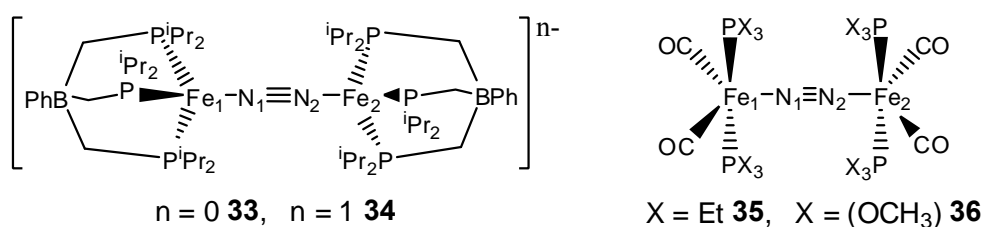
In these structures, the ligands are arranged around the iron centres either in an approximate tetrahedral (**33**, **34**) or trigonal bipyramidal arrangement (**35**, **36**). All Fe-N bond lengths are comparable with **23.[BAr$^F_4$]$_2$** as are the N-N bond lengths excepting structure **34**. In this case the N-N bond length, of the iron(0)-iron(I) dimer complexed by anionic ligands, is 1.171(4) Å which is halfway between that of an N-N triple bond (1.10 Å) and an N-N double bond (1.25 Å).[10]

3.2.6 Preparation of [(FeH(PP$_3$))$_2$(μ-N$_2$)][BPh$_4$]$_2$ 23.[BPh$_4$]$_2$, [(FeH(PP$_3$))$_2$(μ-N$_2$)][BF$_4$]$_2$ 23.[BF$_4$]$_2$ and [(Fe(N$_2$)H(PP$_3$)$_2$][BPh$_4$] 22.[BPh$_4$]

Tetraphenylborate salts of both the dinitrogen cationic complexes **22** and **23** were isolated following literature procedures.[3] Addition of a stoichiometric amount of sodium tetraphenylborate to an ethanol solution of **22.Cl** and **23.Cl$_2$** resulted in the precipitation of a mixture of **22.[BPh$_4$]** and **23.[BPh$_4$]$_2$** as a buff coloured solid. The precipitate was washed with acetone to remove all **22.[BPh$_4$]** resulting in a pure sample of cream coloured **23.[BPh$_4$]$_2$**. The tetraphenylborate salt of **23** is insoluble in most deuterated solvents. It is sufficiently soluble in acetone-d_6 to allow acquisition of NMR spectra but decomposes in this solvent within hours. As expected the ^{31}P{^{1}H} and high field ^{1}H{^{31}P} NMR spectra are almost identical to that of **23.Cl$_2$** (Section 3.2.3).

A solution of FeClH(PP$_3$) **25** and sodium tetraphenylborate in deaerated ethanol was flushed with dinitrogen resulting in the immediate precipitation of **22.[BPh$_4$]** as a peach coloured solid. This product is soluble in acetone-d_6 but decomposes in this solvent within hours. As expected, the ^{31}P{^{1}H} and high field ^{1}H{^{31}P} NMR spectra of **22.[BPh$_4$]** are almost identical to that of **22.Cl** (Section 3.2.3).

The tetrafluoroborate salt of the dinitrogen-bridged cation **23** was isolated by addition of a stoichiometric amount of sodium tetrafluoroborate to an ethanol solution of **22.Cl** and **23.Cl$_2$**. This resulted in the precipitation of **23.[BF$_4$]$_2$** as a buff coloured solid. The tetrafluoroborate salt of **23** is insoluble in most common solvents. As in the case of the tetraphenylborate analogue, **23.[BF$_4$]$_2$** is sufficiently soluble in acetone-d_6 to permit acquisition of NMR spectra but the

sample decomposes within hours. The ^{31}P{^{1}H}and high field ^{1}H{^{31}P} NMR spectra are virtually identical to that of **23.[BPh$_4$]$_2$**. A single resonance occurs in the ^{19}F{^{1}H} NMR spectrum at -147.1 ppm. The hexafluorophosphate salt of **23** was also prepared in an analogous manner.

3.2.7   Treatment of [(FeH(PP$_3$))$_2$(μ-N$_2$)][BPh$_4$]$_2$ 23.[BPh$_4$]$_2$ with base.

Treatment of a suspension of **23.[BPh$_4$]$_2$** in THF with an equimolar amount of base (potassium *t*-butoxide or potassium bis(trimethylsilyl)amide) and gentle heating (approx. 50 ºC for 2 hours) under dinitrogen results in the appearance of a red solution. ^{31}P{^{1}H} and ^{1}H NMR spectroscopy of the filtered solution allows for identification of this red species as the singly deprotonated product [(FeH(PP$_3$))(μ-N$_2$)(Fe(PP$_3$))] **37**. The ^{31}P{^{1}H} NMR spectrum, shown in Figure 3.8, has five resonances at δ 180.7, 176.7, 67.0, 62.0 and 59.6 ppm in the ratio 1:1:3:2:1. These resonances are assigned to the apical phosphorus, P$_A$ (180.6 ppm), and three equivalent terminal phosphorus atoms, P$_E$ (66.9 ppm), of a trigonal bipyramidal iron(0) centre and the four phosphorus atoms, P$_C$ (176.6 ppm), P$_T$ (61.9 ppm) and P$_U$ (59.5 ppm), of the octahedral iron(II) centre. The chemical shifts of the terminal phosphorus atoms P$_T$ and P$_U$ are comparable to those of **23.[BPh$_4$]$_2$** whilst that of the central phosphorus P$_C$ is 4 ppm down field relative to that of **23.[BPh$_4$]$_2$**. The high field region of the ^{1}H NMR spectrum has a multiplet at δ -12.5 ppm which has a splitting pattern very similar to that of **23.[BPh$_4$]$_2$**.
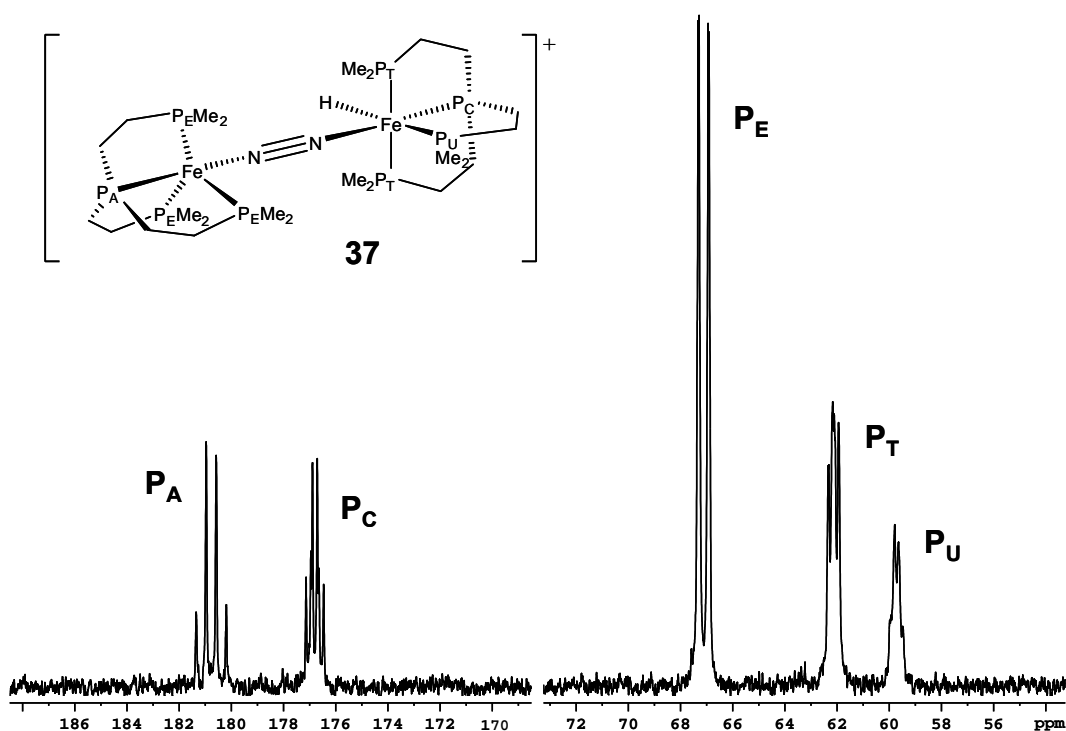
Figure 3.8 $^{31}P\{^1H\}$ NMR (121.5 MHz, 298K) spectra of $[(FeH(PP_3))(\mu-N_2)(Fe(PP_3))][BPh_4]$ **37.[BPh4]** in THF-d_8.

It becomes clear from the $^{31}P\{^1H\}$ NMR spectrum (now run at 162 MHz), which is computer enhanced and expanded in Figure 3.9, that there is coupling between the phosphorus atoms of the different iron centres. For example, the three equivalent P_E terminal phosphorus atoms of the iron(0) centre would appear as a doublet, coupled to the apical phosphorus P_A only, if there was no additional coupling through the bridging dinitrogen. Figure 3.9 clearly demonstrates that this is not the case and that there are small couplings (< 6 Hz) between the phosphorus atoms of the Fe(0) centre and those of the Fe(II) centre across the bridging N_2. A simulation of the spectra has been achieved using the coupling constants given in Table 3.4 and its fit with the actual spectrum is illustrated in Figure 3.9. The P_A-P_E coupling constant of 46.7 Hz is significantly larger than the P_C-P_T coupling of 29.7 Hz which is the largest coupling across the iron(II) centre. This increased coupling constant is indicative of an iron(0) centre.[3, 4]
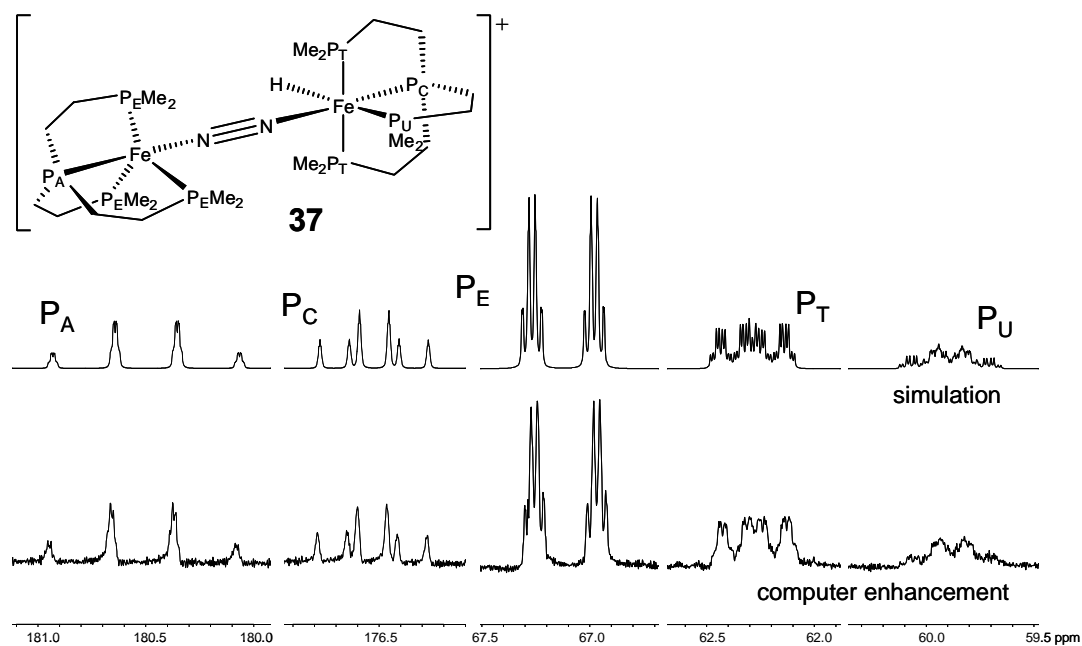
Figure 3.9 Computer enhanced and simulated ^{31}P{^{1}H} NMR (162 MHz) spectra of [(FeH(PP$_3$))(μ-N$_2$)(Fe(PP$_3$))][BPh$_4$] **37.[BPh$_4$]** in THF-d_8.

Table 3.4 Coupling constants (Hz) used in simulation of ^{31}P{^{1}H} NMR (162 MHz) spectrum of [(FeH(PP$_3$))(μ-N$_2$)(Fe(PP$_3$))][BPh$_4$] **37.[BPh$_4$]**

	P$_A$	P$_E$	P$_C$	P$_T$	P$_U$
P$_A$		46.7	0.85	2.0	2.2
P$_E$	46.7		0.90	4.5	5.3
P$_C$	0.85	0.90		29.7	22.0
P$_T$	2.0	4.5	29.7		18.0
P$_U$	2.2	5.3	22.0	18.0	

As might be expected, given the similarities in structure, the P$_C$-P$_T$, P$_C$-P$_U$ and P$_T$-P$_U$ coupling constants of 29.7, 22.0 and 18.0 Hz are very similar to the respective 30.8, 23.1 and 16.2 Hz coupling constants of the symmetrical dinuclear species **23.[BPh$_4$]$_2$**.

71

No examples of long range NMR coupling through a N-N triple bond were found in the literature. The $^5J_{PP}$ coupling constants presented in Table 3.4 are of the same order of magnitude as those reported across a phosphine substituted aromatic ring.[22] The ^{31}P-^{31}P 2D COSY spectrum of **37.[BPh$_4$]** provides evidence of coupling between phosphorus atoms of the same iron centre only. It is likely that the $^5J_{PP}$ couplings across the N-N triple bond are not observed in the ^{31}P-^{31}P 2D COSY experiment because these are an order of magnitude smaller, and hence significantly less sensitive to this NMR technique, than the $^2J_{PP}$ couplings between phosphorus atoms at the same iron centre. Several attempts to adjust the NMR parameters to identify the correlations between phosphorus atoms with smaller coupling constants were unsuccessful. The complex **37.[BPh$_4$]** starts to decompose in solution after a few hours making observation of these 2D COSY couplings more difficult.

It is interesting to note that no significant amount of the doubly deprotonated product (Fe(PP$_3$))$_2$(μ-N$_2$) **38** appears in this reaction. This suggests that the acid base equilibrium favours **37** as shown in Figure 3.10.
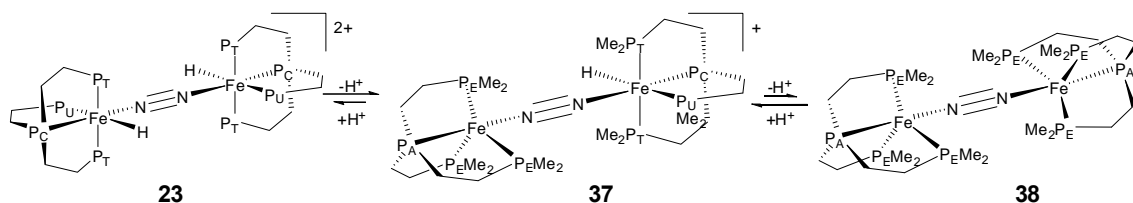
Figure 3.10   Acid base equilibria of **37.[BPh$_4$]**

The deprotonation of **23** to **37,** rather than **37** to **38** is preferred despite the fact that **37** is in solution whereas **23** is present as a suspension of its tetraphenylborate

salt. It can be speculated that resistance of the iron(II) centre of **37** to deprotonation in favour of an iron(II) centre of **23** is due to the electron rich nature of the bridged iron(0) centre. This iron(0) centre is likely to be capable of donating electron density across the N-N triple bond to the iron(II) centre and thus increasing the basicity of this iron and hence the strength of the Fe-H bond at this centre. Thus, the conjugate base and acid of **37**, namely **38** and **23,** are cumulatively less stable than **37** and disproportionation of a solution of **37** into **38** and **23** would not be expected.

The BF$_4$ and PF$_6$ salts of **37** were prepared by analogous reactions of **23.[BF$_4$]$_2$** and **23.[PF$_6$]$_2$** with base.

3.2.8 Preparation of ^{15}N labelled [(FeH(PP$_3$))(μ-^{15}N$_2$)(Fe(PP$_3$))][BPh$_4$] ^{15}N$_2$-37.[BPh$_4$].

It was possible to synthesise the ^{15}N labelled analogue of **37** by treatment of ^{15}**N$_2$-23.[BPh$_4$]$_2$** with a single equivalent of base in THF-d_8 under argon. The ^{31}P{^{1}H} NMR spectrum of [(FeH(PP$_3$))(μ-^{15}N$_2$)(Fe(PP$_3$))][BPh$_4$] ^{15}**N$_2$-37.[BPh$_4$]** has identical chemical shifts to **37.[BPh$_4$]** with a broadening of all resonances due to the coupling to ^{15}N. A 10 Hz P$_A$-^{15}N$_α$ coupling is apparent in the resonance of the P$_A$ phosphine at 180.6 ppm. The ^{15}N NMR spectrum presented in Figure 3.11 shows the two resonances of the bridging dinitrogen at -9.3 and -58.3 ppm assigned to the nitrogen bound to the iron(0) centre and the iron(II) centre respectively. This assignment was made on the basis of 2D ^{31}P-^{15}N HSQC NMR experiments which show a correlation between each ^{15}N resonance and the ^{31}P resonances of the phosphines bound to the respective iron centre. The higher field

position of the nitrogen resonance bound to the iron(II) centre (-58.3 ppm) also correlates well with the chemical shifts of the ^{15}N NMR resonance of the symmetrical species ^{15}N$_2$-23 which is -58.9 ppm in ethanol (Figure 3.6). In addition, the significant downfield shift of the resonance associated with the iron(0) bound nitrogen, N$_\alpha$, is in line with observations for the downfield ^{15}N chemical shift of the metal bound nitrogen of Fe^{15}N$_2$(depe)$_2$[23] (-40.5 ppm, -45.2 ppm unassigned) relative to that of the metal bound nitrogen of [FeH^{15}N$_2$(depe)$_2$]$^+$[9] (-60.7 ppm N$_\alpha$, -42.2 ppm N$_\beta$) (where depe = Et$_2$PCH$_2$CH$_2$PEt$_2$).
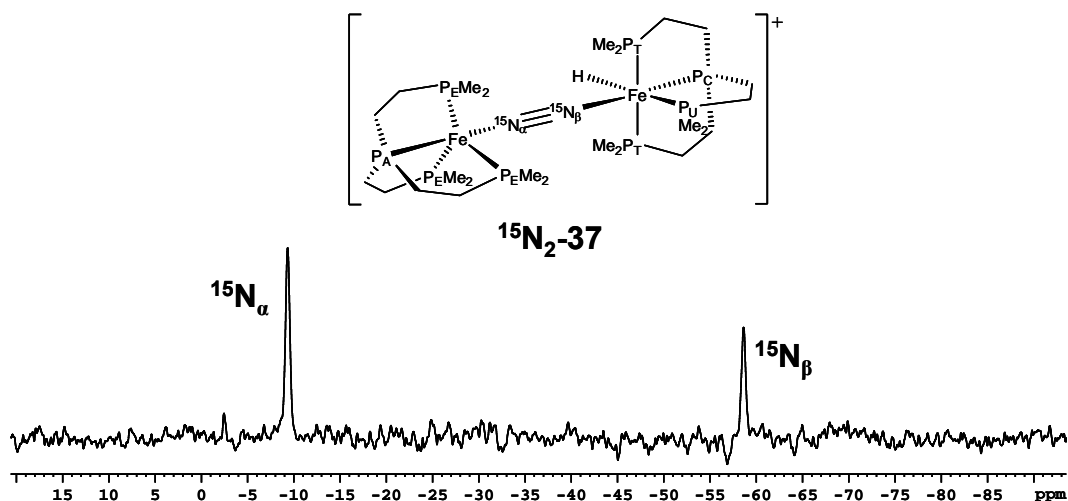
Figure 3.11 ^{15}N{^{1}H} NMR spectrum of [(FeH(PP$_3$))(μ-^{15}N$_2$)(Fe(PP$_3$))][BPh$_4$] ^{15}N$_2$-37.[BPh$_4$] in THF-d_8.

3.2.9 X-Ray Crystallography of [(FeH(PP$_3$))(μ-N$_2$)(Fe(PP$_3$))][BPh$_4$] 37.[BPh$_4$]

Diffraction quality red crystals of [(FeH(PP$_3$))(μ-N$_2$)(Fe(PP$_3$))]$^+$ **37** as its tetraphenylborate salt were grown by layering a THF solution of **37.[BPh$_4$]** with pentane.
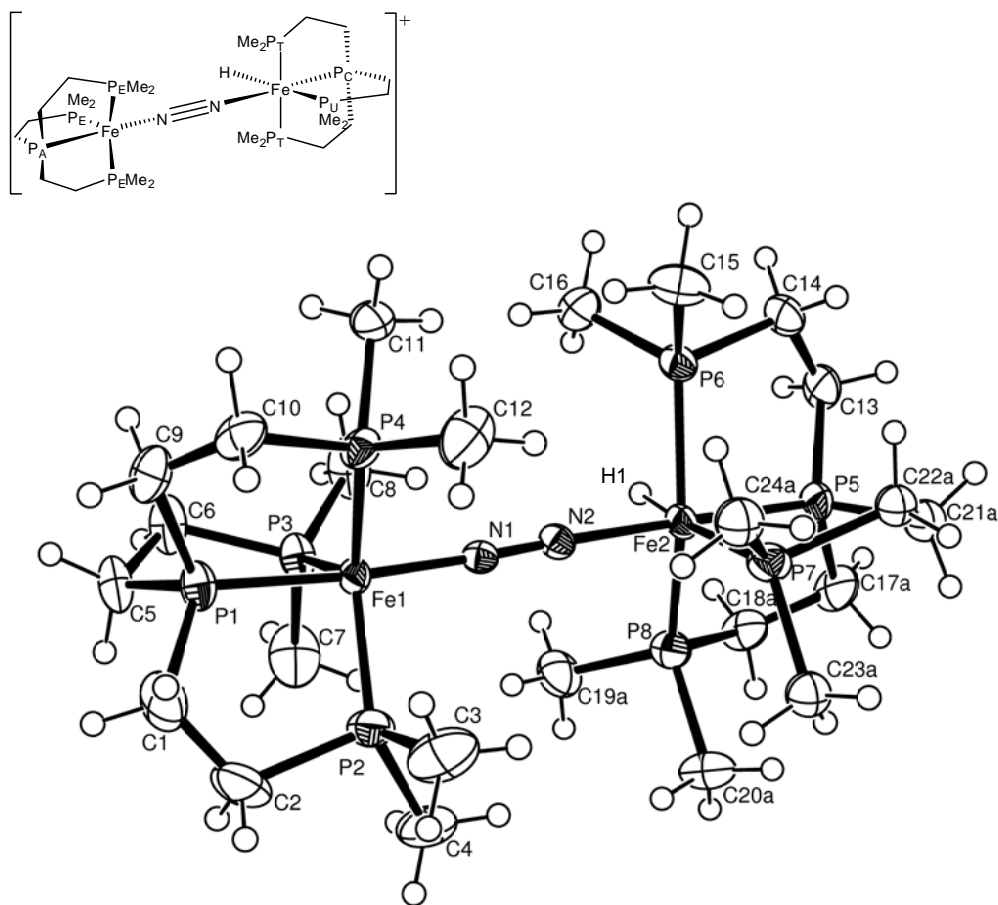
Figure 3.12   ORTEP plot (50% thermal ellipsoids, non-hydrogen atoms) of the complex cation of **37.[BPh$_4$]**. Atoms of 20-50% occupancy have been excluded for clarity.

The crystal contains slight disorder within the PP$_3$ ligand at the iron(II) centre.

Selected bond lengths and angles are presented in Table 3.5 and 3.6 respectively.

Further crystallographic data is contained in Appendix 1 (CD format).

Table 3.5   Bond lengths (Å) for [(FeH(PP$_3$))(μ-N$_2$)(Fe(PP$_3$))][BPh$_4$] **37.[BPh$_4$]**

Fe(1)-P(1)	2.1318(6)	Fe(2)-P(5)	2.1441(6)
Fe(1)-P(2)	2.1602(6)	Fe(2)-P(6)	2.1976(6)
Fe(1)-P(3)	2.1490(6)	Fe(2)-P(7)	2.2022(6)
Fe(1)-P(4)	2.1539(6)	Fe(2)-P(8)	2.1845(6)
Fe(1)-N(1)	1.798(2)	Fe(2)-N(2)	1.904(2)
N(1)-N(2)	1.127(2)	Fe(2)-H(1)	1.47(2)

Table 3.6   Bond angles (°) for [(FeH(PP$_3$))(μ-N$_2$)(Fe(PP$_3$))][BPh$_4$] **37.[BPh$_4$]**

Fe(1)-N(1)-N(2)	177.3(1)	Fe(2)-N(2)-N(1)	177.0(1)
N(1)-Fe(1)-P(1)	175.22(5)	P(2)-Fe(1)-P(1)	86.37(2)
P(3)-Fe(1)-P(1)	84.55(2)	P(4)-Fe(1)-P(1)	84.63(2)
N(1)-Fe(1)-P(2)	98.24(5)	P(3)-Fe(1)-P(2)	120.05(2)
P(4)-Fe(1)-P(2)	117.32(2)	N(1)-Fe(1)-P(3)	94.14(5)
P(4)-Fe(1)-P(3)	120.52(2)	N(1)-Fe(1)-P(4)	92.11(5)
N(2)-Fe(2)-P(5)	177.62(5)	P(6)-Fe(2)-P(5)	85.59(2)
P(7)-Fe(2)-P(5)	86.17(2)	P(8)-Fe(2)-P(5)	85.39(2)
N(2)-Fe(2)-P(6)	95.38(5)	P(7)-Fe(2)-P(6)	101.55(2)
P(8)-Fe(2)-P(6)	150.12(2)	N(2)-Fe(2)-P(7)	95.75(5)
P(8)-Fe(2)-P(7)	106.19(2)	N(2)-Fe(2) P(8)	92.72(5)
N(2)-Fe(2)-H(1)	92.3(8)	P(5)-Fe(2)-H(1)	85.8(8)
P(6)-Fe(2)-H(1)	77.1(8)	P(7)-Fe(2)-H(1)	171.9(8)
P(8)-Fe(2)-H(1)	73.9(8)		

The complex has two distinct iron centres bridged by a dinitrogen ligand. There is an iron(II) centre with the four phosphorus atoms of the PP$_3$ ligand, the dinitrogen and the hydride ligand arranged in a distorted octahedron equivalent to the iron centres of **23.[BAr$^F_4$]$_2$** (Section 3.2.5). This is bridged to an iron(0) centre which has no hydride ligand. The PP$_3$ and dinitrogen ligand are arranged in a distorted trigonal bipyramid with a P$_A$-Fe-N axis. The N-N bond length of 1.127(2) Å is representative of a small degree of activation of the dinitrogen triple bond equivalent in magnitude to that of **23.[BAr$^F_4$]$_2$**.

The structure of the iron(II) centre presents with all Fe-P bonds shorter in length when compared to Fe-P lengths of **23.[BAr$^F_4$]$_2$**. This difference can be attributed to the change in steric stresses at the iron(II) centre caused by the significant difference in the second iron centre now connected to it. The bond angles are

similar with notable exceptions being the N-Fe-P$_T$ bond angles which are 92.7°
and 95.4° in **37.[BPh$_4$]** as compared with 90.8° and 99.2° in **23.[BAr$^F_4$]$_2$**. The
Fe-N-N bond angle is 177.3° compared with 174.5° in **23.[BAr$^F_4$]$_2$**. Again, these
differences most likely reflect the steric, and possibly the electronic, impact of the
different second iron centre.

A search of the Cambridge Structural Database[11, 12] provides few comparative
structures for the trigonal bipyramidal iron(0) centre. Specifically, there are no
crystal structures of iron(0) dinitrogen complexes with tripodal tetradentate
phosphine ligands. A selection of comparative complexes, which can be grouped
as iron(0) dinitrogen complexes and trigonal bipyramidal iron complexes with
tripodal phosphine ligands, are described. Selected bond lengths and angles of
these complexes and the iron(0) centre of **37.[BPh$_4$]** are presented in Table 3.7.

1.   Iron(0) dinitrogen complexes:

Fe(N$_2$)(depe)$_2$[24] **39** and Fe(CO)$_2$(N$_2$)(PEt$_3$)$_2$[20] **40** (this is the monomer of the
dinitrogen bridged dimer **35** described previously (Section 3.2.5)).
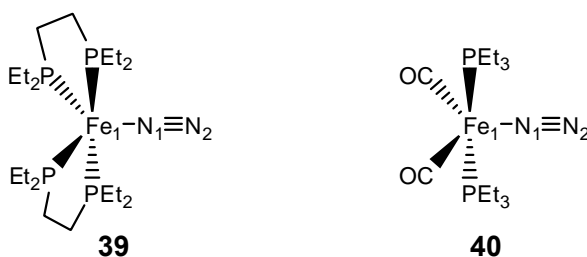
The distribution of the phosphine ligands around the iron centre of **39** shows a
narrowing of N-Fe-P angles from the 90° and 120° of an ideal trigonal
bipyramid.[24] This is in direct comparison with the greater than 90° P$_E$-Fe$_1$-N$_1$

angles for **37.[BPh$_4$]**, a reflection of the constraint applied to the structure by the natural bite of the PP$_3$ **1** ligand.

2. Trigonal bipyramidal iron complexes with tripodal phosphine ligands:

[FeBr(PP$^{Ph}_3$)][BPh$_4$]^{25} **41**, [FeBr(NP$^{Ph}_3$)][PF$_6$]^{25} **42** and Fe(CO)(NP$^i_3$)^{15} **43**.
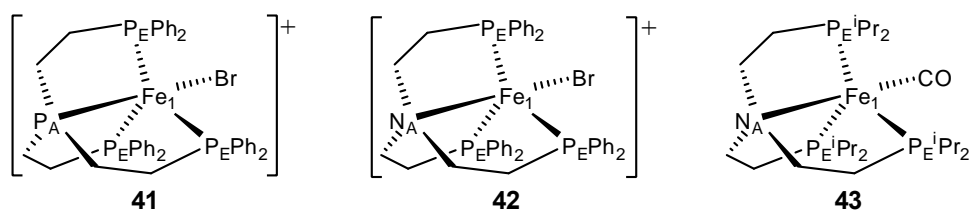
These iron complexes all show the monodentate ligand in an axial position *trans* to the central nitrogen or phosphorus atom of the tetradentate ligand. This is due to the structural constraints placed on the complex by the tetradentate ligands. Complexes **41** and **42** have significantly longer ligand to iron centre bond lengths than **37.[BPh$_4$]**. This might be expected given the large steric bulk of the bromide ligand and the phenyl substituents of the phosphine ligands. Likewise these differences can account for the larger P$_E$-Fe$_1$-X and smaller P$_E$-Fe$_1$-P$_E$ angles in these structures as the terminal phosphines are sterically repulsed by the bromide ligand. In addition the iron centres of structures **41** and **42** have formal oxidation states of (II) which could lead to differences in bond lengths and angles. The donor atom to metal centre bond lengths of **43** are, excepting the Fe$_1$-C bond, also longer than for **37.[BPh$_4$]**. This difference is likely to be due to the differing nature of the phosphine substituents on the ligand. The distribution of the terminal phosphine atoms around the iron centre is also significantly different with P$_E$-Fe$_1$-P$_E$ angles of **43** being 110.5º, 129.3º and 118.4º as compared to 120.1º, 117.3º and 120.5º for **37.[BPh$_4$].** These differences are considered to be

due both to the steric interactions of the terminal phosphine substituents and to the

differing nature of the central atom of the ligand.

Table 3.7   Selected bond lengths (Å) and angles (º) of complexes **37.[BPh$_4$]** (iron(0) centre, this work), **39**[24], **40**[20], **41**[25], **42**[25] and **43**[15].

	37	39	40	41	42	43
Fe$_1$-X	1.798(2)	1.748(8)	1.85(2)	2.369(2)	2.403(4)	1.680(4)
N$_1$-N$_2$	1.127(2)	1.14(1)	1.08(3)			
Fe$_1$-P$_A$/N$_A$	2.1318(6)			2.214(3)	2.65(2)	2.150(2)
Fe$_1$-P$_E$*	2.1602(6)			2.358(3)	2.433(7)	2.2939(8)
Fe$_1$-P$_E$*	2.1490(6)			2.339(3)	2.445(7)	2.2379(8)
Fe$_1$-P$_E$*	2.1539(6)			2.332(3)	2.427(6)	2.2722(7)
Fe$_1$-N$_1$-N$_2$	177.3(1)		179(2)			
P$_A$/N$_A$-Fe$_1$-X	175.22(5)			177.2(1)	176.6(4)	177.4(1)
P$_A$/N$_A$-Fe$_1$-P$_E$ *	86.37(2)			81.9(1)	73.4(4)	85.78(6)
P$_A$/N$_A$-Fe$_1$-P$_E$ *	84.55(2)			82.0(1)	74.3(4)	85.86(6)
P$_A$/N$_A$-Fe$_1$-P$_E$ *	84.63(2)			81.7(1)	75.9(4)	85.10(6)
P$_E$-Fe$_1$-X *	98.24(5)			99.8(1)	103.3(2)	96.78(9)
P$_E$-Fe$_1$-X *	94.14(5)			99.1(1)	106.6(2)	93.33(9)
P$_E$-Fe$_1$-X*	92.11(5)			95.5(1)	106.5(2)	93.16(9)
P$_E$-Fe$_1$-P$_E$ *	120.05(2)			115.2(1)	116.4(2)	110.54(3)
P$_E$-Fe$_1$-P$_E$ *	117.32(2)			122.4(1)	110.1(2)	129.27(3)
P$_E$-Fe$_1$-P$_E$ *	120.52(2)			116.4(1)	112.9(3)	118.37(3)

X = N$_1$, Br or C for **37 39 40**, **41 42** or **43** respectively
* Three equivalent terminal phosphines.

3.2.10 Treatment of [(FeH(PP$_3$))$_2$(µ-N$_2$)][BPh$_4$]$_2$ 23.[BPh$_4$]$_2$ with excess base.

Addition of an excess of potassium *tert*-butoxide to a suspension of **23.[BPh$_4$]$_2$**

under dinitrogen on an NMR scale in THF results in the slow dissolution of the

buff coloured solid to give a red solution of **37.[BPh$_4$]** (by ^{31}P{^{1}H} NMR). Over

the course of several hours the solution turns yellow in colour. The ^{31}P{^{1}H} NMR

spectrum (Figure 3.13) shows the presence of two species assigned as

(Fe(PP$_3$))$_2$(μ-N$_2$) **38** and Fe(N$_2$)(PP$_3$) **44**. Complex **44** has been reported previously from the deprotonation of **22.[BPh$_4$]**.[3] Each species has two resonances in the ratio of 1:3 and these correspond to the apical phosphorus P$_A$ and three equivalent terminal phosphorus atoms P$_E$ of the PP$_3$ **1** ligand arranged around an iron(0) centre in a trigonal bipyramidal fashion. At 182.9 ppm the resonance of the apical phosphorus of **44** is at significantly lower field to that of the dinitrogen bridged species **38** at 170.9 ppm. Each of these apical phosphorus resonances appear as a quartet due to coupling to the three equivalent P$_E$ atoms. The P$_E$ signals of **44** are very slightly lower in field to those of **38** at 66.6 and 66.0 ppm respectively. Each presents as a doublet split by the single P$_A$ atom with the coupling constant of **38** at 57.7 Hz being significantly greater than that of **44** at 45.8 Hz. Hence, the major effect of the second iron centre on the dinitrogen ligand is to the chemical shift of the apical phosphorus located *trans* to the dinitrogen and the ^{31}P-^{31}P coupling across the iron(0) centre. The absence of a hydride peak in the ^{1}H{^{31}P} NMR spectrum lends further weight to the assignment of these resonances. Attempts to isolate these species were unsuccessful. Attempts to crystallise these complexes resulted in the loss of the dinitrogen ligand and the formation of an iron(0) PP$_3$ tetramer (see Section 4.8.2).
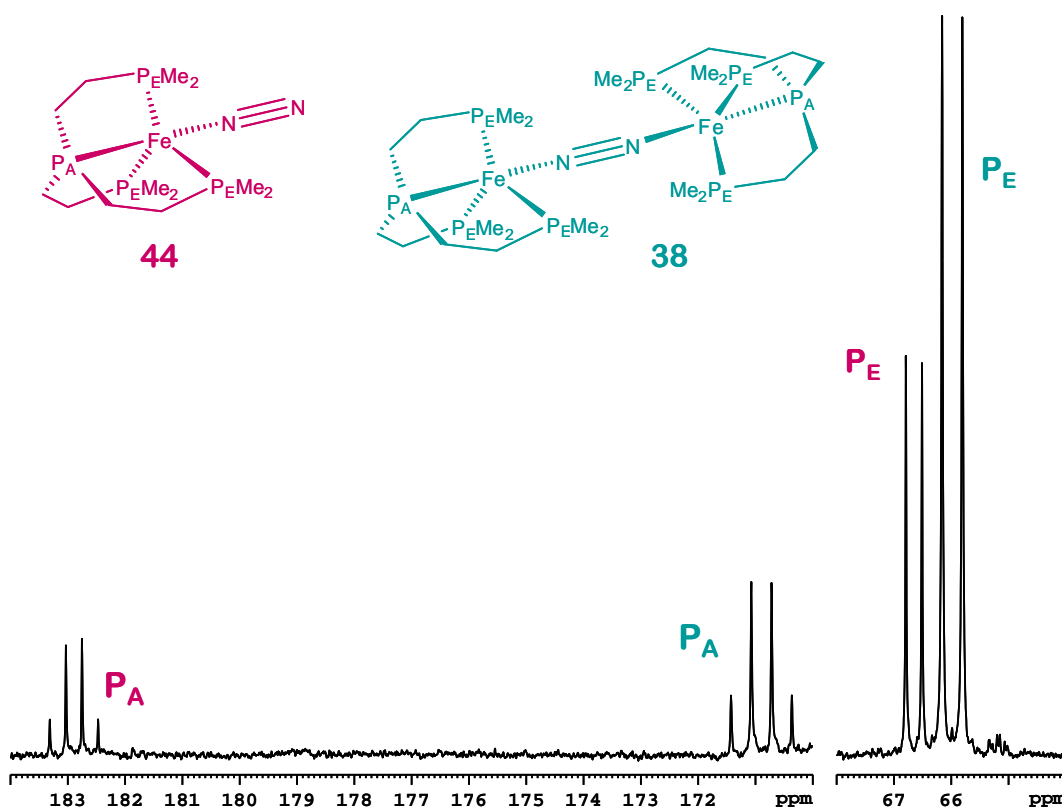
Figure 3.13 ^{31}P{^{1}H} NMR spectra of (Fe(PP$_3$))$_2$(μ-N$_2$) **38** and Fe(N$_2$)(PP$_3$) **44** in THF/THF-d_8.

3.2.11 Treatment of [(FeH(PP$_3$))(μ-^{15}N$_2$)(Fe(PP$_3$))][BPh$_4$] ^{15}N$_2$-37.[BPh$_4$].with base

Treatment of [(FeH(PP$_3$))(μ-^{15}N$_2$)(Fe(PP$_3$))][BPh$_4$] **^{15}N$_2$-37.[BPh$_4$]** with the base potassium t-butoxide was performed on an NMR scale under argon in THF-d_8 in an attempt to synthesise the ^{15}N labelled analogues of **38** and **44**. This led to the formation of Fe(^{15}N$_2$)(PP$_3$) **^{15}N$_2$-44** and an unidentified species by ^{31}P{^{1}H} NMR. The reaction was repeated in deuterated benzene and again 2 species were present. In this case it was possible to identify both species as **^{15}N$_2$-44** and the C-D activation product FeD(Ph-d_5)(PP$_3$) **45**. The ^{31}P{^{1}H} NMR of these products is shown in Figure 3.14.
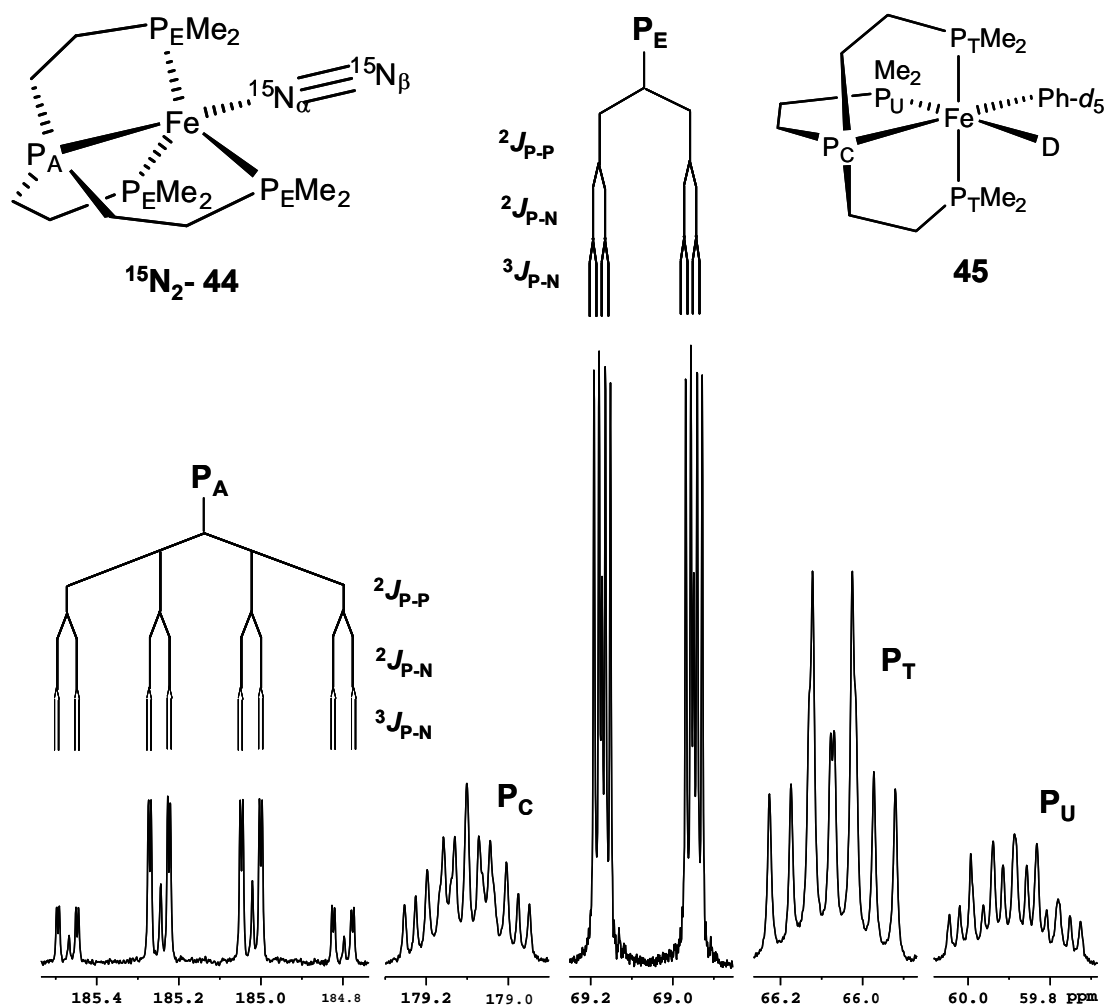
Figure 3.14 ^{31}P{^{1}H} NMR spectra of Fe(^{15}N$_2$)(PP$_3$) ^{15}N$_2$-**44** and FeD(Ph-d_5)(PP$_3$) **45** in benzene-d_6.

It is clear from this NMR spectrum that there has been some contamination of the NMR sample with the ^{14}N species **44** which has signals (P$_A$ quartet and P$_E$ doublet) which are visible and overlap between those of ^{15}N$_2$-**44**. However, it is still possible to elucidate the ^{31}P-^{15}N splitting of the latter complex which is illustrated in Figure 3.14. The resonance of the central phosphine P$_A$ of ^{15}N$_2$-**44** presents as a doublet of doublet of quartets at 185.3 ppm coupling to each nitrogen of the dinitrogen ligand and to the 3 equivalent phosphines P$_E$. The resonance of the terminal phosphines P$_E$ is 3 times the intensity of the P$_A$ signal

and presents as a doublet of doublet of doublets at 69.1 ppm coupled to P$_A$ and to both ^{15}N$_\alpha$ and ^{15}N$_\beta$ of the ^{15}N labelled dinitrogen ligand. The coupling constant between P$_A$ and P$_E$ is 45.4 Hz, as expected this is very similar to that seen in the unlabelled species **44**. The coupling constants between P$_A$ and ^{15}N$_\alpha$ and ^{15}N$_\beta$ are 9.5 and 1.4 Hz respectively whereas the P$_E$ to ^{15}N$_\alpha$ and ^{15}N$_\beta$ coupling constants are 5.5 and 2.6 Hz respectively. The ^{31}P$\{^1$H$\}$ NMR spectrum of ^{15}**N$_2$-44** in THF-d_8 has an identical splitting pattern with very similar coupling constants. However there are noticeable differences in chemical shift with the P$_A$ signal at 183.5 ppm and the P$_E$ signal at 67.2 ppm. A ^{15}N$\{^1$H$\}$ spectrum of ^{15}**N$_2$-44** in THF-d_8 presents two weak resonances for ^{15}N$_\alpha$ and ^{15}N$_\beta$ at -26.7 ppm and -2.5 ppm respectively which have been assigned based on relative chemical shift. These shifts are confirmed by correlations in the 2D ^{31}P-^{15}N HSQC NMR experiment between P$_A$ and both ^{15}N$_\alpha$ and ^{15}N$_\beta$ and between P$_E$ and ^{15}N$_\alpha$. The absence of a P$_A$-^{15}N$_\beta$ correlation is most likely due to the very small (1.4 Hz) nature of this coupling constant.

The resonances for FeD(Ph-d_5)(PP$_3$) **45** in Figure 3.14 present as multiplets at 179.1 ppm, 66.1 ppm and 59.9 ppm representing P$_C$, P$_T$ and P$_U$ respectively with signal intensities in the ratio 1:2:1. Each signal is an unresolved multiplet due to the coupling of the quadrupolar deuteride ligand in addition to the ^{31}P-^{31}P coupling.

Under the reaction conditions described the doubly deprotonated species **38** was not observed. The identification of the C-D activation product from the reaction of ^{15}**N$_2$-37.[BPh$_4$]** with base in benzene-d_6 leads to the conclusion that the

unidentified product of the same reaction in THF-d_8 is also likely to be a C-D activation product. In benzene-d_6, **38** is probably unstable and splits to form a reactive [Fe(PP$_3$)] species and complex **44**. The [Fe(PP$_3$)] species would react with solvent to form the observed C-D activation product (Scheme 3.3).
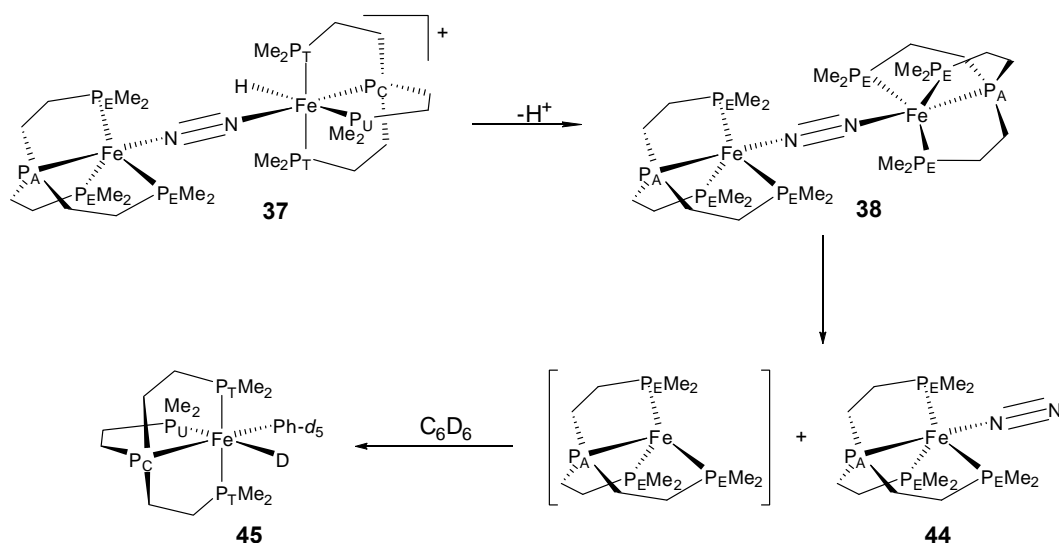
Scheme 3.3

3.3   Treatment of Nitrogen Complexes with Acid.

The complexes **22.[BPh$_4$]**, **23.[BPh$_4$]$_2$**, **23.[BF$_4$]$_2$**, **23.[PF$_6$]$_2$**, **37.[BPh$_4$]**, **37.[BF$_4$]**, **37.[PF$_6$]**, **38** and **44** were treated with acid on an nmr scale in an attempt to protonate the bound dinitrogen. The acids used were hydrochloric, tetrafluoroboric acid and the softer organic acid lutidinium chloride. The possible reduction of nitrogen to ammonia was tested for by detection of ammonium using ^{14}N NMR spectroscopy. The deprotonation products **37.[BPh$_4$]**, **37.[BF$_4$]**, **37.[PF$_6$]**, **38** and **44** were treated with an excess of acid both with and without filtering of the reaction mixture after addition of the deprotonating base. A significant excess of acid was added to the reaction mixture in each case. Typically, a white precipitate and a red solid formed in the reaction mixture. The

^{31}P{^{1}H} NMR spectrum of a typical reaction mixture at this stage showed no signal after reaction with strong acids HCl and HBF$_4$. The ^{31}P{^{1}H} NMR of the reaction mixture after treatment with the softer acid lutidinium chloride showed the reprotonation of species such as **38** and **44** to their conjugate acids **22** (major species) and **23**. The fact that the mononuclear species **22** has a more intense NMR signal than the bridged species **23** may be due to the relative solubilities of the salts of the two species and not necessarily an indication of the relative amounts present in total. After several hours of reaction time, the solvent was removed *in vacuo*. In the case of the softer acid, this was done after addition of hydrochloric acid to ensure that any ammonia present was in the form of ammonium chloride. The resulting solid was dissolved in water with a drop of D$_2$O for NMR lock purposes. The ^{31}P{^{1}H} NMR spectra of these aqueous solutions show the presence of unidentified phosphorus containing species. These are most likely the water soluble, protonated (and potentially decomposed) ligand products. In no case was the presence of ammonium chloride, derived from the bound dinitrogen, seen by NMR spectroscopy.

It has been shown that ammonium chloride concentrations as low as 2 mmol/L or 0.05 mg/1 µmol per nmr sample of 0.5 ml can be detected reliably using ^{14}N NMR spectroscopy collecting 10 k scans.[26] In the work carried out here, the number of scans used in an overnight experiment was at least 6 times this number. In practical terms this means that in a typical 30 mg sample of starting material less than 2% of the nitrogen present needs to be reduced to ammonia to be detectable by ^{14}N NMR spectroscopy. The indophenol test used, for example, by Leigh[1, 2] and Komiya[24], in the quantitative detection of ammonia is a colourimetric test. It

is possible that such a test can provide a false positive with phosphines.[26] The use of ^{14}N NMR spectroscopy eliminates the possibility of an erroneous outcome with ammonium chloride having a well defined ^{14}N NMR spectrum (see Figure 3.15). The highly symmetrical nature of the ammonium cation overcomes the fact that the ^{14}N nucleus is quadrupolar with a spin of 1 which would normally make it a poor candidate for detection by 1D NMR. This technique has been used in the detection of ammonium for over two decades by the botany fraternity.[27, 28]
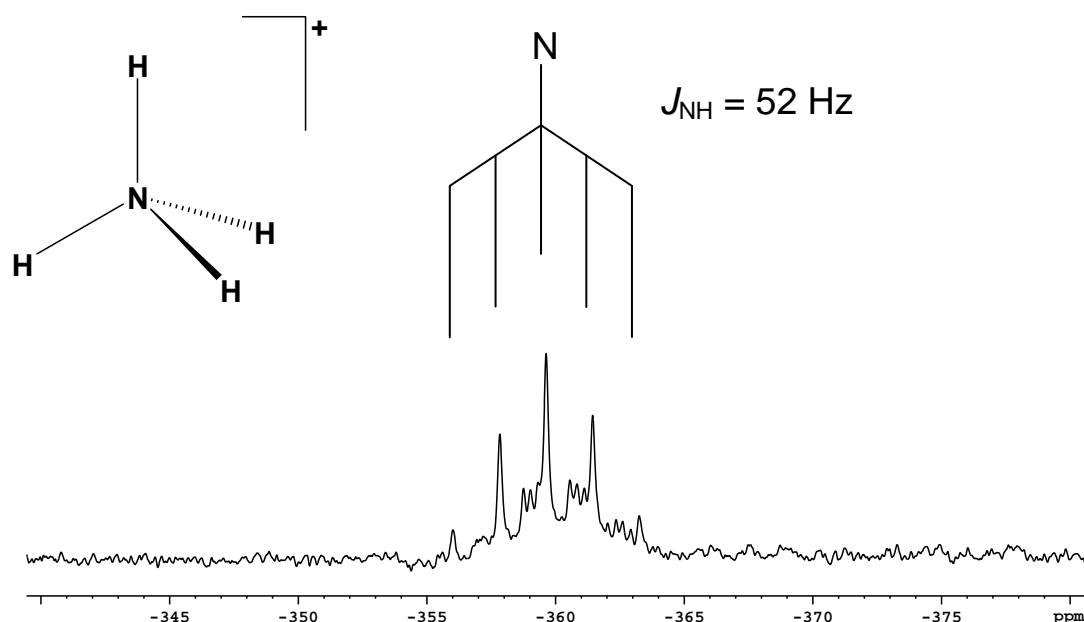
Figure 3.15 ^{14}N NMR of ammonium chloride in H$_2$O/D$_2$O

The ^{14}N NMR spectrum of ammonium chloride in H$_2$O/D$_2$O presents as a quintet with a 52 Hz N-H coupling. Further resonances representative of the deuterium substituted species can also clearly be seen overlapping the main resonance pattern.

In this work no ammonium chloride derived from an iron nitrogen complex was seen. However, in the case where potassium bis(trimethylsilyl)amide was used as

the base in the generation of the iron(0) species an ammonium signal was detected. The spectrum is that provided in Figure 3.15. It was immediately suspected that this ammonium might derive, not from the complexed dinitrogen but, from the base itself. In order to investigate this outcome the experiment was repeated with a ^{15}N labelled dinitrogen complex.
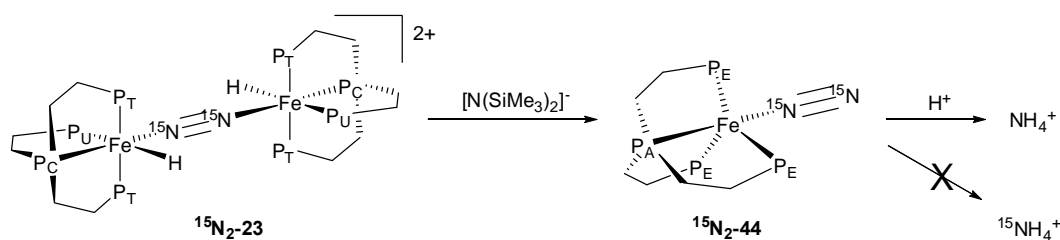
Scheme 3.4

As illustrated in Scheme 3.4, this provided a positive result for ammonium by ^{14}N NMR but no resonance for ammonium in the ^{15}N NMR spectrum proving the source of the ammonium to be the amide base. The ammonia observed is conclusively derived from the based used and this is not an unexpected result given that silicon nitrogen bonds are known to be hydrolytically unstable.[29] It is also possible that the break down of the base could be mediated or catalysed by the iron complexes present. It is worth noting that this result proves the efficacy of ^{14}N NMR spectroscopy in the detection of ammonium in this work.

3.4 Intermediates in the Reduction of the Bound Nitrogen of Iron -PP$_3$ Complexes

An important part of the investigation into the reduction potential of the bound dinitrogen of the iron-nitrogen complexes of PP$_3$ **1** described thus far is the identifying and characterising of possible intermediates. Shrock *et al.*'s

pioneering work[30] into catalytic reduction of nitrogen to ammonia at a single molybdenum centre managed to characterise many of the intermediate species in the proposed catalytic cycle. Here the ammine and hydrazine complexes are clear possible intermediates in any reduction scheme for coordinated dinitrogen. Hydrazine, in addition to ammonia, has been identified many times as a product of dinitrogen reduction at a metal centre.[31] The existence of diazene, hydrazine or ammine ligands in stable iron-PP$_3$ complexes would lend support to the possibility that iron-nitrogen complexes of PP$_3$ could act as catalysts for reduction of dinitrogen.

3.4.1 Preparation of [Fe(NH$_3$)H(PP$_3$)][BPh$_4$], 46.[BPh$_4$]

The preparation of the iron(II) ammine complex [Fe(NH$_3$)H(PP$_3$)][BPh$_4$], **46.[BPh$_4$]** is illustrated in Scheme 3.5.
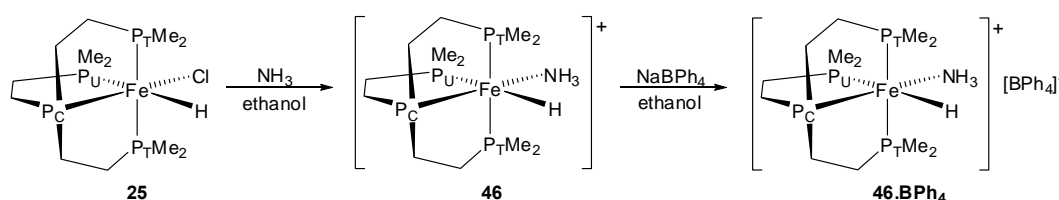
Scheme 3.5

Addition of an ammonia-saturated solution of ethanol to a nitrogen-free ethanol solution of FeClH(PP$_3$) **25** resulted in a colour change from orange to yellow. Addition of a single equivalent of sodium tetraphenylborate, to the filtered reaction mixture after 4 hours, afforded [Fe(NH$_3$)H(PP$_3$)][BPh$_4$] **46.[BPh$_4$]** as a fine yellow solid in 71% yield.

The ^{31}P{^{1}H} NMR spectrum of **46.[BPh$_4$]**, illustrated in Figure 3.16, is typical for an octahedral complex of Fe(II)-PP$_3$ and very similar to the dinitrogen hydride species described previously. The three phosphorus resonances of P$_C$, P$_T$ and P$_U$ present in the ratio 1:2:1 respectively. The P$_C$ resonance is assigned on the basis of its low field position at 179.5 ppm compared to those of P$_T$ and P$_U$ at 59.4 and 56.9 ppm which are assigned on the basis of their relative intensities and splitting patterns. The signal for the hydride ligand appears in the high field area of the ^{1}H NMR spectrum at -13.0 ppm and presents as an unresolved doublet of doublet of triplets, due to coupling to the 4 PP$_3$ **1** phosphorus atoms. This is illustrated in Figure 3.17. In the ^{1}H-^{15}N HSQC spectrum the N-H correlation for the ammonia ligand with a ^{15}N chemical shift of -446 ppm and ^{1}H shift of 1.7 ppm is visible at room temperature but with a more intense signal at lower temperature (230K). The ^{31}P{^{1}H} and ^{1}H high field NMR spectra of **46.[BPh$_4$]** correspond to those of **46** in ethanol seen prior to addition of the counteranion. This fact becomes important when considering the hydrazine reaction in Section 3.4.2.1. The stereochemistry of **46** is not known. However, similarities in NMR spectra to the hydride species in this work and to other Fe(II)-PP$_3$ hydride complexes[3] implies that the hydride ligand is *trans* to the P$_U$ donor atom and the ammonia ligand is *trans* to the central phosphorus P$_C$.
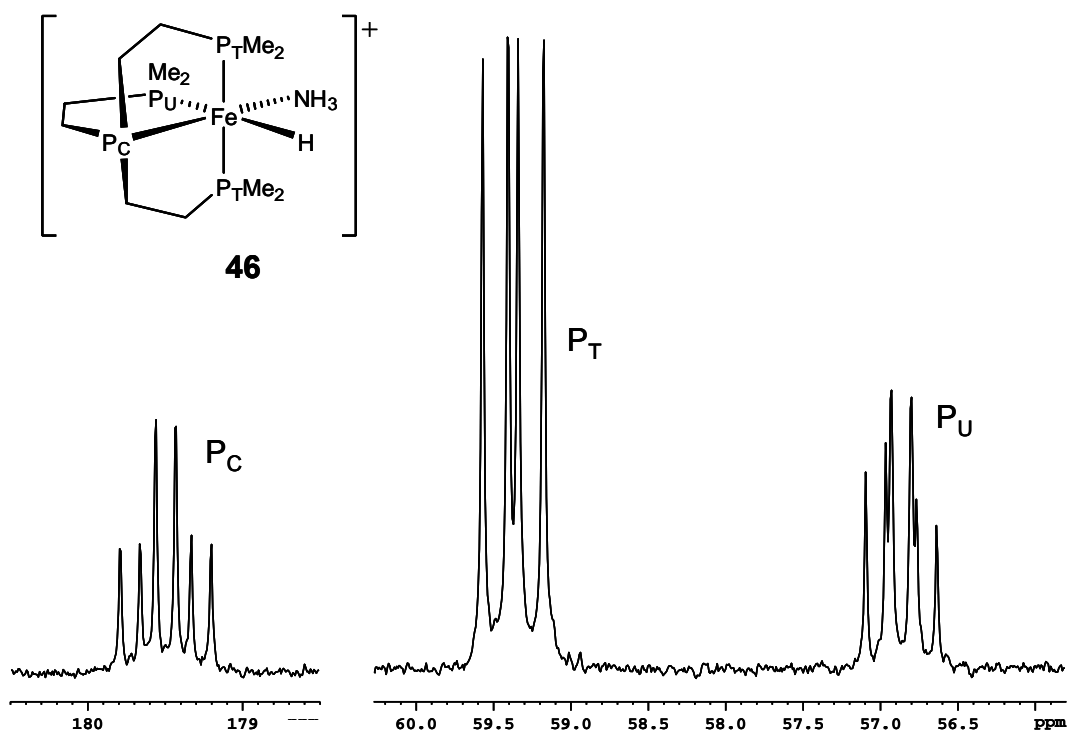
Figure 3.16 ^{31}P{^{1}H} NMR spectrum of [Fe(NH$_3$)H(PP$_3$)][BPh$_4$] **46.[BPh$_4$]** in THF-d_8
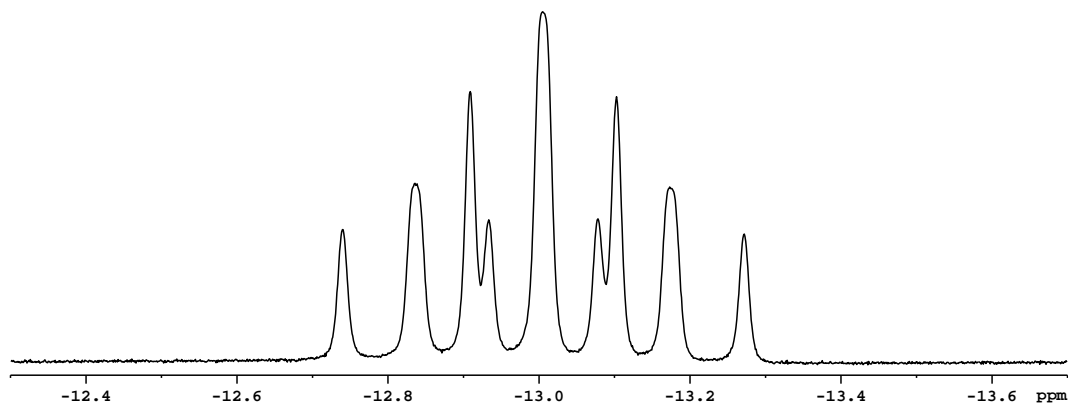
Figure 3.17 ^{1}H NMR spectrum (high field) of [Fe(NH$_3$)H(PP$_3$)][BPh$_4$] **46.[BPh$_4$]** in THF-d_8

3.4.2   Preparation of hydrazine complexes.

Whilst the treatment of FeClH(PP$_3$) **25** with an ethanol solution of ammonia leads to the immediate and complete formation of the ammine complex **46.Cl**, the reaction of **25** with hydrazine results in a variety of species which are time, solvent and concentration dependent. This result might be expected given that

90

hydrazine is known to act as a monodentate, bridging and bidentate ligand.[32] In addition hydrazine is known to disproportionate to ammonia and dinitrogen according to the following equation.[33]

$$3N_2H_{4(g)} \longrightarrow 4NH_{3(g)} + N_{2(g)} \qquad \begin{array}{l} \Delta H^\circ = -337 \text{ kJ mol}^{-1} \\ \Delta S^\circ = -601 \text{ J mol}^{-1} \text{ K}^{-1} \end{array} \qquad (3.1)$$
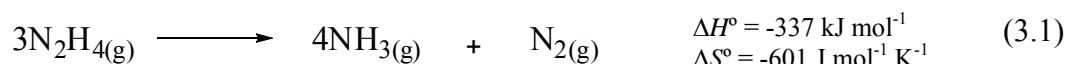
3.4.2.1   Reaction of FeClHPP$_3$ 25 with ^{15}N labelled Hydrazine

The result of addition of approximately 4 equivalents of ^{15}N labelled hydrazine in THF to a solution of **25** (0.24 mmol) in ethanol (0.5 ml) was observed by NMR spectroscopy over the course of several days. A summary of these observations is illustrated in Scheme 3.6.
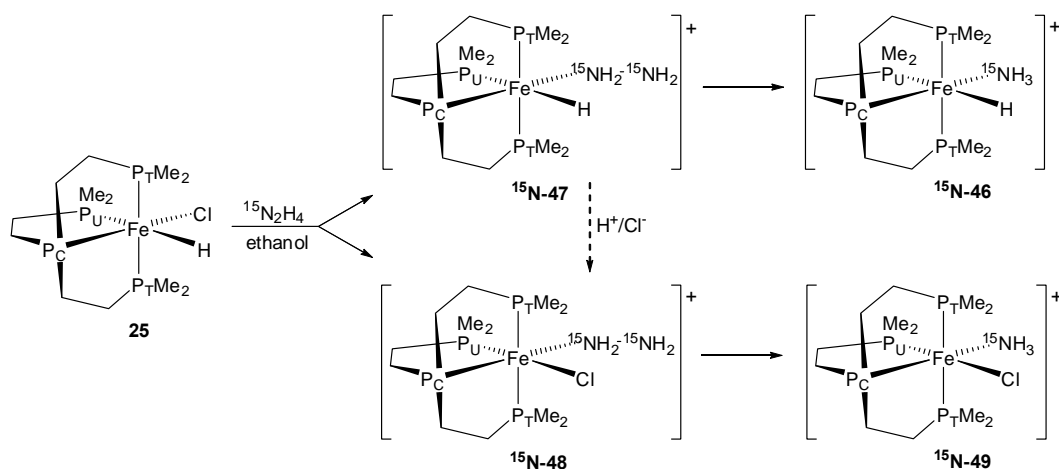
Scheme 3.6

Initially two major new species appear in the ^{31}P{^{1}H} NMR spectrum each of which have corresponding resonances in the ^{15}N spectrum and one of which has a hydride resonance.   These have been assigned as [Fe(^{15}NH$_2$^{15}NH$_2$)H(PP$_3$)]Cl **^{15}N-47.Cl** and more tentatively as [FeCl(^{15}NH$_2$^{15}NH$_2$)(PP$_3$)]$^+$ **^{15}N-48**. The NMR spectra of these species are provided in Figures 3.18 to 3.20.
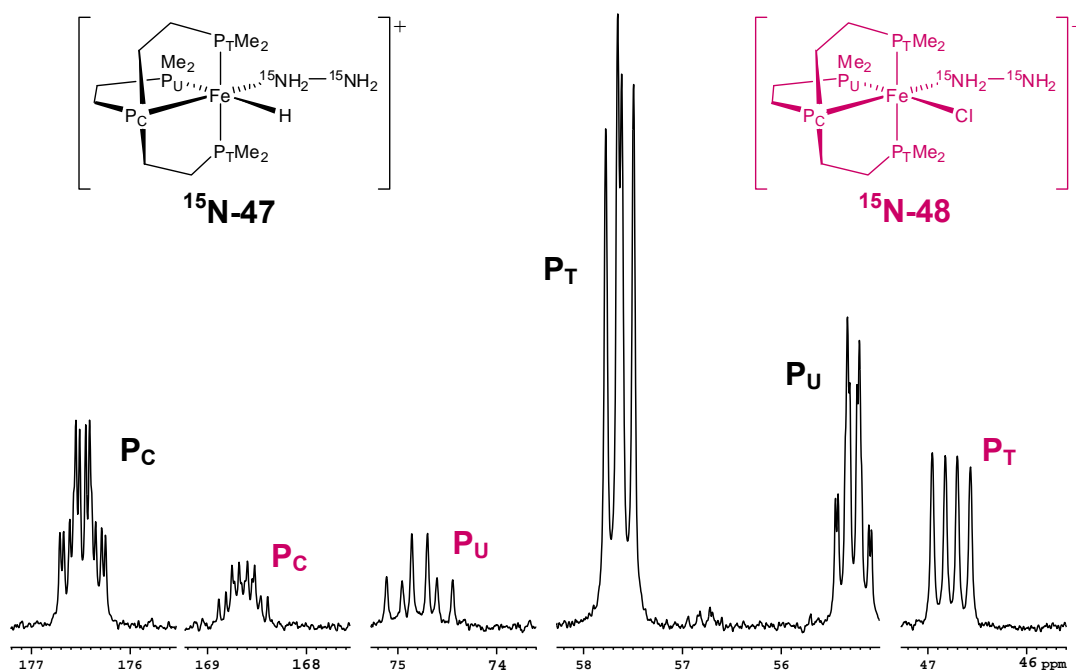
Figure 3.18 ^{31}P{^{1}H} NMR spectrum of [Fe(^{15}NH$_2$^{15}NH$_2$)H(PP$_3$)]Cl ^{15}**N-47.Cl** and [FeCl(^{15}NH$_2$^{15}NH$_2$)(PP$_3$)]$^+$ ^{15}**N-48**. in ethanol/THF/benzene-d_6.

The hydrazine complex cations ^{15}**N-47** and ^{15}**N-48** both present three resonances in the ^{31}P{^{1}H} spectrum in the ratio of 1:2:1 corresponding to the central P$_C$ (assigned based on its low field position) and terminal P$_T$ and P$_U$ donor atoms (assigned based on their relative intensities and splitting patterns) respectively. The P$_T$ resonance of ^{15}**N-47,** with a chemical shift of 57.6 ppm, presents as a doublet of doublets coupling to both the P$_C$ and P$_U$ phosphorus donors but with no apparent $^{2}J_{\text{P-N}}$ coupling to ^{15}N$_\alpha$ of the hydrazine ligand. In contrast the central phosphorus P$_C$ resonance at 176.5 ppm presents with a doublet of doublet of triplets splitting pattern which includes a 6 Hz $^{2}J_{\text{P-N}}$ coupling constant. Likewise, the P$_U$ phosphorus resonance at 55.3 ppm presents as a poorly resolved doublet of doublet of triplets with a $^{2}J_{\text{P-N}}$ coupling constant of 4 Hz. The resonances of ^{15}**N-48** have some striking differences to those of ^{15}**N-47**. The P$_U$ resonance of ^{15}**N-48** at 74.8 ppm is significantly lower field than that of ^{15}**N-47** and presents as a

doublet of triplets coupling to the P_C and P_T donor atoms respectively with no apparent $^2J_{\text{P-N}}$ coupling. The P_T phosphorus resonance appears as a doublet of doublets at 46.8 ppm with no $^2J_{\text{P-N}}$ coupling whereas the P_C resonance presents at 168.7 ppm as a poorly resolved doublet of doublet of triplets with an 11 Hz $^2J_{\text{P-N}}$ coupling constant. In addition, the $^2J_{\text{P-P}}$ coupling constants of P_U with P_C and P_T at 25 and 41 Hz are significantly greater for **^{15}N-48** than **^{15}N-47** at 16 and 19 Hz respectively. These differences reflect the differing steric and electronic effects of the large chloride ligand *trans* to the P_U donor atom in **^{15}N-48** in place of the small highly polarisable strong σ-donating hydride ligand in **^{15}N-47** which is known to have a large *trans*-influence.[34]
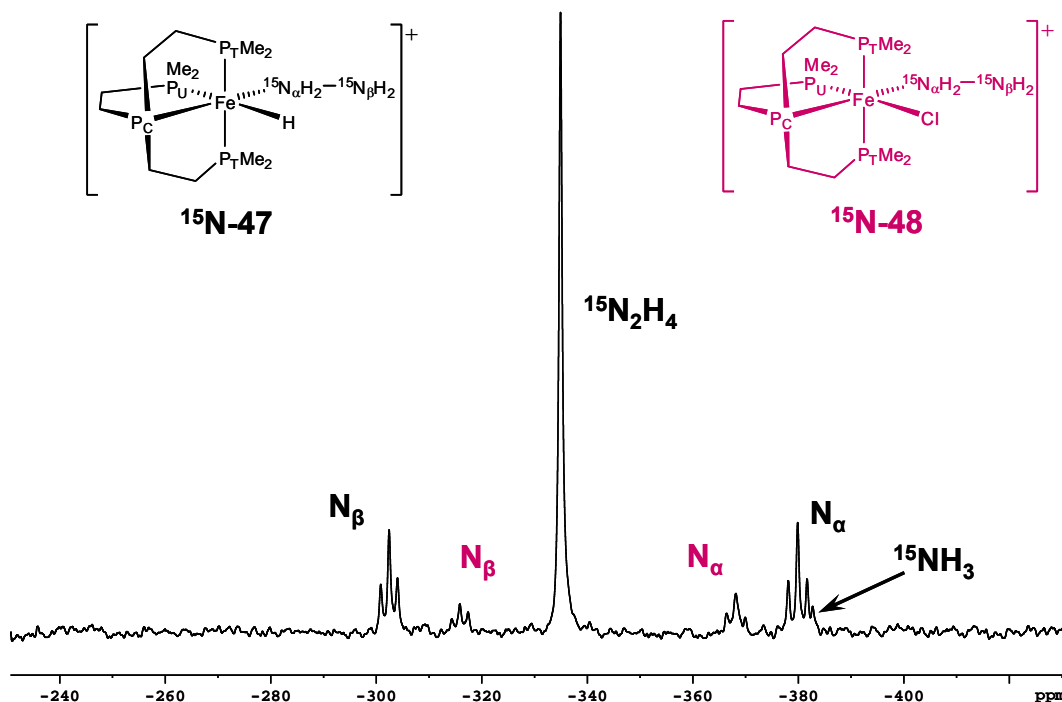
Figure 3.19 ^{15}N NMR spectrum of [Fe(^{15}NH$_2$^{15}NH$_2$)H(PP$_3$)]Cl **^{15}N-47.Cl** and [FeCl(^{15}NH$_2$^{15}NH$_2$)(PP$_3$)]$^+$ **^{15}N-48** in ethanol/THF/benzene-d_6.

The ^{15}N NMR spectrum shows the free hydrazine resonance at -335 ppm and two pairs of resonances representing the nitrogen atoms, N$_\alpha$ and N$_\beta$, of the hydrazine ligands of complexes ^{15}N-47 and ^{15}N-48. Assignment of these ^{15}N resonances between complexes is based on their relative intensities which, at a ratio of 3:1 for ^{15}N-47 and ^{15}N-48, correspond well with those of their respective ^{31}P{^{1}H} signals. The higher field signal has been assigned to N$_\alpha$ and the lower field signal to N$_\beta$ based on literature values for monodentate hydrazine ligands.[32] Each of the complexed hydrazine resonances appears as a triplet being split by the two bound hydrogens. The free hydrazine undergoes rapid proton exchange with the protic solvent[35] resulting in this species appearing as a singlet by ^{15}N NMR. The chemical shift of the ^{15}N-47 N$_\alpha$ resonance at -380.2 ppm is slightly up field to that of ^{15}N-48 N$_\alpha$ at -368.1 ppm whilst the ^{15}N-47 $^1J_{N\alpha-H}$ coupling constant at 71 Hz is very close to that of the ^{15}N-48 $^1J_{N\alpha-H}$ coupling constant of 72 Hz. The ^{15}N-47 and ^{15}N-48 $^1J_{N\beta-H}$ coupling constants are equivalent at 65 Hz with the ^{15}N-47 N$_\beta$ resonance at -302.7 ppm being slightly down field from ^{15}N-48 N$_\beta$ at -315.7 ppm.
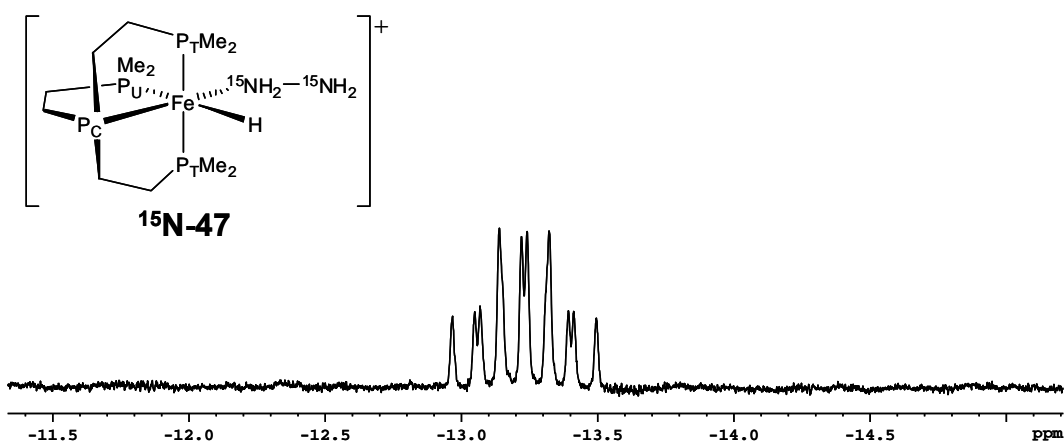
Figure 3.20 Hydride region of ^{1}H NMR spectrum of [Fe(^{15}NH$_2$^{15}NH$_2$)H(PP$_3$)]Cl ^{15}N-47.Cl and [FeCl(^{15}NH$_2$^{15}NH$_2$)(PP$_3$)]$^+$ ^{15}N-48 in ethanol/THF/benzene-d_6.

The high field region of the ^{1}H NMR spectrum presents the hydride resonance of **^{15}N-47** as a multiplet which collapses to a broad singlet upon ^{31}P decoupling. This hydride species is shown to be coupled to the ^{31}P{^{1}H} NMR resonances of **^{15}N-47** by way of a ^{1}H-^{31}P HSQC 2D NMR experiment. In the low field region of the ^{1}H{^{31}P} NMR spectrum it is only possible to locate the hydrazine N$_\alpha$H proton resonances which present as a doublet of triplets at 4.99 ppm for **^{15}N-47** with a $^3J_{\text{H-H}}$ coupling constant of 4 Hz and as a doublet at 5.78 ppm for **^{15}N-48**. In the ^{1}H NMR spectrum the ^{31}P coupling is evident as a broadening of these signals. The N$_\beta$H proton resonances are not visible in these spectra due to the large solvent peaks and have been located at 3.2 and 3.7 ppm for **^{15}N-47** and **^{15}N-48** respectively through a ^{1}H-^{15}N HSQC 2D NMR experiment which also confirms assignment of the N$_\alpha$H protons. The relatively high field shift of the N$_\beta$H proton signals compared to the N$_\alpha$H signals is typical for monodentate hydrazine ligands.[32]

Independent preparation of the complex cation **48** by treatment of the dichloride species **24** with hydrazine (Section 3.4.2.2) confirms the proposed assignment here. Inspection of the chlorohydride starting material **25** by NMR spectroscopy reveals that the dichloride species **24** is present as an insignificant impurity only (less than 2%). This discounts the possibility that the chlorohydrazine species, **^{15}N-48**, has been incidentally formed by reaction of hydrazine with **24**. Instead, the hydride ligand has been displaced from **25,** most likely by protonation and loss of hydrogen gas, the proton source being the ethanol solvent. In a comparable reaction with excess hydrazine in THF, i.e. in the absence of a protic solvent, the **48** to **47** ratio by ^{31}P{^{1}H} NMR was less than 1:20 supporting the proposal that

ethanol assists the formation of the chlorohydrazine complex **48**. In addition, the hydridohydrogen species $[FeH(H_2)(PP_3)]^+$, with $^{31}P\{^1H\}$ NMR resonances at 179.3 (q) and 64.5 (d) ppm[3], is visible in very small quantities by $^{31}P\{^1H\}$ NMR early on in the reaction supporting the presence of a dihydrogen complex as an intermediate in the formation of **48**.

Over the course of several days, further speciation occurs. The next two major species to be formed have been identified as the amminohydride $[Fe(^{15}NH_3)H(PP_3)].Cl$ **^{15}N-46.Cl** and the amminochloride $[Fe(^{15}NH_3)Cl(PP_3)]^+$ **^{15}N-49**. The increase in $^{31}P\{^1H\}$ NMR intensities of these species is accompanied by a decrease in the resonances of species **^{15}N-47** and **^{15}N-48** suggesting that disproportionation of the hydrazine ligand occurs at the iron centre. The $^{31}P\{^1H\}$ NMR resonances of these new species are shown in Figure 3.20. Supporting the argument for disproportionation is a decreasing ^{15}N NMR resonance for hydrazine (-335 ppm) accompanied by the appearance of a strong broad singlet in the ^{15}N NMR spectrum at -383 ppm assigned to ^{15}N ammonia[36] (initially just visible under the **^{15}N-47** N_α triplet in Figure 3.19) and a much weaker resonance at -73 ppm assigned to $^{15}N_2$ gas.
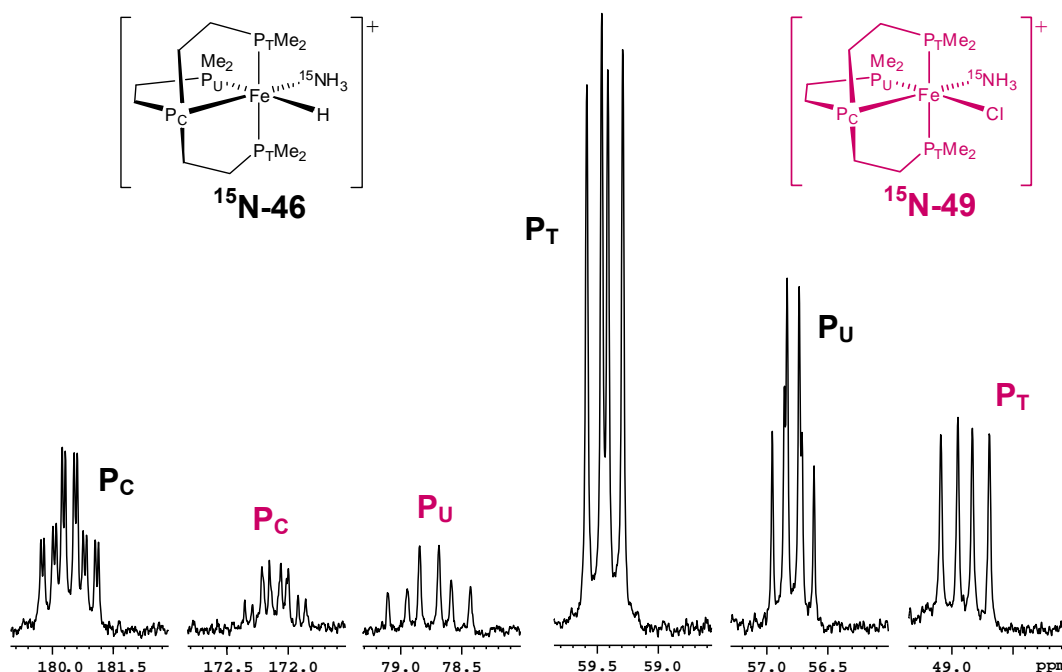
Figure 3.21 ^{31}P{^{1}H} NMR resonances of [Fe(^{15}NH$_3$)H(PP$_3$)]Cl ^{15}N-46.Cl and [FeCl(^{15}NH$_3$)(PP$_3$)]$^+$ ^{15}N-49 in ethanol/THF/benzene-d_6.

The ammine complex cations ^{15}N-46 and ^{15}N-49 present three resonances each in the ^{31}P{^{1}H} spectrum in the ratio of 1:2:1 corresponding to the central P$_C$ (assigned based on its low field position) and terminal P$_T$ and P$_U$ donor atoms (assigned based on their relative intensities and splitting patterns) respectively. The resonances of ^{15}N-46.Cl correspond well with those of the independently synthesised 46.[BPh$_4$] (Section 3.1.1) with an additional 4 Hz $^2J_{P-N}$ coupling constant visible in the low field P$_C$ resonance due to the ^{15}N labelled ammonia ligand situated *trans* to this phosphine. The 2D ^{1}H-^{15}N HSQC NMR experiment reveals the ^{1}H and ^{15}N chemical shifts of the ammonia ligand to be at 1.7 and -443 ppm respectively which again correspond well with the values for 46.[BPh$_4$]. The ^{15}N NMR spectrum allows for the determination of the $^1J_{N-H}$ coupling as 68 Hz. The high field ^{1}H NMR spectrum has a resonance which corresponds well

97

to that of **46.[BPh$_4$]** at -13.1 ppm shown by the 2D ^{1}H-^{31}P HSQC NMR experiment to be coupled to the phosphorus atoms of ^{15}**N-46.Cl**.

The ^{31}P{^{1}H} NMR spectrum of the amminochloride species ^{15}**N-49** has some striking similarities to those of its proposed precursor ^{15}**N-48**. The P$_U$ resonance at 78.8 ppm is significantly lower field than that of the P$_T$ resonance at 48.9 ppm with no $^2J_{P-N}$ coupling apparent in either resonance. The P$_C$ resonance presents at 172.1 ppm as an unresolved doublet of doublet of triplets with a 10 Hz $^2J_{P-N}$ coupling constant. In addition, the $^2J_{P-P}$ coupling constants of P$_U$ with P$_C$ and P$_T$ at 25 and 42 Hz are, like the $^2J_{P-N}$ coupling constants, very similar to those of ^{15}**N-48** and significantly higher than for ^{15}**N-46** at 16 and 20 Hz respectively. ^{15}**N-49** has no resonance in the high field area of the ^{1}H spectrum but does have a ^{1}H-^{15}N correlation in the 2D HSQC experiment at 2.8 and -420 ppm respectively. The corresponding signal in the ^{15}N spectrum, although visible was not sufficiently resolved to glean coupling constant information. The assignment of ^{15}**N-49** as [Fe(^{15}NH$_3$)Cl(PP$_3$)]$^+$ has been lent weight by the successful independent synthesis of the ^{14}N analogue following the addition of an ethanol solution of ammonia to FeCl$_2$PP$_3$ **24** in THF (see Section 3.4.2.4).

The ammine species ^{15}**N-46** and ^{15}**N-49** described above are the two major species which develop over time in this hydrazine reaction. Two further species are also clearly present by ^{31}P{^{1}H} NMR, however, they are as yet unidentified. There are many possibilities for further speciation which include those derived from the hydrazine acting as a bidentate ligand chelating a single iron centre or bridging two iron centres. Other potential intermediates and products resulting from

reactions of hydrazine at a metal centre include amides (-NH$_2$), imides (-NH), diazenes (-N(H)=NH) and hydrazides (-NNH$_2$).[37-39] The information available in this work has not pointed towards such species, however, further experimental work is required to discount them completely.

The synthetic routes to the ammine and hydrazine complexes described are summarised in Figure 3.22. The synthesis of hydrazine complexes is clearly possible although the various speciation and ease with which they react to form ammonia, and other, complexes result in their clean isolation being difficult.
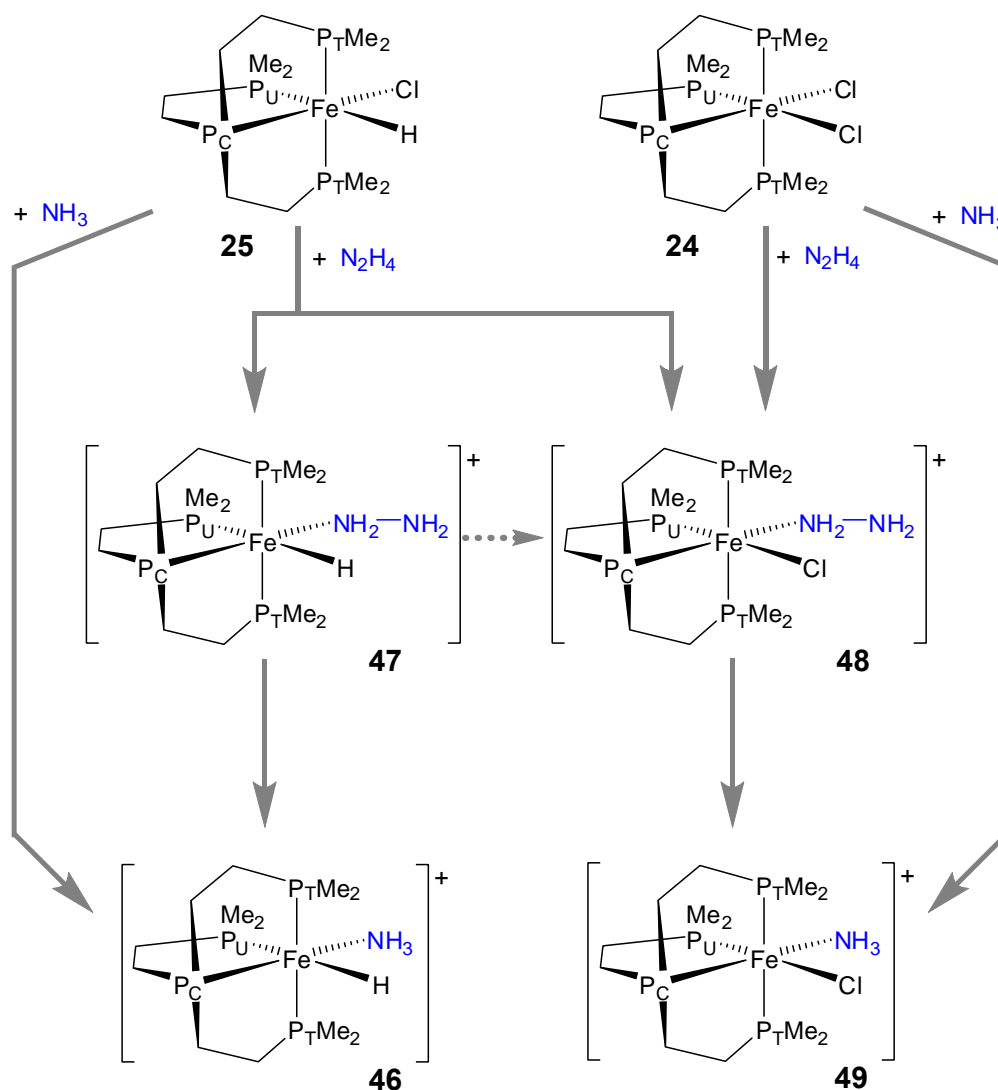
Figure 3.22 Synthetic routes to hydrazine and ammine complexes.

3.4.2.2 [Fe(NH$_2$NH$_2$)H(PP$_3$)][BPh$_4$] 47.[BPh$_4$] and [FeCl(NH$_2$NH$_2$)(PP$_3$)][BPh$_4$] 48.[BPh$_4$]

Isolation of each of these species as their tetraphenylborate salts was possible. Preparation of **47.[BPh$_4$]** was performed by the addition of an equivalent of sodium tetraphenylborate to an NMR scale reaction of excess hydrazine with **25** in ethanol. The two species in this reaction **47.[BPh$_4$]** and **48.[BPh$_4$]** precipitated as yellow powder. A small number of X-ray diffraction quality crystals of **47.[BPh$_4$]** were present allowing determination of a crystal structure. **47.[BPh$_4$]** was separated from **48.[BPh$_4$]** by virtue of its greater solubility in ethanol. This gave NMR spectra which corresponded well to those for the chloride salt of **47**.

Preparation of **48.[BPh$_4$]** was performed by addition of an equivalent of sodium tetraphenylborate to an NMR scale reaction of excess hydrazine with FeCl$_2$(PP$_3$) **24** in ethanol. The resulting solid was sufficiently soluble in THF to allow for accumulation of NMR spectra which corresponded well to those for the chloride salt of **47**. Alternative assignments for **48** have been considered and discounted on the following basis. The similarities between the ^{15}N resonances of **^{15}N-47** and **^{15}N-48**, along with the apparent lack of visible ^{15}N-^{31}P coupling to all but the central phosphine P$_C$ led to the discounting of **48** as a dicationic species with a chelating bidentate hydrazine (η^2-) ligand. Likewise, the lack of visible ^{15}N-^{31}P coupling to all but the Pc phosphine led to the positioning of the hydrazine ligand *trans* to this phosphine. This is based on the larger *trans* ^{15}N-^{31}P couplings seen not only in **^{15}N-47** but also in the dinitrogen species **^{15}N-22** and **^{15}N-23**. In addition, the low field position of the P$_U$ resonance relative to P$_T$ is, complex **25**

excepted, common for six coordinate octahedral Fe-PP_3 complexes with a chloride ligand.[4]

3.4.2.3   X-Ray Crystallography of [FeH(N$_2$H$_4$)(PP$_3$)][BPh$_4$] 47.[BPh$_4$]

The structure of **47.[BPh$_4$]** was determined by X-ray crystallographic analysis of the pale yellow crystals isolated during synthesis.
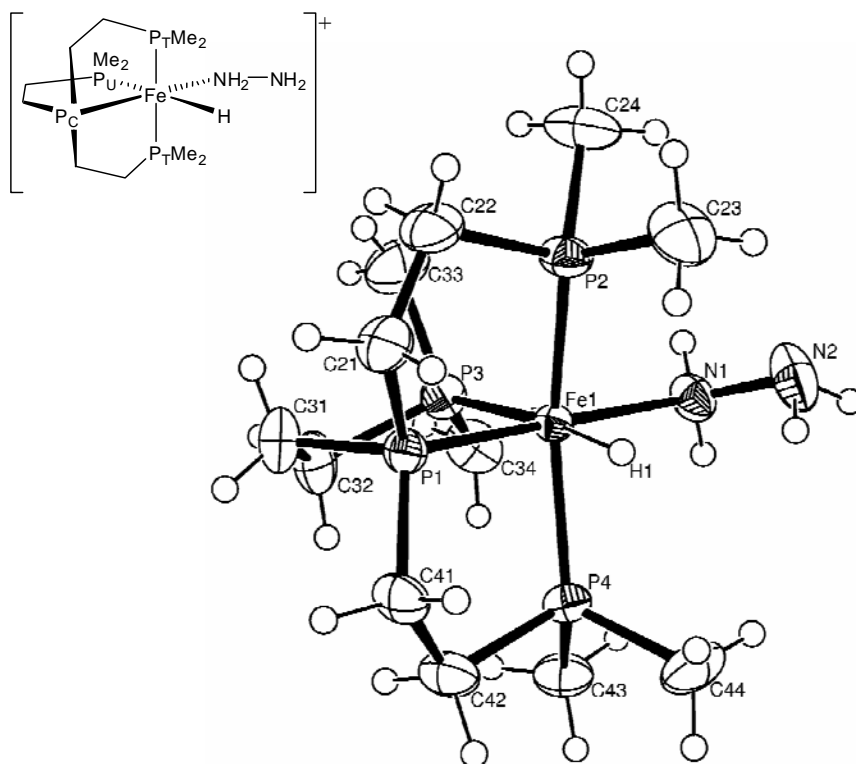
Figure 3.23   ORTEP plot (50% thermal ellipsoids, non-hydrogen atoms) of the complex cation of **47.[BPh$_4$]**.

Selected bond lengths and angles are presented in Tables 3.8 and 3.9 respectively. Further crystallographic data is contained in Appendix 1 (CD format).

Table 3.8 Bond lengths (Å) for [FeH(N$_2$H$_4$)(PP$_3$)][BPh$_4$] **47.[BPh$_4$]**

Fe(1)-P(1)	2.1216(5)	Fe(1)-H(1)	1.529(19)
Fe(1)-P(2)	2.2042(5)	Fe(1)-N(1)	2.0730(16)
Fe(1)-P(3)	2.2196(5)	N(1)-N(2)	1.452(3)
Fe(1)-P(4)	2.1912(5)		

Table 3.9 Bond angles (°) for [FeH(N$_2$H$_4$)(PP$_3$)][BPh$_4$] **47.[BPh$_4$]**

Fe(1)-N(1)-N(2)	115.23(13)	N(1)-Fe(1)-P(1)	177.84(5)
P(2)-Fe(1)-P(1)	86.34(2)	P(3)-Fe(1)-P(1)	86.29(2)
P(4)-Fe(1)-P(1)	85.86(2)	N(1)-Fe(1)-P(2)	92.92(5)
P(3)-Fe(1)-P(2)	104.93(2)	P(4)-Fe(1)-P(2)	153.58(2)
N(1)-Fe(1)-P(3)	95.86(5)	P(4)-Fe(1)-P(3)	99.70(2)
N(1)-Fe(1)-P(4)	93.93(5)	N(1)-Fe(1)-H(1)	91.9(8)
P(1)-Fe(1)-H(1)	86.0(8)	P(2)-Fe(1)-H(1)	77.6(8)
P(3)-Fe(1)-H(1)	171.7(7)	P(4)-Fe(1)-H(1)	76.7(7)

The four phosphorus atoms of the PP$_3$ **1** ligand and the hydrazine and hydride ligands of **47.[BPh$_4$]** are arranged around the iron(II) centre in a distorted octahedron. This distortion is due, in part, to the bite angles of the PP$_3$ ligand which are 86.1° (average) and 86.3° for P$_C$-Fe-P$_T$ and P$_C$-Fe-P$_U$ respectively. The steric bulk of the methyl constituents on the phosphorus atoms combined with the small size of the hydride ligand results in a narrowing of the P-Fe-H angles with these angles being 77.1° (average), 86.0° and 171.7° for P$_T$-Fe-H$_1$, P$_C$-Fe-H$_1$ and P$_U$-Fe-H$_1$ respectively. The Fe-N$_\alpha$-N$_\beta$ bond angle is 115.2° which is slightly larger than the 108° for a perfect tetrahedral sp^3 hybridised arrangement around the N$_\alpha$ atom. The N$_\alpha$-N$_\beta$ length at 1.452 Å is slightly less than that of free hydrazine (1.460 Å).[40]

A search of the Cambridge Structural Database[11, 12] provides no comparative structures with similar co-ligands. However, crystallographic data for the unpublished species *cis*-[Fe(N$_2$H$_4$)H(dmpe)$_2$]Cl[26] **50.Cl** was available and used for comparative purposes.

50.Cl
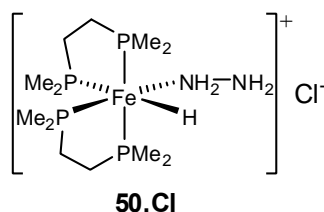
In a similar fashion to **47,** the ligands of **50** are in an approximately octahedral arrangement around the iron(II) centre. The Fe-N$_\alpha$ and N$_\alpha$-N$_\beta$ bond lengths of **50** at 2.095(3) and 1.462(5) Å are slightly longer than those of **47** at 2.0730(16) and 1.452(3) respectively. Likewise, the Fe-N$_\alpha$-N$_\beta$ bond angle of **50** at 117.4(3)° is slightly larger than that of **47** at 115.23(13)°. These small differences most likely reflect the differing characteristics and constraints of the bidentate phosphine ligand compared to the tetradentate ligand in **47** and the different counteranions.

3.4.2.4   [Fe(NH$_3$)Cl(PP$_3$)][BPh$_4$] 49.[BPh$_4$]

Treatment of a red THF solution of FeCl$_2$(PP$_3$) **24** with an ethanol solution of ammonia under argon resulted in an orange suspension, assigned as [Fe(NH$_3$)Cl(PP$_3$)]Cl **49.Cl**. The tetraphenylborate salt of **49** was afforded as a peach coloured powder upon workup of the solution resulting from addition of sodium tetraphenylborate to the suspension of **49.Cl** in THF. The ^{31}P{^{1}H} NMR spectrum of **49.[BPh$_4$]** is presented in Figure 3.24.
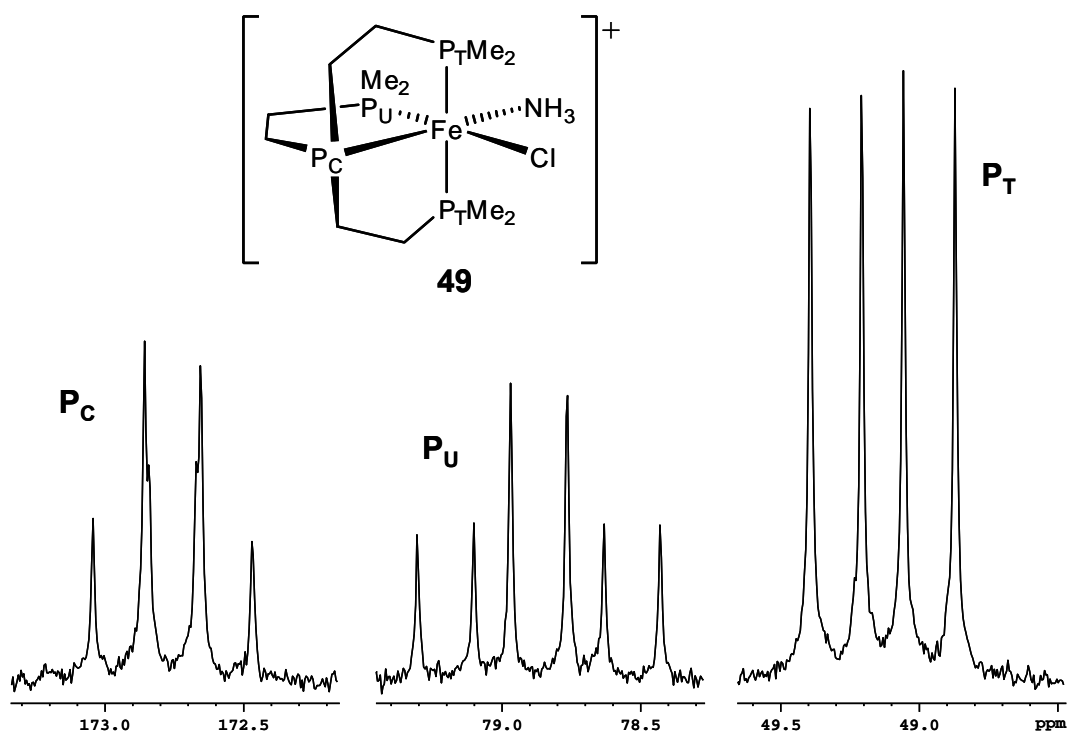
Figure 3.24 ^{31}P$\{^1$H$\}$ NMR spectrum of [Fe(NH$_3$)Cl(PP$_3$)][BPh$_4$] **49.[BPh$_4$]** in THF-d_8.

This spectrum is a very good match for its ^{15}N labelled analogue described in Section 3.4.2.1 less any $^2J_{\text{P-N}}$ coupling. The 3 phosphorus resonances at 172.8, 78.9 and 49.1 ppm are assigned to P$_C$, P$_U$ and P$_T$ respectively on the basis of chemical shift and signal intensity and exhibit coupling constants of 25 Hz for $^2J_{\text{PC-PU}}$, 23 Hz for $^2J_{\text{PC-PT}}$ and 41 Hz $^2J_{\text{PU-PT}}$ respectively. In addition, the ^{1}H-^{15}N 2D HSQC experiment enabled the assignment of ^{1}H and ^{15}N chemical shifts to the ammine ligand at 2.4 and -422 ppm respectively which correspond well with those of ^{15}**N-49** at 2.8 and -420 ppm. The differences in chemical shift between **49** and ^{15}**N-49** are attributed to differences in solvents and solutes present in the two NMR samples.

3.5 Summary of Work on Iron-Nitrogen Complexes of PP$_3$

The known complex cations [Fe(N$_2$)H(PP$_3$)]$^+$ **22** and [(FeH(PP$_3$))$_2$(μ-N$_2$)]$^{2+}$ **23**[3] have been synthesised and **23** further characterised by ^{15}N NMR spectroscopy and X-ray crystallography. The products obtained upon treatment of **23** with base have been identified as the singly deprotonated dinitrogen bridged iron(II)-iron(0) species [(FeH(PP$_3$))(μ-N$_2$)(Fe(PP$_3$))]$^+$ **37**; the doubly deprotonated dinuclear iron(0)-iron(0) species (Fe(PP$_3$))$_2$(μ-N$_2$) **38** and the known mononuclear iron(0) complex Fe(N$_2$)(PP$_3$) **44**.[3] Characterisation of these species has included **37** and **44** by ^{15}N NMR spectroscopy and **37** by X-ray crystallography. Treatment of **22**, **23** and the various deprotonated analogues with acid has not resulted in the detection of ammonium by ^{14}N NMR spectroscopy.

Potential ammine and hydrazine intermediates in any potential reduction of **22** and **23** to yield ammonia have been synthesised. These are the complex cations [Fe(N$_2$H$_4$)H(PP$_3$)]$^+$ **47** and [Fe(NH$_3$)H(PP$_3$)]$^+$ **46**. Characterisation has included ^{15}N NMR spectroscopy and **47** by X-ray crystallography. The ammine and hydrazine complexes [FeCl(N$_2$H$_4$)(PP$_3$)]$^+$ **48** and [FeCl(NH$_3$)(PP$_3$)]$^+$ **49** have also been synthesised. The hydrazine complexes **47** and **48** decompose at room temperature to yield the ammine complexes **46** and **49** respectively. Further work is required to identify other speciation in this reaction.

3.6   References

1.   Hall, D. A.; Leigh, G. J., *J. Chem. Soc., Dalton Trans.* **1996**, (17), 3539-3541.

2.   Leigh, G. J.; Jimenez-Tenorio, M., *J. Am. Chem. Soc.* **1991,** *113*, (15), 5862-3.

3.   Field, L. D.; Messerle, B. A.; Smernik, R. J., *Inorg. Chem.* **1997,** *36*, (26), 5984-5990.

4.   Smernik, R. J., PhD Thesis, University of Sydney, **1996**.

5.   Garrou, P. E., *Chem. Rev.* **1981,** *81*, (3), 229-66.

6.   Atkins, P. W.; Green, J. C.; Green, M. L. H., *J. Chem. Soc., A* **1968**, (9), 2275-80.

7.   Field, L. D.; Messerle, B. A.; Smernik, R. J.; Hambley, T. W.; Turner, P., *Inorg. Chem.* **1997,** *36*, (13), 2884-2892.

8.   Donovan-Mtunzi, S.; Richards, R. L.; Mason, J., *J. Chem. Soc., Dalton Trans.* **1984**, (3), 469-74.

9.   Field, L. D.; Hazari, N.; Li, H. L.; Luck, I. J., *Magn. Reson. Chem.* **2003,** *41*, (9), 709-713.

10. Aylward, G.; Findlay, T., *SI Chemical Data*. 3rd ed.; Jacaranda Wiley Ltd.: Singapore, **1994**.

11. Allen, F. H., *Acta Crystallogr., Sect. B: Struct. Sci.* **2002,** *B58*, (3, 1), 380-388.

12. Bruno, I. J.; Cole, J. C.; Edgington, P. R.; Kessler, M.; Macrae, C. F.; McCabe, P.; Pearson, J.; Taylor, R., *Acta Crystallogr., Sect. B: Struct. Sci.* **2002,** *58*, (3, 1), 389-97.

13. Hazari, A., Unpublished Work, University of Sydney, **2006**.

14. George, T. A.; Rose, D. J.; Chang, Y.; Chen, Q.; Zubieta, J., *Inorg. Chem.* **1995,** *34*, (5), 1295-8.

15. MacBeth, C. E.; Harkins, S. B.; Peters, J. C., *Can. J. Chem.* **2005,** *83*, (4), 332-340.

16. Field, L. D.; Messerle, B. A.; Smernik, R. J.; Hambley, T. W.; Turner, P., *J. Chem. Soc., Dalton Trans.* **1999**, (15), 2557-2562.

17. Field, L. D.; Li, H. L.; Messerle, B. A.; Smernik, R. J.; Turner, P., *J. Chem. Soc., Dalton Trans.* **2004**, (9), 1418-1423.

18. Betley, T. A.; Peters, J. C., *J. Am. Chem. Soc.* **2004,** *126*, (20), 6252-6254.

19. Betley, T. A.; Peters, J. C., *J. Am. Chem. Soc.* **2003,** *125*, (36), 10782-10783.

20. Kandler, H.; Gauss, C.; Bidell, W.; Rosenberger, S.; Buergi, T.; Eremenko, I. L.; Veghini, D.; Orama, O.; Burger, P.; Berke, H., *Chem. Eur. J.* **1995,** *1*, (8), 541-8.

21. Berke, H.; Bankhardt, W.; Huttner, G.; Von Seyerl, J.; Zsolnai, L., *Chem. Ber.* **1981,** *114*, (8), 2754-68.

22. Christina, H.; McFarlane, E.; McFarlane, W., *Polyhedron* **1988,** *7*, (19-20), 1875-9.

23. Hirano, M.; Akita, M.; Morikita, T.; Kubo, H.; Fukuoka, A.; Komiya, S., *J. Chem. Soc., Dalton Trans.* **1997**, (19), 3453-3458.

24. Komiya, S.; Akita, M.; Yoza, A.; Kasuga, N.; Fukuoka, A.; Kai, Y., *J. Chem. Soc., Chem. Commun.* **1993**, (9), 787-8.

25. Sacconi, L.; Di Vaira, M., *Inorg. Chem.* **1978,** *17*, (4), 810-15.

26. Li, H. L., Unpublished Work, University of Sydney, **2004**.

27. Aarnes, H.; Eriksen, A.; Petersen, D.; Rise, F., *J. Exp. Bot.* **2007,** *58*, (5), 929-934.

28. Lundberg, P.; Weich, R. G.; Jensen, P.; Vogel, H. J., *Plant Physiol.* **1989,** *89*, (4), 1380-7.

29. Boncella, J. M.; Coston, C. J.; Cammack, J. K., *Polyhedron* **1991,** *10*, (7), 769-70.

30. Schrock, R. R., *Acc. Chem. Res.* **2005,** *38*, (12), 955-962.

31. Fryzuk, M. D.; Johnson, S. A., *Coord. Chem. Rev.* **2000,** *200-202*, 379-409.

32. Heaton, B. T.; Jacob, C.; Page, P., *Coord. Chem. Rev.* **1996,** *154*, 193-229.

33. Hitchcock, P. B.; Hughes, D. L.; Maguire, M. J.; Marjani, K.; Richards, R. L., *J. Chem. Soc., Dalton Trans.* **1997**, (24), 4747-4752.

34. Coe, B. J.; Glenwright, S. J., *Coord. Chem. Rev.* **2000,** *203*, 5-80.

35. Lagodzinskaya, G. V.; Yunda, N. G.; Manelis, G. B., *Chem. Phys.* **2002,** *282*, (1), 51-61.

36. Wishart, D. S.; Bigam, C. G.; Yao, J.; Abildgaard, F.; Dyson, H. J.; Oldfield, E.; Markley, J. L.; Sykes, B. D., *J. Biomol. NMR* **1995,** *6*, (2), 135-40.

37. Chatt, J.; Fakley, M. E.; Richards, R. L.; Mason, J.; Stenhouse, I. A., *J. Chem. Res., Synop.* **1979**, (10), 322-3.

38. Donovan-Mtunzi, S.; Richards, R. L.; Mason, J., *J. Chem. Soc., Dalton Trans.* **1984**, (7), 1329-32.

39. Schrock, R. R.; Glassman, T. E.; Vale, M. G.; Kol, M., *J. Am. Chem. Soc.* **1993,** *115*, (5), 1760-72.

40. Allen, F. H.; Kennard, O.; Watson, D. G.; Brammer, L.; Orpen, A. G.; Taylor, R., *J. Chem. Soc., Perkin Trans. 2* **1987**, (12), S1-S19.

Chapter 4

Iron and Ruthenium Complexes

4. Synthesis of Iron and Ruthenium Complexes of Tripodal Phosphine Ligands

4.1 Introduction

Selected examples of the successful reduction of dinitrogen at a metal centre are described in Section 1.4.3. Several of these involve the use of constrained polydentate ligands.

The work of Schrock *et al*. describing a catalytic cycle of dinitrogen reduction to ammonia at a molybdenum centre utilises a bulky tripodal tetradentate ligand in a trigonal bipyramidal dinitrogen complex.[1] Peters *et al*. have successfully synthesised an iron nitride species using a tripodal phosphine ligand.[2] In this work the synthesis of iron and ruthenium complexes with tripodal tri or tetradentate phosphine ligands is described. This was done with a view to preparing dinitrogen complexes which could potentially facilitate reduction of the complexed dinitrogen.

4.2 Preparation of Iron Complexes of PP$^i_3$ 12

The ligand $P(CH_2CH_2P(^iPr)_2)_3$, PP$^i_3$, **12** was prepared by the base-catalysed addition of diisopropylphosphine **13** to trivinylphosphine **3** in a reaction analogous to that described in the synthesis of PP$_3$ **1** (Section 2.2).[3]

A series of iron PP$^i_3$ **12** complexes was prepared, including an iron(0) and iron(II) dinitrogen complex. The synthetic route to these complexes is illustrated in Scheme 4.1.
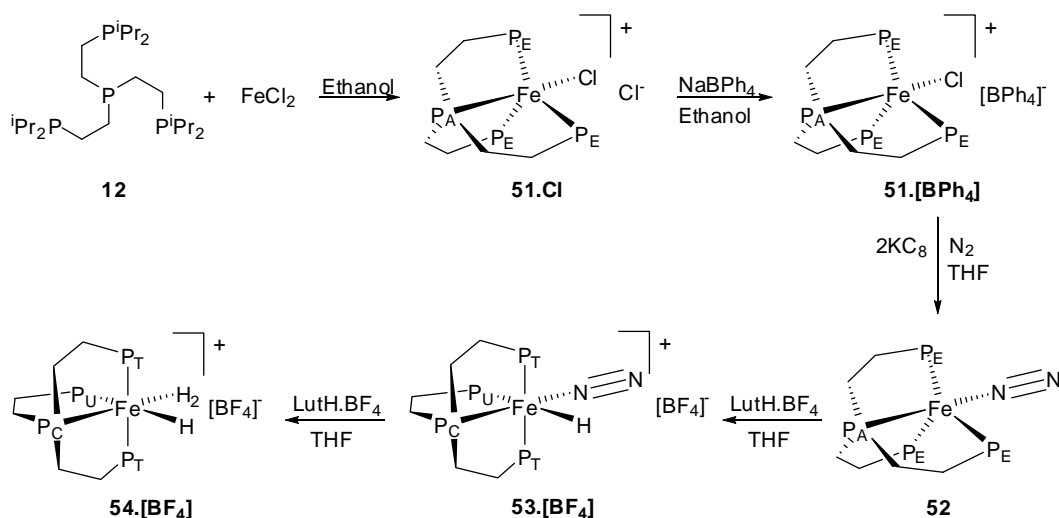
Scheme 4.1

4.2.1 Preparation of [FeCl(PP$^i_3$)][BPh$_4$] 51.[BPh$_4$]

Synthesis of the complex [FeCl(PP$^i_3$)][BPh$_4$] **51.[BPh$_4$]** was performed by addition of an ethanol solution of PP$^i_3$ **12** to one equivalent of iron(II) chloride. This resulted in the immediate formation of a dark violet solution, probably due to the paramagnetic complex **51**. The assignment of a 5-coordinate cationic species, as opposed to the 6-coordinate dichloride, is made based on the existence of similar paramagnetic monochloride complexes of tripodal tetraphosphine ligands with bulky substituents such as phenyl[4] and cyclohexyl[5] groups. After 18 hours, one equivalent of sodium tetraphenylborate was added to the reaction mixture leading to the precipitation of the paramagnetic complex [FeCl(PP$^i_3$)][BPh$_4$] **51.[BPh$_4$]** as a purple powder in high yield (93%). Crystals suitable for analysis by X-ray diffraction were grown by layering a THF solution of **51.[BPh$_4$]** with pentane. The X-ray crystal structure of this complex is discussed in Section 4.2.3.

4.2.2 Preparation of $Fe(N_2)(PP^i_3)$ 52

Synthesis of the iron(0) dinitrogen species **52** was performed using potassium graphite which acts both to abstract the chloride ligand and to reduce the iron centre of **51.[BPh$_4$].** The free ligand site then takes up a dinitrogen ligand from the dinitrogen atmosphere under which the reaction is performed. Potassium graphite (2.2 equivalents) was added to a solution of **51.[BPh$_4$]** in THF and the reaction mixture allowed to stir under dinitrogen for a day. After workup, $Fe(N_2)(PP^i_3)$ **52** was afforded as a dark yellow solid in 52% yield. Crystals suitable for analysis by X-ray diffraction were precipitated from a hot pentane solution of **52** upon cooling. The X-ray crystal structure of this complex is discussed in Section 4.2.3.

The iron(0) species $Fe(N_2)(PP^i_3)$ **52**, unlike its iron(II) precursor **51**, is diamagnetic and has a characteristic splitting pattern in the $^{31}P\{^1H\}$ NMR spectrum for a trigonal bipyramidal complex of a tripodal tetradentate phosphine ligand such as PP^i_3 **12**. This is presented in Figure 4.1. The resonance of the apical phosphine P_A is at relatively low field at 175.8 ppm and presents as a quartet coupled to the 3 equivalent terminal phosphines P_E with a coupling constant of 37 Hz. The three equivalent terminal phosphines P_E present as a doublet at 96.3 ppm due to the P_A phosphine coupling. This signal has three times the intensity of the P_A signal.
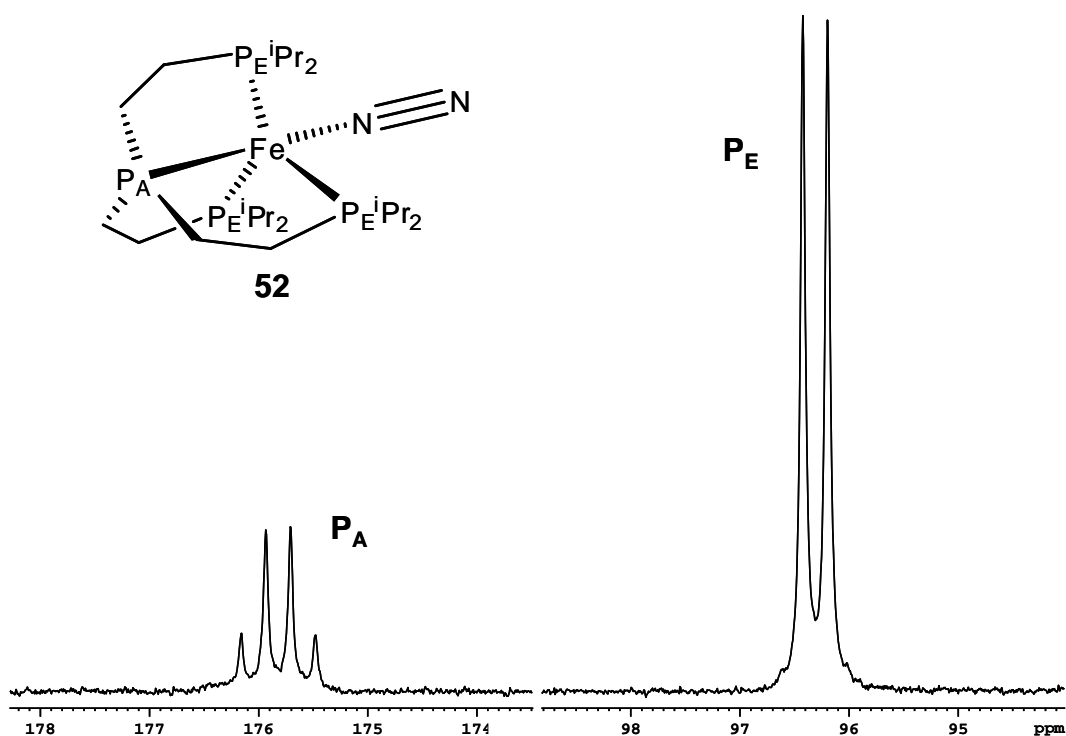
Figure 4.1 $^{31}P\{^1H\}$ NMR spectrum of $Fe(N_2)(PP^i_3)$ **52** in benzene-d_6

^{15}N labelling of complex **52** was achieved by dinitrogen ligand exchange, following the introduction of $^{15}N_2$ gas to a degassed sample of **52** in benzene-d_6. ^{15}N-**52** has a $^{31}P\{^1H\}$ NMR spectrum with chemical shifts similar to those of **52**. The apical phosphine P_A resonance appears as a doublet of quartets with an extra 10 Hz $^2J_{P-N}$ coupling constant. In the ^{15}N NMR spectrum, there is a relatively intense resonance at -71.0 ppm assigned to $^{15}N_2$ and two smaller broad resonances at 18.1 ppm and -18.0 ppm, with equivalent intensities, which are assigned to N_β and N_α respectively on the basis of relative chemical shifts.[6]

4.2.3   X-ray Crystallography of [FeCl(PP$^i_3$)][BPh$_4$] 51.[BPh$_4$] and Fe(N$_2$)(PP$^i_3$) 52.

The crystal structures of $[FeCl(PP^i_3)]^+$ **51** and $Fe(N_2)(PP^i_3)$ **52** are illustrated in Figures 4.2 and 4.3 respectively with selected bond lengths and angles provided in

Tables 4.1 to 4.4. Further crystallographic data is contained in Appendix 1 (CD format).
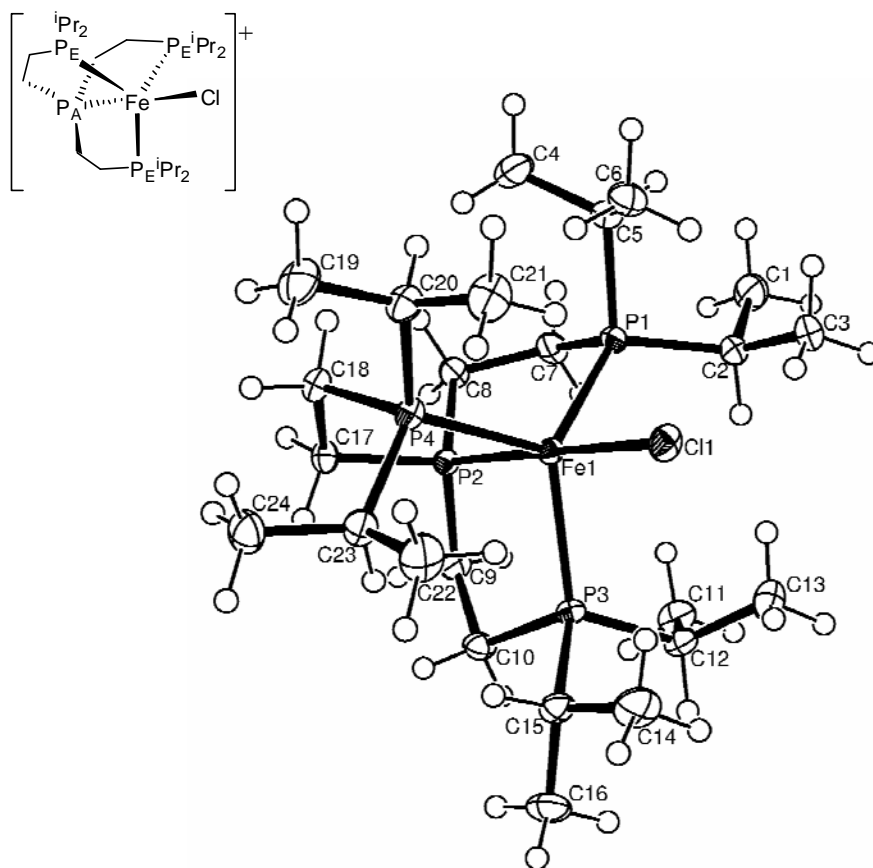
Figure 4.2 ORTEP plot (50% thermal ellipsoids, non-hydrogen atoms) of the complex cation of [FeCl(PP$^i_3$)][BPh$_4$], **51**.

Table 4.1 Selected bond lengths (Å) for [FeCl(PP$^i_3$)][BPh$_4$] **51.[BPh$_4$]**

Fe(1)-Cl(1)	2.2371(3)	Fe(1)–P(1)	2.3694(3)
Fe(1)–P(2)	2.2182(3)	Fe(1)–P(3)	2.3558(3)
Fe(1)–P(4)	2.3940(3)		

Table 4.2 Selected bond angles (º) for [FeCl(PP$^i_3$)][BPh$_4$] **51.[BPh$_4$]**

Cl(1)-Fe(1)-P(2)	178.710(13)	Cl(1)-Fe(1)-P(1)	97.937(12)
Cl(1)-Fe(1)-P(3)	96.524(11)	Cl(1)-Fe(1)-P(4)	98.652(11)
P(2)-Fe(1)-P(1)	82.477(11)	P(2)-Fe(1)-P(3)	82.217(11)
P(2)-Fe(1)-P(4)	82.160(11)	P(1)-Fe(1)-P(3)	119.746(11)
P(1)-Fe(1)-P(4)	120.253(11)	P(3)-Fe(1)-P(4)	114.676(11)
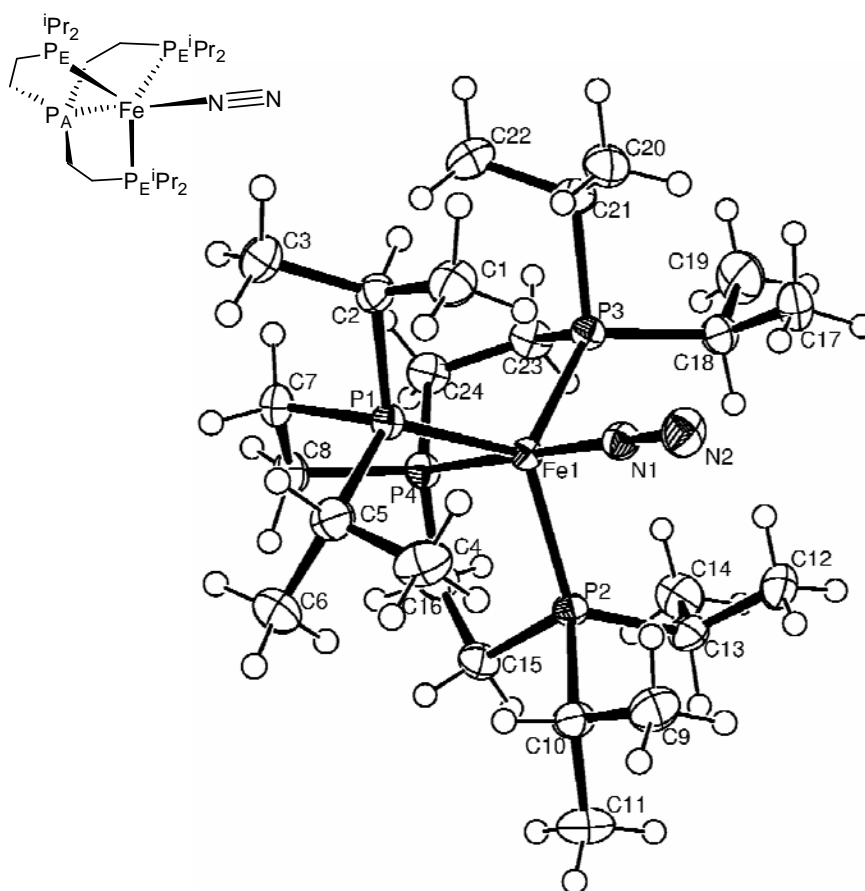
Figure 4.3 ORTEP plot (50% thermal ellipsoids, non-hydrogen atoms) of Fe(N$_2$)(PP$^i_3$) **52**.

Table 4.3 Selected bond lengths (Å) for Fe(N$_2$)(PP$^i_3$) **52**

Fe(1)-N(1)	1.8032(11)	N(1)–N(2)	1.1279(16)
Fe(1)–P(4)	2.1462(4)	Fe(1)–P(1)	2.2185(4)
Fe(1)–P(2)	2.2182(4)	Fe(1)–P(3)	2.2223(4)

Table 4.4 Selected bond angles (º) for Fe(N$_2$)(PP$^i_3$) **52**

Fe(1)-N(1)-N(2)	179.27(12)	N(1)-Fe(1)-P(4)	179.31(4)
N(1)-Fe(1)-P(1)	95.96(4)	N(1)-Fe(1)-P(2)	94.68(4)
N(1)-Fe(1)-P(3)	94.73(4)	P(1)-Fe(1)-P(4)	84.693(15)
P(2)-Fe(1)-P(4)	84.805(16)	P(3)-Fe(1)-P(4)	85.118(15)
P(1)-Fe(1)-P(2)	121.514(15)	P(1)-Fe(1)-P(3)	118.296(15)
P(2)-Fe(1)-P(3)	117.816(14)		

In each case, the 5-coordinate species approximates to a trigonal bipyramid with the monodentate ligand in an axial position. In comparing these structures to the trigonal bipyramidal iron(0) centre of $[(FeH(PP_3)(\mu\text{-}N_2)(Fe(PP_3))]^+$ **37** (Section 3.2.9) the following points are of note. The Fe-P bonds of **51** have an average length of 2.33 Å compared with 2.20 and 2.15 Å for **53** and **37** respectively. This difference reflects the bond lengthening effect of the chloride ligand over the dinitrogen ligand and to a lesser extent that of the isopropyl substituted phosphine ligand **12** over that of the methyl substituted one **1**. The average bite angles, P_A-Fe-P_E, of the tetradentate ligand in the three complexes are 82.3º, 84.9º and 85.2º for **51**, **52** and **37** respectively. The main difference here is due to the large chloride ligand causing a narrowing of the bite angles in complex **51**. When **51** is compared with the PP^{Ph}_3 bromide analogue **42** (Section 3.2.9) there are few differences worthy of note. Small differences in P_E-Fe-P_E angles are apparent due to the larger halide ligand and differing phosphine ligand substituents. The structure of **51** has a high level of correlation in both major bond lengths and angles to the analogous PP^{Cy}_3 chloride $[FeCl(PP^{Cy}_3)]$ $[BPh_4]^5$ $(PP^{Cy}_3 = P(CH_2CH_2P(C_6H_{11})_2)_3)$. The structures of the dinitrogen iron(0) centres **52** and **37** are very similar with the differing phosphine ligands and the bridging iron(II) centre of **37** making little difference. The similarities continue in the N-N triple bond lengths which are 1.13 Å, and the Fe-N bond lengths of 1.80 Å, in each case. The N-N triple bond length indicates modest activation compared to free dinitrogen (1.10 Å).

4.2.4 Preparation of [(Fe(N$_2$)H(PP$^i_3$)][BF$_4$] 53.[BF$_4$]

The result of treating the iron(0) dinitrogen species **52** with one equivalent of the organic acid lutidinium tetrafluoroborate is proposed to be an octahedral iron(II) dinitrogen hydride complex [(Fe(N$_2$)H(PP$^i_3$)]$^+$ **53**. This species is analogous to **22**, the iron(II) dinitrogen hydride species of the PP$_3$ **1** ligand, described in Chapter 3. Immediately after addition of the acid to a THF solution of the dinitrogen complex **52** a red solution forms. This colour persists for a few minutes after which time the solution turns purple. The ^{31}P{^{1}H} NMR spectrum of this purple species, proposed to be **53**, has the three characteristic resonances of an octahedral species of a tripodal tetradentate ligand such as PP$^i_3$ **12**. The ^{31}P{^{1}H} NMR and ^{1}H high field spectra are shown in Figures 4.4 and 4.5 respectively.
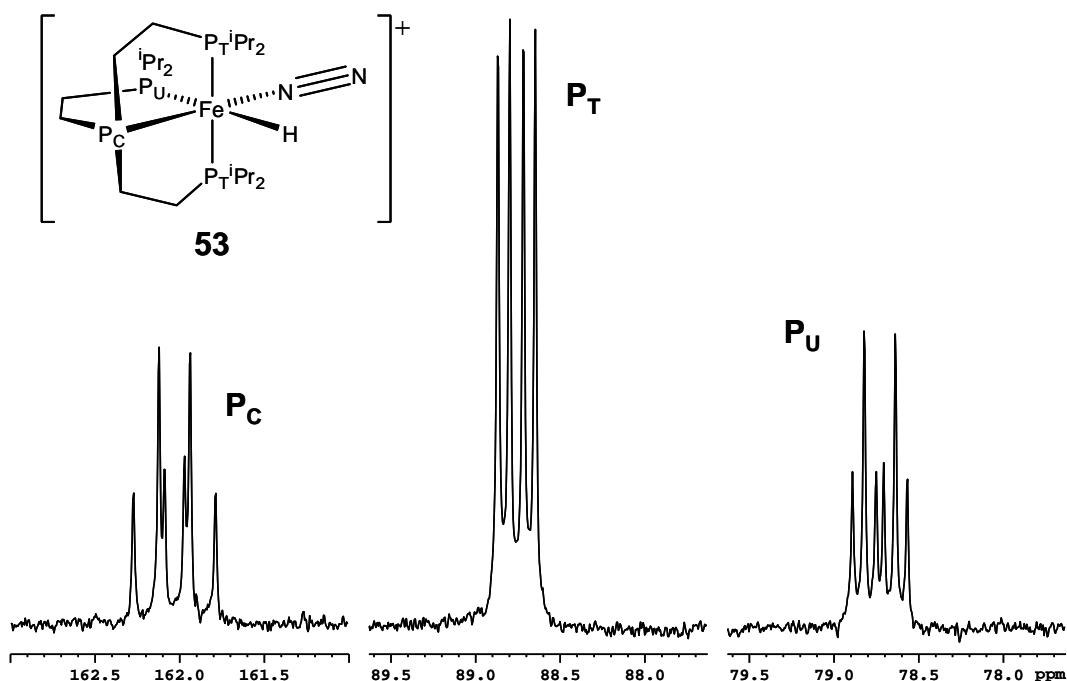
Figure 4.4 ^{31}P{^{1}H} NMR spectrum of [Fe(N$_2$)H(PP$^i_3$)]$^+$ **53** in THF-d_8

The central phosphine P$_C$ signal, at the relatively low field shift of 162.0 ppm, is a doublet of triplets with a coupling constant to P$_U$ and P$_T$ of 29.8 and 24.4 Hz

respectively. The 2 equivalent terminal phosphines P_T have a resonance at 88.8 ppm which presents as a doublet of doublets and has twice the intensity of the signals of P_C and P_U. The coupling constant of P_T to P_U is 11.3 Hz. The resonance of P_U presents as a well resolved doublet of triplets at 78.7 ppm. The coupling constants seen here are similar to those of **22**, the analogous PP_3 **1** species, although the bulkier substituents on the PP^i_3 **12** ligand in **53** lead to significantly different chemical shifts. The P_C signal presents over 10 ppm higher field for **53**, whilst the P_T signal is 26 and the P_U signal 19 ppm lower field in comparison to **22**.
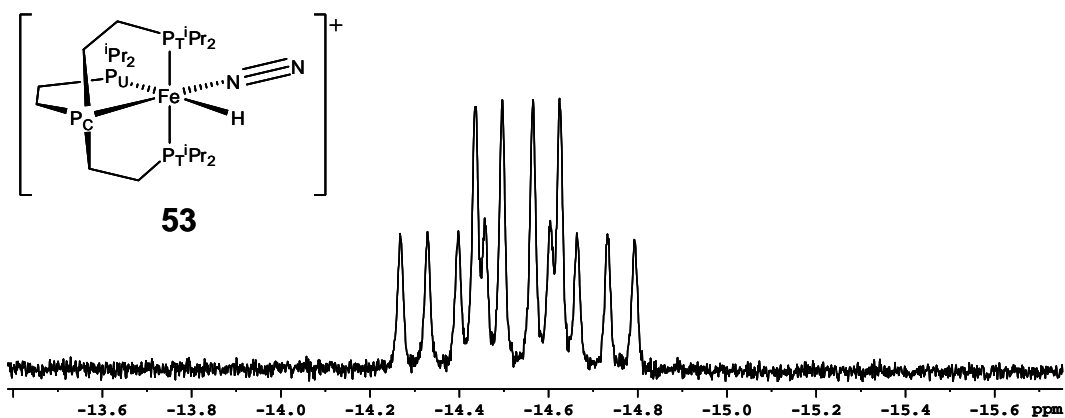
Figure 4.5   High field ^1H NMR spectrum of $[Fe(N_2)H(PP^i_3)]^+$ **53** in THF-d_8

The high field region of the ^1H NMR spectrum presents the characteristic doublet of doublet of triplets resonance of a hydride ligand coupled to the 4 phosphines of the tetradentate ligand. The coupling constants to the phosphines P_C, P_T and P_U are 51.7, 67.2 and 24.4 Hz respectively.

4.2.5   Formation of $[Fe(H_2)H(PP^i_3)][BF_4]$ 54.$[BF_4]$

Treatment of the iron(0) dinitrogen species **52** with 30 equivalents of lutidinium tetrafluoroborate in THF resulted in a red solution which maintained its colour for several hours before turning purple. The $^{31}P\{^1H\}$ NMR spectrum of this reaction

mixture shows the presence of two species. The first set of resonances corresponds with those presented in Figure 4.4 assigned to the dinitrogen hydride species **53.[BF$_4$]**. The second set of resonances are proposed to be those of the molecular hydrogen hydride species [Fe(H$_2$)H(PP$^i_3$)][BF$_4$] **54.[BF$_4$]**. This assignment is based on the differences in the ^{31}P{^{1}H} and ^{1}H NMR spectra when cooled to 200K. These spectra are presented in Figures 4.6 and 4.7.
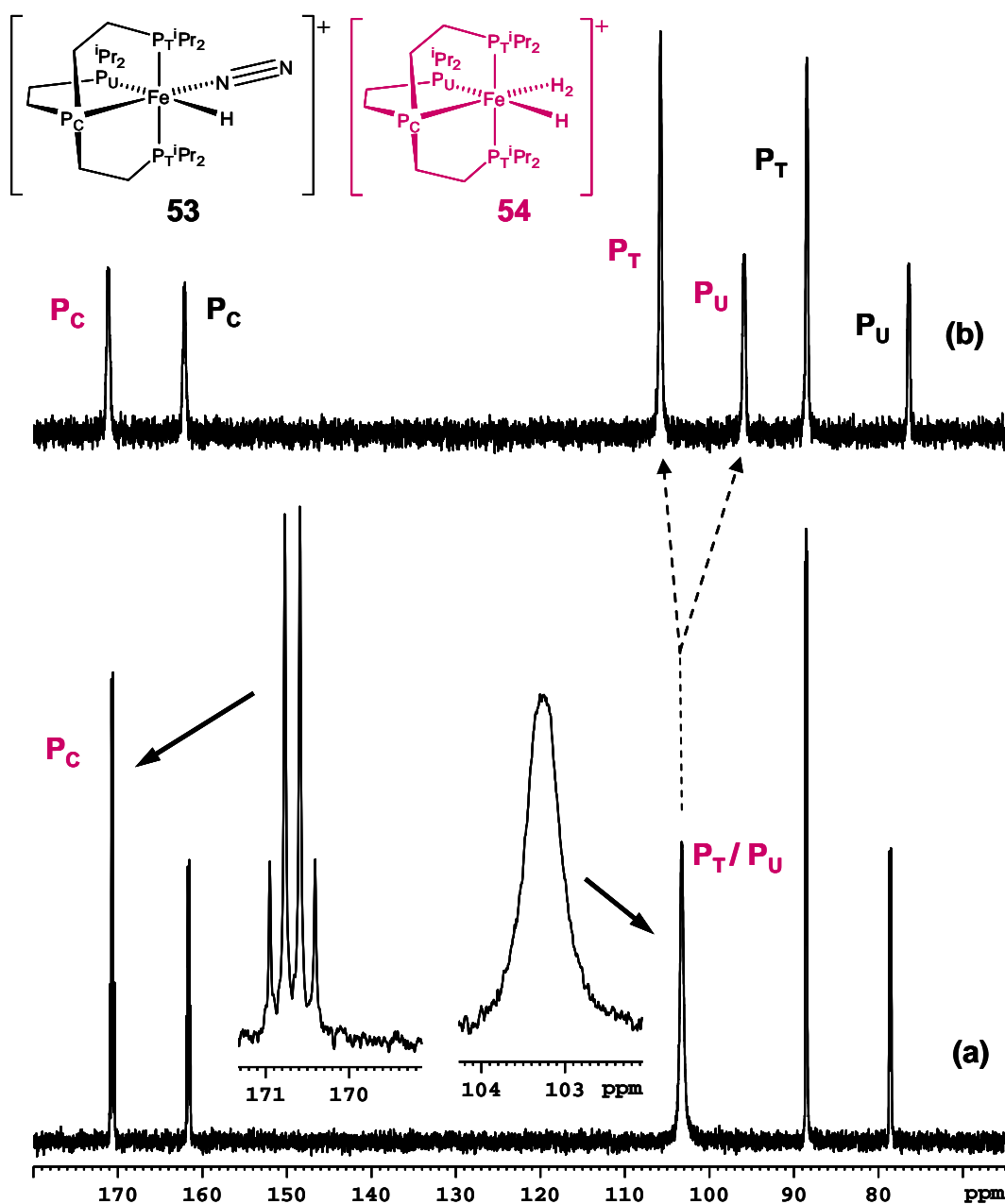
Figure 4.6 ^{31}P{^{1}H} NMR spectrum of [(Fe(N$_2$)H(PP$^i_3$)]$^+$ **53** and [(Fe(H$_2$)H(PP$^i_3$)]$^+$ **54** in THF/THF-d_8 at (a) 300K and (b) 200K.

The $^{31}P\{^1H\}$ NMR spectrum at room temperature presents 5 phosphine resonances. Three of these are assigned, based on their chemical shift and splitting patterns, to $[Fe(N_2)H(PP^i_3)]^+$ **53** as indicated in Figure 4.6. The other two resonances, which present as a quartet at 170.7 ppm and a broad singlet at 103.3 ppm, are assigned to P_C and P_T/P_U respectively of $[Fe(H_2)H(PP^i_3)]^+$ **54**. The terminal phosphines of **54** appear as a broad singlet due to the rapid exchange of the hydride and dihydrogen ligands at this temperature, which in turn exchanges the terminal phosphorus environments. At 200K the rate of exchange has been slowed and the P_T and P_U environments are clearly visible as separate resonances at 105.8 and 95.9 ppm with signal intensities in the ratio of 2:1. The shift of the P_C resonance is not significantly altered by the change in temperature. The splitting patterns of the two species at the lower temperature are not resolved.
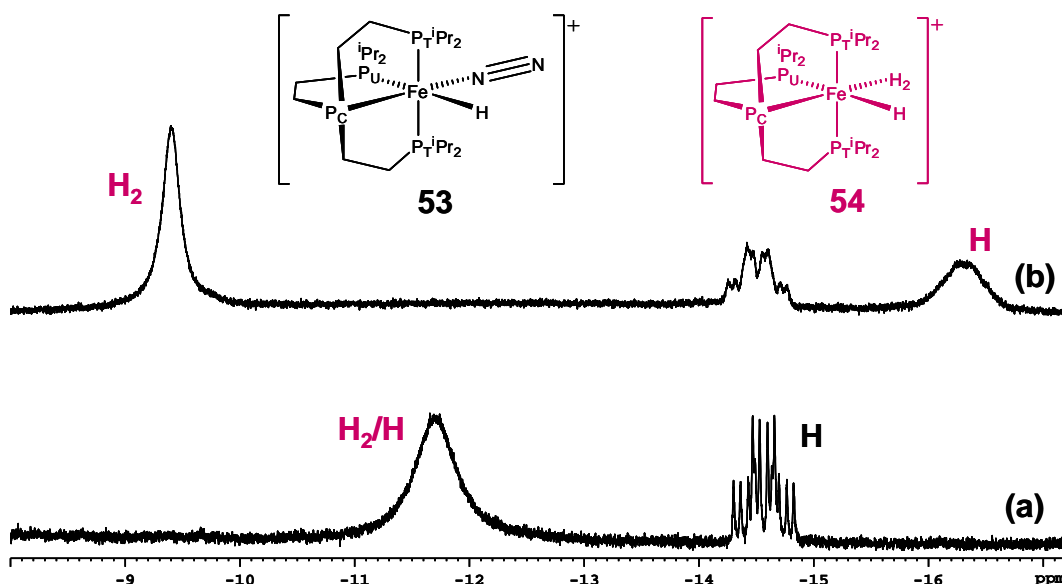
Figure 4.7   High field region of ^1H NMR spectrum of $[Fe(N_2)H(PP^i_3)]^+$ **53** and $[Fe(H_2)H(PP^i_3)]^+$ **54** in THF/THF-d_8 at (a) 300K and (b) 200K.

At 300K the high field region of the ^{1}H NMR spectrum contains the doublet of doublet of triplets signal of the hydride of **53** at $-$ 14.6 ppm, as seen previously in Figure 4.5, and a single broad resonance at -11.7 ppm for the hydride and dihydrogen protons of **54**. The broad appearance of the signal at -11.7 ppm is due to the exchange of the hydride and dihydrogen ligands, a phenomenon that has been reported previously for other dihydrogen hydride species.[7] When cooled to 200K the rate of exchange is slowed and the signals for the dihydrogen and hydride ligands of **54** become distinct. The two new resonances with intensities in the ratio of 2:1 at -9.4 and -16.3 ppm are assigned to the dihydrogen and hydride respectively.

In order for the dihydrogen hydride species **54** to be formed, a source of electrons and/or hydride from the reaction is required. The initial dinitrogen hydride species forms following protonation of the iron(0) centre of the dinitrogen species **52**. In order for an equilibrium between **53** and **54** to be established, as illustrated in Scheme 4.2, dihydrogen is required.
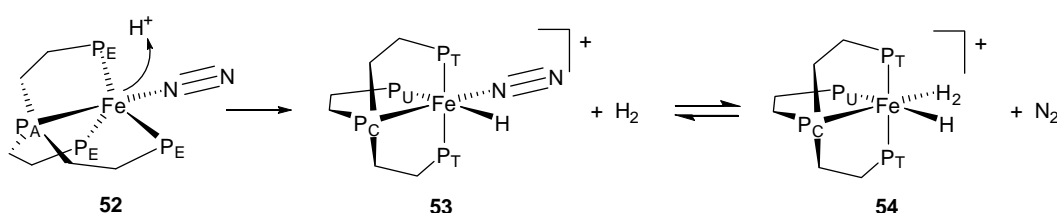
Scheme 4.2

The excess lutidinium tetrafluoroborate is a source of protons. It is proposed that β-hydride elimination from the tetrahydrofuran solvent following C-H activation is the most likely source of hydride for this reaction as illustrated in Scheme 4.3.
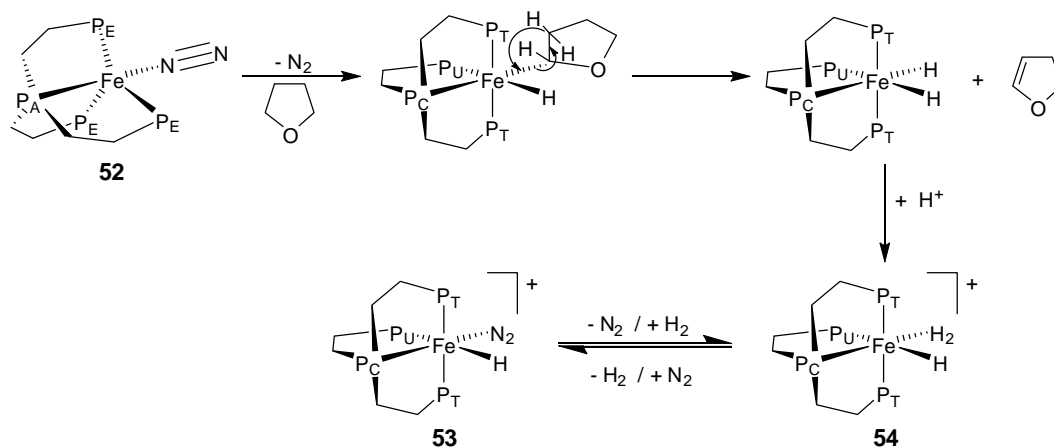
Scheme 4.3

The dihydride intermediate proposed is then protonated to form the molecular hydrogen hydride species **54**.

4.3 Preparation of Ruthenium Complexes of PP$^i_3$ **12**

A series of ruthenium PP$^i_3$ **12** complexes was prepared including a ruthenium(0) and ruthenium(II) dinitrogen complex. The synthetic route to these complexes is illustrated in Scheme 4.4.
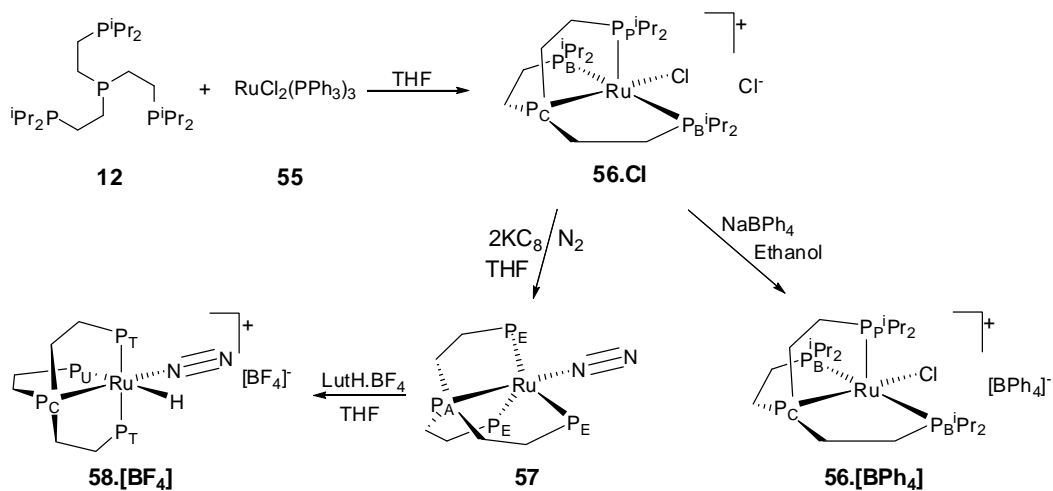
Scheme 4.4

4.3.1 Preparation of [RuCl(PP$^i_3$)]Cl 58.Cl and [RuCl(PP$^i_3$)][BPh$_4$] 58.[BPh$_4$]

Synthesis of the complex [RuCl(PP$^i_3$)][BPh$_4$] **56.[BPh$_4$]** was performed by addition of an equimolar amount of PP$^i_3$ to a THF solution of the ruthenium precursor dichlorotris(triphenylphosphine)ruthenium(II) (RuCl$_2$(PPh$_3$)$_3$) **57**. A red solution formed immediately followed by the precipitation of a cream coloured solid within a matter of minutes. This solid, assigned as [RuCl(PP$^i_3$)]Cl **56.Cl,** was soluble in ethanol. The ^{31}P{^{1}H} NMR spectrum of **56.Cl** is shown in Figure 4.8.
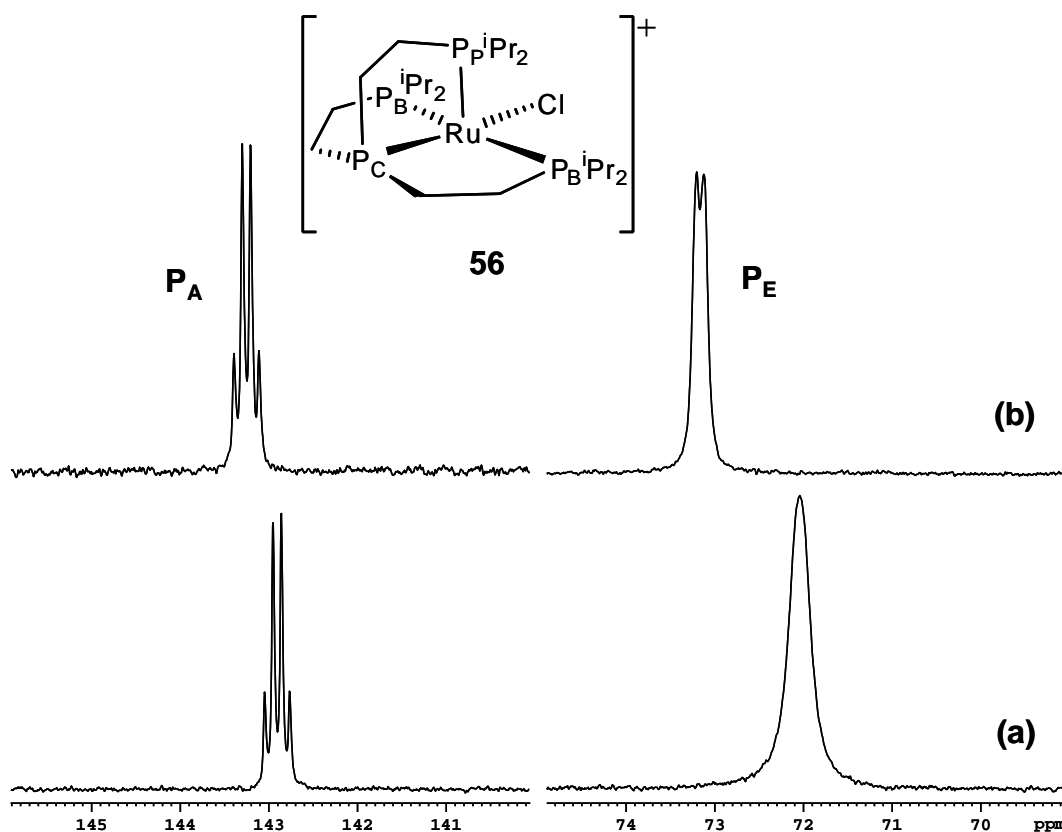
Figure 4.8 ^{31}P{^{1}H} NMR spectrum of [(RuCl(PP$^i_3$)]Cl **56.Cl** in ethanol at (a) 300K and (b) 335K

The structure of this 5-coordinate ruthenium cation has been assigned as that of a distorted square based pyramid based on both NMR spectroscopy and X-ray crystallographic analysis of the tetraphenylborate analogue **56.[BPh$_4$]**. In order to

differentiate between this new configuration and the phosphines of an octahedrally or trigonal bipyramidally arranged complex the terminal phosphine at the pinnacle of the pyramid has been assigned as P_P. The two nominally equivalent terminal phosphines, which are *trans* to each other at the base of the pyramid, are assigned as P_B and the phosphine central to the PP^i_3 ligand as P_C. At 300K the resonances of the central phosphine P_C and the three terminal phosphines P_B/P_P appear as a quartet at 142.9 ppm ($^2J_{P-P}$ = 15.2 Hz) and a broad singlet at 72.1 ppm respectively with signal intensities in the ratio 1:3. At slightly elevated temperatures (335K), there is a modest change in chemical shifts and doublet splitting starts to appear in the P_B/P_P signal. These phenomena have been ascribed to exchange processes which lead to interchange between the three terminal phosphine environments.

Trigonal bipyramid is the more common configuration for 5-coordinate complexes of d^8 electronically configured transition metal centres. The less common 5 coordinate complexes of metal centres with d^6 configuration are best described as square based pyramids. In either case, there is near energetic equality between the two alternative configurations.[8] In 1965, La Placa and Ibers described the X-ray crystallographic structure of the only example of 5-coordinate ruthenium at the time, $RuCl_2(PPh_3)_3$ **55**, as approximating to a square based pyramid.[9] Caulton and Hoffman[8] reviewed the solution structure of this species and showed that at low temperature the $^{31}P\{^1H\}$ NMR presented with inequivalent phosphines, as for the solid state structure. At higher temperatures, the rate of exchange between the phosphorus sites is more rapid and at 303K the spectrum presents as a broadened singlet. A similar process is ascribed here to rationalise

the $^{31}P\{^1H\}$ NMR of $[(RuCl(PP^i_3)]^+$ **56** with the elevated temperature serving to increase the rate of exchange and sharpen the signal of the terminal phosphines as they become equivalent on the NMR time scale. This exchange phenomenon has also been described in the analogous ruthenium complex $[RuCl(PP^{Ph}_3)]^+$ $(PP^{Ph}_3=$ $P(CH_2CH_2PPh_2)_3)$ presenting as an AM_3 spin system in the $^{31}P\{^1H\}$ NMR spectrum at 293K and as an AMQ_2 system, commensurate with square based pyramid geometry, at 163K.[10]

Two further mechanisms which would account for these changes in NMR spectra have been considered. An exchange process involving the outer sphere chloride moving into the inner sphere and out again has been discounted due to the broad nature of the P_B/P_P resonance in the $^{31}P\{^1H\}$ NMR spectrum of **56.[BPh₄]** where there is no second chloride present. Solvent dependent paramagnetism has also been considered. There is precedence in the literature for bidentate phosphine dichloride complexes of iron(II), which are diamagnetic in the solid state, to exhibit a degree of paramagnetism.[11] The paramagnetic character in these complexes is attributed to an equilibrium between a dichloride complex and a dichloride with at least one phosphine decoordinated from the metal centre. Thus, complexes with high and low ligand field strength, leading to both low and high spin configurations, are present in solution. This type of phenomenon would lead to a broadening of resonances in the $^{31}P\{^1H\}$ NMR spectrum, as seen in Figure 4.6, due to partial paramagnetism. At higher temperature the equilibrium could be considered altered such that the high spin configuration is less abundant and the level of paramagnetism is reduced. This would present as a sharpening of the signal in the $^{31}P\{^1H\}$ NMR spectrum as seen. Given that the analogous iron

species **51.Cl** (Section 4.2.1) is paramagnetic in solution this theory has some appeal. However, elements of the second transition series such as ruthenium tend to give low-spin compounds.[12] That is, in the d_6 configuration they are normally diamagnetic. The reasons for this are two-fold: $4d$ orbitals are spatially larger such that double occupation is a lower energy state than for $3d$ orbitals; additionally, a given ligand set produces larger $4d$ orbital splitting than it would $3d$ orbital splitting so that high-spin is a higher energy state for ruthenium than for a given iron analogue.

Addition of one equivalent of sodium tetraphenylborate to an ethanol solution of **56.Cl** results in precipitation of **56.[BPh₄]** as a dark orange solid in 90% yield. The $^{31}P\{^1H\}$ NMR spectrum of **56.[BPh₄]** in acetone-d_6 is very similar to that of **56.Cl** with a P_C resonance at 144.1 ppm presenting as a quartet ($^2J_{P-P}$ = 15.4 Hz) and a P_P/P_B resonance presenting as a broad singlet with 3 times the intensity at 74.0 ppm. Crystals suitable for X-ray diffraction were grown by layering a THF solution of **56.[BPh₄]** with pentane. The crystal structure of this complex, which approximates to a square based pyramid, is discussed in Section 4.3.3.

4.3.2   Preparation of Ru(N₂)(PP^{i}₃) 57

Synthesis of the ruthenium(0) dinitrogen species **57** was performed using potassium graphite to abstract the chloride ligand and reduce the ruthenium centre of **56.Cl**. The free ligand site is then filled by a dinitrogen ligand from the dinitrogen atmosphere under which the reaction is performed. Potassium graphite (2.2 equivalents) was added to a solution of **56.Cl** in THF and allowed to stir under dinitrogen for a day. After workup, Ru(N₂)(PP^{i}₃) **57** was formed as a light

yellow solid in 67% yield. Crystals suitable for analysis by X-ray diffraction were obtained by slow evaporation from a THF solution of **57**. The X-ray crystal structure of this complex is discussed in Section 4.3.3. The $^{31}P\{^1H\}$ NMR spectrum of **57** is shown in Figure 4.9.
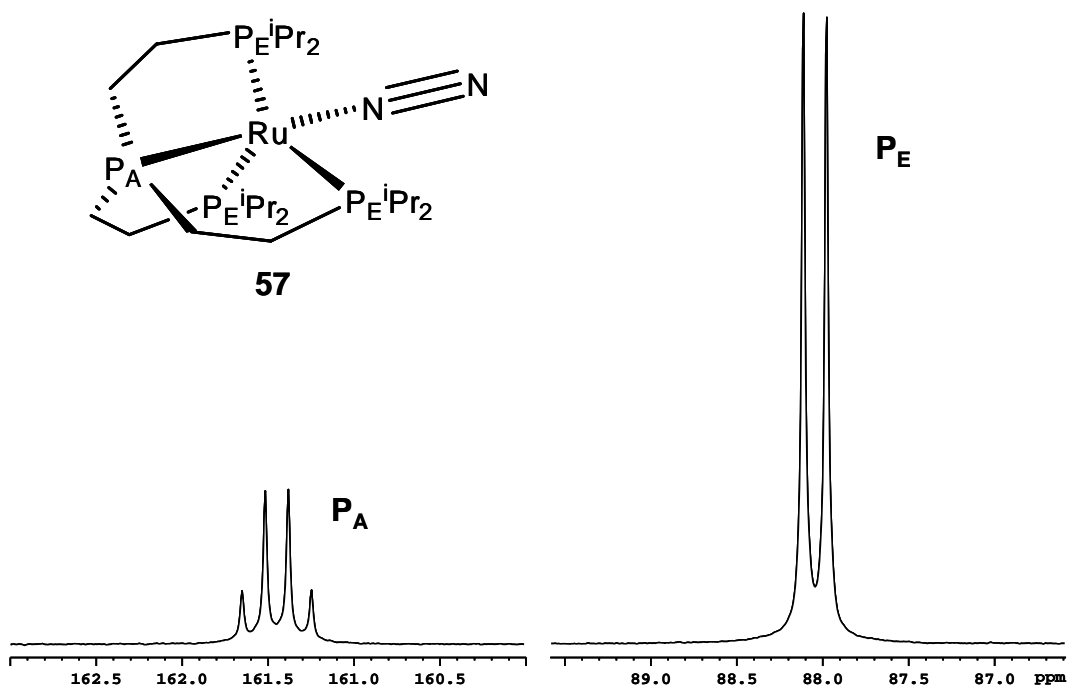
Figure 4.9 $^{31}P\{^1H\}$ NMR spectrum of $Ru(N_2)(PP^i_3)$ **57** in benzene-d_6.

In the $^{31}P\{^1H\}$ NMR spectrum of **57**, the resonances of the apical phosphine P_A and the three equivalent terminal phosphines P_E appear as a quartet at 161.5 ppm ($^2J_{P-P}$ = 21.8 Hz) and a doublet at 88.1 ppm respectively with signal intensities in the ratio 1 to 3. Unlike its precursor **56.Cl,** the signals in the $^{31}P\{^1H\}$ NMR spectrum of **57** are sharp suggestive of a trigonal bipyramidal structure in solution. This is in line with the solid structure discussed in Section 4.3.3.

It was possible to ^{15}N label **57** by exposing a solution of the complex to an atmosphere of $^{15}N_2$ and allowing $^{15}N_2$-**57** to form by exchange of the labile

dinitrogen ligand. The computer enhanced ^{31}P{^{1}H} NMR spectrum of the ^{15}N labelled species illustrated in Figure 4.10 clearly shows the extra couplings of the ^{15}N$_2$ ligand.
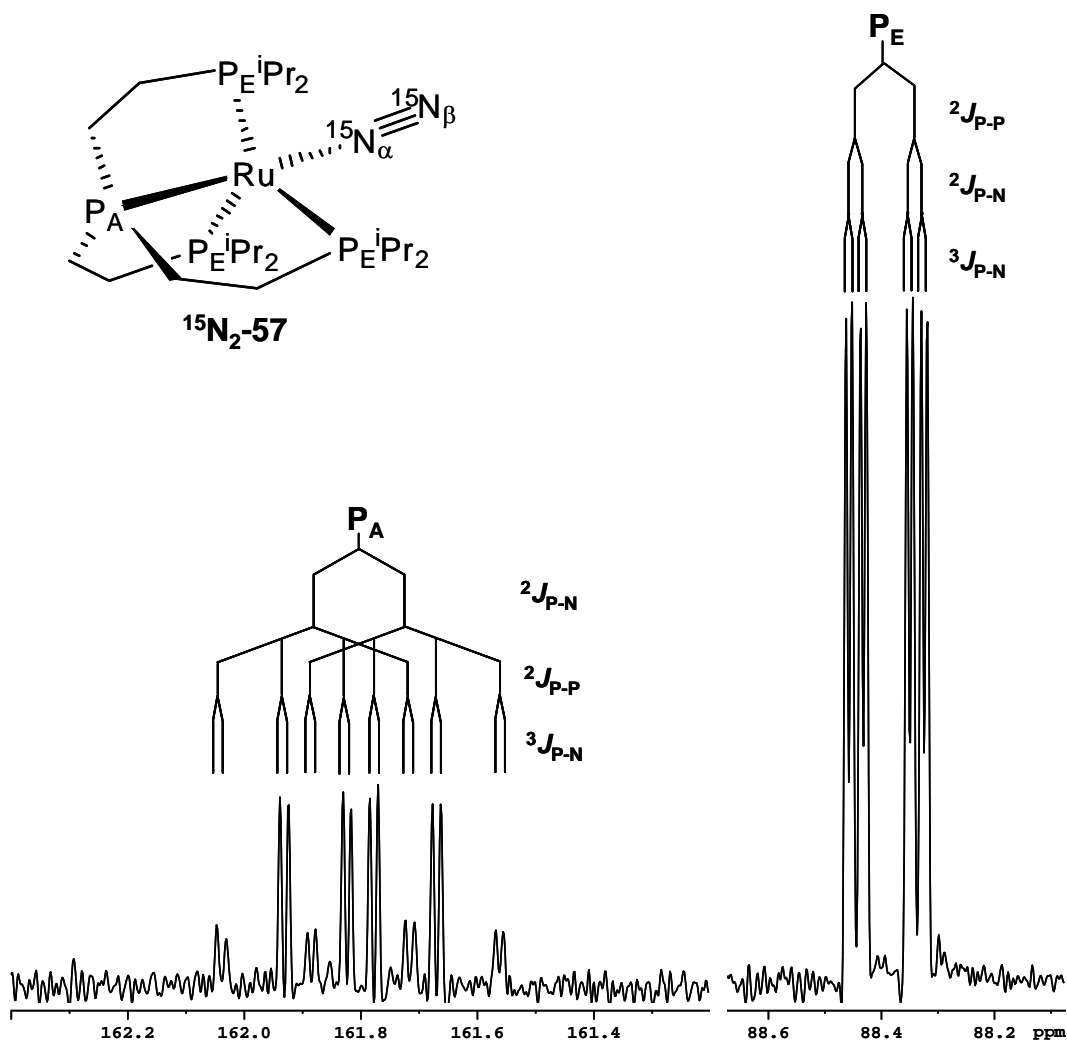
Figure 4.10 Computer enhanced ^{31}P{^{1}H} NMR spectrum of Ru(^{15}N$_2$)(PP$^i_3$) ^{15}N$_2$-**57** in benzene-d_6.

The signal of the apical phosphorus P_A presents as a doublet of doublet of quartets at 161.8 ppm and that of the terminal P_E phosphorus as a doublet of doublet of doublets at 88.4 ppm. The assignment of the ^{31}P-^{15}N coupling constants is based on the assumption that the absolute value of the $^2J_{P-N}$ coupling is larger than the $^3J_{P-N}$ coupling.[6] The $^2J_{P-N}$ coupling constant of the P_A resonance at 31 Hz is

significantly greater than the $^2J_{\text{P-P}}$ coupling constant and an order of magnitude greater than the 3 Hz $^3J_{\text{P-N}}$ coupling constant. This order of magnitude difference between $^2J_{\text{PN}}$ and $^3J_{\text{PN}}$ *trans* coupling constants has been previously noted across the ruthenium centre of a pyrazolyl phosphine complex, namely chloro(triphenylphosphine)bis[bis(1-pyrazolyl)methane]ruthenium(II) chloride,[13] lending weight to the assignment of coupling constants based on size. In contrast, the $^2J_{\text{P-N}}$ and $^3J_{\text{P-N}}$ *cis* coupling constants of the P_E resonance are 5 and 2 Hz respectively.

It was not possible to measure the ^{15}N chemical shifts of **^{15}N$_2$-57** directly, most probably due to fast exchange processes of the weakly bound dinitrogen ligand. The 2D ^{31}P-^{15}N HSQC NMR experiment provided the N_α and N_β chemical shifts as -55.3 and -8.9 ppm respectively. No examples of ruthenium dinitrogen complexes where the resonance of N_β was designated high field with respect to N_α could be found in the literature.[6] The higher field signal was thus assigned to N_α.

4.3.3 X-ray Crystallography of [RuCl(PP$^i_3$)][BPh$_4$] 56.[BPh$_4$] and Ru(N$_2$)(PP$^i_3$) 57

The X-ray crystal structures of [RuCl(PP$^i_3$)].[BPh$_4$] **56.[BPh$_4$]** and Ru(N$_2$)(PP$^i_3$) **57** are illustrated in Figures 4.11 and 4.12 respectively with selected bond lengths and angles provided in Tables 4.5 to 4.8. Further crystallographic data is contained in Appendix 1 (CD format).
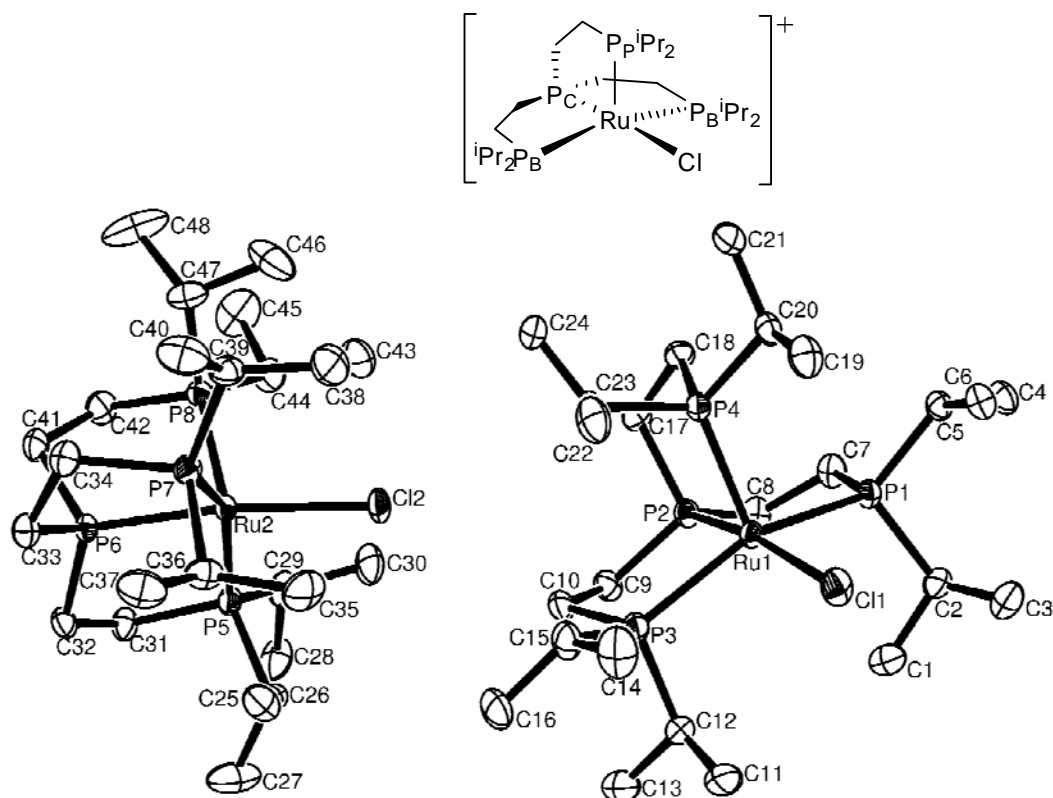
Figure 4.11 ORTEP plot (50% thermal ellipsoids) of the two complex cations of [RuCl(PP$^i_3$)][BPh$_4$], **56**, within each asymmetric unit. Hydrogen atoms have been removed for clarity.

The two structures within the asymmetric unit are sufficiently similar that the crystallographic data of only one of the configurations, namely Ru1, is detailed here. The crystal contains slight disorder around the P8 phosphine arm of the PP$^i_3$ ligand of centre Ru2.

Table 4.5 Selected bond lengths (Å) for [RuCl(PP$^i_3$)][BPh$_4$] **56.[BPh$_4$]**

Ru(1)-Cl(1)	2.4085(6)	Ru(1) –P(2)	2.2321(6)
Ru(1) –P(1)	2.3685(6)	Ru(1) –P(3)	2.3868(6)
Ru(1) –P(4)	2.2533(6)		

Table 4.6   Selected bond angles (°) for [RuCl(PP$^i_3$)][BPh$_4$] **56.[BPh$_4$]**

Cl(1)-Ru(1)-P(2)	167.67(2)	Cl(1)-Ru(1)-P(1)	92.98(2)
Cl(1)-Ru(1)-P(3)	94.91(2)	Cl(1)-Ru(1)-P(4)	110.03(2)
P(2)-Ru(1)-P(1)	83.97(2)	P(2)-Ru(1)-P(3)	82.49(2)
P(2)-Ru(1)-P(4)	82.28(2)	P(1)-Ru(1)-P(3)	151.38(2)
P(1)-Ru(1)-P(4)	99.20(2)	P(3)-Ru(1)-P(4)	103.80(2)

The structure of [RuCl(PP$^i_3$)]$^+$ **56** can be approximated to either a square based

pyramid or a trigonal bipyramid with the P1-Ru1-P3 angle lying between the two

at 151.4 °. However, the Ru1-P4 bond length at 2.25 Å is significantly different to

those of Ru1-P1 and Ru1-P3 both of which are 2.37 Å. For this reason, and those

discussed in Section 4.3.1, the structure has been assigned as a distorted square

based pyramid.
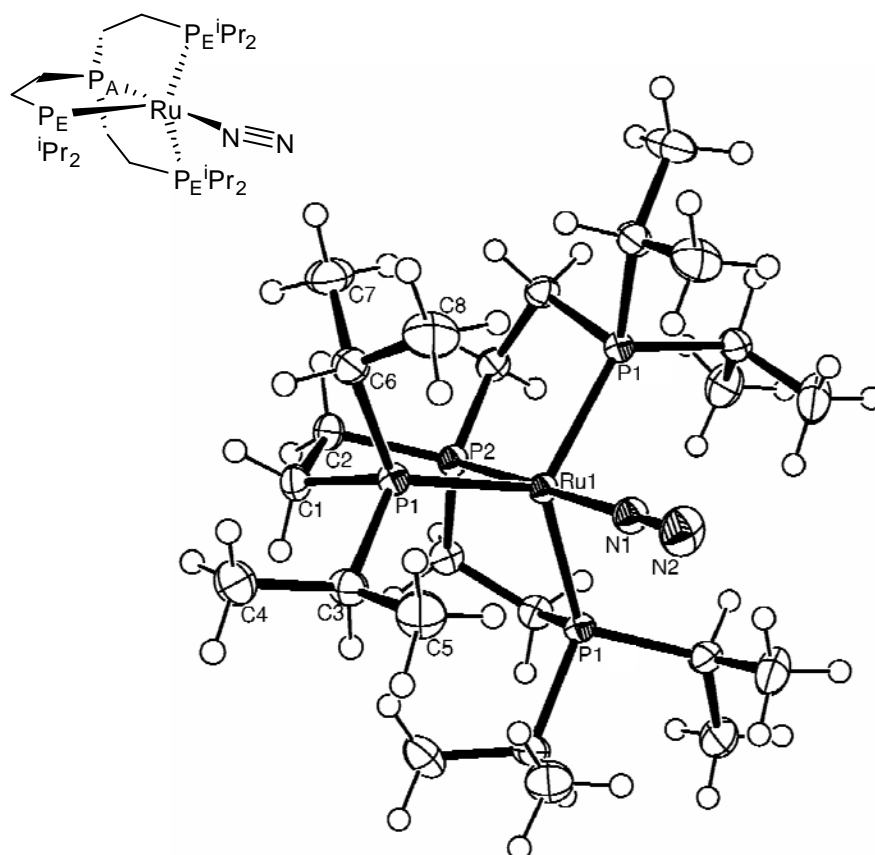
Figure 4.12 ORTEP plot (50% thermal ellipsoids) of Ru(N$_2$)(PP$^i_3$) **57**.

Table 4.7   Selected bond lengths (Å) for $Ru(N_2)(PP^i_3)$ **57**

Ru(1)-N(1)	1.996(3)	N(1)–N(2)	1.109(4)
Ru(1)–P(1)	2.3260(4)	Ru(1)–P(2)	2.2174(8)

Table 4.8   Selected bond angles (º) for $Ru(N_2)(PP^i_3)$ **57**

Ru(1)-N(1)-N(2)	180	N(1)-Ru(1)-P(2)	180
N(1)-Ru(1)-P(1)	96.087(12)	P(1)-Ru(1)-P(2)	83.913(12)
P(1)-Ru(1)-P(1)	118.890(4)		

The structure of $Ru(N_2)(PP^i_3)$ **57** approximates well to a trigonal bipyramid with the three arms of the PP^i_3 ligand being equivalent by symmetry.

A search of the Cambridge Structural Database[14, 15] provides few comparative structures for 5 coordinate species **56** and **57**. Specifically, there are no other examples of ruthenium(0) dinitrogen complexes and no dinitrogen complexes of ruthenium with tripodal phosphine ligands. Three complexes have been identified as suitable for some level of structural comparison. These are the square based pyramid ruthenium(II) complexes $[RuCl(PP^{Ph}_3)][BPh_4]$[10] **59** and $[RuCl_2(PPh_3)_3]$[9] **55** and the ruthenium (II) dinitrogen phosphine complex $[RuCl(N_2)(Diphos)_2](PF_6)$[16] **60** (Diphos = $Ph_2PCH_2CH_2PPh_2$). Selected comparative bond lengths and angles for these structures are presented in Table 4.9
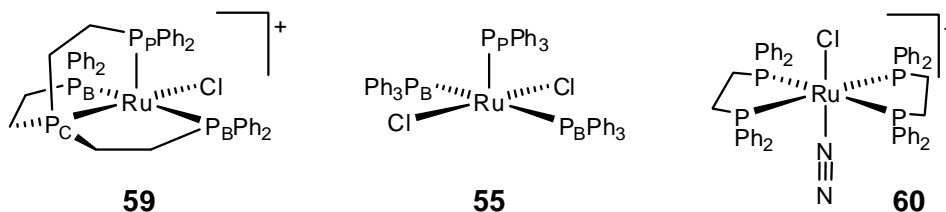
59   **55**   **60**

Table 4.9 Selected bond lengths(Å) and angles(°) of complexes **56**, **57** (this work), **59**,[10] **55**,[9] and **60**.[16]

	56	57	59	55	60
Ru-N/Cl	2.4085(6)	1.996(3)	2.433(3)	2.387(7)	1.96(1) /
				2.388(7)	2.423(4)
N-N		1.109(4)			1.02(1)
Ru-P_P	2.2533(6)		2.216(3)	2.230(8)	
Ru-P_B/P_E	2.3685(6)	2.3260(4)	2.348(3)	2.374(6)	
	2.3868(6)		2.354(3)	2.412(6)	
Ru-P_C	2.2321(6)	2.2174(8)	2.242(3)		
Ru-N-N		180			178.0(1)
P_C-Ru-N/Cl	167.67(2)	180	173.8(1)		
P_B-Ru-P_B	151.38(2)		154.5(1)	156.4(2)	
P_P-Ru-P_B	99.20(2)		97.1(1)	101.1(2)	
	103.80(2)		101.6(1)	104.4(2)	
P_E-Ru-P_E		118.890(4)			
P_C-Ru-P_B/P_E	83.97(2)	83.913(2)	82.9(1)		
	82.49(2)		82.6(1)		
P_C-Ru-P_P	82.28(2)		84.5(1)		

The 3 square based pyramidal structures **56**, **59** and **55** all present a characteristically shorter metal to ligand distance of the pinnacle phosphine P_P than the two base phosphines P_B. The P_B-Ru-P_B angle of **56** at 151.4° is slightly narrower than those of **59** and **55** at 154.5° and 156.4° respectively. The polydentate ligand appears to have a restrictive effect on this angle, the isopropyl substituted PP^i_3 of **56** more so than the phenyl substituted PP^{Ph}_3 ligand of **59**. A further significant difference between **56** and **59** is the central phosphine to chloride angle P_C-Ru-Cl which at 167.7 ° is more acute in **56** than it is in **59** where this angle is 173.8°. The dinitrogen bond length of **60** at 1.0 Å is shorter than that of free dinitrogen (1.1 Å). In contrast, the N-N bond length of the ruthenium(0)

complex **57** approximates to that of free dinitrogen. This lack of activation of the dinitrogen ligand of **57** suggests weak coordination which is in line with the facile displacement of this ligand by $^{15}N_2$ described in Section 4.3.2.

4.3.4 Preparation of [(Ru(N$_2$)H(PP$^i_3$)][BF$_4$] 58.[BF$_4$]

The result of treating the ruthenium(0) dinitrogen species **57** with one equivalent of the organic acid lutidinium tetrafluoroborate is formation of the octahedral ruthenium(II) dinitrogen hydride complex $[Ru(N_2)H(PP^i_3)]^+$ **58**. This species is analogous to the iron(II) dinitrogen hydride species **53** described in Section 4.2.4. Immediately after addition of the acid to a THF solution of the dinitrogen complex **57,** a green solution forms. This colour persists for a few minutes after which time the solution turns yellow. Crystals suitable for analysis by X-ray diffraction were obtained by layering a THF solution of **58.[BF$_4$]** with pentane. The X-ray crystal structure of this complex is discussed in Section 4.3.5.

The $^{31}P\{^1H\}$ NMR spectrum of **58.[BF$_4$]** has the three characteristic resonances of an octahedral complex of a tripodal tetradentate ligand such as PP$^i_3$ **12**. The high field region of the ^1H NMR spectrum presents a multiplet hydride resonance coupled to the phosphines of the tetradentate ligand. These spectra are shown in Figures 4.13 and 4.14.
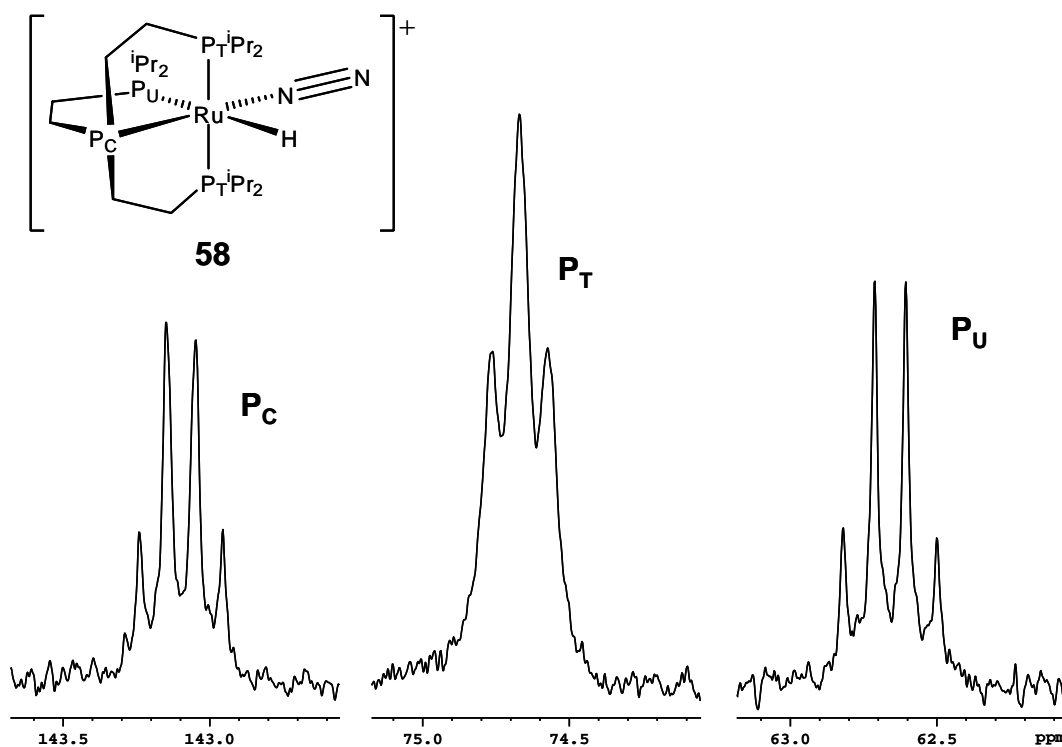
Figure 4.13 ^{31}P{^{1}H} NMR (122 MHz, 298K) spectrum of [RuH(N$_2$)(PP$^i_3$)][BF$_4$] **58.[BF$_4$]** in THF-d_8.

The ^{31}P{^{1}H} resonances, which have intensities in the ratio of 1:2:1 (P$_C$:P$_T$:P$_U$), have been assigned based on chemical shift (low field resonance assigned as P$_C$) and signal intensity. The splitting patterns are not fully resolved but are consistent with the doublet of triplets, doublet of doublets and doublet of triplets of an octahedrally arranged complex for P$_C$, P$_T$ and P$_U$ resonances respectively. This appears to be due to the very close (12.8 – 13.0 Hz) coupling constants of P$_C$ and P$_T$ with P$_U$. Spectra collected at 162 MHz show a broadening of the resonances accompanied by a loss of resolution. It is proposed that this is due to an exchange process, which involves de-coordination and coordination of one or more of the ligands/ donor atoms, occurring on a timeframe coincidental with that of the higher frequency NMR experiment.
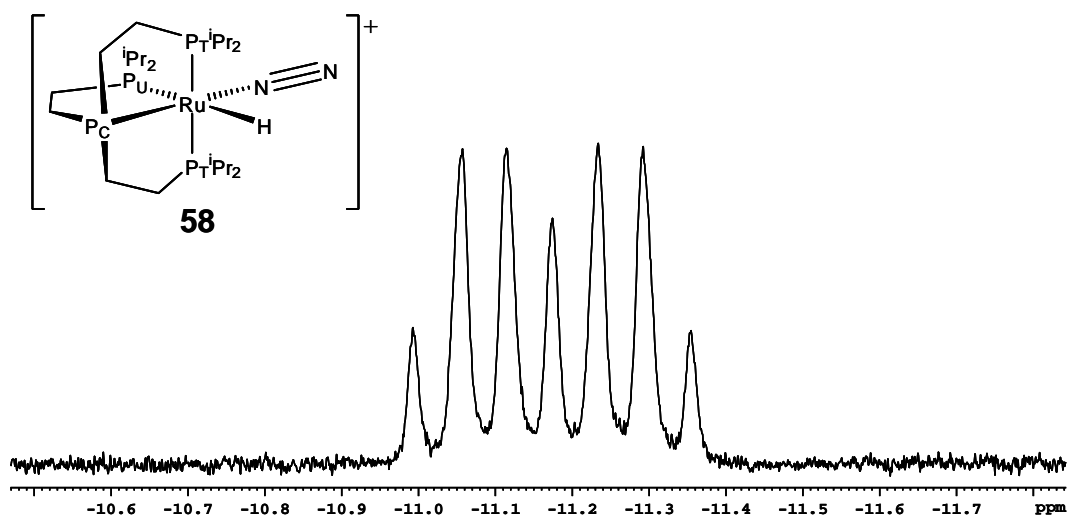
Figure 4.14 High field region of ^{1}H NMR spectrum of $[RuH(N_2)(PP^i_3)][BF_4]$ **58.[BF$_4$]** in THF-d_8.

4.3.5 X-ray Crystallography of $[Ru(N_2)H(PP^i_3)][BF_4]$ 58.[BF$_4$]

The crystal structure of $[Ru(N_2)H(PP^i_3)][BF_4]$ **58.[BF$_4$]** is illustrated in Figure 4.15 with selected bond lengths and angles provided in Tables 4.10 and 4.11. Further crystallographic data is contained in Appendix 1 (CD format).

Table 4.10 Selected bond lengths (Å) for $[Ru(N_2)H(PP^i_3)][BF_4]$.THF **58.[BF$_4$]**

Ru(1)-N(1)	2.022(4)	N(1)-N(2)	1.092(4)
Ru(1)-P(4)	2.4236(11)	Ru(1) –P(1)	2.3538(12)
Ru(1) –P(2)	2.2522(12)	Ru(1) –P(3)	2.3523(12)
Ru(1) –H(1)			

Table 4.11 Selected bond angles (º) for $[Ru(N_2)H(PP^i_3)][BF_4]$.THF **58.[BF$_4$]**

Ru(1)-N(1)-N(2)	178.7(4)	N(1)-Ru(1)-P(2)	178.91(10)
N(1)-Ru(1)-P(1)	95.30(10)	N(1)-Ru(1)-P(3)	96.44(10)
N(1)-Ru(1)-P(4)	97.95(10)	P(1)-Ru(1)-P(3)	149.67(4)
P(1)-Ru(1)-P(2)	83.98(4)	P(1)-Ru(1)-P(4)	105.24(4)
P(2)-Ru(1)-P(3)	83.82(4)	P(2)-Ru(1)-P(4)	83.03(4)
P(3)-Ru(1)-P(4)	100.70(4)		
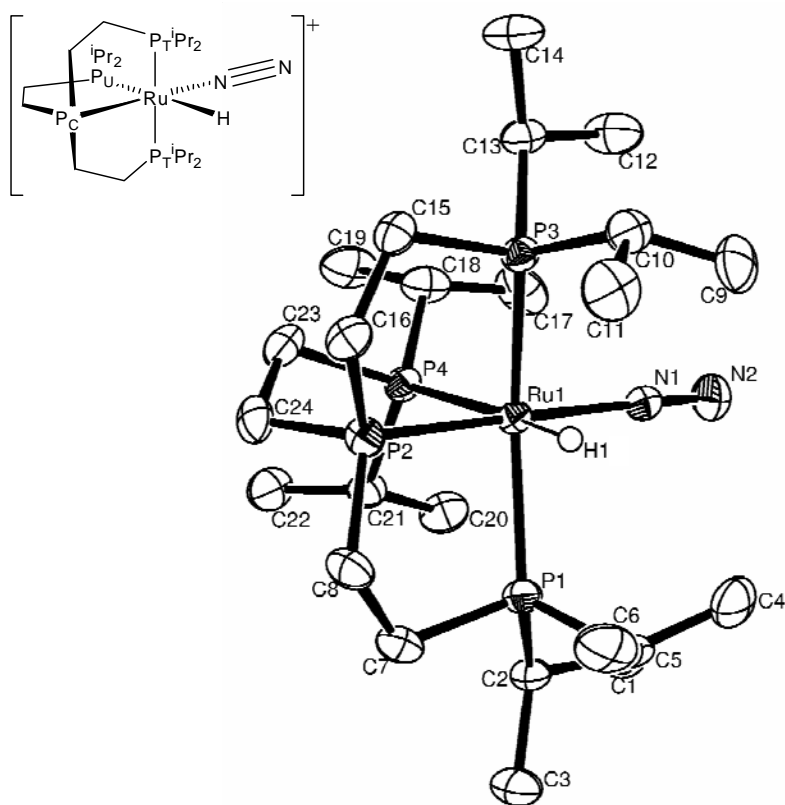
Figure 4.15 ORTEP plot (50% thermal ellipsoids) of the complex cation of $[Ru(N_2)H(PP^i_3)][BF_4].THF$, **58**. Hydrogen atoms (excepting the hydride ligand) have been removed for clarity.

A search of the Cambridge Structural Database[14, 15] provides a selection of comparative structures for the octahedrally arranged ruthenium(II) dinitrogen hydride cation $[Ru(N_2)H(PP^i_3)]^+$ **58.** However, none have all three features sought, namely, a tripodal tetradentatate phosphine, a dinitrogen and a hydride ligand. The species $[RuCl(N_2)(Diphos)_2][PF_6]$[16] **60** described in Section 4.3.3 is the only crystallographically analysed ruthenium dinitrogen species. Four further octahedrally arranged ruthenium(II) complexes of tripodal phosphine ligands, 3 also having a hydride ligand, are presented here. These are $RuH(CCPh)(PP^{Ph}_3)$[17] **61** $(PP^{Ph}_3 = P(CH_2CH_2PPh_2)_3)$, $[Ru(H_2)H(PP^{Ph}_3)][BPh_4].0.5THF$[18] **62,** $[Ru(NCMe)H(NP^{Ph}_3)][BPh_4].(C_6H_6)$[19] $(NP^{Ph}_3 = N(CH_2CH_2PPh_2)_3)$ **63,** and

$RuCl_2((NP^{Ph}_3)^{20}$ **64**. Comparative bond lengths and angles for these structures are presented in Table 4.12.
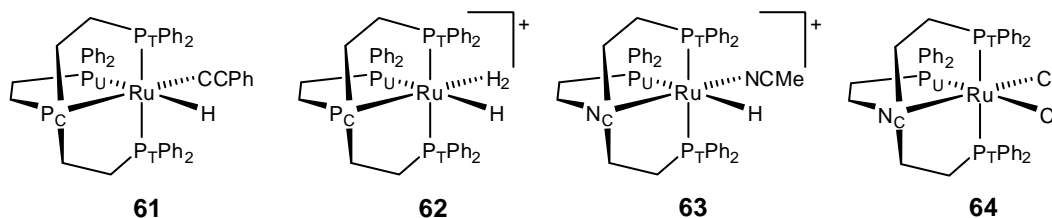
61   **62**   **63**   **64**

Table 4.12   Selected bond lengths(Å) and angles(°) of complexes **58** (this work), **61**,[17] **62**,[18] **63**,[19] and **64**.[20]

	58	61	62	63	64
Ru-P$_C$/N$_C$	2.2522(12)	2.228(2)	2.249(3)	2.169(4)	2.188(7)
Ru-P$_T$	2.3538(12)	2.298(2)	2.350(3)	2.2835(14)	2.346(2)
	2.3523(12)	2.298(2)	2.334(4)	2.2983(15)	2.355(2)
Ru-P$_U$	2.4236(11)	2.335(2)	2.369(3)	2.3386(14)	2.254(2)
Ru-H	1.50(4)	1.57(8)			
P$_C$/N$_C$-Ru-P$_T$	83.98(4)	84.29(8)	84.3(1)	84.42(11)	82.68(19)
	83.82(4)	83.70(8)	83.5(1)	83.86(11)	84.55(19)
P$_C$/N$_C$-Ru-P$_U$	83.03(4)	84.72(9)	84.5(1)	84.04(11)	84.5(2)
P$_T$-Ru-P$_T$	149.67(4)	152.58(8)	153.9(1)	149.34(5)	163.56(8)
P$_T$-Ru-P$_U$	105.24(4)	98.67(8)	100.3(1)	102.70(5)	92.61(8)
	100.70(4)	104.67(8)	99.1(1)	104.13(5)	96.44(9)
P$_C$/N$_C$-Ru-H	86.3(14)	92(3)			
P$_T$-Ru-H	75.1(14)	75(3)			
	76.5(14)	81(3)			
P$_U$-Ru-H	169.2(14)	173(3)			

Despite their significant structural differences the Ru-N bond length of **58** at 2.02 Å is close to that of **60** at 1.96 Å whilst the N-N length at 1.09 Å is slightly longer for **58** than it is for **60** (1.0 Å) and is within the uncertainty range for that of the ruthenium(0) species **57**. The Ru-H bond lengths for **58** and **61** are the same,

within statistical uncertainty, at 1.5 Å. The geometry of **58** is distorted from octahedral with bond angles and lengths similar to those of **61**, **62** and **63**. In each case, the P_T-Ru-P_T angle is significantly less than the idealised 180° as the terminal phosphines with bulky substituents arrange themselves to occupy the space available due to the size of the hydride ligand. Likewise, the P_T-Ru-P_U angles are significantly greater than 90°. The terminal phosphine angles are much closer to those of an ideal octahedron in **64** than in **58** due to the bulky chloride ligands in the former constraining the movement of the phosphines.

4.4   Preparation of a Ruthenium Complex of $P^3P^i_3$ 11

The isopropyl substituted tetradentate phosphine ligand $P(CH_2CH_2CH_2P(^iPr)_2)_3$, $P^3P^i_3$, **11** was prepared by nucleophilic displacement of the bromides of tris(3-bromopropyl)phosphine **16** with lithium diisopropylphosphide **18**. This synthesis is described in Section 2.4.

4.4.1   Preparation of [RuCl($P^3P^i_3$)][BPh$_4$] 65.[BPh$_4$]

Synthesis of the complex [RuCl($P^3P^i_3$)][BPh$_4$] **65.[BPh$_4$]** was performed by addition of one equivalent of the ligand $P^3P^i_3$ **11** to a solution of dichlorotris(triphenylphosphine)ruthenium(II) **55** in THF. This resulted in the immediate formation of a green solution containing most likely [RuCl($P^3P^i_3$)]Cl or RuCl$_2$($P^3P^i_3$). Addition of a stoichiometric amount of sodium tetraphenylborate resulted in the slow appearance of a red solution of [RuCl($P^3P^i_3$)][BPh$_4$] **65.[BPh$_4$]** which, after workup, was obtained as a pink solid in 53% yield. The ^{31}P{^{1}H} NMR spectrum of **65.[BPh$_4$]** is presented in Figure 4.16. Crystals suitable for analysis by X-ray diffraction were grown by layering a THF solution

of **65.[BPh4]** with pentane. The X-ray crystal structure of this complex is discussed in Section 4.4.2.
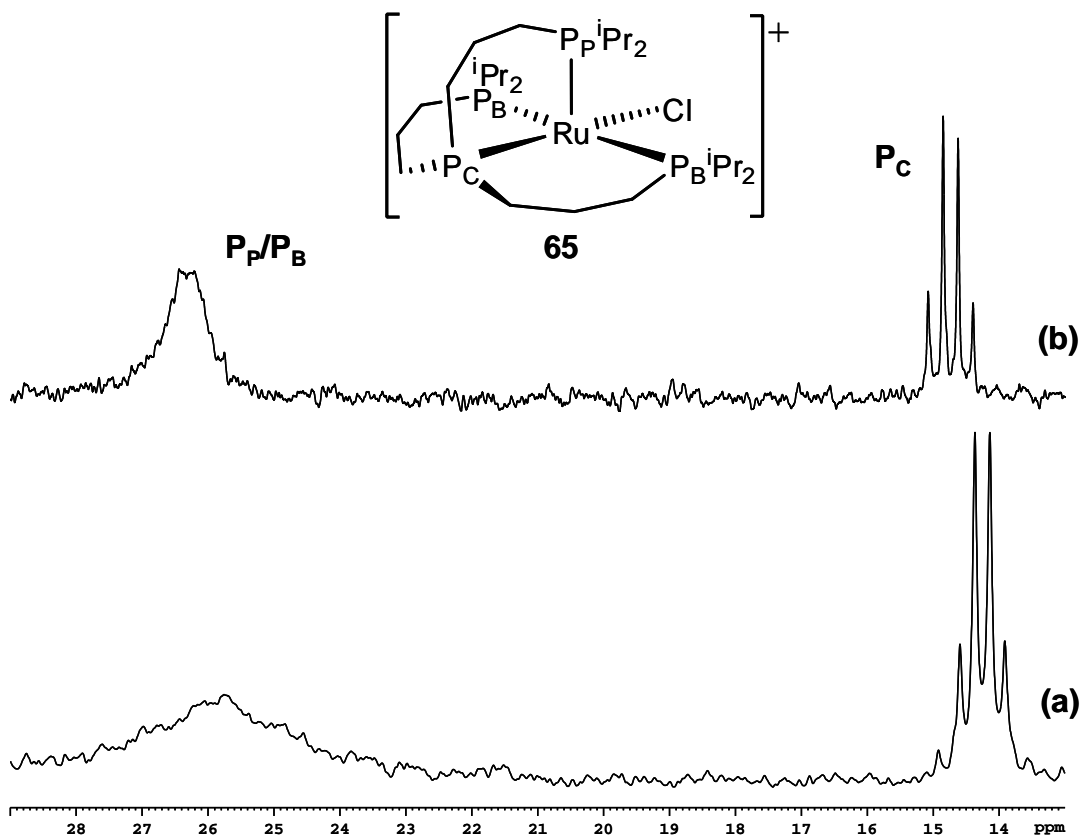
Figure 4.16 $^{31}P\{^1H\}$ NMR spectra of [RuCl(P^{3}P$^i_3$)][BPh4] **65.[BPh4]** in THF-d_8 at (a) 300K and (b) 325K

The $^{31}P\{^1H\}$ NMR spectrum of **65.[BPh4]** presents the three terminal phosphines P$_B$/P$_P$ as a very broad resonance at 25.7 ppm with the central phosphine P$_C$ signal showing as a quartet at 14.2 ppm with a $^2J_{P-P}$ coupling constant of 36.4 Hz. A modest increase (25K) in the temperature of the NMR experiment resulted in an appreciable sharpening of these resonances as illustrated in Figure 4.16. These spectra are analogous to those of [RuCl(PP$^i_3$)][BPh4] **56.[BPh4]**, illustrated in Figure 4.8, Section 4.3.1, and are similarly explained by the facile exchange of the terminal phosphine environments. This exchange results in the complex rapidly switching between square based pyramid and trigonal bipyramid geometry in

solution. At the higher temperature the exchange processes are faster and the averaging of the phosphine environments on an NMR timescale results in a sharpening of the signals. This proposition is supported by a crystal structure which is nominally square based pyramid but in fact lies somewhere between the two conformations. It is interesting to note that the central phosphine P_C resonance is now high field with respect to the terminal phosphine P_B/P_P signals. This reversal in relative chemical shifts from that of **56.[BPh$_4$]** is most likely due to the less strained environment of the central phosphine P_C of the 3-carbon armed, isopropyl substituted ligand $P^3P^i_3$ **11** when complexed to the ruthenium centre of **65**.

4.4.2 X-ray Crystallography of [RuCl(P^{3}P$^i_3$)][BPh$_4$] 65.[BPh$_4$]
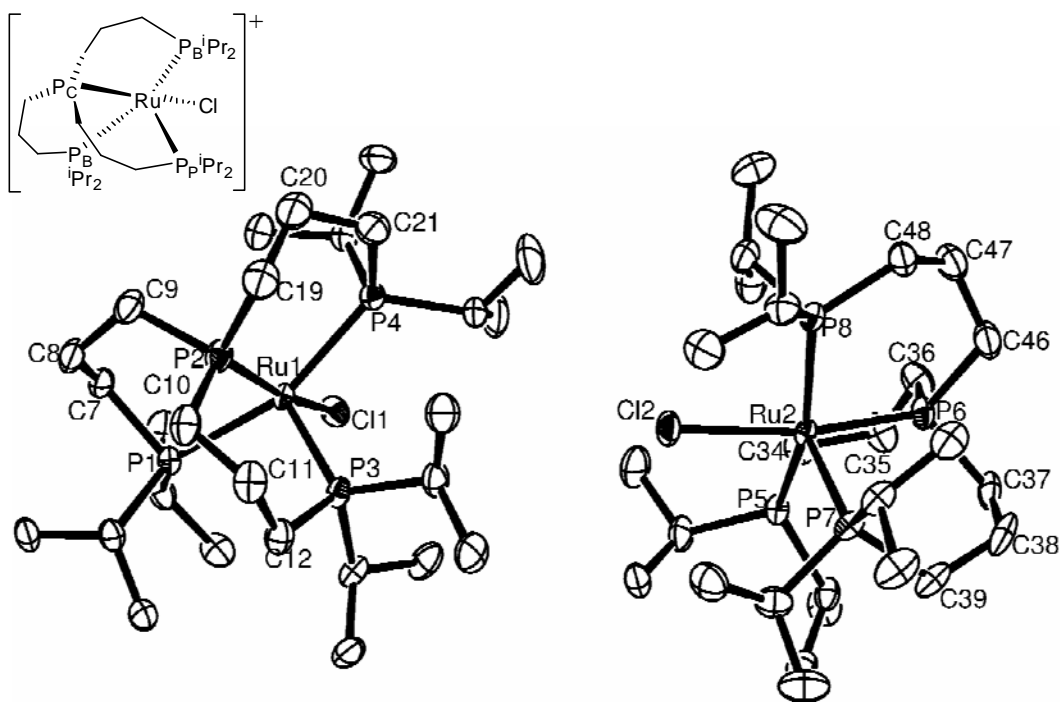
Figure 4.17 ORTEP plot (50% thermal ellipsoids) of the two complex cations of [RuCl(P^{3}P$^i_3$)][BPh$_4$].THF **65**, within each asymmetric unit. Hydrogen atoms have been removed for clarity.

The two structures within the asymmetric unit are sufficiently similar that the crystallographic data of only one of the configurations, namely Ru1, is detailed here. Each asymmetric unit within the crystal structure contains a THF molecule. Selected bond lengths and angles for the structure are presented in Tables 4.13 and 4.14. Further crystallographic data is contained in Appendix 1 (CD format).

Table 4.13   Selected bond lengths (Å) for $[RuCl(P^3P^i_3)][BPh_4]$.THF **65.[BPh$_4$]**

Ru(1)-Cl(1)	2.4351(7)	Ru(1) –P(2)	2.2618(7)
Ru(1) –P(1)	2.4629(6)	Ru(1) –P(3)	2.2536(6)
Ru(1) –P(4)	2.3892(7)		

Table 4.14   Selected bond angles (º) for $[RuCl(P^3P^i_3)][BPh_4]$.THF **65.[BPh$_4$]**

Cl(1)-Ru(1)-P(2)	165.53(2)	Cl(1)-Ru(1)-P(1)	89.28(2)
Cl(1)-Ru(1)-P(3)	103.06(2)	Cl(1)-Ru(1)-P(4)	83.51(2)
P(2)-Ru(1)-P(1)	89.20(2)	P(2)-Ru(1)-P(3)	91.38(2)
P(2)-Ru(1)-P(4)	92.25(3)	P(1)-Ru(1)-P(3)	99.40(2)
P(1)-Ru(1)-P(4)	156.51(2)	P(3)-Ru(1)-P(4)	104.00(2)

The geometry of $[RuCl(P^3P^i_3)]^+$ **65** has been assigned as square based pyramid using the same arguments as for $[RuCl(PP^i_3)]^+$ **56** detailed in Section 4.3.3. In this instance, the P_B-Ru-P_B angle, P1-Ru1-P4, at 156.5º is appreciably closer to that of a square based pyramid than a trigonal bipyramid. In addition the Ru-P_P bond length, Ru1-P3, at 2.254 Å is significantly shorter than the Ru-P_B bond lengths Ru1-P1 and Ru1-P4 (2.463 and 2.389 Å respectively) which is representative of square based pyramid geometry.

A search of the Cambridge Structural Database[14, 15] provides no comparative structures of 5 coordinate complexes of ruthenium with tripodal tetradentate

ligands. There are 3 structures of ruthenium with the tripodal tetradentate ligand P^3P_3 **20,**[21-23] however, these are 6 coordinate arranged in approximate octahedral geometry. Comparison with the analogous PP^i_3 structure $[RuCl(PP^i_3)]^+$ **56** described in Section 4.3.3 results in the following observations. The metal to donor atom lengths of **65** are equivalent to or longer than the analogous lengths in **56**. The P-Ru-P bond angles are all greater in **65** and the Cl-Ru-P bond angles are all more acute than in **56**. Thus the major effect of the 3-carbon armed ligand $P^3P^i_3$ in **65** versus its 2-carbon armed analogue PP^i_3 in **56** is a less strained complex with relaxation of the ligand bite angles and a lengthening of the metal to donor atom bond lengths.

4.5   Preparation of an Iron Complex of N^3P_3 7

The potentially tetradentate, aminophosphine ligand $N(CH_2CH_2CH_2PMe_2)_3$ N^3P_3 **7** was prepared by nucleophilic displacement of the bromides of tris(3-bromopropyl)amine **9** with lithium dimethylphosphide **8**. This synthesis is described in Section 2.3.

4.5.1   Preparation of $[Fe_2Cl_4(N^3P_3)_2]_n$ 66

Stoichiometric amounts of anhydrous iron(II) chloride and N^3P_3 **7** were refluxed in toluene/ethanol for 18 hours resulting in a paramagnetic light blue solution. Upon work up the coordination polymer $[Fe_2Cl_4(N^3P_3)_2]_n$ **66** was afforded as a light blue waxy solid in 48% yield. Layering of an aliquot of the reaction mixture with pentane afforded aqua blue crystals of this polymer suitable for both X-ray diffraction and confirmation of the stoichiometry by microanalysis.

The 2-carbon armed analogues of N^3P_3 **7** with phenyl $(N(CH_2CH_2PPh_2)_3)$[4] and isopropyl $(N(CH_2CH_2P^iPr_2)_3)$[24] substituents have been used to synthesise cationic iron complexes of the form $[FeCl(NP_3)]^+$ which can be considered precursors to dinitrogen complexes. The length, and hence flexibility, of the 3-carbon arms of **7** along with the weak bonding of the central amine leads to **7** bridging as a tridentate ligand rather than chelating as a tetradentate ligand. As such, formation of a monomeric dinitrogen complex precursor was not achieved.

4.5.2   X-ray Crystallography of $[Fe_2Cl_4(N^3P_3)_2]_n$ 66

The molecular structure of $[Fe_2Cl_4(N^3P_3)_2]_n$ is provided in Figure 4.18. Further crystallographic data is contained in Appendix 1 (CD format).
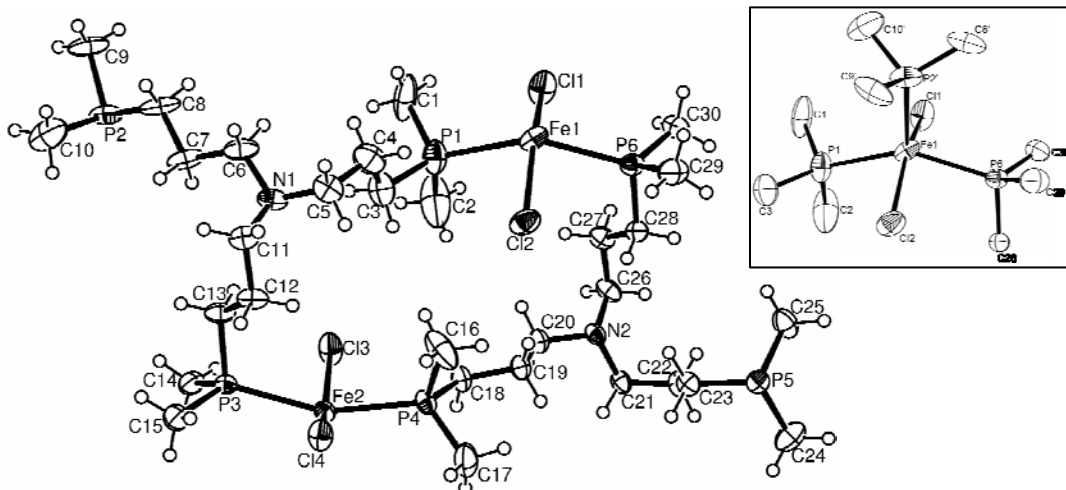
Figure 4.18 ORTEP plot (50% thermal ellipsoids) of the asymmetric unit $Fe_2Cl_4(N^3P_3)_2$ of the polymeric complex $[Fe_2Cl_4(N^3P_3)_2]_n$ **66** with representation of ligands around an iron(II) centre (insert).

The structure has significant disorder which has been omitted for clarity in Figure 4.18. Each iron(II) centre has five ligands arranged in approximate square based pyramid geometry. Two of these are chlorides whilst the other 3 are N^3P_3 **7**

ligands with a single phosphine donor from each. In turn, each N^3P_3 ligand bridges 3 iron(II) centres. The central amine of **7** is non-coordinating in this complex. The overall structure is an 8 by 4 two dimensional polymeric structure with the polynuclear cycle being made up of metal and amine units, for example, "Fe1-N1-Fe2-N2" is the 4 unit cycle represented in Figure 4.18. Representations of this polymeric structure is provided in Figure 4.19.
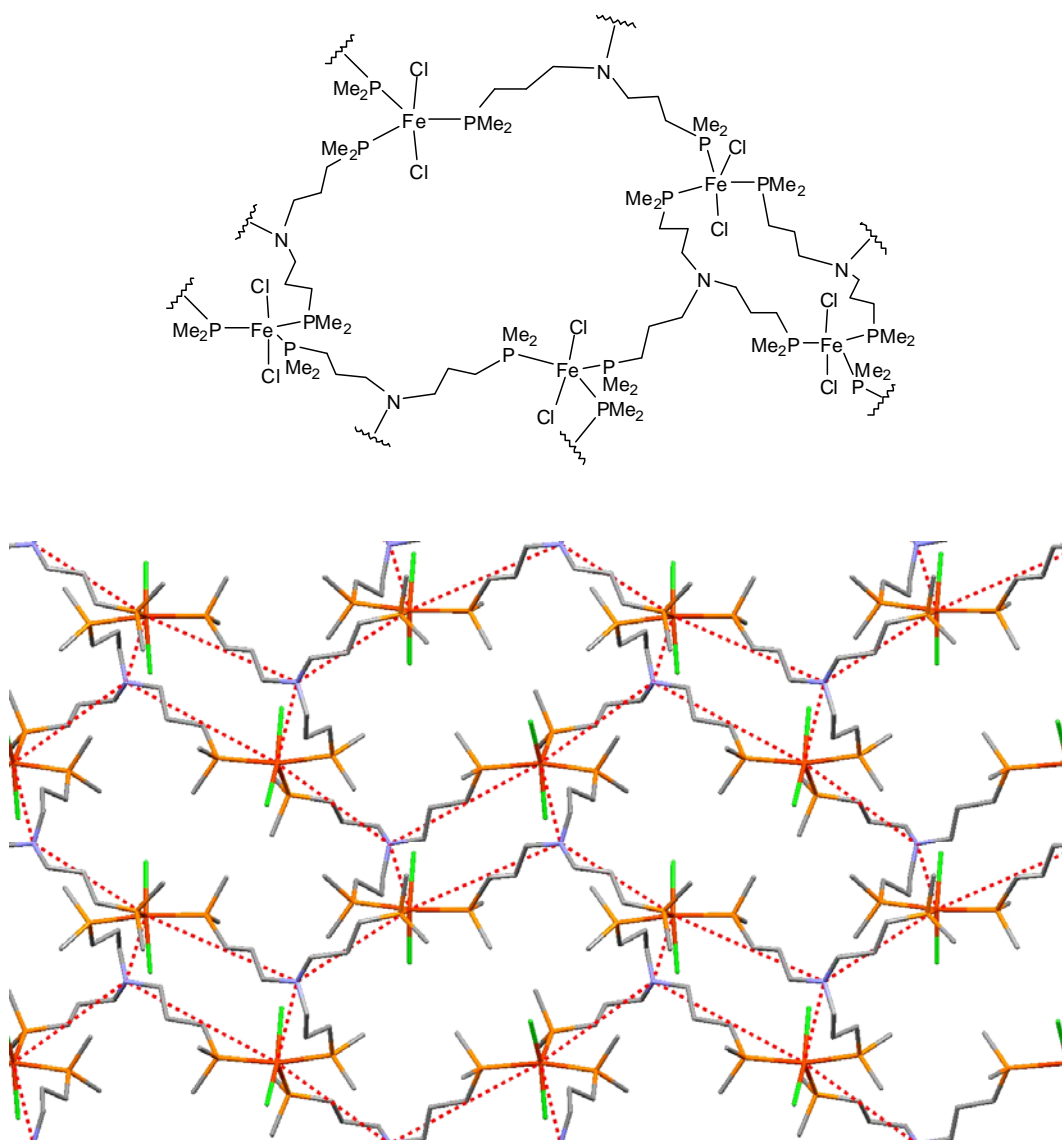
Figure 4.19   Diagrammatic representations of the 8 by 4 two dimensional polymeric structure of $[Fe_2Cl_4(N^3P_3)_2]_n$ **66**.

A search of the literature did not yield any structures of sufficient similarity to warrant a structural comparison. A selection of bond lengths and angles around an iron centre of **66** are provided in Tables 4.15 and 4.16.

Table 4.15   Selected bond lengths (Å) for $[Fe_2Cl_4(N^3P_3)_2]_n$ **66**

Fe(1)-Cl(1)	2.342(2)	Fe(1) –Cl(2)	2.3834(17)
Fe(1) –P(1)	2.677(4)	Fe(1) –P(2)'	2.468(8)
Fe(1) –P(6)	2.5527(17)		

Table 4.16   Selected bond angles (º) for $[Fe_2Cl_4(N^3P_3)_2]_n$ **66**

Cl(1)-Fe(1)-Cl(2)	154.07(5)	P(1)-Fe(1)-P(6)	147.22(9)
P(2)'-Fe(1)-Cl(1)	103.47(19)	P(2)'-Fe(1)-Cl(2)	102.45(19)
P(2)'-Fe(1)-P(1)	111.45(19)	P(2)'-Fe(1)-P(6)	101.09(19)
Cl(1)-Fe(1)-P(1)	86.07(11)	Cl(1)-Fe(1)-P(6)	90.36(7)
Cl(2)-Fe(1)-P(1)	85.33(11)	Cl(2)-Fe(1)-P(6)	83.82(5)

The geometry around the Fe1 centre lies somewhere between that of a square based pyramid and trigonal bipyramid structure. The 3 Fe-P bond lengths are all significantly different with the Fe1-P2' being the shortest which is typical for the pinnacle of a square based pyramid. The Cl1-Fe1-Cl2 and P1-Fe1-P6 bond angles, at 154.1º and 147.2º respectively, are somewhere between those expected for a square based pyramid and a trigonal bipyramid. The iron centre Fe2, although containing some differences in bond lengths and angles to that of Fe1, similarly has a geometry in between that of square based pyramid and trigonal bipyramid. Assignment of square based pyramid geometry is favoured due to one Fe-P bond length (assigned as the pinnacle phosphine) being significantly shorter than the other two Fe-P bond lengths.

4.6   Preparation of an Iron complex of P^i_2 67

The bidentate ligand $CH_2(P^iPr_2)_2$, P^i_2, **67** was obtained as a byproduct in the synthesis of $P^3P^i_3$ **11,** having been distilled from the reaction mixture in the final purification step (see Section 2.4).

4.6.1   Preparation of $[(FeCl)_2(\mu\text{-}Cl)_2(\mu\text{-}P^i_2)_2]$ 68

An equimolar amount of iron(II) dichloride was added to P^i_2 in THF and left for several days under dinitrogen. Filtering of the resultant pale gold crystals gave $[(FeCl)_2(\mu\text{-}Cl)_2(\mu\text{-}P^i_2)_2]$ **68** in 42% yield. The crystalline product was suitable for analysis by microanalysis and by X-ray diffraction, the crystallographic structure is discussed in Section 4.6.2. The $^{31}P\{^1H\}$ NMR spectrum in THF/benzene-d_6 presents the four equivalent phosphine signals as a broadened singlet at 87.1 ppm, the $^1H\{^{31}P\}$ NMR is very broad with no assignable peaks suggesting a phenomenon such as paramagnetism is occurring within the complex.

4.6.2   X-ray Crystallography of $[(FeCl)_2(\mu\text{-}Cl)_2(\mu\text{-}P^i_2)_2]$ 68

The crystal structure of $[(FeCl)_2(\mu\text{-}Cl)_2(\mu\text{-}P^i_2)_2]$ **68** is provided in Figure 4.20. A selection of bond lengths and angles of **68** is provided in Tables 4.17 and 4.18. Further crystallographic data is contained in Appendix 1 (CD format).
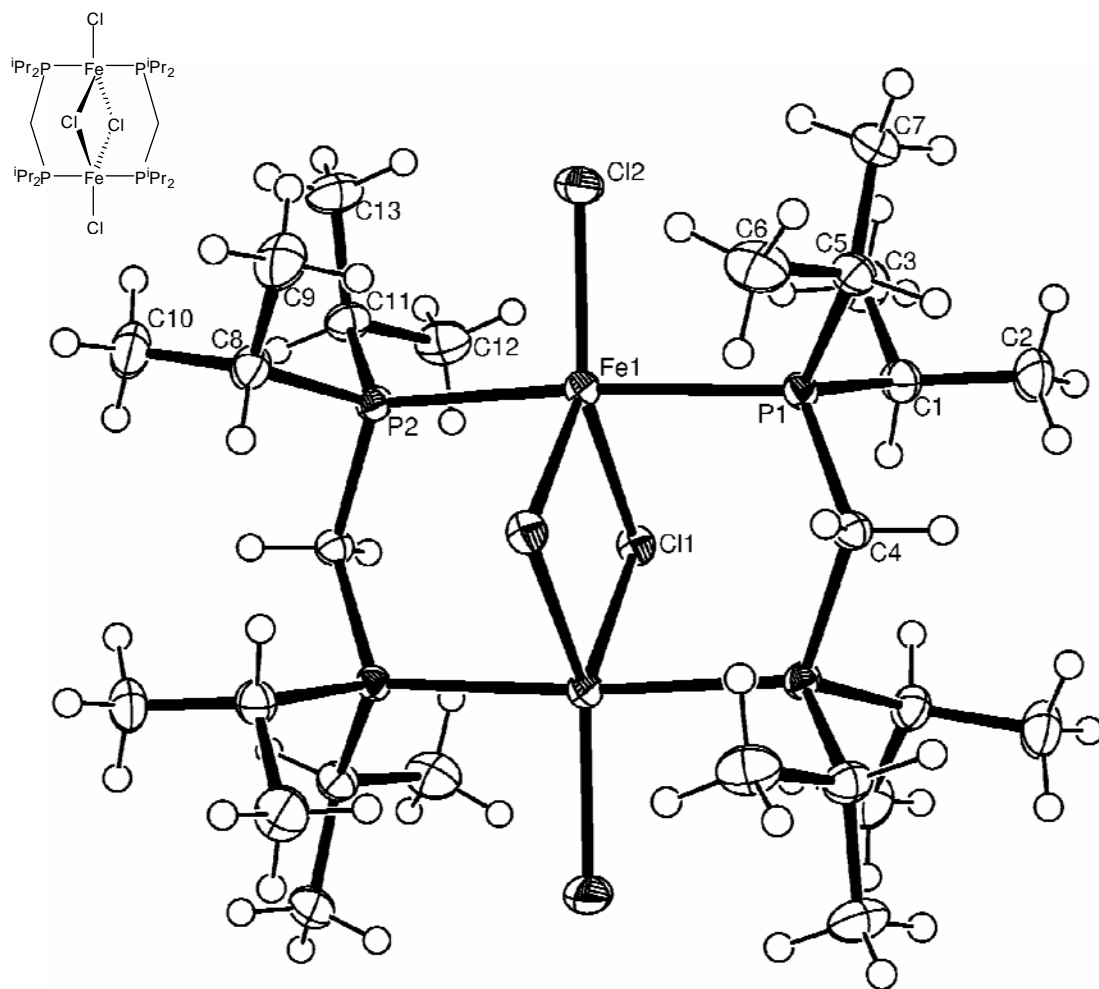
Figure 4.20 ORTEP plot (50% thermal ellipsoids) of $[(FeCl)_2(\mu-Cl)_2(\mu-P^i_2)_2]$ **68**.

The iron (II) dimer **68** is symmetrical by way of an improper-rotation axis. The two iron(II) centres have ligands arranged in, what is best described as, a distorted trigonal bipyramid. The two bridging phosphine ligands serve to increase the Fe1-Fe1 distance from perfect trigonal bipyramid geometry such that the Fe1-Cl1 bond lengths at 2.49 Å are significantly greater than the unconstrained Fe1-Cl2 bond length of 2.30 Å and the Cl1-Fe1-Cl1 bond angle is narrowed to 94°. Given the Fe1-Cl1-Fe1 bond angle of 86° the central Fe1-Cl1-Fe1-Cl1 configuration approximates to a square.

Table 4.17   Selected bond lengths (Å) for $[(FeCl)_2(\mu\text{-Cl})_2(\mu\text{-P}^i_2)_2]$ **68**

Fe(1)-Cl(1)	2.4897(16) 2.495(2)	Fe(1) –P(1)	2.5414(16)
Fe(1) –Cl(2)	2.3037(14)	Fe(1) –P(2)	2.5416(16)

Table 4.18   Selected bond angles (º) for $[(FeCl)_2(\mu\text{-Cl})_2(\mu\text{-P}^i_2)_2]$ **68**

Cl(1)-Fe(1)-Cl(1)	93.76(2)	Cl(1)-Fe(1)-P(2)	89.35(6) 88.27(3)
Cl(1)-Fe(1)-Cl(2)	135.53(3) 130.71(4)	Cl(2)-Fe(1)-P(1)	91.99(4)
Cl(1)-Fe(1)-P(1)	86.47(6) 90.24(4)	Cl(2)-Fe(1)-P(2)	92.23(4)
Fe(1)-Cl(1)-Fe(1)	86.24(2)	P(1)-Fe(1)-P(2)	175.468(15)

A search of the Cambridge Structural Database[14, 15] provides a selection of structures with elements of similarity to the chloride and bidentate phosphine ligand bridged iron(II) dimer **68**.   For example, an analogous chromium(II) complex,   (di-μ-chlorodi-μ-(bis(dimethylphosphino)methane-κ^2P))-bis[chlorochromium(II)],[25] with bis(dimethylphosphino)methane as the bridging phosphine ligand is known. There are several examples of 5-coordinate iron(II) dimers with two bridging chlorides and a third monodentate chloride, however none of these contain phosphine bridging ligands but most commonly have bidentate nitrogen donor ligands in the remaining two coordination sites.[25-28] Two structures which contain P^i_2 as a bridging ligand are: a nickel(II) complex, (di-μ-bromo-μ-bis(diisopropylphosphino)methane-κ^2P)bis[nitrosylnickel(II)],[29] which contains a single bridging P^i_2 and two bridging bromide ligands; and a rhodium(I) complex, (di-μ-(bis(diisopropylphosphino)methane-κ^2P)di-μ-hydrido-bis[carbonylrhodium(I)],[30] which has two bridging P^i_2 ligands and two bridging hydrides. Although not sufficiently similar to warrant a structural comparison

these examples illustrate that the structure adopted by **68,** although known, is unusual for an iron(II) centre.

4.7   Preparation of iron complexes of P^3P_3 19

The 3-carbon armed, tetradentate, phosphine ligand $P(CH_2CH_2CH_2PMe_2)_3$, P^3P_3, **19** was prepared by nucleophilic displacement of the chlorides of tris(3-chloropropyl)phosphine oxide **20** with lithium dimethylphosphide **8** followed by reduction of the central phosphine using trichlorosilane.   This synthesis is described in Section 2.5.

4.7.1   Preparation of $FeCl_2(P^3P_3)$ 69

Synthesis of the known compound $FeCl_2(P^3P_3)$ **69** was performed by addition of an equivalent of the ligand P^3P_3 **19** in THF to anhydrous iron(II) chloride in a method modified slightly from that in the literature.[31]   This resulted in the immediate formation of a violet solution which upon workup gave **69** as a violet powder in 89% yield.   The $^{31}P\{^1H\}$ NMR spectrum of **69**, presented in Figure 4.21, shows the 3 phosphorus resonances; P_C as an unresolved doublet of triplets at 37.2 ppm, P_U as a poorly resolved doublet of triplets at 30.1 ppm and P_T as a doublet of doublets at 7.7 ppm.   In contrast to the analogous PP_3 **1** complexes described throughout Section 3, the P_C resonance is no longer significantly downfield relative to the other two phosphine resonances.   This is attributed to the propyl arms of the P^3P_3 **19** ligand which lead to the P_C phosphorus being a member of significantly less strained chelate rings in complex **69**.   It can also be noted that the P_T resonance is low field relative to the P_U signal, a feature common

to the non-hydride complexes of PP$_3$ **1** with chloride co-ligands described in Section 3.
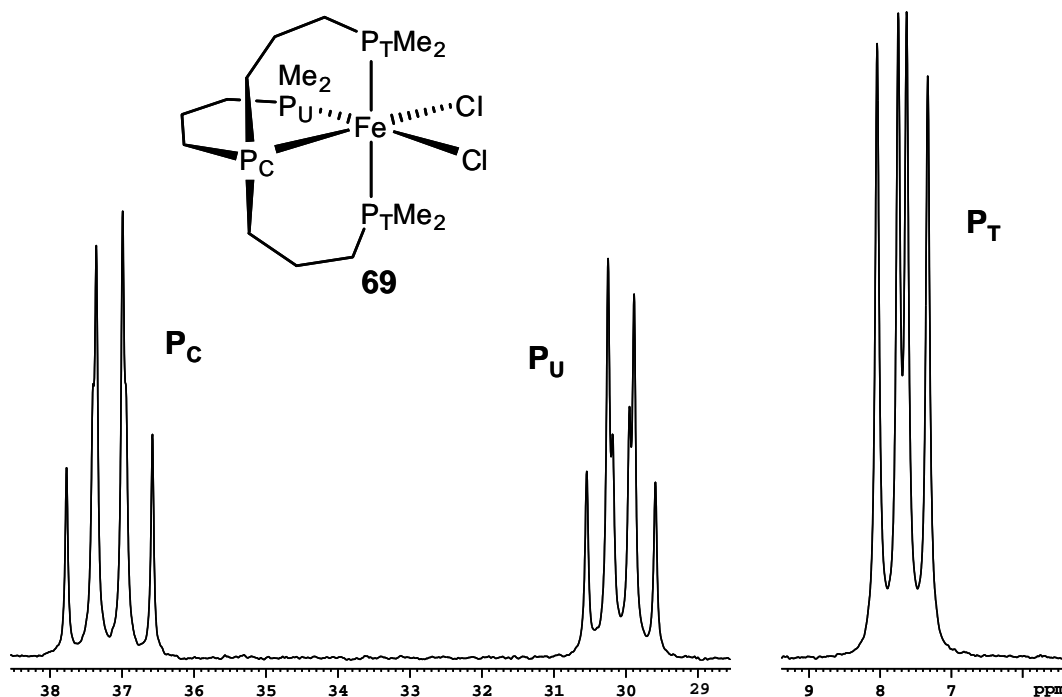
Figure 4.21 ^{31}P{^{1}H} NMR spectrum of FeCl$_2$(P^{3}P$_3$) **69** in THF

4.7.2   Preparation of FeClH(P^{3}P$_3$) 70

Synthesis of the known complex FeClH(P^{3}P$_3$) **70** was performed by addition of a THF solution of LiAlH$_4$ to a solution of FeCl$_2$(P^{3}P$_3$) **69** in THF until such time that no **69** was present by ^{31}P{^{1}H} NMR. This method was a modified procedure to that reported by Antberg *et al.*[32] During addition of the LiAlH$_4$ solution, a colour change from violet to orange occurred. Upon workup, the orange reaction mixture turned brown and was used as an ethanol extract. The ^{31}P{^{1}H} NMR spectrum and high field region of the ^{1}H NMR spectrum of the orange reaction mixture of **70** are presented in Figures 4.22 and 4.23 respectively.
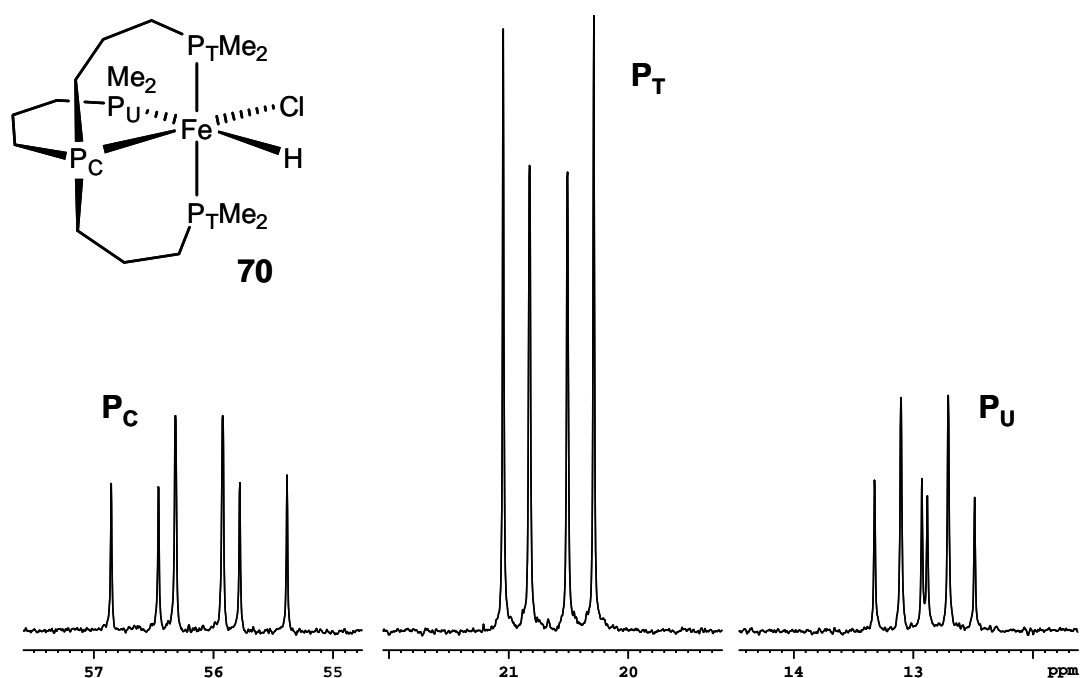
Figure 4.22 $^{31}P\{^1H\}$ NMR spectrum of FeClH(P^{3}P$_3$) **70** in THF/THF-d_8

The phosphorus resonances of **70** present P$_C$ as a doublet of triplets at 56.1 ppm,
P$_T$ as a doublet of doublets at 20.7 ppm and P$_U$ as a doublet of doublets at
12.9 ppm. The intensities of these signals are in the ratio 1:2:1 respectively and
are characteristic for an octahedrally arranged tripodal tetradentate phosphine
ligand complex of iron.

The high field region of the ^1H NMR shows the splitting pattern of a metal bound
hydride coupled to all 4 phosphorus atoms (2 of which are equivalent by NMR) as
a fully resolved doublet of doublet of triplets at -10.7 ppm.
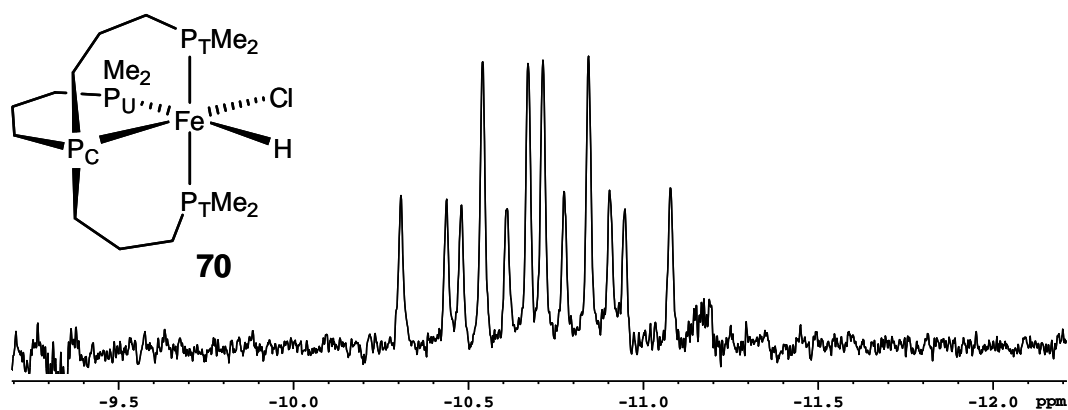
Figure 4.23 High field region of ^1H NMR spectrum of FeClH(P^{3}P$_3$) **70** in THF/THF-d_8

4.7.3 Reaction of FeClH(P^{3}P$_3$) 70 with N$_2$ in Ethanol

Dissolution of FeClH(P^{3}P$_3$) **70** in ethanol under an atmosphere of dinitrogen resulted in the presence of at least two other species by $^{31}P\{^1H\}$ NMR with corresponding hydride peaks in the high field region of the ^1H NMR spectrum. Application of a vacuum to an NMR sample resulted in the loss of these new species, which reappeared upon repressurisation with dinitrogen. This provided some evidence that these species could potentially be dinitrogen hydride complexes. Further work is required to assess whether mononuclear and dinuclear dinitrogen complexes are formed in equilibrium with **70** in a manner analogous to those dinitrogen complexes formed from FeClHPP$_3$ **25** as described in detail in Section 3.2.

4.8 Tetrameric iron complexes of PP$_3$ 1

4.8.1 Preparation of [Fe$_4$Cl$_4$(PP$_3$)$_5$][BPh$_4$]$_4$ 71.[BPh$_4$]$_4$

The main byproduct in the synthesis of FeCl$_2$(PP$_3$) **24** (see Section 3.2.1) has been tentatively assigned by Smernik,[33] from $^{31}P\{^1H\}$ NMR spectra, as the tetrameric

cationic species $[Fe_4Cl_4(PP_3)_5]^{4+}$ **71**. In this work it has been possible to crystallise **71** as its tetraphenylborate salt by addition of sodium tetraphenylborate to an acetone solution of the red THF insoluble residue produced during the synthesis of **24**. The crystal structure of **71** is presented in Figure 4.24.
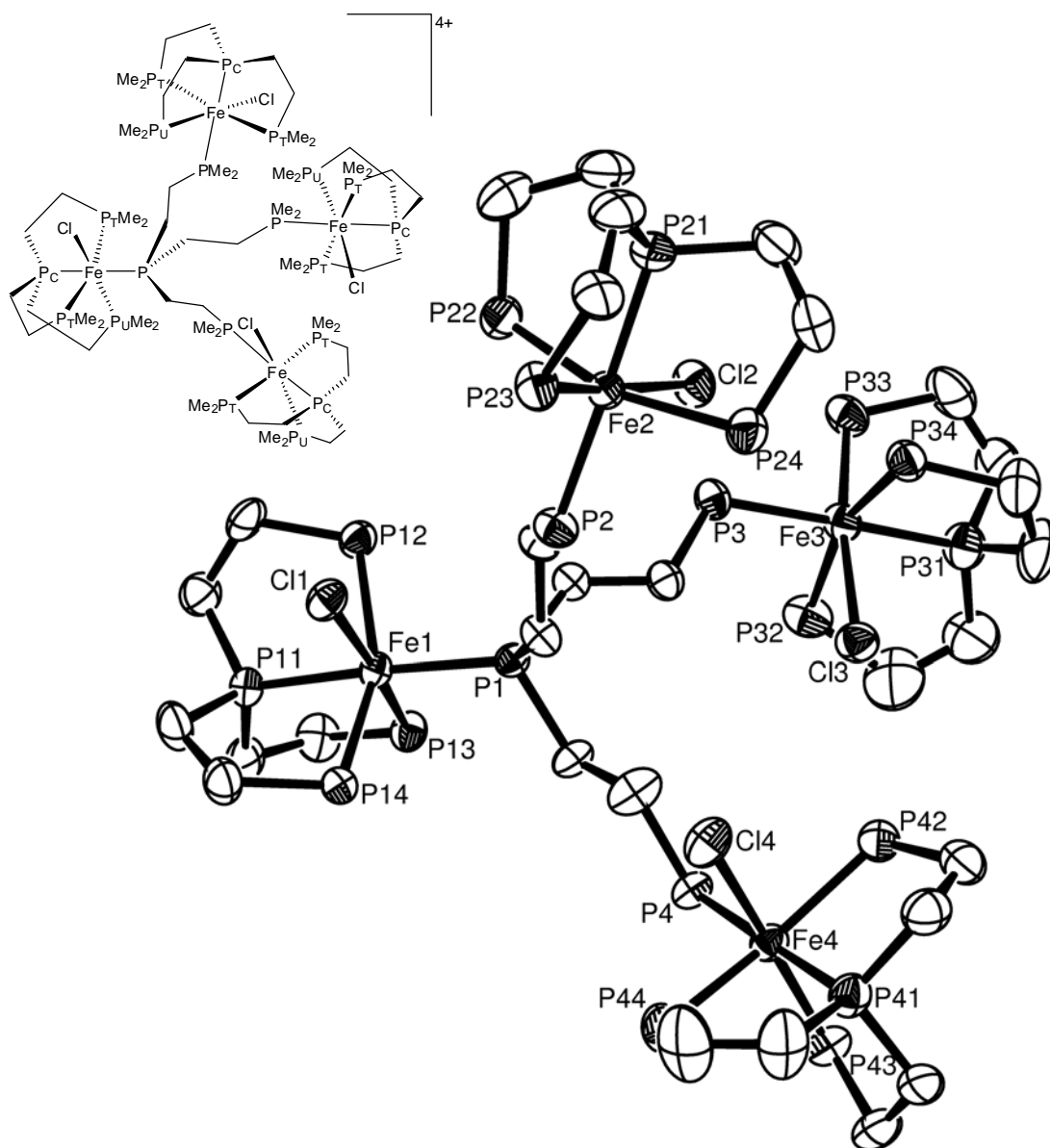
Figure 4.24 ORTEP plot (50% thermal ellipsoids) of the complex cation of $[Fe_4Cl_4(PP_3)_5][BPh_4]_4.3(C_3H_6O).2H_2O$, **71**. Hydrogen atoms and methyl groups from the ligand have been removed for clarity.

The cystallographic analysis supports Smernik's assignment of a central PP_3 **1** ligand bridging 4 "FeCl(PP_3)" moieties. The phosphorus atoms of the bridging ligand are *trans* to the central phosphorus atoms of each "FeCl(PP_3)" group. A selection of bond lengths and angles of **71** are provided in Tables 4.19 and 4.20.

A search of the Cambridge Structural Database[14, 15] provides no structures sufficiently similar to warrant a complete structural comparison. However, when comparing the 4 octahedral iron centres in complex **71** with each other and with the iron complexes of PP_3 **1** presented in Table 3.3 Section 3.2.5, i.e. **30**, **31** and **32**, the following observations can be made. The Fe-P bond lengths in **71** which involve the bridging ligand are 2.26 Å for all but the central phosphine which is 2.28 Å. This difference is likely due to the more bulky substituents on the latter phosphorus. This pattern in bond lengths is not reflected in the Fe-P_C bond lengths, where P_C is that of the chelating ligand and *trans* to a bridging ligand phosphine in each case, which ranges from 2.18 to 2.21 Å. There are no discernible differences in the Fe-Cl bond lengths at 2.38 Å and all the Fe-P bond lengths are commensurate with those of complexes **30**, **31** and **32**. The bond angles for each iron centre show a narrowing from that of the perfect octahedron towards the central phosphine P_C of the chelating ligand. This phenomenon, also seen in **30**, **31** and **33**, is due to the natural bite angle of the PP_3 ligand around the iron(II) centre. The P_T-Fe-P_T angle of the iron centre bound to P_C of the bridging ligand, P12-Fe1-P14, is noticeably more acute at 154.5° than the corresponding angle in the other iron(II) centres which range from 159.0° to 161.6°. This is likely to be due to the greater steric interactions between the larger substituents on the bridging ligand's central phosphine P_C and the chelating ligand on Fe1.

Table 4.19   Selected bond lengths (Å) for [Fe$_4$Cl$_4$(PP$_3$)$_5$][BPh]$_4$.3(C$_3$H$_6$O).2H$_2$O
            71.[BPh$_4$]

Fe(1)-Cl(1)	2.376(2)	Fe(1)-P(1)	2.279(2)
Fe(2)-Cl(2)	2.377(2)	Fe(2)-P(2)	2.259(2)
Fe(3)-Cl(3)	2.379(2)	Fe(3)-P(3)	2.259(2)
Fe(4)-Cl(4)	2.377(2)	Fe(4)-P(4)	2.261(1)
Fe(1)-P(11)	2.207(2)	Fe(1)-P(12)	2.298(2)
Fe(2)-P(21)	2.190(2)	Fe(2)-P(22)	2.274(3)
Fe(3)-P(31)	2.182(2)	Fe(3)-P(32)	2.277(3)
Fe(4)-P(41)	2.197(2)	Fe(4)-P(42)	2.309(3)
Fe(1)-P(13)	2.239(2)	Fe(1)-P(14)	2.291(2)
Fe(2)-P(23)	2.209(2)	Fe(2)-P(24)	2.231(3)
Fe(3)-P(33)	2.214(2)	Fe(3)-P(34)	2.286(3)
Fe(4)-P(43)	2.211(2)	Fe(4)-P(44)	2.267(3)

Table 4.20   Selected bond angles (º) for [Fe$_4$Cl$_4$(PP$_3$)$_5$][BPh$_4$]$_4$.3(C$_3$H$_6$O).2H$_2$O
            71.[BPh$_4$]

P(1)-Fe(1)-Cl(1)	90.86(8)	P(1)-Fe(1)-P(11)	176.91(10)
P(2)-Fe(2)-Cl(2)	90.71(9)	P(2)-Fe(2)-P(21)	177.29(11)
P(3)-Fe(3)-Cl(3)	93.37(9)	P(3)-Fe(3)-P(31)	178.85(11)
P(4)-Fe(4)-Cl(4)	94.20(9)	P(4)-Fe(4)-P4(1)	179.29(10)
P(11)-Fe(1)-P(13)	84.77(9)	P(12)-Fe(1)-P(14)	154.47(9)
P(21)-Fe(2)-P(23)	85.62(10)	P(22)-Fe(2)-P(24)	161.61(10)
P(31)-Fe(3)-P(33)	85.86(11)	P(32)-Fe(3)-P(34)	159.90(11)
P(41)-Fe(4)-P(43)	85.37(11)	P(42)-Fe(4)-P(44)	158.97(11)
P(12)-Fe(1)-P(13)	97.48(9)	P(13)-Fe(1)-Cl(1)	175.25(10)
P(22)-Fe(2)-P(23)	99.16(10)	P(23)-Fe(2)-Cl(2)	171.44(10)
P(32)-Fe(3)-P(33)	100.77(11)	P(33)-Fe(3)-Cl(3)	171.84(10)
P(42)-Fe(4)-P(43)	98.91(10)	P(43)-Fe(4)-Cl(4)	170.55(10)

4.8.2 Preparation of $Fe_4(PP_3)_5$ 72

The synthesis of **38** and **44**, the iron(0) dinitrogen complexes of PP_3 **1**, is described in Section 3.2.10. Attempts to crystallise these complexes, by slow diffusion of solvent from a solution of **38** and **46** in THF, resulted in the loss of dinitrogen and the formation of an iron(0) PP_3 tetramer $Fe_4(PP_3)_5$ **72**. The crystal structure of **72** is presented in Figure 4.25.
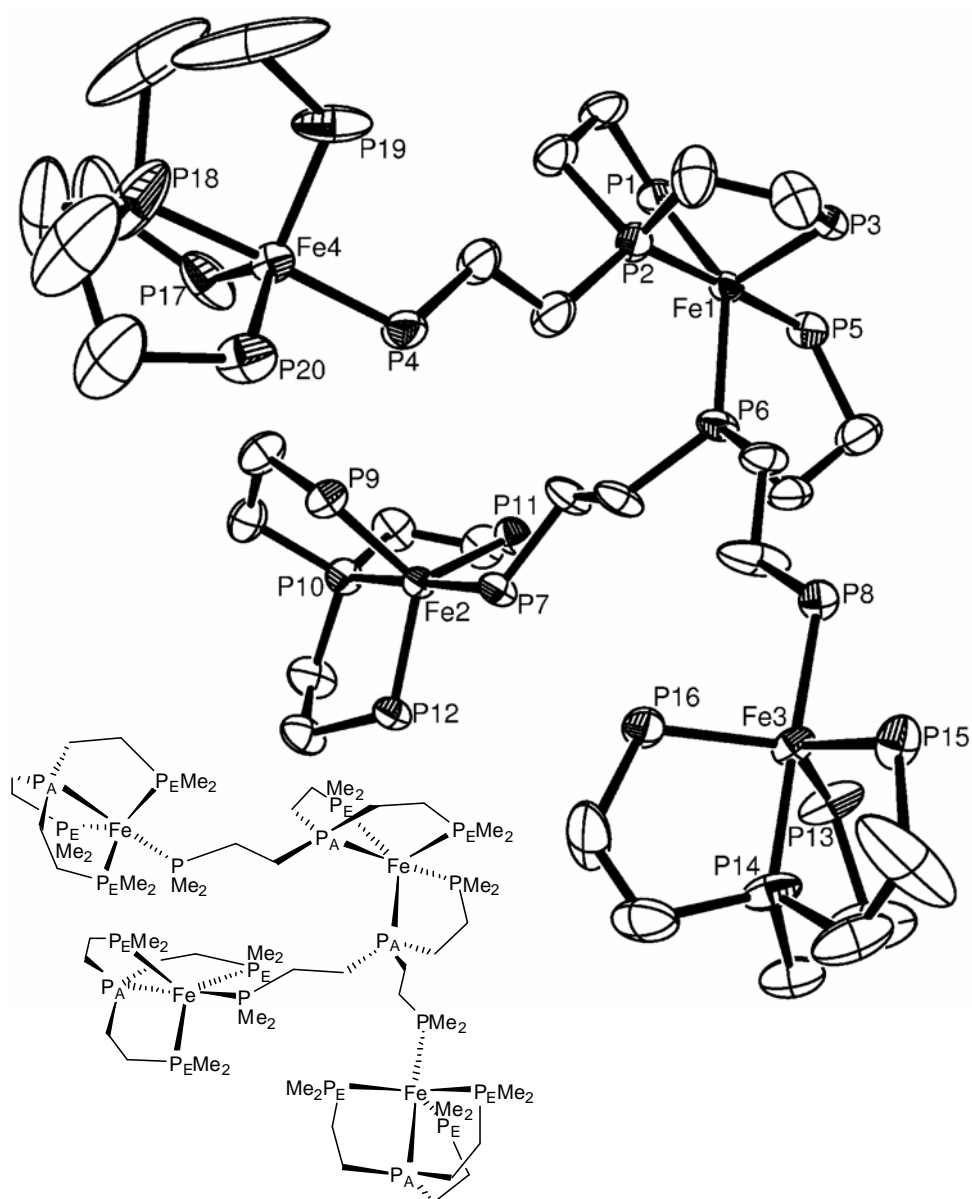
Figure 4.25 ORTEP plot (50% thermal ellipsoids) of the complex $Fe_4(PP_3)_5$.THF **72**. Hydrogen atoms and methyl groups from the ligand have been removed for clarity.

This tetramer has 2 PP_3 ligands which bridge the 4 iron(0) centres, 1 bridges an iron(0) centre, Fe1, to 2 "Fe(PP_3)" moieties whilst the other binds the same iron(0) centre to a 3rd "Fe(PP_3)". Each iron centre has 5 phosphines bound to it in approximate trigonal bipyramidal geometry. Iron centres Fe3 and Fe4, and the PP_3 ligands bonded to them, exhibit disorder. A disordered THF molecule of solvation is present in the crystal but not shown in Figure 4.25. A selection of bond lengths and angles of **72** are provided in Tables 4.21 and 4.22.

A search of the Cambridge Structural Database[14, 15] provides no structures sufficiently similar to warrant a complete structural comparison. However, when comparing the iron centres in complex **72** with each other and with the trigonal bipyramid iron(0) centre of the dinuclear species $[(FeH(PP_3))(\mu-N_2)(Fe(PP_3))]^+$ **37** presented in Section 3.2.8, the following observations can be made. The structure of **72** has 3 iron(0) centres each of which comprise a chelating PP_3 and a terminal phosphine from a bridging PP_3 ligand in an axial position *trans* to the apical phosphine P_A of the chelating ligand. These have Fe-P_A bond lengths which average to 2.12 Å and are significantly shorter than those Fe-P bond lengths of the phosphine *trans* to it which have an average value of 2.17 Å. This difference is likely due to the constraints of the chelating PP_3 ligand which bring the P_A phosphine closer to the metal centre. The equatorial phosphine bond lengths Fe-P_E of these metal centres all lie somewhere between those of the two axial Fe-P bond lengths described. This trend is seen within the iron(0) centre of **37** which has commensurate bond lengths to those discussed here. The bond angles for each of these 3 iron centres show a narrowing from that of the perfect trigonal bipyramid towards the apical phosphine P_A of the chelating ligand. This

phenomenon, also seen in the iron (0) centre of **37**, is due to the natural bite angle of the PP_3 ligand. The angles of the equatorial phosphines P_E-Fe-P_E approximate well to the 120º of the perfect trigonal bipyramid with values ranging from 117º to 123º. Likewise the axial angle P_A-Fe-P of these iron(0) centres at 178º to 179º approximate well to the perfect trigonal bipyramid structure. The 4th iron(0) centre, Fe1, involves binding of an apical and terminal phosphine from one bridging ligand and an apical and two terminal phosphines from a second bridging ligand. This latter ligand (P1 P2 P3 P4) occupies an axial position and 2 equatorial positions with the apical and terminal phosphines respectively. The 2nd axial and 3rd equatorial positions are occupied by the terminal and apical phosphines of the second ligand (P5 P6 P7 P8) respectively. The lack of a single chelating PP_3 ligand removes some of the steric constraints at this iron centre. This is best illustrated by the increased Fe-P_A bond lengths of 2.16 Å and 2.17 Å. All other Fe-P bond lengths at this metal centre are commensurate with those of the 3 iron(0) centres previously described. The bite angle of the PP_3 ligand results in a narrowing of the angle from that of a perfect trigonal bipyramid between the terminal and apical phosphines of each of the donating ligands (P3-Fe1-P2, P1-Fe1-P2 and P5-Fe1-P6). The P-Fe1-P angles between equatorial phosphines at 111º, 112º and 137º deviate significantly from that of a trigonal bipyramid due to the effects of the two PP_3 ligands.

Table 4.21   Selected bond lengths (Å) for $Fe_4(PP_3)_5 \cdot THF$ **72**

Fe(1)-P(2)	2.1675(7)	Fe(1)-P(5)	2.1607(7)
Fe(2)-P(10)	2.1245(6)	Fe(2)-P(7)	2.1712(6)
Fe(3)-P(14)	2.126(7)	Fe(3)-P(8)	2.174(7)
Fe(4)-P(18)	2.122(6)	Fe(4)-P(4)	2.164(7)
Fe(1)-P(1)	2.1531(7)	Fe(2)-P(9)	2.1402(7)
Fe(1)-P(3)	2.1378(6)	Fe(2)-P(11)	2.1399(7)
Fe(1)-P(6)	2.1577(6)	Fe(2)-P(12)	2.1383(6)
Fe(3)-P(14)	2.126(7)	Fe(4)-P(17)	2.154(6)
Fe(3)-P(15)	2.142(7)	Fe(4)-P(19)	2.142(6)
Fe(3)-P(16)	2.140(7)	Fe(4)-P(20)	2.157(7)

Table 4.22   Selected bond angles (º) for $Fe_4(PP_3)_5 \cdot THF$ **72**

P(2)-Fe(1)-P(5)	176.73(3)		
P(10)-Fe(2)-P(7)	179.43(3)		
P(14)-Fe(3)-P(8)	177.8(4)		
P(18)-Fe(4)-P(4)	179.1(5)		
P(1)-Fe(1)-P(3)	111.69(3)	P(2)-Fe(1)-P(1)	84.35(3)
P(1)-Fe(1)-P(6)	137.44(3)	P(2)-Fe(1)-P(3)	86.11(3)
P(3)-Fe(1)-P(6)	110.75(3)	P(2)-Fe(1)-P(6)	95.44(3)
P(9)-Fe(2)-P(11)	120.19(3)	P(10)-Fe(2)-P(9)	85.03(3)
P(9)-Fe(2)-P(12)	118.89(3)	P(10)-Fe(2)-P(11)	84.73(3)
P(11)-Fe(2)-P(12)	118.64(3)	P(10)-Fe(2)-P(12)	85.17(2)
P(13)-Fe(3)-P(15)	119.9(3)	P(14)-Fe(3)-P(13)	85.8(3)
P(13)-Fe(3)-P(16)	118.3(4)	P(14)-Fe(3)-P(15)	84.9(3)
P(15)-Fe(3)-P(16)	119.8(4)	P(14)-Fe(3)-P(16)	85.3(3)
P(17)-Fe(4)-P(19)	117.1(3)	P(18)-Fe(4)-P(17)	85.1(2)
P(17)-Fe(4)-P(20)	122.9(4)	P(18)-Fe(4)-P(19)	85.0(2)
P(19)-Fe(4)-P(20)	117.6(4)	P(18)-Fe(4)-P(20)	84.6(3)

4.9 Summary of Work on the Synthesis of Iron and Ruthenium Complexes of Tripodal Phosphine Ligands

The synthesis of a range of new iron and ruthenium complexes of the novel ligand PP_3^i **12** has been achieved. These include iron(0), iron(II), ruthenium(0) and ruthenium (II) dinitrogen complexes, the characterisation of which has included ^{15}N NMR spectroscopy and X-ray crystallography. A new set of dinitrogen complexes has been made available for further study to determine their potential to facilitate the reduction of dinitrogen to ammonia.

A ruthenium(II) complex of the new tripodal tetradentate ligand $P^3P_3^i$ **11** and an iron(II) polymeric complex of the tripodal tridentate ligand N^3P_3 **7** have been synthesised. In each case characterisation of the new species has included X-ray crystallography. In addition, an unusual iron(II) dimer of known ligand P_2^i **67** and iron(II) and iron(0) tetramers of the PP_3 **1** ligand have been characterised by X-ray crystallography.

Preliminary work with the P^3P_3 **19** ligand gives some evidence for the potential of iron-dinitrogen complexes to form in a system analogous to that described for the PP_3 **1** ligand in Section 3.2. Further work is required to prove this potential.

4.10 References

1. Schrock, R. R., *Acc. Chem. Res.* **2005,** *38*, (12), 955-962.

2. Betley, T. A.; Peters, J. C., *J. Am. Chem. Soc.* **2004,** *126*, (20), 6252-6254.

3. Vuong, K. V.; Field, L. D., Unpublished Work, University of New South Wales, **2006**.

4. Stoppioni, P.; Mani, F.; Sacconi, L., *Inorg. Chim. Acta* **1974,** *11*, (3), 227-30.

5. Jia, G.; Drouin, S. D.; Jessop, P. G.; Lough, A. J.; Morris, R. H., *Organometallics* **1993,** *12*, (3), 906-16.

6. Donovan-Mtunzi, S.; Richards, R. L.; Mason, J., *J. Chem. Soc., Dalton Trans.* **1984**, (3), 469-74.

7. Field, L. D.; Li, H. L.; Messerle, B. A.; Smernik, R. J.; Turner, P., *J. Chem. Soc., Dalton Trans.* **2004**, (9), 1418-1423.

8. Hoffman, P. R.; Caulton, K. G., *J. Am. Chem. Soc.* **1975,** *97*, (15), 4221-8.

9. La Placa, S. J.; Ibers, J. A., *Inorg. Chem.* **1965,** *4*, (6), 778-83.

10. Bianchini, C.; Laschi, F.; Peruzzini, M.; Zanello, P., *Gazz. Chim. Ital.* **1994,** *124*, (6), 271-5.

11. Baker, M. V.; Field, L. D.; Hambley, T. W., *Inorg. Chem.* **1988,** *27*, (16), 2872-6.

12. Cotton, F. A.; Wilkinson, G., *Advanced Inorganic Chemistry*. 5th ed.; Wiley- Interscience: New York, **1988**.

13. Otting, G.; Messerle, B. A.; Soler, L. P., *J. Am. Chem. Soc.* **1997,** *119*, (23), 5425-5434.

14.   Allen, F. H., *Acta Crystallogr., Sect. B: Struct. Sci.* **2002,** *B58*, (3, 1), 380-388.

15.   Bruno, I. J.; Cole, J. C.; Edgington, P. R.; Kessler, M.; Macrae, C. F.; McCabe, P.; Pearson, J.; Taylor, R., *Acta Crystallogr., Sect. B: Struct. Sci.* **2002,** *58*, (3, 1), 389-97.

16.   Takei, I.; Nishibayashi, Y.; Ishii, Y.; Mizobe, Y.; Uemura, S.; Hidai, M., *J. Organomet. Chem.* **2003,** *679*, (1), 32-42.

17.   Bianchini, C.; Frediani, P.; Masi, D.; Peruzzini, M.; Zanobini, F., *Organometallics* **1994,** *13*, (11), 4616-32.

18.   Bianchini, C.; Masi, D.; Peruzzini, M.; Casarin, M.; Maccato, C.; Rizzi, G. A., *Inorg. Chem.* **1997,** *36*, (6), 1061-1069.

19.   Chen, X.; Xue, P.; Sung, H. H. Y.; Williams, I. D.; Peruzzini, M.; Bianchini, C.; Jia, G., *Organometallics* **2005,** *24*, (18), 4330-4332.

20.   Anzellotti, A.; Briceno, A.; Delgado, G.; Diaz de Delgado, G.; Fontal, B., *Acta Crystallogr., Sect. C: Cryst. Struct. Commun.* **2002,** *58*, (Pt 6), m355-7.

21.   Antberg, M.; Dahlenburg, L., *Inorg. Chim. Acta* **1986,** *111*, (1), 73-6.

22.   Antberg, M.; Dahlenburg, L., *Acta Crystallogr., Sect. C: Cryst. Struct. Commun.* **1986,** *C42*, (8), 997-9.

23.   Dahlenburg, L.; Frosin, K. M., *Polyhedron* **1993,** *12*, (4), 427-34.

24.   MacBeth, C. E.; Harkins, S. B.; Peters, J. C., *Can. J. Chem.* **2005,** *83*, (4), 332-340.

25.   Cotton, F. A.; Luck, R. L.; Son, K. A., *Inorg. Chim. Acta* **1990,** *168*, (1), 3-4.

26.   Batten, M. P.; Canty, A. J.; Cavell, K. J.; Ruether, T.; Skelton, B. W.; White, A. H., *Acta Crystallogr., Sect. C: Cryst. Struct. Commun.* **2004,** *C60*, (7), m316-m319.

27.   Gibson, V. C.; O'Reilly, R. K.; Wass, D. F.; White, A. J. P.; Williams, D. J., *Dalton Transactions* **2003**, (14), 2824-2830.

28.   Handley, D. A.; Hitchcock, P. B.; Lee, T. H.; Leigh, G. J., *Inorg. Chim. Acta* **2001,** *316*, (1,2), 59-64.

29.   Vicic, D. A.; Anderson, T. J.; Cowan, J. A.; Schultz, A. J., *J. Am. Chem. Soc.* **2004,** *126*, (26), 8132-8133.

30.   Manger, M.; Laubender, M.; Teichert, M.; Stalke, D.; Werner, H., *J. Organomet. Chem.* **1998,** *569*, (1-2), 189-194.

31.   Antberg, M.; Dahlenburg, L., *Inorg. Chim. Acta* **1985,** *104*, (1), 51-4.

32.   Antberg, M.; Dahlenburg, L., *Z. Naturforsch., B* **1985,** *40B*, (11), 1485-9.

33.   Smernik, R. J., PhD Thesis, University of Sydney, **1996**.

Chapter 5

Summary, Conclusions and Future Work

5. Summary, Conclusions and Future Work

5.1 Iron-Nitrogen Complexes of PP$_3$ 1

In this work, a known dinitrogen bridged complex,[1] $[(FeH(PP_3))_2(\mu\text{-}N_2)]^{2+}$ **23**, was further characterised by ^{15}N NMR spectroscopy and X-ray crystallography. This cation was investigated with particular regard to the potential for activation and reaction of the complexed dinitrogen upon treatment with base and acid. The products obtained on reaction of **23** with base were identified as the singly deprotonated dinitrogen bridged iron(II)-iron(0) species $[(FeH(PP_3))(\mu\text{-}N_2)(Fe(PP_3))]^{+}$ **37**; the doubly deprotonated dinuclear iron(0)-iron(0) species $(Fe(PP_3))_2(\mu\text{-}N_2)$ **38** and the known mononuclear iron(0) complex $Fe(N_2)(PP_3)$ **44**.[1] Complex **44** was characterised by ^{15}N NMR spectroscopy and **37** by both ^{15}N NMR spectroscopy and X-ray crystallography. Treatment of $[(Fe(N_2)H(PP_3)]^{2+}$ **22**, **23**, and the deprotonated products derived from them, with acid did not result in the production of NH_4^{+}. The potential production of NH_4^{+} was assayed by ^{14}N NMR spectroscopy which was demonstrated as an effective method for detection of this cation in the reaction mixture.

None of the dinitrogen complexes studied in this work produced ammonia on treatment with acid. This contrasts with the reports from Leigh[2, 3] and George[4] where NH_3 was formed in similar systems.

A new direction for future work could include the addition an external source of electrons to facilitate the reduction of the bound dinitrogen.

Metal complexes containing coordinated diazene and hydrazine are potential intermediates in the reduction of coordinated dinitrogen to ammonia. The complex cations $[Fe(N_2H_4)H(PP_3)]^+$ **47** and $[Fe(NH_3)H(PP_3)]^+$ **46**, are potential intermediates in any reduction of **22** and **23** to yield ammonia and these were synthesised. Complex **46** was characterised by ^{15}N NMR spectroscopy and **47** by ^{15}N NMR spectroscopy and X-ray crystallography. The ammine and hydrazine complexes $[FeCl(N_2H_4)(PP_3)]^+$ **48** and $[FeCl(NH_3)(PP_3)]^+$ **49** were also synthesised. The hydrazine complexes **47** and **48** decompose at room temperature to yield the ammine complexes **46** and **49** respectively and other, as yet unidentified, species. The successful synthesis of **47** and **46** provides supporting evidence for the potential of **23** to assist in the reduction of dinitrogen to ammonia. The identification of the undefined species observed would be an important part of understanding the chemistry of these potential intermediates.

5.2 Phosphine Ligands

A number of new and known tripodal ligands have been successfully synthesised in this work. The synthesis and characterisation of known ligand $P(CH_2CH_2PMe_2)_3$ PP_3 **1** was achieved by base-catalysed addition of dimethylphosphine **2** across the double bonds of trivinylphosphine **3**. In this synthesis, the phosphine adds regioselectively to the β-carbon due to the directing influence of the central phosphine. This influence is lost in the addition of **2** across the double bond of triallylphosphine **14**.

The synthesis and characterisation of previously unknown ligands $N(CH_2CH_2CH_2PMe_2)_3$ N^3P_3 **7** and $P(CH_2CH_2CH_2P(iPr)_2)_3$ $P^3P^i_3$ **11** was achieved

by the nucleophilic substitution of the bromoalkylamine $N(CH_2CH_2CH_2Br)_3$ **9** and bromoalkylphosphine $P(CH_2CH_2CH_2Br)_3$ **16** precursors with dimethylphosphide **8** and diisopropylphosphide **18** respectively.

The known ligand[5] $P(CH_2CH_2CH_2PMe_2)_3$ P^3P_3 **19** was synthesized by the nucleophilic substitution of its chloroalkylphosphine oxide $P(O)(CH_2CH_2CH_2Cl)_3$ **20** with dimethylphosphide **8**, with subsequent reduction of the central phosphine oxide. This route is more efficient than the established route which proceeds via the radical initiated addition of dimethylphosphine **2** to triallylphosphine **14**.[6] This new synthetic approach has the added benefit of avoiding the increased risks inherent with handling of the highly pyrophoric and volatile starting material **2** for lengthy periods.

The modification of a ligand's substituents has a large influence on its success as a ligand and the chemistry of its complexes. This is illustrated by the increased stability, and ease of synthesis, of chloride complexes of PP^i_3 **12** over those of PP_3 **1** as detailed in this work. The development of new polydentate ligands which provide for complexes with a manageable balance between the desired reactivity and complex stability should be the aim of future work.

5.3 Iron and Ruthenium Complexes

In this work, the synthesis of a range of new iron and ruthenium complexes of the novel ligand $P(CH_2CH_2P(^iPr)_2)_3$ PP^i_3 **52** was achieved. Iron(0) and ruthenium(0) dinitrogen complexes $Fe(N_2)(PP^i_3)$ **52** and $Ru(N_2)(PP^i_3)$ **57** were successfully prepared by the treatment of their chloride precursors **51** and **56** with potassium

graphite under an atmosphere of dinitrogen. Treatment of **52** and **57** with an equivalent of the mild organic acid lutidinium tetrafluoroborate gave the iron(II) and ruthenium(II) complexes $[Fe(N_2)H(PP^i_3)]^+$ **53** and $[Ru(N_2)H(PP^i_3)]^+$ **58**. The characterisation of these dinitrogen species has included ^{15}N NMR spectroscopy and X-ray crystallography. Treatment of **52** with an excess of acid resulted in the dihydrogen hydride species $[Fe(H_2)H(PP^i_3)]^+$ **54**. The reaction chemistry of the dinitrogen complexes **52**, **57**, **53** and **58** with stronger acids or other reagents has yet to be explored.

The iron(II) tetramer $[Fe_4Cl_4(PP_3)_5]^{4+}$ **71**, which was previously[7] postulated as a byproduct in the synthesis of $FeCl_2(PP_3)$ **24**, has been characterised by X-ray crystallography. Characterisation of the iron(0) tetramer $Fe_4(PP_3)_5$ **72**, also by X-ray crystallography, further demonstrates the tendency of PP_3 **1**, and related ligands, to form oligomers.

Also, in this work, a ruthenium(II) complex $[RuCl(P^3P^i_3)]^+$ **65** of the new tripodal tetradentate ligand $P^3P^i_3$ **11** and an iron(II) polymeric complex $[Fe_2Cl_4(NP_3)_2]_n$ **66** of the tripodal tridentate ligand N^3P_3 **7** have been synthesised. In addition, an unusual iron(II) dimer $[(FeCl)_2(\mu\text{-}Cl)_2(\mu\text{-}P^i_2)_2]$ **68** of known ligand P^i_2 **67** has been identified. In each case characterisation of the new species has included X-ray crystallography.

Preliminary reactions of the known complex[8] $FeClH(P^3P_3)$ **70** with dinitrogen provided evidence of the formation of iron-dinitrogen species. However, the

characterisation of the reaction products and exploration of their reaction chemistry should be the subject of future work.

5.4 References

1.   Field, L. D.; Messerle, B. A.; Smernik, R. J., *Inorg. Chem.* **1997,** *36*, (26), 5984-5990.

2.   Leigh, G. J.; Jimenez-Tenorio, M., *J. Am. Chem. Soc.* **1991,** *113*, (15), 5862-3.

3.   Hall, D. A.; Leigh, G. J., *J. Chem. Soc., Dalton Trans.* **1996**, (17), 3539-3541.

4.   George, T. A.; Rose, D. J.; Chang, Y.; Chen, Q.; Zubieta, J., *Inorg. Chem.* **1995,** *34*, (5), 1295-8.

5.   Antberg, M.; Prengel, C.; Dahlenburg, L., *Inorg. Chem.* **1984,** *23*, (25), 4170-4.

6.   Bampos, N.; Field, L. D.; Messerle, B. A.; Smernik, R. J., *Inorg. Chem.* **1993,** *32*, (19), 4084-8.

7.   Smernik, R. J., PhD Thesis, University of Sydney, **1996**.

8.   Antberg, M.; Dahlenburg, L., *Z. Naturforsch., B* **1985,** *40B*, (11), 1485-9.

Chapter 6

Experimental

6 Experimental

6.1 General Procedures

All manipulations of metal complexes and air sensitive reagents described in this thesis were carried out using standard schlenk, vacuum and glove-box techniques under a dry atmosphere of argon or nitrogen.

Solvents were dried, distilled under nitrogen or argon using standard procedures[1] and stored in glass ampoules fitted with Youngs™ teflon taps. Diethyl ether, THF benzene and toluene were dried over sodium wire before distillation from sodium/ benzophenone. Hexane and pentane were distilled from sodium/potassium alloy, whilst acetone was distilled from calcium sulfate. Diethyl ether, THF (inhibitor free), toluene and pentane were also dried and deoxygenated using a Pure Solv 400-4-MD (Innovative Technology) solvent purification system. Methanol and ethanol were distilled from dimethoxy- and diethoxymagnesium respectively. Pyridine was dried over and distilled from potassium hydroxide. DCM was distilled from calcium hydride and kept over activated molecular sieves. Chloroform was deoxygenated by bubbling through a stream of nitrogen or argon for 2 hours prior to use.

Deuterated solvents were purchased from Aldrich, Merck and Cambridge Isotope Laboratories. THF-d_8 and benzene-d_6 were dried over and distilled from sodium/benzophenone, whilst acetone-d_6 was dried and distilled from calcium sulfate and stored over activated molecular sieves. Chloroform-d_1 was used as received. All deuterated solvents, excepting chloroform-d_1 and D_2O, were vacuum distilled immediately prior to use unless otherwise stated.

Starting materials were obtained from Aldrich and/or Merck and used without further purification unless stated otherwise. Tris(3-hydroxypropyl)phosphine (80%) was purchased from Strem Chemicals and used as supplied. Dichlorotris(triphenylphosphine)ruthenium(II) **55** was prepared by the literature[2] method. Potassium *t*-butoxide was sublimed twice prior to use. Lutidinium chloride was prepared by the reaction of 2,6-lutidine with hydrochloric acid in ether. Tetrafluoroboric acid in diethyl ether (50% w/v) and 2 M hydrochloric acid in diethyl ether were degassed with 3 freeze-pump-thaw cycles before use. Lutidinium tetrafluoroborate was prepared via the addition of tetrafluoroboric acid to 2,6-lutidine in water[3] by Dr A Magill and used as provided. Tris(2 diisopropylphosphinoethyl)phosphine (PP$^i_3$) **12** was prepared by Dr K Vuong via the base catalysed addition of diisopropylphosphine **13** to trivinylphosphine **3,** in a method analogous to that for PP$_3$ **1** described in Section 6.4. Potassium graphite[4] was prepared by Dr G Clentsmith and used as provided. Hydrazine (1 M in THF) was degassed with 3 freeze-pump-thaw cycles before use. ^{15}N labelled hydrazine was prepared by Soxhlet extraction of ^{15}N$_2$H$_4$·H$_2$SO$_4$ with liquid ammonia[5] and provided as an oxygen free THF solution (approx. 0.5 M) by Dr H L Li. Saturated solutions of ammonia in ethanol were prepared by bubbling ammonia gas through ethanol for an hour.

The bulk compressed gases argon (>99.99%) and nitrogen (99.5%) were obtained from the British Oxygen Company (BOC) and used without further purification. ^{15}N labelled dinitrogen was obtained from Cambridge Isotopes Laboratories and used without further purification.

Infrared spectra were recorded using a Shimadzu 8400 Series FTIR or an Avatar 370 FTIR spectrometer with samples prepared as a nujol or fluorolube mull. Microanalyses were carried out at the Campbell Microanalytical Laboratory, University of Otago, New Zealand. Single crystal X-ray analyses were performed by Dr Paul Jensen and Dr Peter Turner at the University of Sydney, Dr Tony Willis at the Australian National University and Dr Scott Dalgarno at the Heriot-Watt University, Scotland. Electron impact mass spectra (EI) were recorded on a Finnigan Polaris Q mass spectrometer at the University of Sydney using an electron energy of 70 eV. Electrospray mass spectra (ESI) were recorded on a Finnigan LCQ mass spectrometer at the University of Sydney. Data is quoted in the form x(y) where x is the mass/charge ratio and y is the percentage abundance relative to the base peak. High resolution mass spectra (HRMS) were recorded on a Bruker Apex 4.7T FTICR (Fourier Transform Ion Cyclotron Resonance) mass spectrometer at the Research School of Chemistry, Australian National University. In reporting mass spectral data, M is the molecular weight of the compound of interest.

6.2   NMR Spectroscopy

Air-sensitive NMR samples were prepared in an argon or nitrogen filled glove box or on a high vacuum line by vacuum transfer of solvent into an NMR tube fitted with a concentric teflon valve. ^{1}H, ^{15}N and ^{31}P NMR spectra were recorded on Bruker DPX(300), Bruker Avance DRX400 and Bruker DPX(500) NMR spectrometers operating at 300.17, 400.13, 500.13 MHz (^{1}H); 30.41, 40.56, 50.70 (^{15}N); and 121.49, 161.98, 202.49 MHz (^{31}P) respectively. ^{13}C and ^{14}N spectra were recorded on a Bruker Avance DRX400 at 100.61 MHz and 28.92 MHz

respectively and ^{19}F spectra were recorded on a Bruker DPX(300) at 282.40 MHz. All spectra were recorded at 300K, unless stated otherwise. [1]H and ^{13}C spectra were referenced to solvent resonances whilst ^{14}N and ^{15}N spectra were referenced to external neat nitromethane at 0.00 ppm. [19]F and ^{31}P spectra were referenced to external neat hexafluorobenzene at 163.00 ppm and trimethyl phosphite at 140.85 ppm respectively. NMR data were processed on a PC using standard Bruker software (XWINNMR, TOPSPIN 1.3 and XWINPLOT). Chemical shifts (δ) are quoted in ppm. Uncertainties in chemical shifts are typically ±0.01 ppm for ^{1}H and ±0.05 ppm for ^{13}C, ^{31}P, ^{15}N and [19]F. Scalar coupling constants (J) are given in Hz and typically have an uncertainty of ±0.1 Hz for [1]H-^{1}H and ±0.5 Hz for all other couplings. The following abbreviations are used in the reporting of NMR resonance multiplicities: s singlet, d doublet, t triplet, q quartet, p pentet, h heptet, m multiplet and br broad. The following 2D NMR techniques were used in the assignment of compounds: COSY *co*rrelation *s*pectroscop*y*, NOESY *n*uclear *o*verhauser *e*ffect *s*pectroscop*y*, HSQC *h*eteronuclear correlation through *s*ingle *q*uantum *c*oherence, HMQC *h*eteronuclear correlation through *m*ultiple *q*uantum *c*oherence and HMBC *h*eteronuclear *m*ultiple *b*ond *c*orrelation. NMR simulations were run using Spinworks 2.5 software (written by Kirk Marat, University of Manitoba). Where necessary, experimental spectra were computer enhanced by applying a Gaussian multiplication to the FID prior to performing a Fourier transform on the data.

The following sections outline the specific experimental procedures undertaken in this work.
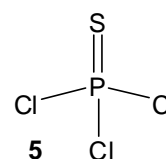
6.3   Synthesis of Dimethylphosphine, Me₂PH 2

Dimethylphosphine was prepared by the desulfurisation and cleavage of tetramethyldiphosphine disulfide following the method of Trenkle and Vahrenkamp.[6]
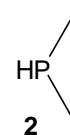
6.3.1   Trichlorophosphine Sulfide, PSCl₃ 5

Trichlorophosphine sulfide was prepared following a modified version of the method reported by Smernik.[7]

A mixture of phosphorus trichloride (210 g, 1.5 mol) and sulfur powder (50 g, 1.6 mol) was gently refluxed with the addition of aluminium trichloride (2.0 g, 0.015 mol) in two lots. A vigorous reaction occurred which resulted in a self-sustaining reflux until a clear yellow/brown solution was obtained. This solution was then placed on an oil bath and refluxed for a further 30 minutes at 100°C. The resulting mixture was distilled affording trichlorophosphine sulfide as a colourless liquid (254 g, 84%) b.p. 121-123°C.

^{31}P NMR (162 MHz, chloroform-d_1): δ 29.0 (1P, s).

6.3.2   Methylmagnesium Iodide, MeMgI

A solution of iodomethane (340 g, 2.4 mol) in diethyl ether (800 ml) was added to magnesium turnings (60 g, 2.5 mol) in diethyl ether (600 ml) over approximately 4 hours with stirring. A crystal of iodine was added to initiate the reaction. The resulting grey solution was stirred for 16 hours and used directly in the next step.

6.3.3 Tetramethyldiphosphine Disulfide, Me$_2$P(S)-P(S)Me$_2$ 4

Tetramethyldiphosphine disulfide was prepared following a

modified method from that of Parshall.[8]
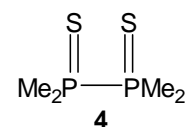
A solution of PSCl$_3$ (140 g, 0.80 mol) in diethyl ether (85 ml) was added over a

period of 3 hours to the diethyl ether solution of MeMgI (2.4 mol) leading to the

formation of a white precipitate. The temperature was maintained at 0-5°C during

the course of this addition. The reaction mixture was then warmed to room

temperature over a period of 2 hours and subsequently poured onto crushed ice

(approx. 500 g). Sulfuric acid (900 ml, 10%) was added with care and the mixture

was agitated until no further gas evolution was observed. The resultant white

solid was collected by filtration, washed with water and air dried.

Recrystallisation from ethanol gave tetramethyldiphosphine disulfide (50.3 g,

68%) as a white crystalline solid.

^{31}P$\{^{1}$H$\}$ NMR (162 MHz, chloroform-d_1): δ 32.2 (2P, s).

^{1}H$\{^{31}$P$\}$ NMR (400 MHz, chloroform-d_1): δ 1.94 (12H, s).

6.3.4 Dimethylphosphine, (CH$_3$)$_2$PH 2

Dimethylphosphine was prepared following the method of Trenkle and

Vahrenkamp.[6]
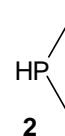
Tetramethyldiphosphine disulfide (31 g, 0.16 mol), tri-n-butylphosphine (66 g,

0.33 mol) and water (3.0 g, 0.16 mol) were added to a round-bottom flask fitted

with a short fractionating column connected to a condenser cooled to 0°C and a

collecting vessel cooled to -78°C. The reaction mixture was slowly heated to

140°C (approx. 1 hour) using an oil bath. After this time the reaction mixture appeared as a homogenous solution and the temperature was increased to 170°C. The volatile dimethylphosphine was distilled under nitrogen from the reaction mixture (b.p. 20°C) and subsequently trap to trap distilled to afford a clear, malodorous, highly air sensitive liquid (13 g, 88%).

$^{31}P\{^{1}H\}$ NMR (162 MHz, THF): δ -99.0 (1P, s).

6.4 Synthesis of Tris(2-dimethylphosphinoethyl)phosphine, P(CH₂CH₂P(CH₃)₂)₃, PP₃ 1

Tris(2-dimethylphosphinoethyl)phosphine was prepared by the base catalysed addition of dimethylphosphine to trivinylphosphine in a method modified from that of Morris *et al.* used in the synthesis of analogous tripodal tetradentate phosphine ligands.[9]
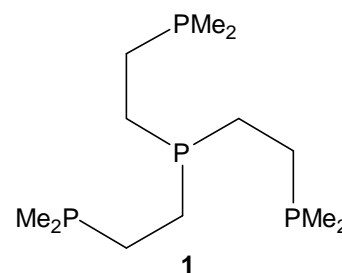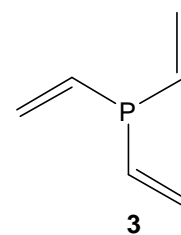
6.4.1 Vinylmagnesium Bromide, CH₂CHMgBr

Vinyl bromide (23 g, 0.21 mol) was condensed into THF (40 ml) cooled to -78°C. This solution was added dropwise to a stirred suspension of magnesium turnings (5.1 g, 0.21 mol) in THF (80 ml) maintaining a moderately vigorous reaction. The reaction was initiated by addition of a crystal of iodine and heat. On completion of the reaction the magnesium turnings were consumed leaving a brown solution of vinylmagnesium bromide in THF. This solution was used directly in the preparation of trivinylphosphine.

6.4.2 Trivinylphosphine, P(CHCH₂)₃ 3

In a method modified from that of Maier *et al.*,[10] trimethyl phosphite (6.6 g, 0.053 mol) in THF (20ml) was added dropwise to 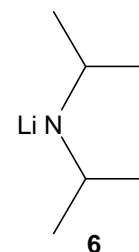a THF solution of vinylmagnesium bromide (from Section 6.4.1) causing a gentle reflux to occur. During the course of the reaction the colour of the solution changed from brown to yellow. The solvent and product were distilled from the reaction mixture in two fractions between 64-78°C. The first fraction distilled at 64-68°C was THF only and discarded. The second fraction was a solution of trivinylphosphine in THF. This was used directly without further purification.

$^{31}P\{^{1}H\}$ NMR (162 MHz, THF): δ -19.8 (1P, s).

### 6.4.3 Lithium Diisopropylamide, LiN(CH(CH₃)₂)₂ 6

Diisopropylamine (10 g, 0.10 mol) was added to a flask containing hexane (20 ml) at -78°C. *n*-Butyllithium (2.5 M in hexane, 40 ml, 0.10 mol) was added dropwise over a 30 min period with stirring. The reaction mixture was then stirred for a further 30 min at -78°C before being allowed to warm to room temperature. During the course of the reaction, the clear solution took on the appearance of a white emulsion as the lithium diisopropylamide precipitated out. The solvent was removed *in vacuo* leaving lithium diisopropylamide as a white solid.

6.4.4 Tris(2-dimethylphosphinoethyl)phosphine, P(CH₂CH₂P(CH₃)₂)₃, PP₃ 1

PP$_3$ **1** was prepared in a method modified from that of

Morris *et al.* used in the synthesis of analogous tripodal

tetradentate phosphine ligands.[9]
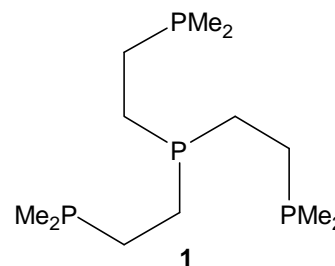
Dimethylphosphine (13 g, 0.21 mol) was added to a

solution of trivinylphosphine (*ca* 0.05 mol) in THF (100 ml). Lithium

diisopropylamide (ca 0.1 mol) in THF (40 ml) was added in stages with stirring

over a 15 min period to control the vigour of the reaction. During the course of

the reaction effervescence occurred and the solution turned bright yellow. Once

addition of the base was complete and no trivinylphosphine **3** remained ($^{31}P\{^1H\}$

NMR) the solution was cooled to -78°C and methanol (approx. 20 ml) added to

quench the base catalyst. This resulted in a colour change from yellow to off

white. The reaction mixture was allowed to warm to room temperature and the

solvents then removed *in vacuo*. The resulting off white solid was extracted with

benzene (50 ml) and the extract was filtered through celite. The benzene was

removed *in vacuo* leaving PP$_3$ as a white solid (7.4 g, 50% from trimethyl

phosphite).

$^{31}P\{^1H\}$ NMR (162 MHz, benzene-d_6): δ -19.6 (1P, q, $^3J_{P-P}$ = 20.7 Hz, **P**(CH₂)₃);

-47.7 (3P, d, **P**Me₂); (lit[7] -19.8 1P, -48.6 3P).

6.5 Synthesis of Tris(3-dimethylphosphinopropyl)amine, N(CH$_2$CH$_2$CH$_2$P(CH$_3$)$_2$)$_3$, N^{3}P$_3$ 7

Tris(3-dimethylphosphinopropyl)amine was prepared by the nucleophilic substitution of bromide in tris(3-bromopropylamine) with dimethylphosphide in a method modified from that of Peters *et al.* used in the synthesis of analogous tripodal tridentate phosphinoamine ligands.[11]
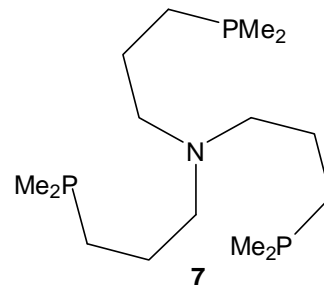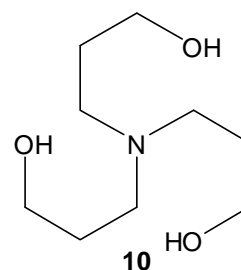
6.5.1 Tris(3-bromopropyl)amine), N(CH$_2$CH$_2$CH$_2$Br)$_3$ 9

Tris(3-bromopropylamine) was prepared following a slightly modified method to that of Piguet *et al.*[12]
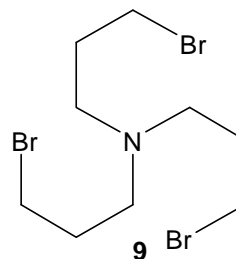
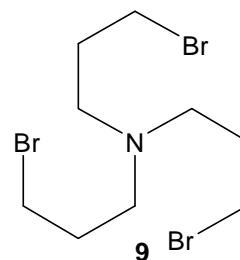#### 6.5.1.1 Tris(3-hydroxypropyl)amine, N(CH$_2$CH$_2$CH$_2$OH)$_3$ 10

3-Chloro-1-propanol (25 ml, 0.30 mol), 3-amino-1-propanol (10 ml, 0.13 mol) and sodium carbonate (34 g, 0.32 mol) were refluxed in absolute ethanol (75 ml) for 24 hours. The reaction mixture was allowed to cool to room temperature and the solvent removed *in vacuo* affording a clear oil of slightly impure tris(3-hydroxypropyl)amine which was used directly in the next step without further purification.

^{1}H NMR (300 MHz, chloroform-d_1): δ 4.74 (3H, b, O**H**); 3.57 (6H, t, $^3J_{H-H}$ = 6.0 Hz, C**H$_2$**OH); 2.57 (6H, t, $^3J_{H-H}$ = 7.2 Hz, NC**H$_2$**); 1.66 (6H, m, CH$_2$C**H$_2$**CH$_2$).

6.5.1.2 Tris(3-bromopropyl)amine, $N(CH_2CH_2CH_2Br)_3$ 9

Phosphorus tribromide (25 ml, 0.26 mol) was added dropwise to a stirring solution of tris(3-hydroxypropyl)amine (approx. 0.13 mol) in chloroform (150 ml). The reaction mixture was then refluxed for 18 hours. Once cooled to room temperature the excess phosphorus tribromide was quenched by the slow addition of ethanol (100 ml). The solvents were then removed *in vacuo* and the resulting clear liquid left at ambient temperature for 24 hours during which time large white crystals of $N(CH_2CH_2CH_2Br)_3$ 9 formed. The crystals were isolated by filtration and washed with an ice cold mixture of water and methanol then dried in a vacuum desiccator for 48 hours (19.0 g, 38% based on 3-amino-1-propanol).

^{1}H NMR (300 MHz, chloroform-d_1): δ 3.40 (6H, t, $^3J_{H-H}$ = 6.2 Hz, C**H**$_2$Br); 2.46 (6H, t, $^3J_{H-H}$ = 6.5 Hz, NC**H**$_2$); 1.91 (6H, m, CH$_2$C**H**$_2$CH$_2$).

LRMS (ESI$^+$, methanol) *m/z*: 380 ([M+H]$^+$, 43%), 300 ([M-Br+H]$^+$,100).

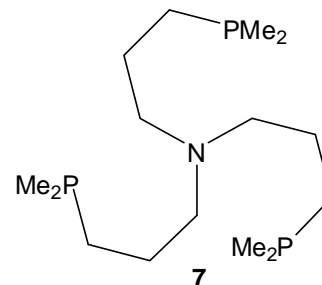### 6.5.2 Lithium Dimethylphosphide, $LiP(CH_3)_2$ 8

The lithium dimethylphosphide was prepared following a modified method by Fryzuk *et al.*[13]
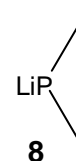
n-Butyllithium (2.5 M in hexane, 24.3 ml, 0.061 mol) was added via canula to dimethylphosphine (3.76 g, 0.0606 mol) at -78°C with stirring. The reaction mixture was allowed to warm to room temperature and the solvent removed *in vacuo*. The white solid was then dissolved in approximately 50 ml THF resulting in a yellow solution which was used directly in the next step.

6.5.3 Tris(3-dimethylphosphinopropyl)amine, N(CH$_2$CH$_2$CH$_2$P(CH$_3$)$_2$)$_3$, N^{3}P$_3$ 7

The lithium dimethylphosphide solution from the previous step was added dropwise to a stirring solution of tris(3-bromopropyl)amine (7.0 g, 0.018 mol) in THF (approx. 20 ml) at 0°C. The reaction mixture was then left to stir at room temperature for 18 hours. The solvent was removed in *vacuo* and deaerated water (approx. 50 ml) added with care at 0°C until all excess lithium phosphide had been destroyed (evidenced by a cessation in sputtering of the reaction mixture). Benzene (approx. 50 ml) was added and the mixture stirred for 30 minutes. The organic layer was then decanted off, dried over anhydrous magnesium sulfate and filtered. Removal of the solvent *in vacuo* gave tris(3-dimethylphosphinopropyl)amine as a clear oil (4.76 g, 80%).

^{31}P{^{1}H} NMR (162 MHz, benzene-d_6): δ -51.8 (3P, s).

^{1}H{^{31}P} NMR (400 MHz, benzene-d_6): δ 2.42 (6H, t, $^3J_{\text{H-H}}$ = 7.1 Hz, NC**H**$_2$); 1.57 (6H, m, CH$_2$C**H**$_2$CH$_2$); 1.26 (6H, t, $^3J_{\text{H-H}}$ = 8.3 Hz, C**H**$_2$P); 0.86 (18H, s, PC**H**$_3$).

^{13}C{^{1}H} NMR (101 MHz, benzene-d_6): δ 55.8 (d, $^3J_{\text{C-P}}$ = 12 Hz, N**C**H$_2$); 30.4 (d, $^1J_{\text{C-P}}$ = 14 Hz, **C**H$_2$P); 24.2 (d, $^2J_{\text{C-P}}$ = 11 Hz, CH$_2$**C**H$_2$CH$_2$); 14.4 (d, $^1J_{\text{C-P}}$ = 15 Hz, P(**C**H$_3$)$_2$).

HRMS (EI) *m/z*: [M+H]$^+$ 324.2126 (calc. 324.2139).

LRMS (ESI$^+$, methanol) *m/z*: 430 (100%), 324 ([M+H]$^+$, 61), 262 ([M-PMe$_2$]$^+$, 55).

6.6 Synthesis of Tris(3-dimethylphosphinopropyl)phosphine, $P(CH_2CH_2CH_2P(CH_3)_2)_3$ P^3P_3 19

Tris(3-dimethylphosphinopropyl)phosphine was prepared by the nucleophilic substitution of chloride in tris(3-chloropropyl)phosphine oxide with dimethylphosphide followed by reduction of the central phosphine.
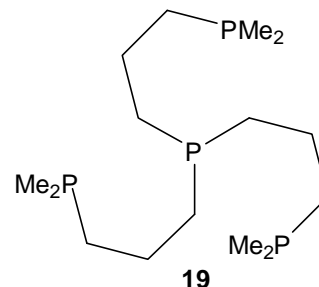
6.6.1 Tris(3-chloropropyl)phosphine oxide, $P(O)(CH_2CH_2CH_2Cl)_3$ 20

Tris(3-chloropropyl)phosphine oxide was prepared using a modified procedure by Kaden *et al.*[14] where thionyl chloride was used in the conversion of a diol to a dichloro species.
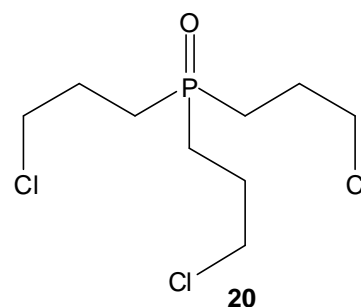
Tris(3-hydroxypropyl)phosphine (16.5 g, 0.0793 mol) and dry pyridine (16 ml, 0.20 mol) were dissolved in approximately 150 ml DCM. Thionyl chloride (25 ml, 0.34 mol) was added dropwise causing a vigorous reaction which resulted in the reaction mixture taking on a gelatinous appearance until approximately half the thionyl chloride had been added. Once addition was completed the reaction mixture, which had a cloudy dark orange appearance, was refluxed gently with stirring for two hours then allowed to cool to room temperature and stirred for a further 16 hours resulting in a light brown solution with a small amount of solid visible. Hydrochloric acid (50 ml, 1.0 M) was added with caution after which the organic layer was separated and washed with saturated sodium carbonate until all effervescence ceased (approx. 50 ml). The resulting organic layer was separated,

dried over magnesium sulfate and filtered. The solvent was then removed *in vacuo* to afford tris(3-chloropropyl)phosphine oxide as an off white solid (14.4 g, 65%).

$^{31}P\{^{1}H\}$ NMR (162 MHz, benzene-d_6): δ 47.3 (1P, s).

$^{1}H\{^{31}P\}$ NMR (400 MHz, benzene-d_6): δ 3.52 (6H, m, **CH$_2$**Cl); 1.97 (6H, m, CH$_2$**CH$_2$**CH$_2$); 1.79 (6H, m, P(O)**CH$_2$**).

$^{13}C\{^{1}H\}$ NMR (101 MHz, benzene-d_6): δ 45.4 (d, $^{3}J_{C\text{-}P}$ = 16 Hz, **CH$_2$**Cl); 25.9 (d, $^{1}J_{C\text{-}P}$ = 66 Hz, P(O)**CH$_2$**); 24.9 (s, CH$_2$**CH$_2$**CH$_2$).

HRMS (EI) *m/z*: [M+H]$^{+}$ 279.0224 (calc. 279.0239).

LRMS (ESI^{+}, methanol) *m/z*: 319 (68%), 301 ([M+Na]$^{+}$, 100), 287 (74), 279 ([M+H]$^{+}$, 59), 243 ([M-Cl]$^{+}$, 68).

6.6.2 Tris(3-dimethylphosphinopropyl)phosphine oxide, P(O)(CH$_2$CH$_2$CH$_2$P(CH$_3$)$_2$)$_3$ 21

Tris(3-chloropropyl)phosphine oxide (3.16 g, 0.0113 mol) was dissolved in approximately 20 ml THF and cooled to 0°C. A yellow solution of lithium dimethylphosphide (prepared from dimethylphosphine (2.1 g, 0.034 mol) as described in Section 6.5.2) in approximately 20 ml THF was added and the reaction mixture was allowed to warm to room temperature resulting in a pale brown solution which was stirred under nitrogen for 16 hours. The solvent was removed *in vacuo,* and 75 ml of water added with caution followed by 75 ml of benzene. The organic layer was decanted, dried over magnesium sulfate, filtered
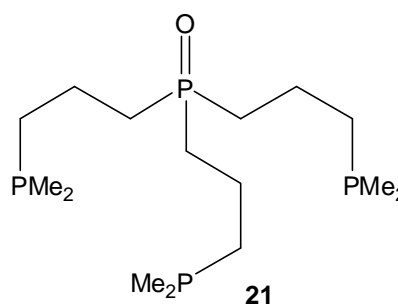
and the solvent removed *in vacuo* to give tris(3-dimethylphosphinopropyl)phosphine oxide as a white solid (2.69 g, 67%).

$^{31}P\{^{1}H\}$ NMR (162 MHz, benzene-d_6): δ 46.2 (1P, s, **P**(O)); -52.4 (3P, s, **P**Me$_2$).

$^{1}H\{^{31}P\}$ NMR (400 MHz, benzene-d_6): δ 1.38-1.70 (12H, br m, P(O)C**H**$_2$C**H**$_2$); 1.27 (6H, m, C**H**$_2$P(CH$_3$)$_2$); 0.80 (18H, s, C**H**$_3$).

HRMS (EI) *m/z*: [M+H]$^{+}$ 357.1798 (calc. 357.1795).

LRMS (ESI^{+}, methanol) *m/z*: 357 ([M+H]$^{+}$, 100%).

6.6.3 Tris(3-dimethylphosphinopropyl)phosphine, P(CH$_2$CH$_2$CH$_2$P(CH$_3$)$_2$)$_3$, P^{3}P$_3$ 19

Trichlorosilane (6 ml, 60 mmol) was added to tris(3-dimethylphosphinopropyl)phosphine oxide (2.69 g, 7.56 mmol) in THF (approx. 60 ml) and the reaction mixture refluxed under nitrogen for 18 hours. The reaction mixture was then cooled to 0°C and quenched by the addition of deaerated aqueous sodium hydroxide solution (40% w/w, 100 g) with stirring. After warming to room temperature, toluene (approx. 100 ml) was added and the reaction mixture left stirring for several hours until 2 clear fractions were evident. The organic layer was then decanted, dried over anhydrous magnesium sulfate and filtered. The solvent was removed *in vacuo* to afford tris(3-dimethylphosphinopropyl)phosphine as a white solid (1.81 g, 70%).
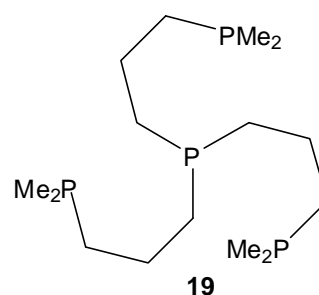
$^{31}P\{^{1}H\}$ NMR (162 MHz, benzene-d_6): δ -31.5 (1P, s, **P**(CH$_2$)$_3$); -51.2 (3P, s, **P**Me$_2$) (lit.[15] -34.4 1P, -54.2 3P).

6.7 Synthesis of Tris(3-diisopropylphosphinopropyl)phosphine, $P(CH_2CH_2CH_2P(CH(CH_3)_2)_2)_3$, $P^3P^i_3$ 11

Tris(3-diisopropylphosphinopropyl)phosphine was prepared by the nucleophilic substitution of bromide in tris(3-bromopropyl)phosphine with lithium diisopropylphosphide.

11
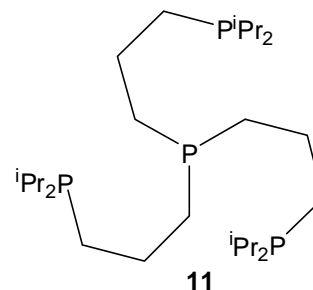
6.7.1 Tris(3-bromopropyl)phosphine 16

Phosphorus tribromide (4.3 ml, 0.046 mol) was added dropwise to a stirring suspension of tris(3-hydroxypropyl)phosphine (7.7 g, 0.037 mol) in chloroform (30 ml). The reaction mixture was then stirred

16
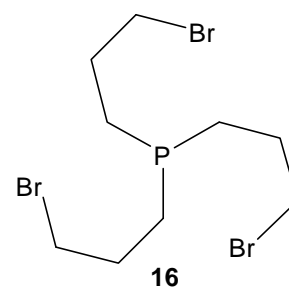
at room temperature for 18 hours. Saturated aqueous sodium carbonate solution (approx. 30 ml) was added to the reaction mixture until all effervescence ceased. The organic layer was then separated and dried over magnesium sulfate. The solution was filtered and the solvent was removed *in vacuo* to give tris(3-bromopropyl)phosphine as a clear liquid (9.0 g, 62%). This product was used immediately in the next step without further purification.

^{31}P NMR (162 MHz, benzene-d_6): δ -34.1 (1P, h, $^2J_{P-H}$ = 7 Hz)

^{1}H{^{31}P} NMR (400 MHz, benzene-d_6): δ 2.99 (6H, m, C**H**$_2$Br); 1.56 (6H, m, PC**H**$_2$); 1.06 (6H, m, CH$_2$C**H**$_2$CH$_2$).

^{13}C{^{1}H} NMR (101 MHz, benzene-d_6): δ 34.7 (d, $^3J_{C-P}$ = 14 Hz, **C**H$_2$Br); 29.4 (d, $^1J_{C-P}$ = 16 Hz, P**C**H$_2$); 25.5 (d, $^2J_{C-P}$ = 15 Hz, CH$_2$**C**H$_2$CH$_2$).

6.7.2   Diisopropylphosphine, $((CH_3)_2CH)_2PH$ 13

Diisopropylphosphine was prepared following a modification of the method by Krogh-Jespersen, Goldman *et al.*[16]
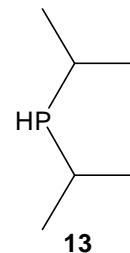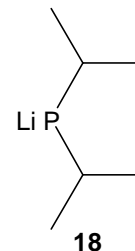
A solution of chlorodiisopropylphosphine (26 ml, 0.16 mol) in diethyl ether (50 ml) was added dropwise to a suspension of lithiumaluminium tetrahydride (3.0 g, 0.080 mol) in diethyl ether (approx. 200 ml) at 0°C over the course of an hour with stirring. The reaction mixture was then allowed to warm to room temperature and stirred for a further 18 hours. The reaction mixture was then filtered and distilled under nitrogen. An azeotropic mixture of diethyl ether and diisopropylphosphine was collected between 40°C and 118°C (11.5 g determined by integration of ^1H NMR spectrum, 60%).

$^{31}P\{^1H\}$ NMR (122 MHz, benzene-d_6): δ -15.8 (1P, s)

^1H NMR (300 MHz, benzene-d_6): δ 2.63 (1H, br s, **H**P); 1.77 (2H, m, PC**H**); 0.93 (6H, d, $^3J_{H\text{-}H}$ = 7.0 Hz, C**H**$_3$); 0.88 (6H, d, $^3J_{H\text{-}H}$ = 6.9 Hz, C**H**$_3$).

6.7.3   Lithium Diisopropylphosphide, $LiP(CH(CH_3)_2))_2$ 18

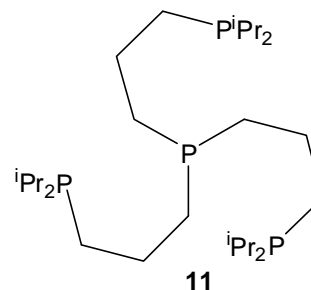The lithium phosphide was prepared following a modified method by Fryzuk *et al.*[13]

n-Butyllithium (1.6 M in hexane, 60 ml, 0.097 mol) was added to diisopropylphosphine (48% w/w in diethyl ether, 24 g, 0.097 mol) at 0°C with stirring. The reaction was allowed to warm to room temperature and THF (50 ml) was added resulting in a red solution which was used directly in the next step (Section 6.7.4).

6.7.4 Tris(3-diisopropylphosphinopropyl)phosphine, P(CH$_2$CH$_2$CH$_2$P(CH(CH$_3$)$_2$)$_2$)$_3$, P^{3}P$^i_3$ 11

The lithium diisopropylphosphide solution from the previous step (Section 6.7.3) was added to a stirring solution of tris(3-bromopropyl)phosphine (9.0 g, 0.023 mol) in THF (approx. 100 ml) at 0°C. The reaction mixture was then left to stir at room temperature for 18 hours. The solvent was removed *in vacuo* and deaerated water (approx. 50 ml) added with care at 0°C until all excess lithium phosphide had been destroyed. Benzene (approx. 50 ml) was then added and the mixture stirred for 30 minutes. The organic layer was decanted, dried over anhydrous magnesium sulfate and filtered resulting in a brown solution. Attempts to decolourise the solution by stirring with deactivated charcoal and filtering through celite were unsuccessful. The solvents were removed *in vacuo* and the resulting brown oil was heated under vacuum (0.4 mbar) to distill off any impurities, including bis(diisopropylphosphino)methane **P$^i_2$ 67** (b.p. 76°C at 0.4 mbar), leaving tris(3-diisopropylphosphinopropyl)phosphine as a brown oil (6.56g, 56%).

^{31}P{^{1}H} NMR (162 MHz, benzene-d_6): δ 1.9 (3P, s, **P**^{i}Pr$_2$); -34.7 (1P, s, **P**(CH$_2$)$_3$).

^{1}H{^{31}P} NMR (400 MHz, benzene-d_6): δ 1.75 (6H, m, CH$_2$**CH$_2$**CH$_2$); 1.58 (6H, m, **CH**(CH$_3$)$_2$); 1.53 (6H, m, PC**H$_2$**CH$_2$); 1.42 (6H, t, $^3J_{H-H}$ = 8 Hz, **CH$_2$**P(C$_3$H$_7$)$_2$); 1.05 (18H, d, $^3J_{H-H}$ = 7 Hz, **CH$_3$**); 1.03 (18H, d, $^3J_{H-H}$ = 7 Hz, **CH$_3$**).

^{13}C{^{1}H} NMR (101 MHz, benzene-d_6): δ 29.8 (dd, J_{C-P} = 12 Hz, 15 Hz, P**CH$_2$**CH$_2$); 25.4 (dd, J_{C-P} = 20 Hz, 14 Hz, CH$_2$**CH$_2$**CH$_2$); 24.1 (dd, J_{C-P} = 20 Hz, 10 Hz, **CH$_2$**P(C$_3$H$_7$)$_2$); 23.7 (d, $^1J_{C-P}$ = 14 Hz, P(**CH**(CH$_3$)$_2$); 20.4 (d, $^2J_{C-P}$ = 16 Hz, P(CH(**CH$_3$**)$_2$); 19.0 (d, $^2J_{C-P}$ = 10 Hz, P(CH(**CH$_3$**)$_2$).

HRMS (EI) *m/z*: [M+H]$^+$ 509.3716 (calc. 509.3724).

LRMS (ESI$^+$, methanol) *m/z*: 542 ([M+2O+H]$^+$, 73%), 525 ([M+O+H]$^+$, 79), 510 ([M+H]$^+$, 100).

6.8   Iron and Ruthenium Complexes

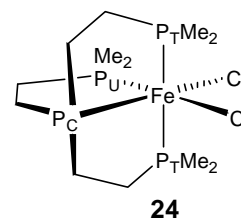### 6.8.1   Lithium Aluminium Hydride Solution, LiAlH$_4$

The method used was based on that reported by Turnbull.[17]

THF (100 ml) was refluxed for 18 h in a Soxhlet apparatus with lithiumaluminium tetrahydride powder (3.0 g, 0.079 mol).   The resulting grey solution was used without determination of concentration (approx. 0.5 M[17]).

6.8.2   [OC-6-32] dichloro(tris(2-dimethylphosphinoethyl)phosphine-κ^4*P*)iron(II), FeCl$_2$(PP$_3$) 24

The method used was based on that reported by Smernik.[7]

24

Solutions of anhydrous iron(II) chloride (200 mg, 1.6 mmol) and PP$_3$ **1** (470 mg, 1.6 mmol) in THF (50 ml each) were added at equal rates over a period of 4 hours to THF (approx. 85 ml) with rapid stirring.   The reaction mixture was maintained at 0°C under an atmosphere of argon, affording a red solution and a small amount of reddish brown solid.   The red solution of FeCl$_2$(PP$_3$) **24** was used directly in the next step without further purification.

6.8.3 [OC-6-24] chlorohydrido(tris(2-dimethylphosphinoethyl)phosphine-κ^4*P*)iron(II), FeClH(PP$_3$) 25

A THF solution of lithiumaluminium tetrahydride (approx. 0.5 M) was added dropwise to the red solution of FeCl$_2$(PP$_3$) **24** in THF from the previous step (Section 6.8.2)


25
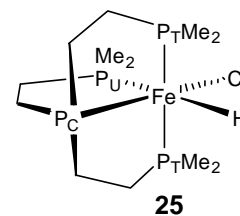
at 0°C causing a colour change from red to bright yellow. The colour change was used to determine the endpoint of the reaction. The solvent was removed *in vacuo* and the resulting orange solid dissolved in benzene (approx. 5 ml). This solution was filtered under argon and the solvent removed *in vacuo* affording FeClH(PP$_3$) **25** as an orange solid (100 mg, 16%).

^{31}P{^{1}H} NMR (162 MHz, benzene-d_6): δ 184.8 (1P, dt, $^2J_{\text{P(C)-P(T)}}$ = 30.3 Hz, $^2J_{\text{P(C)-P(U)}}$ = 23.5 Hz, **P$_C$**); 61.5 (2P, dd, $^2J_{\text{P(T)-P(U)}}$ = 22.5 Hz, **P$_T$**); 60.2 (1P, dt, **P$_U$**) (lit[18] 184.8 **P$_C$**, 61.3 **P$_T$**, 60.0 **P$_U$**).

^{1}H{^{31}P} NMR (400 MHz, benzene-d_6, high field): δ -11.74 (1H, s, Fe-**H**) (lit[18] -11.63).

6.8.4 μ-(dinitrogen)bis[hydrido(tris(2-dimethylphosphinoethyl)phosphine-κ^4*P*)iron] dichloride, [(FeH(PP$_3$))$_2$(μ-N$_2$)]Cl$_2$ 23.Cl$_2$ and [OC-6-34] [(dinitrogen)hydrido(tris(2-dimethylphosphinoethyl)phosphine-κ^4*P*)iron] chloride, [Fe(N$_2$)H(PP$_3$)]Cl 22.Cl

23.Cl$_2$ **22.Cl**
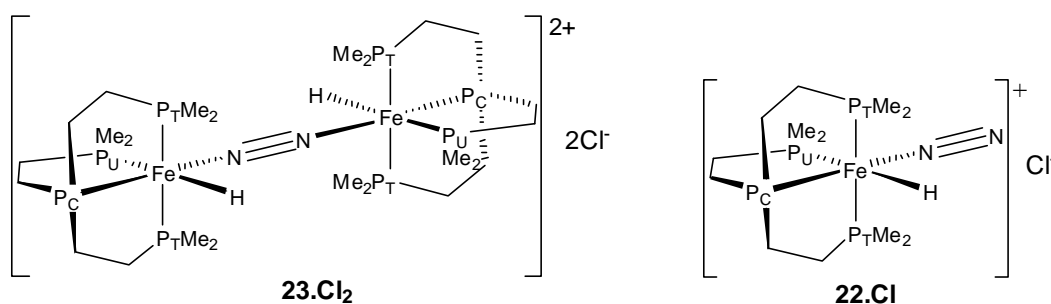
The procedure used was that based on Field *et al.*[18]

A typical procedure for the preparation of $[(FeH(PP_3))_2(\mu\text{-}N_2)]Cl_2$ and $[Fe(N_2)H(PP_3)]Cl$ in ethanol is described:

FeClH(PP_3) **25** (100 mg, 260 μmol) was dissolved in ethanol (approx. 5 ml) and allowed to stand under nitrogen for one week. This resulted in a dark orange solution containing both the mononuclear and dinuclear dinitrogen complexes **22.Cl** and **23.Cl_2**.

$[(FeH(PP_3))_2(\mu\text{-}N_2)]Cl_2$ **23.Cl_2**

$^{31}P\{^1H\}$ NMR (162 MHz, ethanol): δ 172.3 (2P, dt, $^2J_{P(C)\text{-}P(T)}$ = 31.0 Hz, $^2J_{P(C)\text{-}P(U)}$ = 24.0 Hz, **P_C**); 62.1 (4P, dd, $^2J_{P(T)\text{-}P(U)}$ = 14.6 Hz **P_T**,); 59.4 (2P, dt, **P_U**).

$^1H\{^{31}P\}$ NMR (400 MHz, ethanol, high field): δ -12.75 (2H, s, Fe-**H**).

$[Fe(N_2)H(PP_3)]Cl$ **22.Cl**

$^{31}P\{^1H\}$ NMR (162 MHz, ethanol): δ 171.9 (1P, dt, $^2J_{P(C)\text{-}P(T)}$ = 30.4 Hz, $^2J_{P(C)\text{-}P(U)}$ = 26.8 Hz , **P_C**); 62.9 (2P, dd, $^2J_{P(T)\text{-}P(U)}$ = 17.4 Hz, **P_T**); 60.9 (1P, dt, **P_U**).

$^1H\{^{31}P\}$ NMR (400 MHz, ethanol, high field): δ -12.91 (1H, s, Fe-**H**).

The ^{15}N labelled analogues of these complexes were synthesised by dissolution of FeClH(PP_3) **25** (50-100 mg, 130-260 μmol) in nitrogen free ethanol (1 ml) in an NMR tube fitted with a concentric teflon tap under argon. The solution was degassed by 3 freeze-pump-thaw cycles followed by introduction of $^{15}N_2$ to the NMR tube.

$[(FeH(PP_3))_2(\mu\text{-}^{15}N_2)]Cl_2$ **$^{15}N_2$-23.Cl_2**

$^{15}N\{^1H\}$ NMR (40.6 MHz, ethanol): δ -58.7 (2N, m).

$[Fe(^{15}N_2)H(PP_3)]Cl$ **$^{15}N_2$-22.Cl**
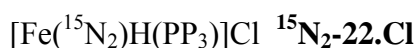
$^{15}N\{^1H\}$ NMR (40.6 MHz, ethanol): δ -34.2 (1N, br s, Fe-N**N**);

-63.4 (1N, m, Fe-**N**).

6.8.5   μ-(^{15}N-dinitrogen)bis[hydrido(tris(2-dimethylphosphinoethyl)-phosphine-κ^4P)iron] bis[tetra(3,5-bis(trifluoromethyl)phenyl)borate], [(FeH(PP$_3$))$_2$(μ-^{15}N$_2$)][BAr$^F_4$]$_2$ ^{15}N$_2$-23.[BAr^F]$_2$

^{15}N$_2$-23.[BAr^F]$_2$
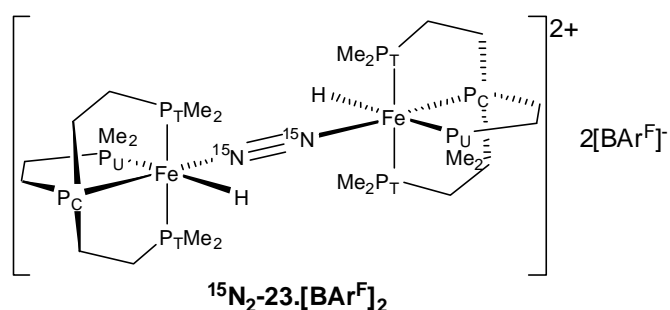
Crystals of the ^{15}N labelled dication [(FeH(PP$_3$))$_2$(μ-N$_2$)]$^{2+}$ **23** as its

bis[tetra(3,5-bis(trifluoromethyl)phenyl)borate] salt suitable for X-ray diffraction

were grown by addition of sodium tetra(3,5-bis(trifluoromethyl)phenyl)borate

(100 mg, 11 μmol) to an ethanol solution (2 ml) of **^{15}N$_2$-23.Cl$_2$** and **^{15}N$_2$-22.Cl**

described above. The solution was then left under an atmosphere of argon in a

sealed vial for several weeks during which time pale orange crystals formed.

6.8.6   μ-(dinitrogen)bis[hydrido(tris(2-dimethylphosphinoethyl)phosphine-κ^4P)iron] bis[tetraphenylborate], [(FeH(PP$_3$))$_2$(μ-N$_2$)][BPh$_4$]$_2$ 23.[BPh$_4$]$_2$

The procedure used was that based on Field *et al.*[18]

23.[BPh$_4$]$_2$
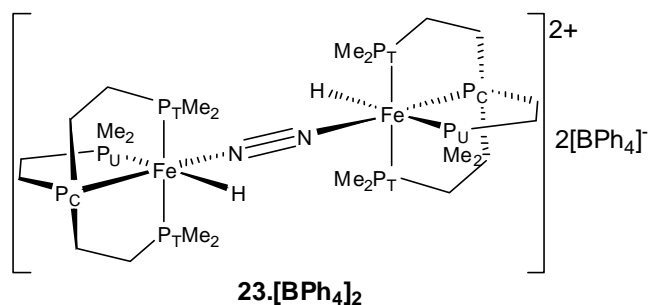
A solution of FeClH(PP$_3$) **25** (100 mg, 260 μmol) in ethanol (5 ml) was allowed to stand under nitrogen for 5 days. After this time sodium tetraphenylborate (100 mg, 290 μmol) was added and a buff coloured precipitate formed immediately. This precipitate was filtered, washed with acetone and subsequently ethanol and then dried under nitrogen to give [(FeH(PP$_3$))$_2$(μ-N$_2$)][BPh$_4$]$_2$ **23.[BPh$_4$]$_2$** (181 mg, 95%).

^{31}P{^{1}H} NMR (162 MHz, acetone-d_6): δ 173.0 (dt, 2P, $^2J_{P(C)-P(T)}$ = 30.8 Hz, $^2J_{P(C)-P(U)}$ = 23.1 Hz, **P$_C$**); 62.6 (dd, 4P, $^2J_{P(T)-P(U)}$ = 16.2 Hz, **P$_T$**); 59.9 (dt, 2P, **P$_U$**) (lit.[18] 172.7 **P$_C$**, 62.2 **P$_T$**, 59.6 **P$_U$**).

^{1}H NMR (400 MHz, acetone-d_6, high field): δ -12.63 (2H, ddt, Fe-**H**, $^2J_{P(C)-H}$ = 44.1 Hz, $^2J_{P(U)-H}$ = 28.7 Hz , $^2J_{P(T)-H}$ = 63.1 Hz) (lit.[18] -12.50).

6.8.7 [OC-6-34] [(dinitrogen)hydrido(tris(2-dimethylphosphinoethyl) phosphine-κ^4*P*)iron] [tetraphenylborate], [Fe(N$_2$)H(PP$_3$)][BPh$_4$] 22.[BPh$_4$]

The procedure used was that based on Field *et al.*[18]

22.[BPh$_4$]
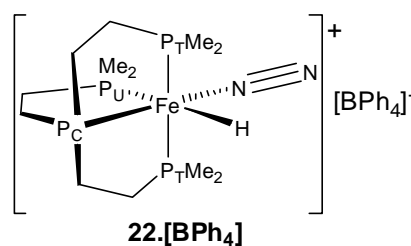
FeClH(PP$_3$) **25** (20 mg, 50 μmol) was dissolved in degassed ethanol (approx. 10 ml) containing sodium tetraphenylborate (20 mg, 60 μmol) under argon. Nitrogen gas was bubbled through the orange solution for an hour causing the precipitation of a small amount of peach coloured solid. This solid was collected by filtration and dried under nitrogen to afford [Fe(N$_2$)H(PP$_3$)][BPh$_4$] **22.[BPh$_4$]** as a fine powder (approx. 20 mg, 50%).

$^{31}P\{^1H\}$ NMR (162 MHz, acetone-d_6): δ 172.6 (1P, dt, $^2J_{P(C)-P(T)}$ = 30.4 Hz,

$^2J_{P(C)-P(U)}$ = 26.5 Hz, $\mathbf{P_C}$); 63.6 (2P, dd, $^2J_{P(T)-P(U)}$ = 17.5 Hz, $\mathbf{P_T}$); 61.7 (1P, dt, $\mathbf{P_U}$)

(lit.[18] 172.3 $\mathbf{P_C}$, 63.2 $\mathbf{P_T}$, 61.4 $\mathbf{P_U}$).

^1H NMR (400 MHz, acetone-d_6, high field): δ -12.78 (1H, m, Fe-$\mathbf{H}$) (lit.[18] -12.66)

6.8.8 μ-(dinitrogen)bis[hydrido(tris(2-dimethylphosphinoethyl)phosphine-$\kappa^4 P$)iron] bis[tetrafluoroborate], [(FeH(PP$_3$))$_2$(μ-N$_2$)][BF$_4$]$_2$ 23.[BF$_4$]$_2$

The procedure used was that based on Field *et al.*[18]

A solution of FeClH(PP$_3$) **25** (100 mg, 260 μmol) in ethanol

23.[BF$_4$]$_2$
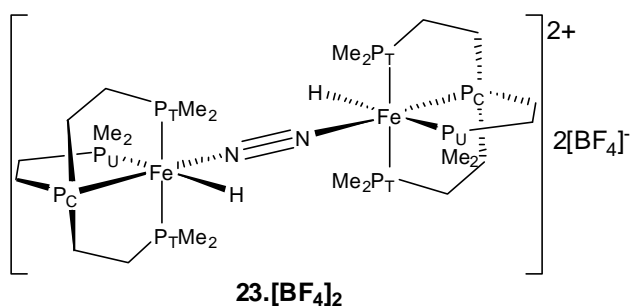
(5 ml) was allowed to stand under nitrogen for 5 days. After this time a solution

of sodium tetrafluoroborate (28 mg, 260 μmol) in ethanol was added and a buff

coloured precipitate formed over the course of an hour. This precipitate was

filtered and dried under nitrogen to give [(FeH(PP$_3$))$_2$(μ-N$_2$)][BF$_4$]$_2$ **23.[BF$_4$]$_2$**

(45 mg, 38%).

$^{31}P\{^1H\}$ NMR (162 MHz, acetone-d_6): δ 173.0 (1P, dt, $^2J_{P(C)-P(T)}$ = 30.4 Hz;

$^2J_{P(C)-P(U)}$ = 24.6 Hz, $\mathbf{P_C}$); 62.5 (2P, dd, $^2J_{P(T)-P(U)}$ = 16.4 Hz, $\mathbf{P_T}$); 59.8 (1P, dt, $\mathbf{P_U}$).

$^1H\{^{31}P\}$ NMR (400 MHz, acetone-d_6, high field): δ -12.6 (2H, br s, Fe-$\mathbf{H}$).

$^{19}F\{^1H\}$ NMR (282 MHz, acetone-d_6) δ -147.1 (8F, s).

In a similar procedure **23.[PF$_6$]$_2$** was synthesised by addition of potassium

hexafluorophosphate to a solution of FeClH(PP$_3$) **25** in ethanol which was

allowed to stand under nitrogen for 5 days. This resulted in $^{31}P\{^1H\}$ and $^1H\{^{31}P\}$ NMR spectra which were very similar to those for **23.[BPh$_4$]$_2$** and **23.[BF$_4$]$_2$**.

23.[PF$_6$]$_2$

$^{31}P\{^1H\}$ NMR (162 MHz, acetone-d_6): δ 172.8 (1P, dt, $^2J_{P(C)-P(T)}$ = 30.4 Hz; $^2J_{P(C)-P(U)}$ = 24.4 Hz, **P$_C$**); 62.4 (2P, dd, $^2J_{P(T)-P(U)}$ = 16.3 Hz, **P$_T$**); 59.7 (1P, dt, **P$_U$**).

$^1H\{^{31}P\}$ NMR (400 MHz, acetone-d_6, high field): δ -12.6 (2H, br s, Fe-**H**).

6.8.9 μ-(dinitrogen)[hydrido-1-bis(tris(2-dimethylphosphinoethyl) phosphine)-1κ^{4}P,2κ^{4}P-diiron] [tetraphenylborate], [(FeH(PP$_3$))(μ-N$_2$)(Fe(PP$_3$))][BPh$_4$] 37.[BPh$_4$]

37.[BPh$_4$]
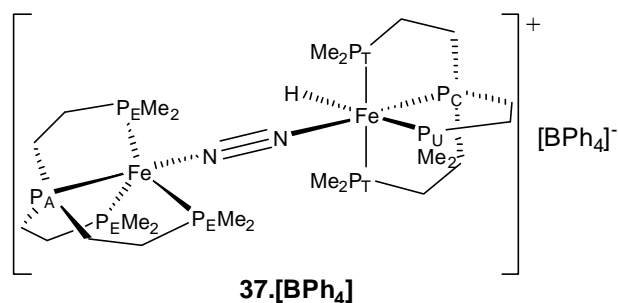
Potassium *t*-butoxide (8 mg, 71 μmol) was added to a suspension of [(FeH(PP$_3$))$_2$(μ-N$_2$)][BPh$_4$]$_2$ **23.[BPh$_4$]$_2$** (96 mg, 70 μmol) in THF (approx. 4 ml). The reaction mixture was stirred with gentle heating (approx. 50ºC) for 2 hours after which it had the appearance of a red solution with some whitish solid present. The solution was filtered and layered with pentane to give [(FeH(PP$_3$))(μ-N$_2$)(Fe(PP$_3$))][BPh$_4$] as red crystals (15 mg, 21%) suitable for analysis by X-ray diffraction. An identical product was seen when the base used in this reaction was potassium bis(trimethylsilyl)amide.

Anal Found: C 54.34, H 7.91, N 2.49. C$_{48}$H$_{81}$BFe$_2$N$_2$P$_8$ (MW 1056.31) requires C 54.57, H 7.73, N 2.65%.

$^{31}P\{^1H\}$ NMR (121.5 MHz, THF-d_8): δ 180.7 (1P, ddtq, $^2J_{P(A)-P(E)}$ = 46.7 Hz, $^5J_{P(A)-P(U)}$ = 2.2 Hz, $^2J_{P(A)-P(T)}$ = 2.0 Hz, $^2J_{P(A)-P(C)}$ = 0.85 Hz, $\mathbf{P_A}$); 176.7 (1P, ddtq, $^2J_{P(C)-P(T)}$ = 29.7 Hz, $^2J_{P(C)-P(U)}$ = 22.4 Hz, $^2J_{P(C)-P(E)}$ = 0.90 Hz, $\mathbf{P_C}$); 67.0 (3P, dddt, $^2J_{P(E)-P(U)}$ = 5.3 Hz, $^2J_{P(E)-P(T)}$ = 4.5 Hz, $\mathbf{P_E}$); 62.0 (2P, dddq, $^2J_{P(T)-P(U)}$ = 18.0 Hz, $\mathbf{P_T}$); 59.6 (1P, ddtq, $\mathbf{P_U}$).*

$^1H\{^{31}P\}$ NMR (400 MHz, THF-d_8, high field): δ -12.5 (1H, br s, Fe-$\mathbf{H}$).

The ^{15}N labelled analogue of this complex was synthesised by treatment of $^{15}\mathbf{N_2}$-**23.[BPh$_4$]$_2$** (100 mg, 85 μmol) in THF-d_8 (0.7 ml) with potassium t-butoxide (4.5 mg, 40 μmol) under argon. The reaction mixture was heated to approximately 60ºC for an hour in an NMR tube fitted with a concentric teflon tap. The resulting dark red solution of $^{15}\mathbf{N_2}$-**37.[BPh$_4$]** was then filtered prior to analysis by NMR spectroscopy.

[(FeH(PP$_3$))(μ-^{15}N$_2$)(Fe(PP$_3$))][BPh$_4$] $^{15}\mathbf{N_2}$-**37.[BPh$_4$]**

$^{31}P\{^1H\}$ NMR (243 MHz, THF-d_8): δ 180.6 (1P, m, $^2J_{P(A)-N}$ = 10 Hz, $\mathbf{P_A}$); 176.6 (1P, m, $\mathbf{P_C}$); 66.9 (3P, m, $\mathbf{P_E}$); 61.9 (2P, m, $\mathbf{P_T}$); 59.5 (1P, m, $\mathbf{P_U}$).

$^1H\{^{31}P\}$ NMR (500 MHz, THF-d_8, high field): δ -12.6 (1H, m, Fe-$\mathbf{H}$).

$^{15}N\{^1H\}$ NMR (50.7 MHz, THF-d_8): δ -9.3 (1N, s, P$_A$-Fe-$\mathbf{N}$), -58.3 (1N, s, P$_C$-Fe-$\mathbf{N}$).
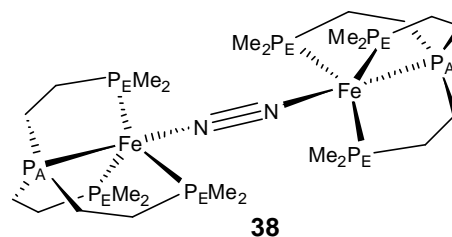
The BF$_4$ and PF$_6$ salts of **39** were prepared by analogous reactions of **25.[BF$_4$]$_2$** and **25.[PF$_6$]$_2$** with base. The $^{31}P\{^1H\}$ and $^1H\{^{31}P\}$ NMR are the same as those of **37.[BPh$_4$]$_2$** above.

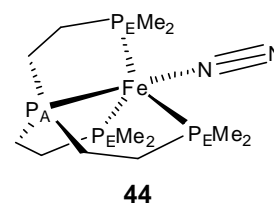* Scalar coupling constants derived from computer simulation of spectrum – see Section 3.2.7

6.8.10 μ-(dinitrogen)bis[(tris(2-dimethylphosphinoethyl)phosphine)-κ⁴P)iron], (Fe(PP₃))₂(μ-N₂) 38 and [TBPY-5-15] [dinitrogen(tris(2-dimethylphosphinoethyl)phosphine)-κ⁴P)iron], Fe(N₂)(PP₃) 44

[(FeH(PP$_3$))$_2$(μ-N$_2$)][BPh$_4$]$_2$ **23.[BPh₄]₂** (95 mg, 70 μmol) was placed in an nmr tube under dinitrogen with THF (0.5 ml) and shaken to form a slurry. To this a large excess of potassium *t*-butoxide was added (30 mg, 270 μmol). The buff coloured solid slowly dissolved to give a red solution (shown by ^{31}P{^{1}H} NMR to be **37.[BPh₄]** after 24 hours) which then turned into a yellow solution with some light coloured solid evident. After 3 days the solution was shown by ^{31}P{^{1}H} NMR to contain two major species namely (Fe(PP$_3$))$_2$(μ-N$_2$) **38** and Fe(N$_2$)(PP$_3$) **44**.

38

44

Fe(N$_2$)(PP$_3$) **44**:

^{31}P{^{1}H} NMR (121.5 MHz, THF): δ 182.9 (1P, q, **P$_A$**, $^2J_{P(A)-P(E)}$ = 45.3 Hz); 66.6 (3P, d, **P$_E$**) (lit.[18] 181.7 **P$_A$**, 66.0 **P$_E$**).

(Fe(PP$_3$))$_2$(μ-N$_2$) **38**:

^{31}P{^{1}H} NMR (121.5 MHz, THF): δ 170.9 (1P, q, **P$_A$**, $^2J_{P(A)-P(E)}$ = 57.7 Hz); 66.0 (3P, d, **P$_E$**).

The ^{15}N analogue of **44** was prepared by treatment of an NMR sample of [(FeH(PP$_3$))(μ-^{15}N$_2$)(Fe(PP$_3$))][BPh$_4$] ^{15}N$_2$-37.[BPh₄] (25 mg, 11 μmol) in THF-d_8 (0.5 ml) with potassium *t*-butoxide (1 mg, 10 μmol). This reaction resulted in two

major products. The first was assigned as **^{15}N-44** whilst the second, believed to be

a C-D activation product, remained unidentified.

Fe(^{15}N$_2$)(PP$_3$) **^{15}N$_2$-44**:

^{31}P{^{1}H} NMR (202.5 MHz, THF-d_8): δ 183.5 (1P, ddq, $^2J_{P(A)\text{-}P(E)}$ = 45.4 Hz,

$^2J_{P(A)\text{-}N}$ = 9.6 Hz, $^3J_{P(A)\text{-}N}$ = 1.4 Hz, **P$_A$**); 67.3 (3P, ddd, $^2J_{P(E)\text{-}N}$ = 5.6 Hz,

$^3J_{P(E)\text{-}N}$ = 2.4 Hz, **P$_E$**).

^{15}N{^{1}H} NMR (50.7 MHz, THF-d_8): δ -2.5 (1N, s, Fe-N**N**), -26.7 (1N, s, Fe-**N**).

The ^{15}N analogue of **44** was also synthesised in an analogous manner by treatment

of an NMR sample of **^{15}N$_2$-37.[BPh$_4$]** with potassium t-butoxide in benzene-d_6

(0.5 ml). This reaction also resulted in two major products. The first was

assigned as **^{15}N-44** whilst the second was assigned as the C-D activation product

FeD(Ph-d_5)(PP$_3$) **45**.

Fe(^{15}N$_2$)(PP$_3$) **^{15}N-44**:

^{31}P{^{1}H} NMR (202.5 MHz, benzene-d_6): δ 185.3 (1P, ddq, $^2J_{P(A)\text{-}P(E)}$ = 45.4 Hz,

$^2J_{P(A)\text{-}N}$ = 9.5 Hz, $^3J_{P(A)\text{-}N}$ = 1.4 Hz, **P$_A$**); 69.1 (3P, ddd, $^2J_{P(E)\text{-}N}$ = 5.5 Hz,

$^3J_{P(E)\text{-}N}$ = 2.6 Hz, **P$_E$**).

FeD(Ph-d_5)(PP$_3$):

^{31}P{^{1}H} NMR (202.5 MHz, benzene-d_6): δ 179.1 (1P, m, **P$_C$**); 66.1 (2P, m, **P$_T$**),

59.9 (1P, m, **P$_U$**).

6.8.11 Treatment of iron dinitrogen complexes with acid.

In a typical reaction, 30 – 60 mg of **23.[BPh₄]₂** (20-40 μmol) was placed in an NMR tube under dinitrogen or argon and 0.5 ml 2M HCl (500 μmol) in diethyl ether was added causing effervescence and the immediate formation of both a white and a red solid. The reaction mixture was either shaken ensuring immediate access of the acid to all dinitrogen salt or left undisturbed to allow the reaction to proceed more slowly over the course of several hours. Reaction progress was monitored by $^{31}P\{^{1}H\}$ NMR. In order to test for any ammonia produced during the reaction, and present as ammonium salt, the solvent was removed *in vacuo* and the remaining solid dissolved in water with a drop of D_2O for lock purposes. ^{14}N NMR was used to detect the presence of NH_4^+ (around -360 ppm). A similar procedure was also performed on **22.[BPh₄]**, **23.[BF₄]₂**, **23.[PF₆]₂** and with the alternative acids tetrafluoroboric acid and lutidinium chloride. No NH_4^+ was detected in all cases.

6.8.12 Treatment of iron dinitrogen complexes with base then acid.

In a typical reaction, 30 – 85 mg of **23.[BPh₄]₂** (20-55 μmol) was placed in an NMR tube with 1 ml of THF under dinitrogen or argon and an excess of potassium *t*-butoxide added (200 -300 μmol). The NMR tube was heated gently until a deep red (**37.[BPh₄]**) or yellow (**38/44**) solution developed. The solution was then either treated directly or filtered first and then treated with an excess of acid as described above (approx. 0.5-1 ml 2M HCl in diethyl ether) causing effervescence and the immediate formation of both a white and a red solid. The reaction mixture was either shaken ensuring immediate access of the acid to all dinitrogen complex or left undisturbed to allow the reaction to proceed more

slowly over the course of several hours. Reaction progress was monitored by $^{31}P\{^1H\}$ NMR. The presence of ammonium was tested for as described in Section 6.8.11. Potassium bis(trimethylsilyl)amide was used as an alternative base and tetrafluoroboric acid and lutidinium chloride as alternative acids. Similar procedures were also performed with **22.[BPh₄]**, **23.[BF₄]₂**, **23.[PF₆]₂**. No ammonium was detected except in the following:

This procedure was applied to **23.[BPh₄]₂** using the base potassium bis(trimethylsilyl)amide and HCl in diethyl ether as the acid to produce NH_4^+.

^{14}N (28.9 MHz, water/D_2O): δ -359.5 (N, p, $^1J_{N-H}$ = 52 Hz, **NH_4^+**).

This procedure was applied to **$^{15}N_2$-23[BPh₄]₂** using the base potassium bis(trimethylsilyl)amide and HCl in diethyl ether as the acid to produce NH_4^+.

^{14}N (28.9 MHz, water/D_2O): δ -359.5 (N, p, $^1J_{N-H}$ = 52 Hz, **NH_4^+**).

^{15}N (40.6 MHz, water/D_2O): no signal.

6.8.13 [OC-6-34] [amminehydrido(tris(2-dimethylphosphinoethyl) phosphine-κ⁴*P*)iron] [tetraphenylborate], [Fe(NH₃)H(PP₃)][BPh₄] 46.[BPh₄]

FeClH(PP₃) **25** (108 mg, 277 μmol) was added to an ammonia saturated solution of ethanol (approx. 10 ml) under argon and stirred for 4 hours. After this time the light orange solution was filtered

46.[BPh₄]

and added to one equivalent of sodium tetraphenylborate (95 mg, 280 μmol). Upon stirring a fine yellow solid precipitated from the solution. The solvent was
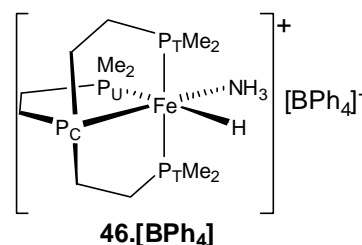
removed *in vacuo* and the yellow solid then extracted with THF (approx. 15 ml). This solution was filtered and the solvent removed *in vacuo* to afford [Fe(NH$_3$)H(PP$_3$)][BPh$_4$] **46.[BPh$_4$]** as a fine yellow powder (137 mg, 71%).

^{31}P{^{1}H} NMR (162 MHz, THF-d_8): δ 179.5 (1P, dt, $^2J_{P(C)-P(T)}$ = 28.1 Hz, $^2J_{P(C)-P(U)}$ = 15.7 Hz, **P$_C$**); 59.4 (2P, dd, $^2J_{P(T)-P(U)}$ = 19.9 Hz, **P$_T$**); 56.9 (1P, dt, **P$_U$**).

^{1}H{^{31}P} NMR (400 MHz, THF-d_8): δ 7.61 (8H, br s, B**Ph$_{ortho}$**); 6.84 (8H, m, B**Ph$_{meta}$**); 6.70 (4H, m, B**Ph$_{para}$**); 1.7 (3H, s, N**H$_3$**)†; 1.57-1.25 (12H, m, C**H$_2$**); 1.39 (6H, s, P$_T$C**H$_3$**); 1.27 (6H, s, P$_T$C**H$_3$**); 1.23 (6H, s, P$_U$C**H$_3$**); -13.00 (1H, s, Fe-**H**).

^{1}H-^{15}N HSQC (40.6 MHz, THF-d$_8$, 230K): δ -445.6 (3H, br s, Fe-**N**H$_3$).

IR (nujol): ν 3352 w, 3273 w (NH), 1784 m ν(FeH) cm^{-1}.

6.8.14 [OC-6-34] [^{15}N-hydrazinehydrido(tris(2-dimethylphosphinoethyl) phosphine-κ^4*P*)iron] chloride, [Fe(^{15}NH$_2$^{15}NH$_2$)H(PP$_3$)]Cl ^{15}N-47.Cl and [OC-6-34] [chloro^{15}N-hydrazine(tris(2-dimethylphosphinoethyl) phosphine-κ^4*P*)iron] chloride, [FeCl(^{15}NH$_2$^{15}NH$_2$)(PP$_3$)]Cl ^{15}N-48.Cl

Approximately 2 ml of *ca* 0.5 M ^{15}N labelled hydrazine (1 mmol) in THF was added to a solution of FeClH(PP$_3$) **25** (90 mg, 240 μmol) in ethanol (0.5 ml) under argon. The solution immediately turned light yellow and was shown to contain two major hydrazine complexes by NMR.

^{15}N-47.Cl

^{15}N-48.Cl

---
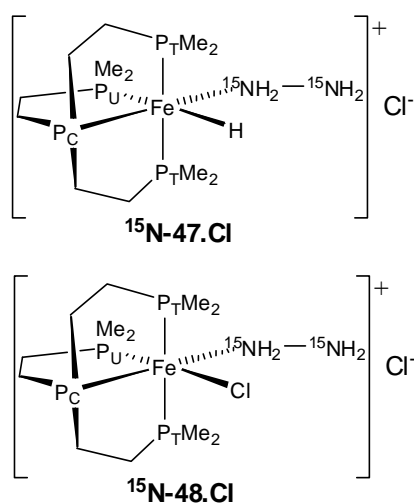
† By ^{1}H-^{15}N HSQC

$[Fe(^{15}NH_2{}^{15}NH_2)H(PP_3)]Cl$ **^{15}N-47.Cl**

$^{31}P\{^1H\}$ NMR (162 MHz, ethanol/THF/benzene-d_6): δ 176.5 (1P, ddt, $^2J_{P(C)-P(T)} = 26.0$ Hz, $^2J_{P(C)-P(U)} = 16.2$ Hz, $^2J_{P(C)-N} = 6$ Hz, **P_C**); 57.6 (2P, dd, $^2J_{P(T)-P(U)} = 19.2$ Hz, **P_T**); 55.3 (1P, ddt, $^2J_{P(U)-N} = 4$ Hz, **P_U**).

$^1H\{^{31}P\}$ NMR (400 MHz, ethanol/THF/benzene-d_6): δ 4.99 (2H, dt, Fe-N**H_2**, $^1J_{H-N} = 71$ Hz, $^3J_{H-H} = 4$ Hz); 3.16 (2H, Fe-NH$_2$N**H_2**‡); -13.2 (1H, s, Fe-**H**).

^{15}N NMR (40.6 MHz, ethanol/THF/benzene-d_6): δ -302.7 (1N, t, $^1J_{N-H} = 65$ Hz, Fe-NH$_2$**N**H$_2$); -380.2 (1N, t, $^1J_{N-H} = 71$ Hz, Fe-**N**H$_2$).

$[FeCl(^{15}NH_2{}^{15}NH_2)(PP_3)]Cl$ **^{15}N-48.Cl**

$^{31}P\{^1H\}$ NMR (162 MHz, ethanol/THF/benzene-d_6): δ 168.7 (1P, ddt, $^2J_{P(C)-P(T)} = 21.4$ Hz, $^2J_{P(C)-P(U)} = 25.4$ Hz, $^2J_{P(C)-N} = 11$ Hz, **P_C**); 74.8 (1P, dt, $^2J_{P(U)-P(T)} = 41.2$ Hz, **P_U**); 46.8 (2P, dd, **P_T**).

$^1H\{^{31}P\}$ NMR (400 MHz, ethanol/THF/benzene-d_6): δ 5.78 (2H, d, Fe-N**H_2**, $^1J_{H-N} = 72$ Hz); 3.65 (2H, Fe-NH$_2$N**H_2**‡).

^{15}N NMR (40.6 MHz, ethanol/THF/benzene-d_6): δ -315.7 (1N, Fe-NH$_2$**N**H$_2$, t, $^1J_{N-H} = 65$ Hz); -368.1 (1N, t, $^1J_{N-H} = 72$ Hz, Fe-**N**H$_2$).

6.8.15 [OC-6-34] [hydrazinehydrido(tris(2-dimethyl phosphinoethyl) phosphine-κ^4P)iron] [tetraphenylborate], $[Fe(NH_2NH_2)H(PP_3)][BPh_4]$ 47.[BPh$_4$]

Approximately 0.2 ml of 1 M hydrazine in THF was added to a solution of
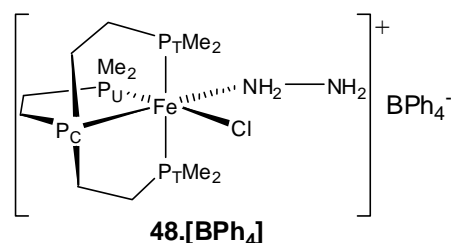

47.[BPh$_4$]

---
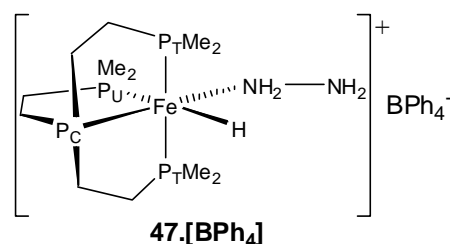
‡by ^{1}H-^{15}N HSQC

FeClH(PP$_3$) **25** (*ca* 15 mg, 40 µmol) in ethanol (1 ml) under argon. The orange solution immediately turned pale yellow and was observed to contain two species by ^{31}P{^{1}H} NMR (**47** and **48**). Addition of one equivalent of sodium tetraphenylborate (13 mg, 38 µmol) resulted in the immediate appearance of a yellow precipitate. Small yellow crystals of **47.[BPh$_4$]**, suitable for analysis by X-ray diffraction, were collected at this stage. Separation of the two species precipitated was achieved by addition of ethanol (approx. 5 ml) to dissolve **47.[BPh$_4$]**. The solution was filtered and the solvent removed *in vacuo* to give [Fe(NH$_2$NH$_2$)H(PP$_3$)][BPh$_4$] **47.[BPh$_4$]** as a yellow powder in good purity and sufficient yield for analysis by NMR.

^{31}P{^{1}H} NMR (162 MHz, ethanol/THF-d_8): δ 176.7 (1P, dt, $^2J_{P(C)-P(T)}$ = 26.8 Hz, $^2J_{P(C)-P(U)}$ = 16.0 Hz, **P$_C$**); 57.8 (2P, dd, $^2J_{P(T)-P(U)}$ = 20.2 Hz, **P$_T$**); 55.4 (1P, dt, **P$_U$**).

^{1}H{^{31}P} NMR (400 MHz, ethanol/THF-d_8, high field): δ -13.2 (1H, br s, Fe-**H**).

6.8.16 [OC-6-34] [chlorohydrazine(tris(2-dimethylphosphinoethyl) phosphine-κ^4*P*)iron] [tetraphenylborate], [FeCl(NH$_2$NH$_2$)(PP$_3$)][BPh$_4$] 47.[BPh$_4$]

Approximately 0.5 ml of 1 M hydrazine in THF was added to an ethanol solution of FeCl$_2$(PP$_3$) **24** (*ca* 20 mg, 50 µmol) (isolated by filtering of the red THF solution described in Section 6.8.2 and subsequent removal of the solvent *in vacuo*). The red ethanol solution turned yellow and was seen to contain one species by NMR **48.Cl.**

48.[BPh$_4$]

$(^{31}P\{^1H\}$ NMR (162 MHz, ethanol/THF): δ 168.7 (1P, dt, $^2J_{P(C)-P(U)}$ = 25.6, Hz,

$^2J_{P(C)-P(T)}$ = 21.3 Hz, $\mathbf{P_C}$); 74.7 (1P, dt, $^2J_{P(U)-P(T)}$ = 41.3 Hz, $\mathbf{P_U}$); 46.9 (2P, dd, $\mathbf{P_T}$)).

Addition of a single equivalence of sodium tetraphenylborate (17 mg, 50 μmol) to the solution of **48.Cl** resulted in the immediate appearance of a yellow precipitate. The solution was filtered to afford a yellow powder, assigned as $[FeCl(NH_2NH_2)(PP_3)][BPh_4]$ **48.[BPh$_4$]**, sufficiently soluble in THF for analysis by NMR.

$^{31}P\{^1H\}$ NMR (162 MHz, THF-d_8): δ 167.8 (P, dt, $\mathbf{P_C}$, $^2J_{P(C)-P(U)}$ = 23.8, Hz,

$^2J_{P(C)-P(T)}$ = 21.5 Hz); 75.0 (1P, dt, $\mathbf{P_U}$, $^2J_{P(U)-P(T)}$ = 40.4 Hz); 46.3 (2P, dd, $\mathbf{P_T}$).

$^1H\{^{31}P\}$ NMR (400 MHz, THF-d_8): δ 5.31 (2H, s, Fe-N$\mathbf{H_2}$); 3.62 (2H, br, Fe-NH$_2$N$\mathbf{H_2}$).

6.8.17 [OC-6-34] [amminechloro(tris(2-dimethylphosphinoethyl)phosphine-κ^4P)iron] [tetraphenylborate], [Fe(NH$_3$)Cl(PP$_3$)][BPh$_4$] 49.[BPh$_4$]

A THF (100 ml) solution of FeCl$_2$(PP$_3$) **24** was prepared following the procedure described in Section 6.8.2 using 100 mg anhydrous iron(II) chloride (0.79 mmol) and 235 mg PP$_3$ **1**

49.[BPh$_4$]
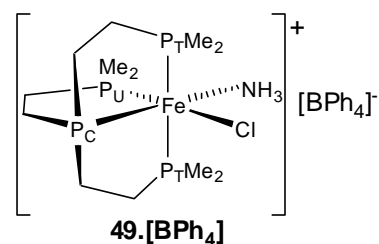
(0.79 mmol). This solution was filtered and used without further purification. A saturated solution of ammonia in ethanol (approx 10 ml) was added causing an orange suspension to form. The solvents were removed *in vacuo* and sodium tetraphenylborate (approx 300 mg, 0.9 mmol) was added to the resulting orange powder. THF (approx 50 ml) was then added to the mixture of solids to form an orange solution upon stirring. The solvent was removed *in vacuo* and the orange

solid redissolved in THF and filtered to remove the unwanted sodium salts. The filtrate was evaporated to dryness *in vacuo* and the solid residue washed with ethanol and then dried. This afforded [Fe(NH$_3$)Cl(PP$_3$)][BPh$_4$] **49.[BPh$_4$]** as a peach coloured powder (150 mg, 25% based on FeCl$_2$).

^{31}P{^{1}H} NMR (121 MHz, THF-d_8): δ 172.8 (1P, dt, $^2J_{P(C)-P(U)}$ = 24.8 Hz, $^2J_{P(C)-P(T)}$ = 22.8 Hz, **P$_C$**); 78.9 (1P, dt, $^2J_{P(U)-P(T)}$ = 40.8 Hz, **P$_U$**); 49.1 (2P, dd, **P$_T$**).

^{1}H{^{31}P} NMR (300 MHz, THF-d_8): δ 7.32 (8H, br s B**Ph$_{ortho}$**); 6.88 (8H, br m, B**Ph$_{meta}$**); 6.72 (4H, br m, B**Ph$_{para}$**); 2.44 (2H, m, P$_T$C**H**H'); 2.42 (3H, s, N**H$_3$**)§; 2.16 (2H, m, C**H**H'CH$_2$P$_T$); 1.95 (2H, m, CH**H'**CH$_2$P$_T$); 1.78 (2H, m, P$_T$CH**H'**); 1.62 (2H, m, C**H$_2$**CH$_2$P$_U$); 1.62 (2H, m, C**H$_2$**CH$_2$P$_U$); 1.52 (6H, s, P$_T$C**H$_3$**); 1.42 (2H, m, C**H$_2$**P$_U$)1.41 (6H, s, P$_T$C**H$_3$**); 1.19 (6H, s, P$_U$C**H$_3$**).

^{1}H-^{15}N HSQC (40.6 MHz, THF-d$_8$): δ-442.1 (Fe-**N**H$_3$).

6.8.18 [TBPY-5-13] [chlorotris(2-diisopropylphosphinoethyl)phosphine-κ^{4}P)iron] [tetraphenylborate], [FeCl(PP$^i_3$)][BPh$_4$] 51.[BPh$_4$]

Anhydrous iron(II) dichloride (0.286 g, 2.26 mmol) was added to tris(2-diisopropylphosphinoethyl)-phosphine PP$^i_3$ **12** (1.05 g, 2.24 mmol) in ethanol (approx. 25 ml) under nitrogen. The reaction mixture, which immediately developed a dark violet colour, was left to stir under nitrogen for 18 hours. Sodium tetraphenylborate (0.900 g, 2.60 mmol) was then added resulting in the immediate precipitation of a violet solid which was filtered to afford the paramagnetic title compound [FeCl(PP$^i_3$)][BPh$_4$] **51.[BPh$_4$]** as a purple powder

51.[BPh$_4$]

---
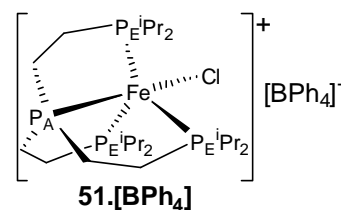
§ By ^{1}H-^{15}N HSQC

(1.83 g, 93%). Crystals suitable for X-ray diffraction were grown by layering a THF solution of the complex with pentane.
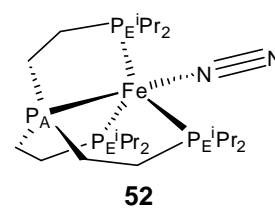
Anal Found: C 65.72, H 8.29 $C_{48}H_{74}BClFeP_4$ (MW 877.11) requires C 65.73, H 8.50%.

HRMS (EI) *m/z*: $[M]^+$ 557.2210 (calc. 557.2214).

LRMS (ESI^+, methanol) *m/z*: 557 ($[M+H]^+$, 100%), 467 ($[PP^i_3+H]^+$, 35).

6.8.19 [TBPY-5-23] [(dinitrogen)(tris(2-diisopropylphosphinoethyl) phosphine-$κ^4$P)iron], Fe(N$_2$)(PP$^i_3$) 52

Potassium graphite (75 mg, 0.55 mmol) was added to a solution of [FeCl(PP$^i_3$)][BPh$_4$] **51.[BPh$_4$]** (230 mg, 262 mmol) in THF (approx. 15 ml). The reaction mixture was stirred under nitrogen for 24 hours. The resulting black suspension was filtered to afford an orange solution. The solvent was removed *in vacuo* and the resulting solid extracted into pentane (approx. 10 ml). This yellow solution was then filtered and the solvent removed *in vacuo* to afford Fe(N$_2$)(PP$^i_3$) **52** as a dark yellow solid (75 mg, 52%). Crystals suitable for analysis by X-ray diffraction were precipitated upon cooling of a hot pentane solution of **52**.

52

Anal Found: C 52.31, H 9.93, N 3.85 $C_{24}H_{54}FeN_2P_4$ (MW 550.44) requires C 52.37, H 9.89, N 5.09%. Elemental analysis performed on crystalline product suggests some loss of weakly bound dinitrogen ligand upon application of vacuum during analytical procedure.

^{31}P{^{1}H} NMR (162 MHz, benzene-d_6): δ 175.8 (1P, q, $^2J_{P(A)-P(E)}$ = 36.7 Hz, **P$_A$**); 96.3 (3P, d, **P$_E$**).

$^1H\{^{31}P\}$ NMR (400 MHz, benzene-d_6): δ 2.29 (6H, m, P_EC**H**(CH$_3$)$_2$); 1.35 (6H, m, P_AC**H**$_2$); 1.28 (18H, m, C**H**$_3$); 1.25 (18H, m, C**H**$_3$); 1.10 (6H, m, P_EC**H**$_2$).

$^{13}C\{^1H\}$ NMR (101 MHz, benzene-d_6): δ 34.3 (m, **C**H$_3$); 29.0 (m, P_E**C**H$_2$); 28.8 (m, P_A**C**H$_2$); 20.5 (d, $^1J_{C-P}$ = 11 Hz, P_E**C**H(CH$_3$)$_2$).

IR (fluorolube): ν 1985 s (N≡N) cm^{-1}.

LRMS (ESI$^+$, methanol) *m/z*: 523 ([Fe(PP$^i_3$)+H]$^+$, 100%), 522 (81).

The ^{15}N labelled analogue of this complex was synthesised by exchange of the labile dinitrogen ligand over 2 hours. Fe(N$_2$)(PP$^i_3$) **52** (approx 20 mg, 80 μmol) was dissolved in benzene-d_6 (0.5 ml) in an NMR tube fitted with a concentric teflon tap under dinitrogen. The solution was frozen in liquid nitrogen and the headspace was evacuated followed by introduction of ^{15}N$_2$ to the NMR tube.

Fe(^{15}N$_2$)(PP$^i_3$) ^{15}**N$_2$-52**

$^{31}P\{^1H\}$ NMR (202 MHz, benzene-d_6): δ 175.6 (1P, dq $^2J_{P(A)-(E)}$ = 36.7 Hz, $^2J_{P(A)-N}$ = 9.7 Hz, **P$_A$**,); 96.1 (3P, d, **P$_E$**).

^{15}N NMR (50.7 MHz, benzene-d_6) δ 18.1 (1N, Fe-N**N**); -18.0 (1N, Fe-**N**)

6.8.20 [OC-6-43] [(dinitrogen)hydrido(tris(2-diisopropylphosphinoethyl)phosphine-κ^4P)iron] [tetrafluoroborate], [Fe(N$_2$)H(PP$^i_3$)][BF$_4$] 53.BF$_4$

Fe(N$_2$)(PP$^i_3$) **52** (20 mg, 36 μmol) and lutidinium tetrafluoroborate (7 mg, 36 μmol) were stirred in THF (approx. 2 ml) under nitrogen to afford a red solution which turned purple within an hour. The
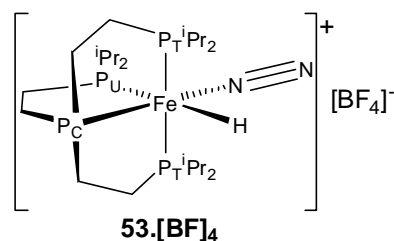
53.[BF]$_4$

solution was layered with pentane and after 24 hours was filtered to afford

$[Fe(N_2)H(PP^i{}_3)][BF_4]$ **53.[BF$_4$]** as a purple solid (16 mg, 70 %).

$^{31}P\{^1H\}$ NMR (121.5 MHz, THF-d_8): δ 162.0 (1P, dt, $^2J_{P(C)\text{-}P(U)}$ = 29.8 Hz,

$^2J_{P(C)\text{-}P(T)}$ = 24.4 Hz, **P$_C$**); 88.8 (2P, dd, $^2J_{P(T)\text{-}P(U)}$ = 11.3 Hz, **P$_T$**); 78.7 (1P, dt, **P$_U$**).

$^1H\{^{31}P\}$ NMR (400 MHz, THF-d_8): δ 2.6-2.4 (8H, m, P$_T$**CH$_2$CH$_2$**); 2.57 (2H, m,

P$_T$**CH**); 2.15 (2H, m, P$_U$**CH**); 2.10-1.80 (4H, m, P$_U$**CH$_2$CH$_2$**); 1.73 (2H, m,

P$_T$**CH'**);1.50 (6H, d, $^3J_{H\text{-}H}$ = 7 Hz, P$_U$CH(**CH$_3$**)); 1.41 (6H, d, $^3J_{H\text{-}H}$ = 7 Hz,

P$_T$CH(**CH$_3$**)); 1.34 (6H, d, $^3J_{H\text{-}H}$ = 7 Hz, P$_U$CH(**CH$_3$**)); 1.31 (6H, d, $^3J_{H\text{-}H}$ = 7 Hz,

P$_T$CH(**CH$_3$**)); 1.27 (6H, d, $^3J_{H\text{-}H}$ = 7 Hz, P$_T$CH'(**CH$_3$**)); 1.13 (6H, d, $^3J_{H\text{-}H}$ = 7 Hz,

P$_T$CH'(**CH$_3$**)); -14.53 (1H, s, Fe-**H**).

^1H NMR (400 MHz, THF-d_8, high field): δ -14.53 (1H, ddt, Fe-**H,**

$^2J_{H\text{-}P(T)}$ = 67.2 Hz, $^2J_{H\text{-}P(C)}$ = 51.7 Hz, $^2J_{H\text{-}P(U)}$ = 24.4 Hz).

IR (fluorolube): 2095 s, ν(N≡N) cm^{-1}.

6.8.21 [OC-6-43] [dihydrogenhydrido(tris(2-diisopropylphosphinoethyl) phosphine-$κ^4P$)iron] [tetrafluoroborate], [Fe(H$_2$)H(PP$^i{}_3$)][BF$_4$] 54.[BF$_4$]

Fe(N$_2$)(PP$^i{}_3$) **52** (20 mg, 36 μmol) and lutidinium tetrafluoroborate (210 mg, 1.1 mmol, 30 equivalents) were stirred in THF (approx. 2 ml) under nitrogen to afford a red solution which turned purple after several
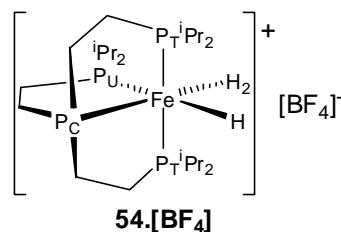
54.[BF$_4$]

hours. After 24 hours $^{31}P\{^1H\}$ NMR indicated that there were two products:

$[Fe(N_2)H(PP^i{}_3)][BF_4]$ **53.[BF$_4$]** (NMR as given in Section 6.8.20) and

$[Fe(H_2)H(PP^i{}_3)][BF_4]$ **54.[BF$_4$]**.

^{31}P{^{1}H} NMR (121.5 MHz, THF): δ 171.0 (1P, q, $^2J_{\text{P-P}}$ = 29.3 Hz); 103.6 (3P, br s, $\mathbf{P_T}$, $\mathbf{P_U}$).

^{1}H NMR (400 MHz, THF, high field) δ -11.7 (3H, br s, Fe-$\mathbf{H/H_2}$).

^{31}P{^{1}H} NMR (121.5 MHz, THF, 190K): δ 171.3 (1P, m, $\mathbf{P_C}$); 105.8 (2P, br s, $\mathbf{P_T}$); 96.0 (1P, br s, $\mathbf{P_U}$).

^{1}H NMR (400 MHz, THF, 190K, high field): δ -9.4 (2H, br s, Fe-$\mathbf{H_2}$); -16.3 (1H, br s, Fe-$\mathbf{H}$).

6.8.22 [TBPY-5-13] [chloro(tris(2-diisopropylphosphinoethyl)phosphine-κ^{4}P)ruthenium] chloride, [RuCl(PP$^i_3$)]Cl 56.Cl

Dichlorotris(triphenylphosphine)ruthenium(II) **55** (0.78 g, 0.82 mmol) and tris(2-diisopropylphosphinoethyl)-phosphine PP$^i_3$ **12** (0.38 g, 0.82 mmol) were stirred in

56.Cl
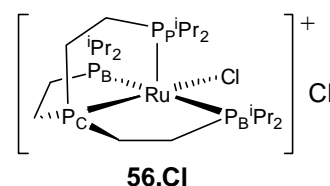
THF (approx. 25 ml). A red solution formed immediately followed by the precipitation of a cream coloured solid after approximately 5 min. This solid was collected by filtration and washed with THF to give [RuCl(PP$^i_3$)]Cl (392 mg, 80%).
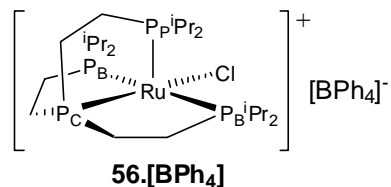
^{31}P{^{1}H} NMR (162 MHz, ethanol): δ 142.9 (1P, q, $^2J_{\text{P(C)-P(B/P)}}$ = 15.2 Hz, $\mathbf{P_C}$); 72.1 (3P, d, $\mathbf{P_{B/P}}$).

HRMS (EI) m/z: [M]$^+$ 603.1909 (calc. 603.1908).

LRMS (ESI$^+$, methanol) m/z: 621 ([RuCl(PP$^i_3$)+H$_2$O]$^+$, 100%), 619 ([RuCl(PP$^i_3$)+OH]$^+$, 95), 603 ([RuCl(PP$^i_3$)+H]$^+$, 56), 517 (68).

6.8.23 [TBPY-5-13] [chloro(tris(2-diisopropylphosphinoethyl)phosphine-κ^{4}P)ruthenium] [tetraphenylborate], [RuCl(PP$^i_3$)][BPh$_4$] 56.[BPh$_4$]

Sodium tetraphenylborate (60 mg, 180 μmol) was added to a solution of [RuCl(PP$^i_3$)]Cl **56.Cl** (104 mg, 163 μmol) in ethanol (approx. 10 ml) resulting in the immediate formation of a dark orange precipitate. This precipitate was filtered and washed with ethanol to afford [RuCl(PP$^i_3$)][BPh$_4$] **56.[BPh$_4$]** (135 mg, 90%) as a dark orange powder. Crystals suitable for X-ray diffraction were grown by layering a THF solution of the complex with pentane.

56.[BPh$_4$]

Anal Found: C 62.29, H 7.97 C$_{48}$H$_{74}$BClP$_4$Ru (MW 922.33) requires C 62.51, H 8.09%.

^{31}P{^{1}H} NMR (162 MHz, acetone-d_6): δ 144.1 (1P, q, $^2J_{P(A)\text{-}P(B/P)}$ = 15.4 Hz, **P$_C$**); 74.0 (3P, br s, **P$_{B/P}$**)

^{1}H{^{31}P} NMR (400 MHz, acetone-d_6): δ 7.38 (8H, br m B**Ph$_{ortho}$**); 6.97 (8H, m, B**Ph$_{meta}$**); 6.82 (4H, m, B**Ph$_{para}$**); 2.32 (6H, t, $^3J_{H\text{-}H}$= 7.2 Hz, P$_C$**CH$_2$**); 2.17 (6H, h, $^3J_{H\text{-}H}$= 7.3 Hz, P$_{B/P}$**CH**(CH$_3$)$_2$); 2.17 (6H, m, P$_{B/P}$**CH$_2$**); 1.55 (18H, d, C**H$_3$**); 1.20 (18H, d, C**H$_3$**).

^{13}C{^{1}H} NMR (101 MHz, acetone-d_6): δ 164.9 (m, B**Ph$_{ipso}$**);136.8 (s, B**Ph$_{ortho}$**); 125.7 (m, B**Ph$_{meta}$**); 122.0 (s, B**Ph$_{para}$**); 30.0 (m, P$_E$**CH**(CH$_3$)$_2$); 26.2 (m, P$_E$**CH$_2$**); 25.9 (d, $^1J_{C\text{-}P}$= 30.5 Hz, P$_A$**CH$_2$**); 19.7 (s, C**H$_3$**); 19.5 (s, C**H$_3$**).

6.8.24 [TBPY-5-23] [(dinitrogen)(tris(2-diisopropylphosphinoethyl) phosphine-$\kappa^4 P$)ruthenium], Ru(N$_2$)(PP$^i_3$) 57

Potassium graphite (109 mg, 0.81 mmol) was added to a suspension of [RuCl(PP$^i_3$)]Cl **56.Cl** (144 mg, 226 mmol) in THF (approx. 15 ml). The reaction mixture was stirred under nitrogen for 18 hours after which it was filtered to
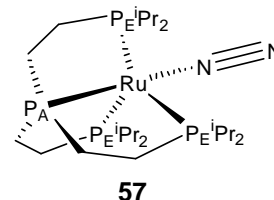
57

afford a dark yellow solution. The solvent was removed *in vacuo* and the resulting dark yellow solid was dissolved in pentane, filtered and the solvent removed *in vacuo* once more to afford Ru(N$_2$)(PP$^i_3$) **57** (90 mg, 67%) as a yellow solid.

^{31}P{^{1}H} NMR (162 MHz, benzene-d_6): δ 161.5 (1P, q, $^2J_{P(A)-P(E)}$ = 21.8 Hz, **P$_A$**); 88.1 (3P, d, **P$_E$**).

^{1}H {^{31}P} NMR (400 MHz, benzene-d_6): δ 2.11 (6H, m, $^3J_{H-H}$ = 7.2 Hz, P$_E$**CH**(CH$_3$)$_2$); 1.27 (6H, m, P$_A$**CH$_2$**); 1.28 (18H, d, **CH$_3$**); 1.16 (6H, m, P$_E$**CH$_2$**); 1.13 (18H, m, C**H$_3$**).

^{13}C{^{1}H} NMR (101 MHz, benzene-d_6): δ 33.8 (m, P$_E$**CH**(CH$_3$)$_2$); 30.1-29.3 (m, P$_A$**CH$_2$CH$_2$**); 20.4 (s, P$_E$CH(**CH$_3$**)$_2$); 20.2 (s, P$_E$CH(**CH$_3$**)$_2$).

IR (fluorolube): 2083 s, ν (N≡N) cm^{-1}.

The ^{15}N labelled analogue of this complex was synthesised by exchange of the labile dinitrogen ligand over 2 hours. Ru(N$_2$)(PP$^i_3$) **57** (approx 20 mg, 80 μmol) was dissolved in benzene-d_6 (0.5 ml) in an NMR tube fitted with a concentric teflon tap under dinitrogen. The solution was frozen with liquid nitrogen and the headspace evacuated followed by introduction of ^{15}N$_2$ to the NMR tube.

$Ru(^{15}N_2)(PP^i_3)$ **$^{15}N_2$-57**

$^{31}P\{^1H\}$ NMR (202 MHz, benzene-d_6): δ 161.8 (1P, ddq, **P_A**, $^2J_{P(A)-N}$ = 31.4 Hz, $^2J_{P(A)-P(E)}$ = 21.9 Hz, $^3J_{P(A)-N}$ = 2.9 Hz); 88.4 (3P, ddd, **P_E**, $^2J_{P(E)-N}$ = 5.2 Hz, $^3J_{P(E)-N}$ = 2.1 Hz).[**]

^{15}N NMR (50.7 MHz, benzene-d_6) δ -8.9 (1N, Ru-N**N**); -55.3 (1N, Ru-**N**N).[††]

6.8.25 [OC-6-43] [(dinitrogen)hydrido(tris(2-diisopropylphosphinoethyl) phosphine-κ^4P)ruthenium] [tetrafluoroborate], [Ru(N$_2$)H(PP$^i_3$)][BF$_4$] 58.[BF$_4$]

Lutidinium tetrafluoroborate (17 mg, 100 mmol) was added to a solution of $Ru(N_2)(PP^i_3)$ **57** (60 mg, 100 mmol) in THF (approx. 15 ml). The solution turned green for several minutes before
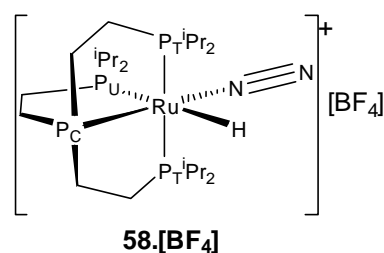
58.[BF$_4$]

reverting to yellow. After stirring for an hour the solution was filtered and the solvent reduced *in vacuo* to approx. 2 ml. This solution was then layered with pentane to afford yellow crystals of [Ru(N$_2$)H(PP$^i_3$)][BF$_4$] **58.[BF$_4$]** (52 mg, 75%). Anal Found: C 42.41, H 7.82, N 3.85 $C_{24}H_{55}BF_4N_2P_4Ru$ (MW 683.48) requires C 42.18, H 8.11, N 4.10%.

$^{31}P\{^1H\}$ NMR (122 MHz, 298K, THF-d_8): δ 143.1 (1P, m, **P_C**); 74.7 (2P, m, **P_T**); 62.7 (2P, m, **P_U**).

$^1H\{^{31}P\}$ NMR (400 MHz, THF-d_8): δ 2.6-2.4 (6H, m, , P_C**CH**$_2$); 2.07 (2H, m, P_T**CH**); 2.49 (2H, m, P_T**CH'**); 2.07 (2H, m, P_U**CH**); 1.80 (2H, m, P_U**CH**$_2$); 1.71 (4H, m, P_T**CH**$_2$); 1.44 (6H, d, $^3J_{H-H}$ = 7.6 Hz, P_UCH(**CH**$_3$)); 1.33 (6H, d,

---

[**] computer enhancement of spectrum required
[††] by ^{31}P-^{15}N HSQC

$^3J_{\text{H-H}}$ = 7.4 Hz, P$_U$CH(C**H**$_3$)); 1.38 (6H, d, $^3J_{\text{H-H}}$ = 7.0 Hz, P$_T$CH(C**H**$_3$)) 1.29 (6H,

d, $^3J_{\text{H-H}}$ = 6.6 Hz, P$_T$CH(C**H**$_3$)); 1.23 (6H, d, $^3J_{\text{H-H}}$ = 6.5 Hz, P$_T$CH'(C**H**$_3$));

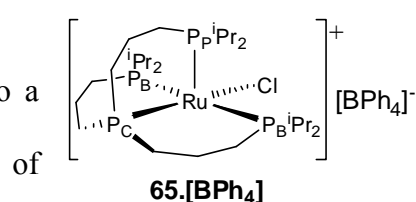1.08 (6H, d, $^3J_{\text{H-H}}$ = 6.7 Hz, P$_T$CH'(C**H**$_3$)); -11.17 (1H, s, Ru-**H**).

6.8.26 [TBPY-5-13] [chloro(tris(3-diisopropylphosphinopropyl)phosphine-κ^{4}P)ruthenium] [tetraphenylborate], [RuCl(P^{3}P$^i_3$)][BPh$_4$] 65.[BPh$_4$]

Tris(3-diisopropylphosphinopropyl)phosphine P^{3}P$^i_3$ **11** (456 mg, 0.896 mmol) was added to a brown solution of

65.[BPh$_4$]

dichlorotris(triphenylphosphine)ruthenium(II) **55** (860 mg, 0.896 mmol) in THF (approx. 30 ml) resulting in an immediate change of the solution colour to green. A stoichiometric amount of sodium tetraphenylborate (306 mg, 0.894 mmol) was added and the solution slowly turned red with stirring. After 3 hours the solvent was removed *in vacuo* to give [RuCl(P^{3}P$^i_3$)][BPh$_4$] **65.[BPh$_4$]** as a pink solid which was then recrystallised twice from THF layered with pentane (300 mg, 53%). Crystals suitable for X-ray diffraction were collected.

Anal Found: C 63.71, H 8.27 C$_{51}$H$_{80}$BClP$_4$Ru (MW 964.41) requires C 63.52, H 8.36%.

^{31}P{^{1}H} NMR (162 MHz, THF-d_8): δ 25.7 (3P, br, **P**$_{\text{B/P}}$); 14.2 (1P, q, $^2J_{\text{P(C)-P(B/P)}}$ = 36.4 Hz, **P**$_C$).

^{1}H NMR (400 MHz, THF-d_8): δ 7.29 (8H, m, B**Ph**$_{\text{ortho}}$); 6.86 (8H, m, B**Ph**$_{\text{meta}}$); 6.72 (4H, m, B**Ph**$_{\text{para}}$); 2.64 (6H, h, $^3J_{\text{H-H}}$ = 6.9 Hz, P$_{\text{B/P}}$C**H**(CH$_3$)$_2$); 1.96 (6H, m, CH$_2$C**H**$_2$CH$_2$); 1.83 (6H, m, P$_{\text{B/P}}$C**H**$_2$); 1.39 (9H, d, P$_{\text{B/P}}$CH(C**H**$_3$)); 1.12 (9H, d, P$_{\text{B/P}}$CH(C**H**$_3$)); 1.06 (6H, m, P$_C$C**H**$_2$).

$^{13}C\{^1H\}$ NMR (101 MHz, THF-d_8): δ 165.6 (m, B**Ph**$_{ipso}$);137.6 (s, B**Ph**$_{ortho}$); 126.1 (m, B**Ph**$_{meta}$); 122.2 (s, B**Ph**$_{para}$); 30.8 (m, P$_{B/P}$**C**H(CH$_3$)$_2$); 29.1 (m, P$_{B/P}$**C**H$_2$); 26.7 (m, **C**H$_2$**C**H$_2$**C**H$_2$); 21.3 (s, P$_{B/P}$CH(**C**H$_3$)); 20.9 (s, P$_{B/P}$CH(**C**H$_3$)); 20.6 (m, P$_C$**C**H$_2$).

6.8.27 [bis-{μ$_3$(tris(3-dimethylphosphinopropyl)amine-κ^{3}P)} bis-(dichloroiron(II))]$_n$, [Fe$_2$Cl$_4$(N^{3}P$_3$)$_2$]$_n$ 66
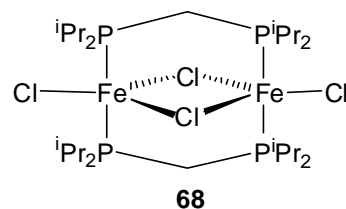

66
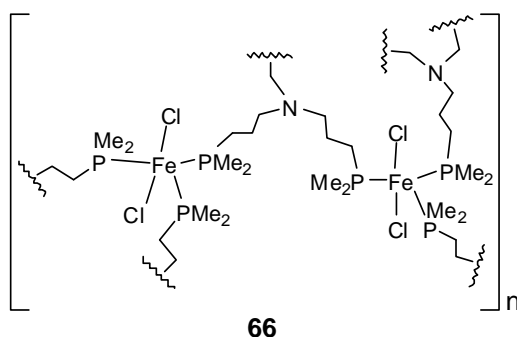
Anhydrous iron(II) chloride (156 mg, 1.24 mmol) and tris(3-dimethylphosphinopropyl)amine N^{3}P$_3$ **7** (508 mg, 1.57 mmol) were refluxed in toluene:ethanol (90%:10%) (approx. 125 ml) for 18 hours to give a light blue solution. After cooling the solution was filtered during which time a waxy solid started to precipitate. The solvent was removed *in vacuo* to afford the paramagnetic polymer [Fe$_2$Cl$_4$(N^{3}P$_3$)$_2$]$_n$ **66** as a blueish white solid (312 mg, 48%). Layering of an aliquot of the filtered reaction mixture with pentane afforded aqua blue crystals suitable for X-ray diffraction.

Anal Found: C 40.49, H 8.07, N 3.17 (C$_{30}$H$_{72}$Cl$_4$Fe$_2$N$_2$P$_6$)n (MW 900.15n) requires C 40.02, H 8.06, N 3.11%.

6.8.28 (Di-μ-chlorodi-μ-(bis(diisopropylphosphino)methane-$\kappa^2 P$))-di[chloroiron(II)], [(FeCl)$_2$(μ-Cl)$_2$(μ-P$^i_2$)$_2$] 68

Anhydrous iron(II) dichloride (approx. 20 mg, 160 μmol) was added to a solution of bis(diisopropylphosphino)methane P$^i_2$ **67** (approx. 40 mg, 160 μmol) in THF (approx. 5 ml). The reaction mixture was left under dinitrogen for several days during which time golden coloured crystals of [(FeCl)$_2$(μ-Cl)$_2$(μ-P$^i_2$)$_2$] formed (25 mg, 42%). These crystals were suitable for analysis by X-ray diffraction.
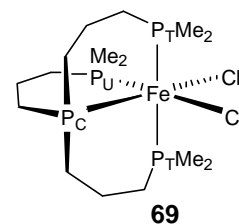
Anal Found: C 41.69, H 7.81 C$_{26}$H$_{60}$Cl$_4$Fe$_2$P$_4$ (MW 750.11) requires C 41.63, H 8.06%.

^{31}P{^{1}H} NMR (162 MHz, THF-d_8): δ 87.1 (4P, br s).

^{1}H{^{31}P} NMR (400 MHz, THF-d_8): δ 3.3-0 (60H, br m).

6.8.29 [OC-6-32] dichloro(tris(2-dimethylphosphinopropyl)phosphine-$\kappa^4 P$)iron(II), FeCl$_2$(P^{3}P$_3$) 69

A modified procedure of that reported by Antberg *et al.*[19] was used. Anhydrous iron(II) chloride (71 mg, 0.56 mmol) and tris(2-dimethylphosphinopropyl)phosphine (180 mg, 0.56 mmol) were stirred in THF (approx. 10 ml) for 2 hours. The purple reaction mixture was then filtered and the solvent removed *in vacuo* to afford FeCl$_2$(P^{3}P$_3$) **69** as a violet powder (218 mg, 89%).

^{31}P{^{1}H} NMR (162 MHz, THF): δ 37.2 (1P, dt, $^2J_{P(C)-P(T)}$ = 66.9 Hz, $^2J_{P(C)-P(U)}$ = 50.4 Hz, **P$_C$**); 30.1 (1P, dt, $^2J_{P(U)-P(T)}$ = 48.1 Hz, **P$_U$**); 7.7 (2P, dd, **P$_T$**) (lit.[20] 38.4 **P$_C$**, 31.2, **P$_U$**, 8.9 **P$_T$**).

6.8.30 [OC-6-32] chlorohydrido(tris(2-dimethylphosphinopropyl)phosphine-κ^4P)iron(II), FeClH(P^{3}P$_3$) 70

A modified procedure of that reported by Antberg et al.[21] was

used. An NMR sample of FeCl$_2$(P^{3}P$_3$) **69** (200 mg,

0.46 mmol) in THF was treated with a THF solution of

LiAlH$_4$ until **69** was no longer present by ^{31}P{^{1}H} NMR. The
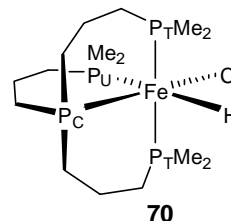
orange reaction mixture turned brown when filtered. The solvent was removed *in vacuo* and then extracted into ethanol to be used directly in the next step.

^{31}P{^{1}H} NMR (162 MHz, THF/THF-d_8): δ 56.1 (1P, dt, $^2J_{P(C)-P(T)}$ = 65.1 Hz, $^2J_{P(C)-P(U)}$ = 47.8 Hz, **P$_C$**); 20.7 (2P, dd, $^2J_{P(T)-P(U)}$ = 26.8 Hz, **P$_T$**); 12.9 (1P, dt, **P$_U$**) (lit.[20] 57.8 **P$_C$**, 22.0 **P$_T$**, 14.5 **P$_U$**).

^{1}H{^{31}P} NMR (400 MHz, THF/THF-d_8, high field): δ -10.7 (1H, s, Fe-**H**) (lit.[20] -10.4).

^{1}H NMR (400 MHz, THF/THF-d_8, high field): δ -10.7 (1H, ddt, $^2J_{P(T)-H}$ = 70.1 Hz, $^2J_{P(A)-H}$ = 52.4 Hz, $^2J_{P(C)-H}$ = 38.9 Hz, Fe-**H**) (lit.[20] -10.4).

6.8.31 Reaction of FeClH(P^{3}P$_3$) 70 with dinitrogen in ethanol

Exposure of the ethanol solution of FeClH(P^{3}P$_3$) (Section 6.8.30) to an atmosphere of dinitrogen resulted in the presence of at least two new sets of resonances by ^{31}P{^{1}H} NMR over the course of several days. The new resonances disappeared on application of a vacuum suggesting that neither can be attributed to an ethoxyhydrido complex. The first appearing of these new resonances has been tentatively attributed to the formation of an octahedral dinitrogen complex as occurs in the analogous reaction of FeClH(PP$_3$) **25**, namely [Fe(N$_2$)H(P^{3}P$_3$)]$^+$ **22** or its dimer [(FeH(P^{3}P$_3$))(μ-N$_2$)]$^{2+}$ **23**.

First set of resonances to appear after 1 day:

$^{31}P\{^{1}H\}$ NMR (121.5 MHz, ethanol/THF-d_8) δ 28.2 (1P, m, $\mathbf{P_C}$); 15.5 (2P, m, $\mathbf{P_T}$); 5.1 (1P, m, $\mathbf{P_U}$).

$^{1}H\{^{31}P\}$ (300.2 MHz, ethanol/THF-d_8, high field) δ -11.3 (1H, s, Fe-$\mathbf{H}$).
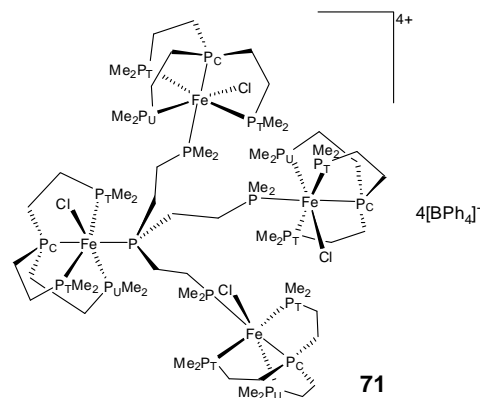
Second set of resonances to appear after several days:

$^{31}P\{^{1}H\}$ NMR (121.5 MHz, ethanol/THF-d_8) δ 24.0 (m), 14.8 (m), 3.6 (m).

$^{1}H\{^{31}P\}$ (300.2 MHz, ethanol/THF-d_8, high field) δ -13.6 (s).

6.8.32 μ$_4$-(tris(2-dimethylphosphinoethyl)phosphine-κ^4P)-tetra[chloro(tris(2-dimethylphosphinoethyl)phosphine-κ^4P)iron(II)] tetrakis[tetraphenylborate], [Fe$_4$Cl$_4$(PP$_3$)$_5$][BPh$_4$]$_4$ 71.[BPh$_4$]$_4$

Solutions of anhydrous iron(II) chloride (200 mg, 1.6 mmol) and PP$_3$ **1** (470 mg, 1.6 mmol) in THF (50 ml each) were added at equal rates over a period of 4 hours to THF (approx. 85 ml) with rapid stirring. The reaction mixture was maintained at 0°C under an atmosphere of argon, affording a red solution of FeCl$_2$(PP$_3$) **24** and a small amount of reddish brown solid. The solid, believed[7] to be [Fe$_4$Cl$_4$(PP$_3$)$_5$]Cl$_4$ **71.Cl$_4$** was collected by filtration and dissolved in acetone to which approximately 5 mg of sodium tetraphenylborate was added resulting in the precipitation of a red crystalline solid suitable for analysis by X-ray diffraction.

6.8.33 μ_3-(tris(2-dimethylphosphinoethyl)phosphine-1κP, 2κP, 4$\kappa^2 P$)-μ_2-(tris(2-dimethylphosphinoethyl)phosphine-3κP, 4$\kappa^3 P$)-tri[(tris(2-dimethylphosphinoethyl)phosphine-$\kappa^4 P$)iron(0)]iron(0), [Fe$_4$(PP$_3$)$_5$] **72**

The yellow THF solution of (Fe(PP$_3$))$_2$(μ-N$_2$) **38** and Fe(N$_2$)(PP$_3$) **44** from Section 6.8.10 was allowed to lose its solvent by slow evaporation. This resulted in the formation of small crystals of the tetramer **72** suitable for analysis by X-ray diffraction.

72
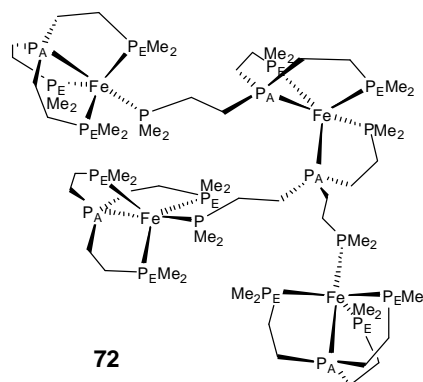
6.9   References

1.   Perrin, D. D. A., W. L. F., *Purification of Laboratory Chemicals*. 3rd ed.; Pergamon Press: Oxford, **1993**.

2.   Hallman, P. S.; Stephenson, T. A.; Wilkinson, G., *Inorg. Synth.* **1970,** *12*, 237-40.

3.   Ohmori, H.; Takanami, T.; Shimada, H.; Masui, M., *Chem. Pharm. Bull.* **1987,** *35*, (6), 2558-60.

4.   Weitz, I. S.; Rabinovitz, M., *J. Chem. Soc., Perkin Trans. 1* **1993**, (1), 117-20.

5.   Glassman, T. E.; Vale, M. G.; Schrock, R. R., *J. Am. Chem. Soc.* **1992,** *114*, (21), 8098-109.

6.   Trenkle, A.; Vahrenkamp, H., *Z. Naturforsch., B* **1979,** *34B*, (4), 642-3.

7.   Smernik, R. J., PhD Thesis, University of Sydney, **1996**.

8.   Parshall, G. W., *Org. Synth.* **1965,** *45*, 102-4.

9.   Jia, G.; Drouin, S. D.; Jessop, P. G.; Lough, A. J.; Morris, R. H., *Organometallics* **1993,** *12*, (3), 906-16.

10. Maier, L.; Seyferth, D.; Stone, F. G. A.; Rochow, E. G., *J. Am. Chem. Soc.* **1957,** *79*, 5884-9.

11. MacBeth, C. E.; Harkins, S. B.; Peters, J. C., *Can. J. Chem.* **2005,** *83*, (4), 332-340.

12. Renaud, F.; Decurnex, C.; Piguet, C.; Hopfgartner, G., *J. Chem. Soc., Dalton Trans.* **2001**, (12), 1863-1871.

13. Fryzuk, M. D.; Carter, A.; Westerhaus, A., *Inorg. Chem.* **1985,** *24*, (5), 642-8.

14. Baumeister, J. M.; Alberto, R.; Ortner, K.; Spingler, B.; August Schubiger, P.; Kaden, T. A., *J. Chem. Soc., Dalton Trans.* **2002**, (22), 4143-4151.

15. Antberg, M.; Prengel, C.; Dahlenburg, L., *Inorg. Chem.* **1984,** *23*, (25), 4170-4.

16. Zhu, K.; Achord, P. D.; Zhang, X.; Krogh-Jespersen, K.; Goldman, A. S., *J. Am. Chem. Soc.* **2004,** *126*, (40), 13044-13053.

17. Turnbull, A. J., PhD Thesis, University of Sydney, **2000**.

18. Field, L. D.; Messerle, B. A.; Smernik, R. J., *Inorg. Chem.* **1997,** *36*, (26), 5984-5990.

19. Antberg, M.; Dahlenburg, L., *Inorg. Chim. Acta* **1985,** *104*, (1), 51-4.

20. Bampos, N., PhD Thesis, University of Sydney, **1993**.

21. Antberg, M.; Dahlenburg, L., *Z. Naturforsch., B* **1985,** *40B*, (11), 1485-9.

Appendix

A1 X-ray Crystallographic Data (CD contents)

Complex		File on CD
$[(FeH(PP_3))_2(\mu\text{-}{}^{15}N_2)][BAr^F_4]_2$	$^{15}N_2$-23.[BAr$^F_4$]$_2$	23.cif
$[(FeH(PP_3))(\mu\text{-}N_2)(Fe(PP_3))][BPh_4]$	37.[BPh$_4$]	37.cif
$[Fe(NH_2NH_2)H(PP_3)][BPh_4]$	47.[BPh$_4$]	47.cif
$[FeCl(PP^i_3)][BPh_4]$	51.[BPh$_4$]	51.cif
$Fe(N_2)(PP^i_3)$	52	52.cif
$[RuCl(PP^i_3)][BPh_4]$	56.[BPh$_4$]	56.cif
$Ru(N_2)(PP^i_3)$	57	57.cif
$[Ru(N_2)H(PP^i_3)][BF_4]$	58.[BF$_4$]	58.cif
$[RuCl(P^3P^i_3)][BPh_4]$	65.[BPh$_4$]	65.cif
$[Fe_2Cl_4(N^3P_3)_2]_n$	66	66.cif
$[(FeCl)_2(\mu\text{-}Cl)_2(\mu\text{-}P^i_2)_2]$	68	68.cif
$[Fe_4Cl_4(PP_3)_5][BPh_4]_4$	71.[BPh$_4$]$_4$	71.cif
$[Fe_4(PP_3)_5]$	72	72.cif